New nano-oxide catalysts for CO2 hydrogenation reaction

Dominik Wierzbicki

AGH University of Science and Technology

Faculty of Energy and Fuels

Sorbonne Université

Institut Jean Le Rond D'Alembert

PhD Thesis

New nano-oxide catalysts for CO_2 hydrogenation reaction

Nowe nanotlenkowe katalizatory do reakcji uwodornienia CO_2

Dominik Wierzbicki

PhD supervisors:

Prof. dr hab. Teresa Grzybek (AGH, Kraków), supervisor

Prof. Maria Elena Galvez (SU, Paris), supervisor

Dr hab. Monika Motak (AGH, Kraków), co-supervisor

Prof. Patrick Da Costa, (SU, Paris), co-supervisor

Kraków 2018

OŚWIADCZAM, ŚWIADOMY ODPOWIEDZIALNOŚCI KARNEJ ZA POŚWIADCZENIE NIEPRAWDY, ŻE NINIEJSZĄ PRACĘ DOKTORSKĄ WYKONAŁEM OSOBIŚCIE I SAMODZIELNIE ORAZ IŻ NIE KORZYSTAŁEM ZE ŹRÓDEŁ INNYCH NIŻ WYMIENIONE W PRACY.

Dominik Wierzbicki

The research presented in this PhD thesis was carried out on Sorbonne University, Institut Jean Le Rond D'Alembert and on Faculty of Energy and Fuels at AGH University of Science and Technology within the cotutelle agreement between AGH in Kraków and UPMC in Paris.

Acknowledgements

I would like to thank my supervisors Prof. Teresa Grzybek, Prof. Maria Elena Galvez, Dr hab. Monika Motak and Prof. Patrick Da Costa, for the patient guidance, encouragement and advice they provided throughout my time as their student. I have been very lucky to have supervisors who cared so much about my work, and who responded to my questions and queries so promptly.

I would also like to thank all my colleagues from Faculty of Energy and Fuels, AGH and Insitut Jean Le Rond D'Alembert, SU for helping me keep things in perspective.

Finally, my deep and sincere gratitude to my Family for their continuous and unparalleled love and support. This journey wouldn't be possible without them, and I dedicate this milestone to them.

List of Abbreviations

CCS – Carbon Capture and Storage

CCU – Carbon Capture and Utilization

CNs – Carbon nanotubes

CP – co-precipitation

DEA – diethanolamine

DFT – Density Functional Theory

DME – Dimethyl ether

DRIFT – Diffuse Reflectance Infrared Fourier Transformation

ECBM - Enhanced Coal Bed Methane Recovery

EGR – Enhanced Gas Recovery

EOR – Enhanced Oil Recovery

FT – Fischer-Tropsch synthesis

FTIR – Fourier Transform Infrared Spectroscopy

GHG – Greenhouse Gases

GHSV – Gas Hourly Space Velocity

HERFD-XANES – High Energy Resolution Fluorescence Detection X-Ray Absorption Near Edge Spectroscopy

HTs – hydrotalcites

IAD – Integrated Absolute Difference

IGCC – Integrated Gasification Combined Cycle

ICP – Inductively Coupled Plasma

IMP – impregnation

LCF – Linear Combination Fitting

LDHs – Layered double hydroxides

MEA – Monoethanoloamine

MeOH – methanol

MTBE – methyl tert-butyl ether

MTG – methanol to gasoline

MTO – methanol to olefins

NP – nanoparticles

POM – partial methane oxidation

RWGS – Reverse Water Gas shift

SEM – Scanning Electron Microscopy

SSITKA – Steady State Isotopic Transient Kinetic Analysis

TEM – Transmission Electron Microscopy

TG – Thermogravimetry

TOF – Turnover Frequency

TPD – Temperature Programmed Desorption

TPR – Temperature Programmed Reduction

WGS – Water Gas Shift

XAS – X-ray Absorption Spectroscopy

XES – X-ray Emission Spectroscopy

XRD – X-ray diffraction

XRF – X-Ray Fluorescence

CONTENTS

1. Introduction

Energy is one of the fundamental needs in modern society. It is forecasted that consumption will increase further with the economic growth. The increasing energy demand creates a number of challenges for the global population, whose energy infrastructure relies largely on fossil fuels.

One of the important tasks is to mitigate the effects of greenhouse gas emissions from fossil fuel combustion, which are rising continuously. The scientific community has agreed that the increasing concentration of carbon dioxide from anthropogenic sources in the atmosphere is responsible for the climate change and increasing of global average temperature. According to the International Energy Agency the energy consumption is responsible for ca. 69% of greenhouse gases emitted by humankind and CO_2 contributes to 90% of the greenhouse gases released from energy consumption. The emissions of carbon dioxide into atmosphere are growing with every year and reached a record value of 36Gt in 2015, which forced governments to look for strategies for CO_2 emissions reduction. European Union set a long-term goal by year 2050, which implies the reduction of greenhouse gases emissions by 80-95% with respect to the levels from 1990. In order to reach this goal, different technologies have to be implemented, such as carbon dioxide capture and storage (CCS) or capture and utilization (CCU). As CCS technologies have a limited capacity and fossil fuels, as predicted, will still be the main source of energy, CCU technologies, which in comparison to CCS are non-passive, seem to be a better solution of this problem. The utilization of CO_2 in comparison to storage is more attractive, especially if it can be recycled into valuable chemical products such as e.g. methane, methanol or higher hydrocarbons. Currently there are a few industrial processes utilizing carbon dioxide, such as e.g. synthesis of polycarbonates, urea or salicylic acid

[1, 2]. However, the amount utilized in these processes corresponds only to a few percentages of the potentially available CO_2.

Moreover, the CO_2 hydrogenation offers the storage of excess energy in the form of chemicals, e.g. methane (or higher hydrocarbons), with hydrogen supplied via water electrolysis using excess energy. Thus, for countries such as Germany, which renewable energy sector is growing very quickly and a lot of excess energy is produced, such strategy would be of great advantage. The infrastructure for gas transportation, that already exists enables to use methane as an energy carrier. CO_2 hydrogenation is treating carbon dioxide as raw material and may simultaneously lead to (i) production of gaseous or liquid fuels (ii) reduction of carbon dioxide emissions and (iii) storage of the excess energy in chemical compounds. CO_2 methanation may have also other applications, such as e.g. syngas purification for ammonia production.

The CO_2 methanation reaction is thermodynamically favorable, however, the complete reduction (to methane) of fullly oxidized carbon, is an eight electron reaction with significant kinetics limitations, which makes it necessary to implement an active catalyst in order to achieve reasonable conversion degrees. Ni, Ru and Rh based catalysts have been revealed as the most active materials for this process. The most widely studied catalytic systems are nickel-based, presenting almost the same activity in methanation and being much cheaper and more available than noble metals, making such catalysts more interesting from a commercial standpoint. However, the catalytic activity and selectivity at lower temperatures (250°C) still needs to be enhanced in order to introduce this process on industrial scale.

The proposed strategies towards increasing the activity of the nickel-based catalysts include the application of different supports and/or promoters. Basing on literature reports concerning nickel-based catalysts for carbon dioxide methanation

reaction, it is possible to define some crucial properties of catalysts for this process, such as e.g basic properties and metallic nickel crystallite size. It postulated that medium-strength basic sites are directly involved in the reaction of CO_2 methanation. Another report showed that CO_2 methanation is favored on catalysts with smaller metallic nickel particle size. The positive effect of MgO addition to the catalysts, or its application as support, was attributed to its high basicity, which enhanced CO_2 adsorption capacity on the catalysts surface. Another important issue are promoters for this process e.g. lanthanum was considered as support of this reaction because of its basic properties.

Among different materials considered as catalysts for CO_2 methanation, hydrotalcites seem to be very promising. Hydrotalcite-derived materials possess some unique properties coming from the precursor. The most important one is that the composition of such materials can be strictly controlled during the synthesis. Different types of cations introduced into the hydrotalcite structure are homogenously distributed, as they are randomly arranged in the brucite-like layers. The product of thermal decomposition of the precursor exhibits basic properties, which is crucial for the methanation of carbon dioxide reaction.

The number of literature studies focused on hydrotalcite-derived mixed oxides as catalysts for the process of carbon dioxide methanation is rather limited. Thus, there are is a lot of uncertainties and open questions which need to be addressed, concerning:

- the influence of nickel content in brucite-like layers,
- the influence of promoters (e.g. La or Fe),
- the effect of different methods of promoter introduction.

The main goal of this PhD thesis is to fill these gaps. The main thesis is that through the implementation of different Ni/Mg/Al ratios, different promoters and various modification methods, it is possible to tailor the properties of the catalysts in order to

increase their activity and selectivity in the reaction of carbon dioxide methanation. The studies presented in this thesis confirm this hypothesis.

2. Aim of the PhD thesis

The aims of this PhD thesis were to:

- Prepare nickel containing hydrotalcite-derived materials, characterize them using different techniques in order to establish their physico-chemical properties and test them as catalysts in the reaction of CO_2 methanation.
- Tailor basic and redox properties and determine the importance of both types of sites in CO_2 methanation by varying the ratio of Ni/Mg.
- Establish the influence of lanthanum and iron as promoters on the catalytic properties of hydrotalcite-derived mixed oxide catalysts.
- Establish the influence of different methods of La incorporation on the catalytic properties of Ni/Mg/La/Al hydrotalcites.

The obtained results allowed to prove the hypothesis that the catalytic properties of hydrotalcite-derived mixed oxides can be tailored, and that the appropriate composition of the precursors allows to increase the catalytic activity in the reaction of carbon dioxide methanation at low temperature and normal pressure.

3. Climate change and possible solutions

The rising levels of CO_2 in the atmosphere increased concerns and social awareness about the climate change caused by the emission of greenhouse gases originating from combustion of fossil fuels for power generation and other industrial activities. Lowering the emissions of carbon dioxide from anthropogenic sources includes the transition to carbon-free sources of electricity, such as renewables or utilizing biomass as a feedstock for valuable chemicals, as well as CO_2 capture from stationary sources and direct capture of CO_2 from the atmosphere. Apart from different technological status of such methods, it should be considered that even the most advanced of them have some limitations. Thus, it will be necessary to apply all these solutions in order to efficiently reduce the CO_2 emissions. The transition to renewable energy sources, the most obvious of the proposed solutions, creates an additional important problem, which is the energy availability on demand. This requires the storage of excess renewable energy. One of the proposed solutions is the storage in the form of chemical compounds. The carbon dioxide hy drogenation offers the possibility of storage of excess energy from renewable sources in the form of chemicals such as methane or higher hydrocarbons, with hydrogen provided via water electrolysis.

3.1. Carbon dioxide emissions

The emissions of carbon dioxide into atmosphere are constantly increasing since the pre-industrial era and reached the level of 36 Gt in 2015, resulting in a drastic increase of CO_2 concentration from ca. 280 ppm in the end of 1800s to ca. 405 ppm in November 2017, with an average growth of ca. 2ppm per year in the last 10 years. According to International Energy Agency (IEA), the energy consumption is responsible for ca. 69% of greenhouse gases emitted by the humankind, with CO_2 contributing to 90% of the

greenhouse gases released from energy consumption. An additional problem is a huge increase of 150% in global total primary energy supply, which was mainly caused by the worldwide economic growth and development. Despite a large development of new renewable, as well as nuclear energy sources, the total world energy supply has been relatively unchanged over the past 40 years, and fossil fuels still are the main energy supply contributing to ca. 82% of the worlds primary energy use. Carbon dioxide emissions are strongly associated with the combustion of fossil fuels, with the highest contribution of coal and oil. Until 2000 the emissions of CO_2 caused by oil combustion exceeded those from coal. The situation was changed due to the fast development of countries such as China or India, which have large coal reserves, and the rapid increase in the energy intensive industrial processes.

The main sources of carbon dioxide emission are:

- Electricity and heat production (42%),
- Transportation (23%), and
- Industry (19%).

As many countries, such as China, India or Poland, still strongly relay on fossil fuels, it is predicted that the situation will not change in the coming years.

The top CO_2 emitters are China, USA, Russia, Japan, Germany, Korea, Canada, Iran and Saudi Arabia and these countries account for two thirds of global carbon dioxide emissions [3]. As shown in Fig. 3.1 the highest carbon dioxide emission region is Asia with China being the number one emitter. In 2014 both largest emitters of CO_2 in the world, USA and China, increased CO_2 emissions by 0.9% with respect to 2013. On the other hand, European Union successfully decreased the emissions of CO_2 in 2014 by 5.4% due to the lower consumption of fossil fuels for power generation [4].

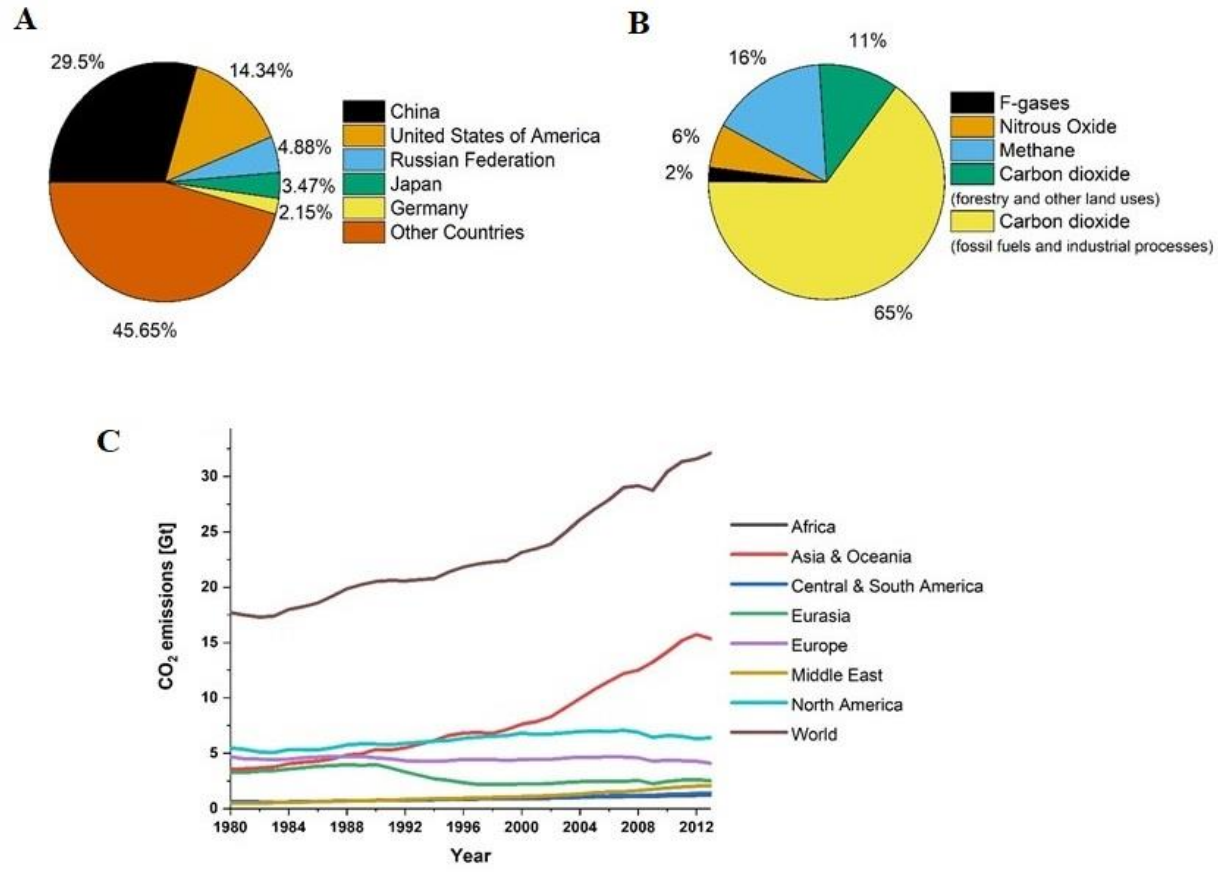

Figure 3.1 The greenhouse gas emissions and CO_2 emissions: share of CO_2 emissions by region in 2015 (A), global greenhouse gas emissions in 2010 (B), and global CO_2 emissions by region (1980 to 2015) [5].

It is very important to understand the global driving factors of carbon dioxide emission in order to find efficient solutions to reduce the GHG emissions. The growing world population, increasing demand for energy and practically unchanged carbon intensity of the energy mix, resulted in significant increase of CO_2 emissions during few decades. The increase of CO_2 concentration in the last 150 years was mainly caused by well developed countries, which today apply GHG emissions reduction policies. However, at the same time the developing countries emit huge amounts of GHG. Thus, some efforts have to be undertaken by all countries in order to develop in a sustainable way.

The first international agreement, which forced countries to reduce greenhouse gases emissions was the Kyoto Protocol linked to the UNFCCC - United Nations Framework Convention on Climate Change, which was adopted in 1997 and implemented in 2005 [6]. The first commitment period stated that industrialised countries were obligated to reduce the GHG emissions (CO_2, CH_4, N_2O, HFCs, PFCs, SF_6) by 5% against 1900s levels during years 2008-2012. The levels of reduction were specified for each participating country and each GHG, depending on political and economic situation. In the second commitment period from 2013-2020 the participating countries should reduce the GHG emissions by 18% with respect to 1990s levels. In order to bring the protocol into force, it requires ratification of two-thirds of 144 participating countries. Until now 175 parties have ratified the Paris Agreement out of 197. The Paris Agreement entered into force on 4 November 2016 [7].

European Union has already implemented the 20/20/20 policy, which sets targets that should be reached by 2020 [7]:

- GHG emissions 20% lower than those from 1990s levels,
- At least 20% share of renewables in the energy sector, and
- 20% improvement in energy efficiency.

In 2014 and 2016 the CO_2 emissions in EU decreased by 5.4% and 0.4%, respectively [7]. The European Union adopted also a new 2030 climate and energy framework in October 2014, which sets three key targets to be reached by year 2030 [7], at least:

- 40% lower emissions of GHG than those from 1990s levels,
- 27% share of renewables in energy sector, and
- 27% improvement in energy efficiency.

The development of low-carbon economy assumes that:

- EU should lower GHG emissions by at least 80% in comparison to 1990s,
- The milestones to achieve the goal are cuts by 40% and 60% by 2030 and 2040, respectively,
- All sectors need to contribute, and
- The low-carbon transition is feasible and affordable.

3.2. Reduction of CO_2 emissions

In order to limit the temperature increase within 2°C by 2050, the International Energy Agency developed a model, which showed that the annual carbon dioxide emissions shouldn't exceed 15 Gt. To achieve this goal, increasing both the energy efficiency and the application of renewable energy sources have to be further developed. Since the concept of CCS is limited, Carbon Capture, a combination of CCS and carbon utilization CCU i.e. Utilization and Storage (CCUS) methods gained significant attention and are believed to be the solution to this problem.

The first step to mitigate carbon dioxide emissions from the existing power generators is CO_2 capture, which is, or will be, applied to large scale stationary emission sources such as e.g. fuel processing plants, as well as certain other industrial sources. Post-combustion and pre-combustion, as well as oxy-combustion CO_2 capture technique are the solutions proposed (Figure 3.2). Post-combustion CO_2 capturing systems, which are the most widely studied, should remove CO_2 from outgases of industrial processes or power plants, which enables the control of emissions. In the pre-combustion scheme, carbon dioxide is removed before the fuel combustion to prevent its release into the atmosphere. Pre-combustion CO_2 removal systems are usually applied to gasification combined cycle plants, such as IGCC, where CO_2 originates from gasification and WGS

reactions [8, 9]. On the other hand, in the oxy-combustion technique oxygen is used to burn fuels, resulting in a concentrated CO_2 stream at the exit of the process [10]. Out of these three methods, post-combustion CO_2 capture techniques are most technologically mature and could be implemented at the existing applications. There are already some examples using such solutions on a large scale. In 2014, the first coal-fired power plant started CO_2 capture from flue gases (Boundary Dam power plant, 120 MW, Canada). Another example may be the 320 MW power plant at Shady Point, USA firing coal or co-firing coal and biomass, removing 15% of CO_2 from flue gas i.e. 800 t/day. Other e.g. Petra Nova Carbon Capture, 1.4 Mt post combustion CO_2 capture, since January 2017 (Texas, USA,) or Illinois Industrial CCS (1 Mt injection capacity) [11].

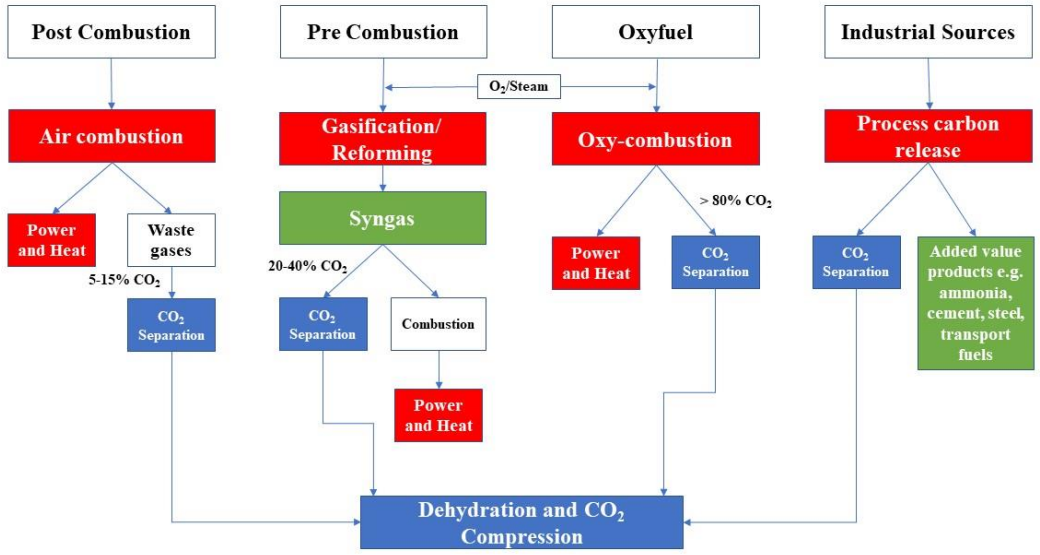

Figure 3.2 Carbon Dioxide Capture Systems From Stationary Sources (adapted from [12])

In case of the pre-combustion CO_2 capture system, carbon dioxide is captured after the reaction of steam with carbon monoxide that remained after the reaction of the fuel with oxygen or air and/or steam.

In the oxy-fuel combustion techniques the fuel reacts with a stream of pure oxygen, resulting in a flue gas that consists mainly CO_2 and H_2O. The main disadvantages of this

method are high temperature of the flame resulting from combustion of the fuel in pure oxygen, and high cost of oxygen separation from air. The flue gas may be returned to the boiler in order to change the temperature.

The most often proposed post-combustion carbon dioxide capture technique is based on absorption method and requires a CO_2 capturing absorbent, which will efficiently remove it from a mixture of 4-14 vol.%. Due to the low concentration of carbon dioxide, the flue gas stream forms a significant kinetic limitation for the development of such capturing technology. The novel technologies are mostly focused on finding membranes or adsorbents.

The technology of post-combustion CO_2 capture currently most developed is chemical absorption. It is realized by scrubbing by an aqueous amine solvent. It has already been applied on industrial scale [13]. In this process carbon dioxide is absorbed in an aqueous solution at low temperature (close to ambient), followed by regeneration of the absorbent by stripping with water vapor at 100-120℃. Water is subsequently condensed in order to obtain pure CO_2 [13]. The most commonly used absorbents are monoethanolamine (MEA), diethanolamine (DEA) or potassium carbonate, out of which MEA has been shown to have the highest efficiency and is thus most often proposed [10, 13, 14]. When new absorbents are developed their performance is compared to the performance of MEA, which is used as a baseline [15]. The solution of the absorbent contains around 20-30% of MEA dissolved in water in order to prevent corrosion [8]. The major drawbacks connected with this technology is the low cyclic carbon dioxide capture capacity of the absorbents, corrosive nature of the absorbents, the amount of energy utilized for regeneration and losses of the absorbent due to degradation in the presence of oxygen [16]. Additionally, the method requires appropriate cleaning of flue gas of other

pollutants, such as NOx, SO_2 and particulate matter, in order to avoid considerable losses of MEA [17].

Another possible solution could be using solid adsorbents, as their utilization eliminates corrosion problems when compared to liquid absorbents. Both physical and chemical adsorbents are under research. The most important features of physical adsorbents are selectivity and amount adsorbed. Due to the fact that flue gas contains air, water and impurities, such as e.g. SO_x and NO_x, an adsorbent for post-combustion CO_2 capture should be characterized by higher selectivity for carbon dioxide over other components of flue gases. The most extensively studied physical adsorbents for CO_2 capture are activated carbons, metal organic frameworks, zeolites, carbon nanotubes and molecular sieves [8]. Their advantage is a weak interaction with CO_2, so carbon dioxide can be easily released under mild conditions. On the other hand, the weak interaction with CO_2 results in low selectivity for carbon dioxide in the presence of water. Of all mentioned adsorbents activated carbon seems to fulfill all requirements for a good adsorbent, such as low price, high specific surface area and low amount of energy supplied for regeneration [18]. The recent developments of adsorbents include the incorporation of amine sites integrated into metal organic frameworks in order to increase the CO_2 selectivity and to increase the interaction adsorbent-CO_2 [19].

Other techniques that may effectively separate carbon dioxide from flue gases are membranes. This technique could be applied for high pressure flue gases, where the driving force is the difference in pressure. Ceramics, metals or polymers found application for separation of hydrogen, carbon dioxide or oxygen from flue gases. Due to high cost required for carbon dioxide capture and technical problems, this method has not as yet found application on a scale as large as required for power stations.

3.3. Storage of captured CO_2

The next steps in CCS methods are drying of CO_2 and transport, followed by the storage of captured carbon dioxide in order to prevent its release into the atmosphere. One of the possibilities of handling this problem is to find a suitable reservoir that can store a large amount of CO_2 for a long time. However, CO_2 storage technologies suffer from technical and infrastructural issues. Among storing technologies, the following are most often considered: enhanced oil or gas recovery (EOR, EGR), geological storage or enhanced coal bed methane recovery (ECBM).

Enhanced Oil Recovery has been successfully demonstrated on a large scale e.g. in the Weyburn oil field [20] and Sleipner gas field [21]. EOR provides currently ca. 5% of total United States crude oil production and is predicted to increase in the upcoming decades because of the increasing oil prices [22, 23]. Geological storage of carbon dioxide is another proposed way of sequestration. There is already a significant technical experience with injection of CO_2 into underground reservoirs as a part of enhanced oil recovery (EOR) projects. Geological storage involves the injection of carbon dioxide into a depleted fossil fuel field. However, it has not been proven with any certainty that carbon dioxide will stay underground for long periods [24]. Nevertheless, this method has a huge potential of CO_2 storage the highest of all proposed solutions. The main locations for geological storage, that are taken into consideration, are depleted hydrocarbons reservoirs, deep coal seams and saline aquifers, the latter having the highest capacity potential for CO_2 storage [24, 25]. Both geological storage and mineral trapping suffers from some critical issues. For both of them CO_2 has to be compressed at an emission source and transported to the site of disposal and then injected underground. Currently if there is no pipeline infrastructure that could connect the source of emission with geological storage facility, this may be is the major challenge for these technologies [26].

In Enhanced Coal Bed Methane Recovery (ECBM) carbon dioxide is injected into a deep depleted coal field in order to recover the methane sorbed in a coal bed. The recovered methane may be further used for electricity production or exported to market. In comparison to EOR and EGR methods, which are mature technologies, ECBM is still under development. The main disadvantage connected with this method is that the mine cannot be exploited anymore [27].

One of the main problems connected with storage is to establish standards and technologies in order to accurately monitor the CO_2 and prevent leaks. An uncontrolled leak can be devastating not only for environment but also the human health, as demonstrated by e.g. natural release of CO_2 in Lake Nyos in Cameroon which killed 1700 people.

3.4. *Carbon dioxide utilization*

The image of carbon dioxide has drastically changed during last few decades. CO_2 is no longer considered as a harmful pollutant, but as an interesting C_{1+} building block. The carbon dioxide capture and separation techniques, that are already applied or under development, can provide a highly pure CO_2 stream for production of other chemical compounds. The utilization of CO_2 may be divided into two groups with (i) CO_2 used directly without any conversion, and (ii) carbon dioxide converted into chemicals. CO_2 already found some application without conversion, in e.g. food processing, preservation, beverage carbonation, fire suppression, enhanced oil recovery or in supercritical state as a solvent. The current industrial processing of CO_2 results in its conversion to valuable chemicals, such as urea, methanol, salicylic acid, formic acid, or pharmaceuticals production. However, its use as chemical feedstock has still a huge potential [28, 29].

Current and potential technologies, which can utilize CO_2 as raw material for production of synthetic fuels and added value chemicals is presented in Figure 3.3. It is

predicted that the amount of industrial processes involving CO_2 as raw material will be developed in the upcoming decades, which will create a new CO_2 based economy. It is worth noting that all these processes require the presence of catalysts, which clearly points to the importance of catalytic studies of those reactions on lab- and/or pilot scale.

Carbon dioxide conversion to fuels, rather than organic compounds, is expected to play a major role in the CO_2 emission management strategies, because of the fact that the market for fuels is much bigger than that for organic chemicals. Centi *et al.* [28] suggested that around 5-10% of current CO_2 emissions is suitable for the production of fuels, corresponding to ca. 1.75-3.5 Gt CO_2 reduced per year. Most of the reactions of CO_2 conversion require energy, thus in order to supply the amount of required energy it is important to develop renewable technologies. Ecofys and Carbon Count provided a classification of the diverse range of CCU applications [30]. They used a taxonomical approach using sectors of CCU technologies as a base of their classification, with applications differentiated more in a functional than technical groups. The classification, illustrated by Table 3.1, covers the following applications:

- CO_2 to fuels – technologies that may provide new types of energy, such as renewable methanol or biofuels from algae,
- Enhanced commodity production – where CO_2 could be used to boost the production of some goods. CO_2 is already applied in this way but it could be modified in areas such as urea yield boosting, or as a substitute in existing technologies e.g. for steam in a power cycle,
- Enhanced hydrocarbon production – covering the use of CO_2 for recovery of hydrocarbons from subsurface (EOR),
- CO_2 mineralization, and
- Chemicals production.

Considering this classification, Bocin Dimitru & Tsimas [31] discussed additionally the technological maturity of the methods. The main considered categories are: research stage, demonstration phase, economically feasible method and mature market technology.

Table 3.1 CCU technologies classification and maturity (adapted from [31])

CCU category	**CCU technology**	***Research***	***Demonstration***	***Economical Feasibility***	***Mature market***
CO_2 to fuels	• Hydrogen (renewable methanol)		■	■	
	• Hydrogen (formic acid)	■	■		
	• Algae (to biofuels	■	■		
	• Photocatalytic processes	■			
	• Nanomaterial catalysts	■			
Enhanced production	• Power cycles (using $scCO_2$)	■			
	• Urea, methanol				■
Enhanced recovery	• CO_2-EOR				■
	• CO_2-EGR		■		
	• ECBM		■		
CO_2 - mineralisation	• Production of cement	■	■		
	• CO_2 concrete curing		■	■	
	• Bauxite residue carbonation (red mud)			■	
	• Carbonate mineralisation (other)	■	■		
Production of chemicals	• Sodium carbonate				■
	• Polymers	■	■		
	• Other chemicals (e.g. acetic acid)	■			
	• Algae (for chemicals)		■	■	
Legend	Main activities ■	Some activies ■			

Research in the Table 3.1 means that while basic science is understood the technology is feasible and some laboratory and bench scale testing has been carried out. ***Demonstration phase*** means that the technology has already been operated on a pilot scale, but further development is required before it will be ready for commercialization on a full scale. ***Economically feasible*** is a well-developed technology, which may be applied commercially under certain conditions. ***Mature market*** is the one that was already been commercialized on the full scale and can be easily modified for new applications involving non-captive CO_2. Additionally, Ecofys and Carbon Count conducted a technology readiness assessment of the CCU categories, which is given in Table 3.2 [32]. Technology Readiness Level (TRL) is an effective tool to assess the development level of technologies, starting from its basic concept (TRL 1) to commercial scale (TRL 9). Table 3.2. presents selected CCU technologies, which were considered to be the most promising technological pathways identified by various reports. The Table presents the potential CO_2 uptake and DG Joint Research Center in-house TRLs assessment levels [33].

Table 3.2 The overview of European most promising CCU technology pathways and the DG JRC CO_2 reuse technologies with their potential CO_2 uptake (adapted from [33])

CCU technology	Potential CO_2 uptake (Mt/y)	Technology Readiness Level
Methanol	> 300	4 - 6
Mineralisation	> 300	3 - 6
Polymerisation	5 to 30	8 - 9
Formic acid	> 300	2 - 4
Urea	5 to 30	9
ECBM recovery	30 to 300	6
Enhanced geothermal systems	5 to 30	4
Algae cultivation	> 300	3 - 5
Concrete curing	30 to 300	4 - 6
Bauxite residue managment	5 to 30	4 - 5
Fuels engineered micro-organism	> 300	2 - 4
CO_2 injection to methanol synthesis	1 to 5	2 - 4

In the second group, carbon dioxide is converted to chemicals or fuels through carboxylation or reduction [34]. There are already some industrial processes utilizing CO_2 as feedstock e.g. production of urea, salicylic acid, cyclic carbonates or polycarbonates.

All the mentioned reactions together use around 130 Mt of CO_2 per year, with urea production consuming the highest amount of CO_2.

Mineral carbonation is a chemical process, which involves the conversion of CO_2 into a solid mineral such as e.g. calcite ($CaCO_3$) or magnesite ($MgCO_3$). This method is believed to be a long-term storage option, as carbonate is the most stable form of carbon. Thus, this method seems to be environmentally safe and does not require additional monitoring [35, 36]. According to the studies of Keleman *et al.* Samail ophiolite in Oman contains enough magnesium to store the whole amount of CO_2 from atmosphere in the form of magnesite [37]. It is suggested in literature that through in-situ carbonation reaction by drilling into the geological formation it is possible to obtain high reaction rates due to generation of heat from the carbonation reaction [36, 38].

Enhanced commodity production belongs to market mature technologies. The main areas are urea production and CO_2 as applied to power cycles. Urea is produced by the reaction between ammonia and CO_2 (Eq. 3.1) at around 185-190°C with pressure ranging from 180-200 atm. This process can be divided into two steps. During the first, fast and exothermic reaction, ammonium carbamate ($H_2N\text{-}COONH_4$) is formed through the contact of liquid ammonia with CO_2. In the second, slow and endothermic reaction, which is a rate determining step, ammonium carbamate is decomposed to water and urea.

$$CO_2 + 2NH_3 \rightleftharpoons H_2NCOONH_4 \rightleftharpoons CO(NH_2)_2 + H_2O \qquad \text{(Eq. 3.1)}$$

As large amounts of CO_2 are separated during production of H_2 supplying ammonia plants via steam reforming and WGS reaction the facilities are often placed close to urea plants. Currently urea production process is the main consumer of CO_2 as feedstock with around 112 Mt of carbon dioxide consumed annually [39].

Similarly, CO_2 is used to react with ethylene diamines giving 2-imidazolidinones, which are cyclic ureas (Eq. 3.2)

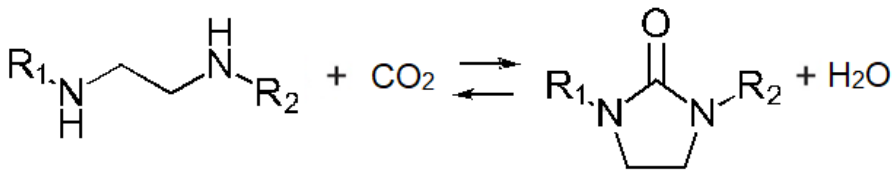

(Eq. 3.2)

Kolbe-Schmitt reaction, which is given by Eq. 3.3 is also utilizing CO_2 as feedstock.

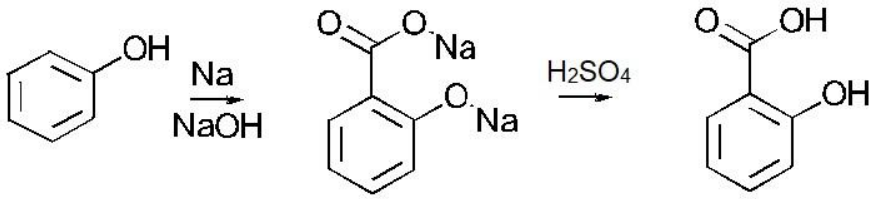

(Eq. 3.3)

In this process CO_2 reacts with sodium phenolate anion via electrophilic substitution to produce salicylic acid. Salicylic acid can be used to manufacture a large number of fine chemicals, such as e.g. synthetic aspirin (acetylsalicylic acid), salol (phenyl salicylates) or amide of salicyl (salicylic amide).

Liquid Light company produced mono-ethylene glycol (MEG), which found application in industrial manufacturing of polyester obtained through oxalic acid (electrochemical production) as intermediate.

The production of carbonates, cyclic carbonates or polycarbonates currently involves the reaction between appropriate alcohols and toxic phosgene. And interesting alternative

would be to use CO_2 (Eq. 3.3) or epoxides (Eq. 3.4) instead of phosgene in order to obtain respectively, carbonates and cyclic carbonates.

Coal gasification has been known for many decades and found application on industrial scale in early 1800s in the production of heat and light. However, with development of natural gas and oil technologies the further development of this process was abandoned. Today gasification technologies again gained attention and are strongly developed. In this process coal is converted into suitable gas fuel through the reaction with gasification agents i.e. air, steam, CO_2 or mixtures, resulting in a product of mixed carbon monoxide, hydrogen, methane and carbon dioxide. The main reactions involved in gasification are [40]:

$$C + O_2 \rightleftharpoons CO_2 \quad \text{(Eq. 3.4)}$$

$$C + ½O_2 \rightleftharpoons CO \quad \text{(Eq. 3.5)}$$

$$CO + ½O_2 \rightleftharpoons CO_2 \quad \text{(Eq. 3.6)}$$

$$C + H_2O \rightleftharpoons H_2 + CO \quad \text{(Eq. 3.7)}$$

$$C + CO_2 \rightleftharpoons 2CO \quad \text{(Eq. 3.8)}$$

$$CO + H_2O \rightleftharpoons CO_2 + H_2 \quad \text{(Eq. 3.9)}$$

$$C + 2H_2 \rightleftharpoons CH_4 \quad \text{(Eq. 3.10)}$$

The gasification of coal is a complex process involving pyrolysis and exothermic partial combustion (Eq. 3.4 – Eq. 3.6), with the latter providing enough heat for the endothermic gasification (Eq. 3.7 and Eq. 3.8). The methane formation process can be accompanied by a catalyst due to the presence of ash. WGS reaction can occur in this process (Eq. 3.9). This process could contribute to the reduction of CO_2 emissions through utilization of CO_2 as gasification agent. Additionally, it was found that CO_2 in a gasification mixture can increase the efficiency of this process and reduce coal and oxygen consumption [41].

There are other prospective applications of CO_2, such as conversion to fuels, utilization in biotechnological processes and production of biomass. The opinion that CO_2 molecule is stable is misinterpreted and CO_2 is considered as unreactive, which implies that any chemical conversion requires high amounts of energy. This is why the use of CO_2 as feedstock for chemicals is considered as inappropriate. Indeed, it is true when O_2 would be considered, but there are several reactions that do not need any external source of energy to convert CO_2 where the co-reactant (e.g. hydroxides, amines or olefins) provide enough energy for initiation of the reaction even at low temperatures.

3.4.1. CO_2 - as C_1 building block

Carbon dioxide may gain attention as an interesting C_1 building block for the synthesis of valuable chemicals. Hydrogen is a high energy molecule and could be used as a prospective reagent to transform CO_2. The utilization of CO_2 as a feedstock for the chemicals production would then contribute to alleviating global climate changes, as well as provide challenges in exploration of new possibilities for both catalytic and industrial development. Some possible products that could be obtained by carbon dioxide hydrogenation by either direct or indirect routes, are shown in Figure 3.3. There are five major products of CO_2 hydrogenation, which may be obtained directly: methane, methanol, formaldehyde, formic acid and carbon monoxide. The products of carbon dioxide hydrogenation are influenced by the used catalyst and operating conditions of the process.

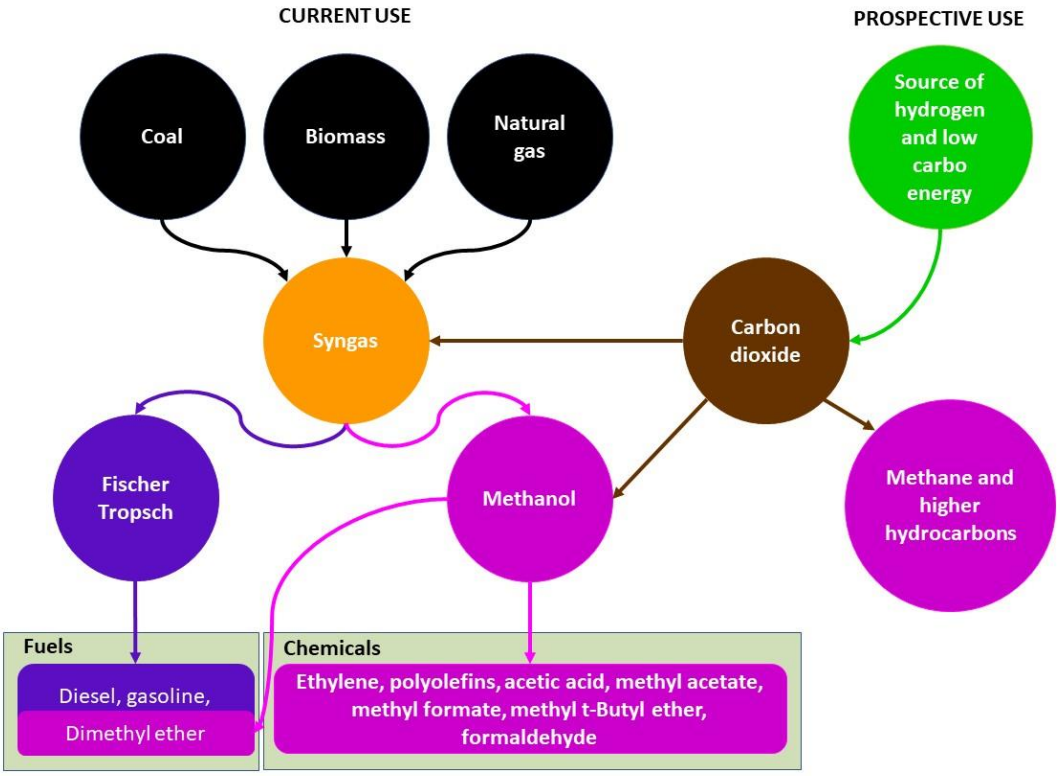

Figure 3.3 Possible chemical products that can be obtained via CO_2 hydrogenation (adapted from [42])

Indirect routes include e.g. production of synthesis gas or methanol formation as intermediates for further processing. The indirect route could be a multi-stage approach that utilizes different reactors with different catalysts to perform simultaneously a multi-step synthesis leading to highly valuable products.

Methanol

Methanol is a very important chemical, applied widely in industry, with a combined production of over 100 Mt annually. It is manufactured industrially using CO produced from methane (Eq. 3.11). In some industrial processes CO_2 is used as an additive to consume excess hydrogen (Eq. 3.12).

$$CO + 2H_2 \rightleftharpoons CH_3OH \qquad \Delta H_R^{298K} = -90.5 \text{ kJ/mol} \qquad \text{(Eq. 3.11)}$$

$$CO_2 + 3H_2 \rightleftharpoons CH_3OH + H_2O \qquad \Delta H_R^{298K} = -49.5 \text{ kJ/mol} \qquad \text{(Eq. 3.12)}$$

The reaction is mainly catalyzed by a Cu/ZnO-based catalyst. On the other hand, methanol could be produced directly from CO_2 with one of the CCU technologies. However, the source of hydrogen is a very important issue. Peters *et al.* [43]analyzed various hydrogen sources for methanol production taking into account conventional methanol synthesis with hydrogen obtained via steam reforming of natural gas and methanol synthesis from a mixture of CO_2/H_2 with hydrogen obtained (i) from natural gas, (ii) via water electrolysis using fossil fuel-derived energy or (iii) via water electrolysis using hydropower. The results showed that only for the latter case, the implementation of methanol production from carbon dioxide and hydrogen would result in a decrease of CO_2 emissions. It should be mentioned here that CRI technology of production of "renewable" methanol is based on a similar idea, with necessary energy obtained from geothermal sources.

Formic Acid

Formic acid is another interesting chemical, that could be produced directly from carbon dioxide (Eq. 3.13). It found many industrial applications, e.g. in food production, leather industry and agriculture [44, 45]. Currently the demand for formic acid is ca. 0.7Mt annually. A number of processes have been developed to produce formic acid. However, the catalysts were mostly based on expensive metals, such as rhodium, ruthenium and iridum, which, from the industrial point of view, is not acceptable [46, 47]. Therefore, copper, nickel and iron-based materials were proposed as prospective catalysts for this reaction [45, 48, 49]. Additionally, as the reaction is thermodynamically unfavorable under standard conditions, all catalytic tests reported in literature were performed at high pressures ranging from 5 to 50 bars at relatively low temperatures ranging from 20 to 120°C [49].

$$CO_2 + H_2 \rightleftharpoons HCOOH \quad \Delta H_R^{298K} = -7.45 \text{ kJ/mol} \qquad \text{(Eq. 3.13)}$$

Formaldehyde

Formaldehyde (HCHO) is a very important bulk chemicals and found application in over 50 types of processes, including the production of resins, adhesives, plastics, paints and foams. Currently formaldehyde is manufactured at a series of high-temperature reactions, starting from steam reforming of natural gas to obtain syngas, subsequent synthesis of methanol followed by oxidation to formaldehyde. This chain-process results in a high energy consumption, and therefore finding a more efficient and environmentally friendly approach to obtain this product is crucial.

Two possible routes for HCHO synthesis based on the utilization of CO_2 are proposed in literature (i) utilizing formic acid or (ii) carbon monoxide as intermediates [50-52]. In the first approach CO_2 is hydrogenated into formic acid (Eq. 3.14), followed by dehydration-hydrogenation to form formaldehyde (Eq. 3.15).

$$CO_2 + H_2 \rightleftharpoons HCOOH \qquad \Delta H_R^{298K} = -7.45 \text{ kJ/mol} \qquad \text{(Eq. 3.14)}$$

$$HCOOH + H_2 \rightleftharpoons HCHO + H_2O \qquad \Delta H_R^{298K} = -1.25 \text{ kJ/mol} \qquad \text{(Eq. 3.15)}$$

In the second approach CO_2 is hydrogenated to CO via RWGS reaction (Eq. 3.16), followed by hydrogenation of CO to formaldehyde (Eq. 3.17).

$$CO_2 + H_2 \rightleftharpoons CO + H_2O \qquad \Delta H_R^{298K} = 11.19 \text{ kJ/mol} \qquad \text{(Eq. 3.16)}$$

$$CO + H_2 \rightleftharpoons HCHO \qquad \Delta H_R^{298K} = -19.89 \text{ kJ/mol} \qquad \text{(Eq. 3.17)}$$

Higher hydrocarbons

Another promising route of CO_2 utilization is a direct production of hydrocarbons (alkanes and alkenes), via direct Fischer-Tropsch process starting from CO_2 and H_2. The conventional Fischer-Tropsch synthesis is based on syngas. The production of olefins is

ca. 200 Mt per year and results in 1.2-1.8 tons of carbon dioxide emitted per ton of the product [53]. The emissions of carbon dioxide could be significantly decreased if CO_2 would be applied as feedstock. However, there is still no appropriate catalyst for this reaction, which should be active in both RWGS and FT reactions. The path to higher hydrocarbons involves either RWGS reaction followed by FT synthesis, or methanol synthesis with subsequent hydrocarbons formation.

4. Carbon dioxide methanation

Methanation is a chemical reaction where CO and/or CO_2 is converted to methane. However, due to low price and high availability of natural gas only few plants apply this process on large scale e.g. Great Plains Synfuel in North Dakota (U.S., 1500 MW) operational since 1984 [54] and most recently AFUL Chantrerie in Nantes (France, 14 Nm^3/day) [55]. Recently, because of the increasing demand for natural gas and the necessity of the reduction of GHG emissions, the production of synthetic natural gas from CO_2 (SNG) has gained attention. Methanation of carbon dioxide, is an exothermic catalytic process of H_2 and CO_2 taking place at moderate temperature and pressure in the presence of metal-based catalysts, which leads to the formation of methane and water, as shown in Eq. 4.1.

$$CO_2 + 4H_2 \rightleftharpoons CH_4 + 2H_2O \qquad \Delta H_R^{298K} = -165 \text{ kJ/mol} \qquad \text{(Eq. 4.1)}$$

Some side reactions can also take place during methanation: (i) reverse water gas shift (RWGS), (ii) CO methanation and (iii) reverse dry reforming.

$$CO_2 + H_2 \rightleftharpoons CO + H_2O \qquad \Delta H_R^{298K} = 41 \text{ kJ/mol} \qquad \text{(Eq. 4.2)}$$

$$CO + 3H_2 \rightleftharpoons CH_4 + H_2O \qquad \Delta H_R^{298K} = -206 \text{ kJ/mol} \qquad \text{(Eq. 4.3)}$$

$$2CO + 2H_2 \rightleftharpoons CH_4 + CO_2 \qquad \Delta H_R^{298K} = -247 \text{ kJ/mol} \qquad \text{(Eq. 4.4)}$$

RWGS reaction is mildly endothermic, while the other three reactions are highly exothermic, which results in the formation of large amounts of heat during the process. In order to keep the appropriate temperature for CO_2 methanation an efficient heat removal is of great importance. Through RWGS reaction CO_2 molecule with low reactivity is split into CO and H_2O, followed by hydrogenation of CO through methanation and reverse dry reforming.

Beside the main reactions some side reactions can also take place during CO_2 methanation, such as Boudouard reaction, CO reduction, CO_2 reduction, methane decomposition and/or the formation of alkanes and alkenes, as given by reactions shown in (Eq 4.5 – 4.10)

$$2CO \rightleftharpoons C + CO_2 \quad \text{(Eq. 4.5)}$$

$$CO + H_2 \rightleftharpoons C + H_2O \quad \text{(Eq. 4.6)}$$

$$CO_2 + 2H_2 \rightleftharpoons C + 2H_2O \quad \text{(Eq. 4.7)}$$

$$CH_4 \rightleftharpoons C + 2H_2 \quad \text{(Eq. 4.8)}$$

$$nCO + (2n+1)H_2 \rightleftharpoons CnH_{2n+2} + nH_2O \quad \text{(Eq. 4.9)}$$

$$nCO + 2nH_2 \rightleftharpoons C_nH_{2n} + nH_2O \quad \text{(Eq. 4.10)}$$

The first four reactions lead to catalyst deactivation by carbon deposits. Slight amounts of higher hydrocarbons are found in the products of CO_2 methanation. However, the selectivity to CH_4 is strongly dependent on the active material used as catalyst.

The obtained gas should fulfil specific requirements similar to those of the natural gas distributed in the system, the latter containing typically more than 80% of methane. The general concept of CO_2 methanation process is shown in Figure 4.1. Additionally, it was proposed that CO_2 methanation can be implemented for biogas, which contains mainly CH_4, CO_2 and H_2 (in low amounts), in order to increase its quality.

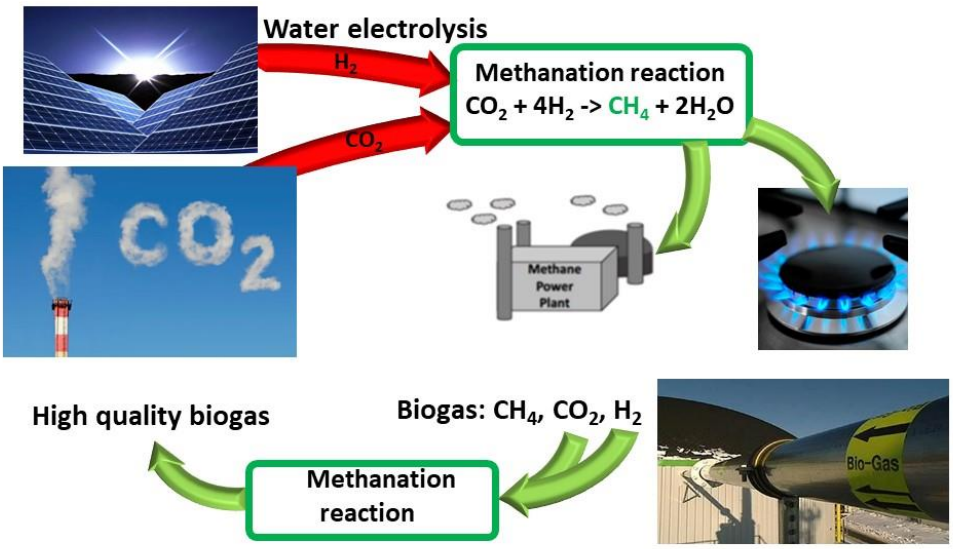

Figure 4.1 Concept of CO_2 methanation / possible application

Out of all hydrogenation processes mentioned in Chapter 3.4., up till now CO_2 methanation is the best developed, with a few projects on with small-scale industrial installations being tested. Table 4.1 lists selected European installations.

Table 4.1 Power-to-Methane plants in European Union (source: europeanpowertogas.com)

Installation	Methanation principle	Power [kW]	Electrolysis	Status
Etogas - Audi AG	Chemical	6300	Alkaline	Operational
Solothurn (Store&Go project)	Biological	700	PEM	Planned
Niederaussem	Chemical	300	PEM	Finished
Foulum - Electrochaea	Biological	250	PEM	Finished
Alzey – Exytron (Exytron GmbH)	Unknown	63	Alkaline	Planned
Rostock – Exytron Demonstrationsanlage	Unknown	21	Unkown	Operational
Stralsund (Fachhochschule Stralsund)	Unknown	20	Alkaline	Planned
Rozenburg	Chemical	10	PEM	Operational

PEM – Polymer electrolyte membrane electrolysis

4.1. Reaction Mechanism

Methanation of carbon dioxide is a catalytic reaction with either CH_4 or CO as the main products. The selectivity in the reaction is dependent on the type of metal used as a catalyst. Most of the studies focused on finding the reaction pathway were performed with a stioichiometric ratio H_2:CO_2 4:1 or with high excess of hydrogen up to 100:1. The mechanism of carbon dioxide methanation reaction has been studied by a number of research groups. However, there is no agreement on the mechanism of carbon dioxide methanation reaction and it should be noted that there is also no agreement on the reaction kinetics and mechanism for CO methanation. The overall reaction of carbon dioxide

methanation, despite the complexity of the elementary steps of the reaction, is represented by Eq. 4.11:

$$CO_2 + 4H_2 \rightleftharpoons CH_4 + 2H_2O \qquad \Delta H_{298} = -165 \text{ kJ mol}^{-1} \qquad \text{(Eq. 4.11)}$$

Literature proposes associative or dissociative mechanisms. As presented in Fig. 4.2. the former involves the formation of oxygenates as intermediates, that are subsequently hydrogenated to CH_4, while the latter assumes that CO_2 dissociates to adsorbed CO and O, followed by hydrogenation to methane. However, there is an accepted, in general, that CO is the main intermediate in CO_2 methanation.

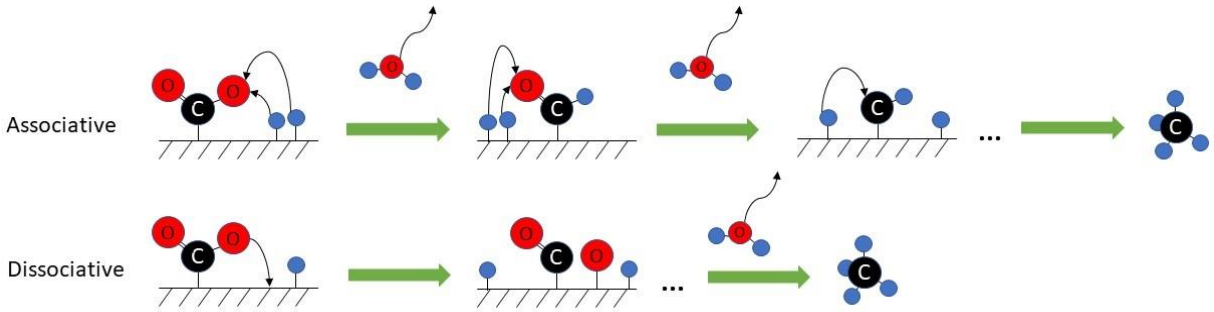

Figure 4.2 Carbon dioxide associative and dissociative methanation scheme (adapted from [56, 57])

The associative methanation mechanism involves the associative adsorption of CO_2 and H_2, followed by hydrogenation into methane. This mechanism was supported by in-situ FT-IR studies of Aldana *et al.* [58] carried out on Ni-containing Ce-Zr catalyst. The obtained spectra revealed the existence of carbonate on the support and bands of carbonyl bonded to metallic nickel. The increase of temperature resulted in hydrogenation of carbonate (CO_3) to bicarbonate (HCO_3) followed by rapid dehydration to formate (HCOO). The hydrogen atoms are believed to originate from H_2 dissociated on metallic Ni particles. The authors observed also that the bands arising from carbonyls on metallic nickel remained unchanged. Thus, it was stated that CO and CH_4 were formed in different mechanisms. While methane was produced by hydrogenation of formate species adsorbed on the catalysts surface, carbon monoxide resulted from carbon dioxide reduction on Ce^{3+}

sites. The in-situ FTIR spectroscopy studies of Shild *et al.* confirmed that formate is the essential intermediate for the production of methane [59].

Prairie *et al.* [60] studied the CO_2 methanation reaction on Ru-containing Al_2O_3 and TiO_2 catalysts using DRIFT spectroscopy. The obtained spectra revealed the existence of formate adsorbed on the support and carbonyl on Ru/Ru oxide. The authors concluded that carbonyl was produced via reverse water gas shift reaction (RWGS) of adsorbed CO_2 through formate species. Upham *et al.* claim that hydrogenation of carbonyl to methane is the rate-limiting step [61]. They came to this conclusion basing on transient experiments on ruthenium supported on ceria. They introduced CO_2 before H_2 or H_2 before CO_2. When CO_2 was introduced first, both CH_4 and CO were produced. On the other hand, when H_2 was introduced first, ceria was reduced, which resulted in reduction of CO_2 to CO on Ce^{3+}, without the formation of methane. Thus, it was proposed that methane was formed through hydrogenation of associatively adsorbed CO_2 while CO originated from CO_2 reduction over Ce^{3+}.

Studies of Westermann [62] and Pan *et al.* [63] regarded formate as CH_4 and CO precursors. Westermann *et al.* [62] studied Ni-impregnated zeolite USY by in-situ FTIR spectroscopy. They found that at temperatures below 200°C carbonates were hydrogenated to formate adsorbed on nickel particles, and then the increase of temperature led to the dehydration of formate into carbonyl, followed by formation of CO or hydrogenation to CH_4, and then desorption. The increase in nickel content led to increased CO_2 adsorption capacity while carbonate species were not observed when for USY not promoted with Ni.

Pan *et al.* [63] obtained similar results during in-situ FTIR CO_2 methanation studies. The obtained spectra showed five types of adsorption species: monodentate and bidentate carbonates hydrogenated to formate, followed formation of CO and/or

hydrogenation of the latter to CH_4. The observations made during temperature-programmed studies indicated that formate was the major intermediate for CH_4 production.

Schild *et al.* [59] studied carbon dioxide methanation over amorphous nickel supported on zirconia and confirmed the presence of CO on the catalyst's surface. However, there was no proof of RWGS reaction. On the other hand, formate species as intermediates were observed, which is in good agreement with the work of Barrault et al [64].

Thus, the related studies suggest that CO_2 methanation proceeds via reactions shown in Eq. 4.12-4.14.

$$CO_{2\ gas} \rightleftharpoons CO_{2\ ads} \quad \text{(Eq. 4.12)}$$

$$CO_{2\ ads} + H_{2\ ads} \rightleftharpoons HCOO_{ads} + H_{ads} \quad \text{(Eq. 4.13)}$$

$$HCOO_{ads} + H_{ads} \rightleftharpoons H_2O_{ads} + CO_{ads} \quad \text{(Eq. 4.14)}$$

The literature, however, proposes also another, dissociative mechanism of CO_2 methanation. It assumes that methanation of carbon dioxide is a combination of CO_2 conversion to CO via reverse water gas shift reaction, and the subsequent CO conversion to methane, as described by reactions (Eq. 4.15 and 4.16).

$$CO_2 + H_2 \rightleftharpoons CO_{ads} + H_2O \quad \text{(Eq. 4.15)}$$

$$CO_{ads} + 3H_2 \rightleftharpoons CH_4 + H_2O \quad \text{(Eq. 4.16)}$$

This suggests that adsorbed CO_2 dissociates on the catalyst surface, while the formation of CH_4 follows the CO methanation mechanism. Borgschulte *et al.* [65] tested nickel-containing zirconia supported catalysts and postulated that the CO formed via RWGS reaction is an important intermediate in CO_2 methanation. However, in order to increase the reaction yield of methane and to minimize the CO release, water had to be removed.

Weatherbee *et al.* [66] confirmed that the first step of CO_2 methanation was the dissociative adsorption of hydrogen as well as of CO_2, the latter to CO_{ads} and O_{ads}. It was postulated that CO could either desorb or dissociate into C_{ads} and O_{ads} (Eq. 4.25), followed by hydrogenation of adsorbed carbon and carbene to methane according to Eq. 4.17-4.21:

$$C_{ads} + H_{ads} \rightleftharpoons CH_{ads} \quad \text{(Eq. 4.17)}$$

$$CH_{ads} + H_{ads} \rightleftharpoons CH_{2\,ads} \quad \text{(Eq. 4.18)}$$

$$CH_{2ads} + H_{ads} \rightleftharpoons CH_{3\,ads} \quad \text{(Eq. 4.19)}$$

$$CH_{3ads} + H_{ads} \rightleftharpoons CH_{4\,ads} \quad \text{(Eq. 4.20)}$$

$$CH_{4ads} \rightleftharpoons CH_{4\,gas} \quad \text{(Eq. 4.21)}$$

Water was assumed to have been formed from atomic oxygen, as given by Eq. 4.22-4.24:

$$O_{ads} \rightleftharpoons OH_{ads} \quad \text{(Eq. 4.22)}$$

$$OH_{ads} + H_{ads} \rightleftharpoons H_2O_{ads} \quad \text{(Eq. 4.23)}$$

$$H_2O_{ads} \rightleftharpoons H_2O_{gas} \quad \text{(Eq. 4.24)}$$

According to Coenen *et al.* [67] the rate-determining step in methanation on nickel catalysts is either the CO dissociation to surface carbon (Eq. 4.25), or dissociation of CHO (Eq. 4.26 and 4.27):

$$CO_{ads} \rightleftharpoons C_{ads} + O_{ads} \quad \text{(Eq. 4.25)}$$

$$CO_{ads} + H_{ads} \rightleftharpoons CHO_{ads} \quad \text{(Eq. 4.26)}$$

$$CHO_{ads} + H_{ads} \rightleftharpoons C_{ads} + H_2O_{gas} \quad \text{(Eq. 4.27)}$$

Taking into account that the mechanism of CO_2 methanation may be influenced by reaction temperature, pressure, as well as a catalyst used and its particle size,

Andersson *et al.* [68] postulated that at temperatures below 850K, dissociation of CHO as the intermediate could be the rate-determining step.

The presence of CO_{ads} on the surface of $Rh/\gamma\text{-}Al_2O_3$ catalysts was shown during in-situ DRIFT measurements [69]. CO_2 dissociation on the catalyst surface was proven by simultaneous oxidation of rhodium by oxygen species. The results of DRIFT measurements performed on similar catalysts by Beuls *et al.* [70] confirmed that the dissociation of CO_2 is responsible for the oxidation of rhodium, thus supporting the mechanism proposed by Jacquemin et al [69].

On the other hand, the investigations of CO_2 methanation on ruthenium supported on alumina carried out by steady state isotopic transient kinetic analysis (SSITKA) coupled with DRIFTs proved that the redox mechanism should be neglected [71]. The experiments were performed under atmospheric pressure and excess of H_2. The exchange of $^{12}CO_2$ to $^{13}CO_2$ resulted in reduced intensity of $^{12}CO_{ads}$, and the simultaneous increase in the intensity of the band arising from $^{13}CO_{ads}$. At the same time the slow response of bands arising from formate during the isotope exchange test suggested that formate was not the major intermediate in this reaction. As a result, it was concluded that the mechanism of CO_2 methanation proceeded through dissociative adsorption of CO_2 resulting in formation of CO_{ads} and O_{ads}, considered as the rate determining step.

Marwood *et al.* [72] performed steady-state transient measurements coupled with IR spectroscopy studies on Ru/TiO_2 catalyst. The mechanism involving the formation of CO_{ads} as an intermediate in the pathway to methane was proposed. Additionally, formate was considered as a by-product strongly bonded with the support. However, the hydrogenation steps could not be observed by IR spectroscopy. Since interfacial formate species were formed on the support, a pathway involving hydrogen carbonates was proposed as a precursor of these species, which were characterized by a transient

response, consistent with the response of CO precursor. Solymosi *et al.* [73, 74] proposed that the formate ions formed on the catalysts metal species migrate rapidly towards the support during the reaction of CO_2 methanation, suggesting that the observed bands of formate correspond to a by-product adsorbed on the support.

Concluding, the mechanism of carbon dioxide methanation is yet not fully understood, with two possible pathways proposed in literature. This process can proceed either via direct carbon dioxide reaction to methane or through formation of carbon monoxide as an intermediate in this reaction. The formation of formate as the main reaction intermediate has been suggested by many authors for the direct CO_2 methanation pathway. In general, it was accepted that in the case of CO_2 reaction to CO reverse water gas shift reaction is occurring as the intermediate in methanation of CO_2, followed by hydrogenation of the adsorbed CO. Carbon monoxide can be also alternatively formed by the dissociative adsorption of carbon dioxide on the catalysts surface.

4.2. CO_2 methanation thermodynamics calculation

Thermodynamic calculations are very useful in the assessment of reactions involved in the methanation system and allow to predict the optimal conditions of the reaction. The most commonly discussed parameters influencing conversion of CO_2, methane selectivity and carbon deposition are: temperature, pressure, H_2/CO_2 ratio, the addition of other reactants (H_2O, CH_4, O_2). Thermodynamic calculations performed for complex chemical systems based on Gibbs energy minimization can answer several questions such as (i) the type of thermodynamically stable products of the reaction, (ii) selectivity to this product together with the yield, (iii) if the reaction is exothermal or endothermal. From the existing literature, it may be concluded that methanation process is favoured at low temperatures, high pressure and high H_2/CO_2 ratio.

Table 4.2 Possible reactions involved in CO_2 methanation

Reaction type	Formula	ΔH_{298K} (kJ mol^{-1})
CO_2 methanation	$CO_2 + 4H_2 \rightleftharpoons CH_4 + 2H_2O$	-165.0
CO reduction	$CO + H_2 \rightleftharpoons C + H_2O$	-131.3
CO_2 reduction	$CO_2 + 2H_2 \rightleftharpoons C + 2H_2O$	-90.1
inversed dry reforming of methane	$2CO + 2H_2 \rightleftharpoons CH_4 + CO_2$	-247.3
Boudouard reaction	$2CO \rightleftharpoons C + CO_2$	-172.4
water-gas shift	$CO + H_2O \rightleftharpoons CO_2 + H_2$	-41.2
methane cracking	$CH_4 \rightleftharpoons 2H_2 + C$	74.8
-	$nCO + (2n+1)H_2 \rightleftharpoons C_nH_{2n+2} + nH_2O$	-
-	$nCO + 2nH_2 \rightleftharpoons C_nH_{2n} + nH_2O$	-

The analysis of Gao *et al.* [75] showed that low temperatures (<250°C) are optimal for CO_2 methanation, where the CO_2 conversion and CH_4 selectivity can reach almost 100%. On the contrary, the reaction rate is increasing with increased temperature. The increase of temperature up to 500ºC is also favorable for the reverse water-gas shift (RWGS) reaction, thus CO_2 methanation should be performed up to 500ºC. Additionally, increasing the reaction temperature can result in carbon deposition, as well as sintering of the catalytic active material. Considering the Le Chatelier principle, CO_2 methanation is favored at increased pressure. According to Gao *et al.* [75] increasing the pressure is effective up to a certain point with negligable effect of pressure above that point. The optimum pressure, that will cause no sintering of the catalyst, was proposed to be between 10 and 30 atm. Theoretically, no carbon deposition occurs during CO_2 methanation if the H_2/CO_2 ratio is stoichiometric or higher. The side reactions and their respective temperatures at which they are favored are shown in Fig. 4.3.

Basing on the thermodynamic calculations for CO_2 methanation reaction presented in literature [75-81], some general conclusions concerning conditions appropriate for carbon dioxide methanation reaction can be formulated:

- **In order to convert almost 100% of CO_2 to CH_4 with ca. 100% selectivity temperature should not exceed 300ºC,**
- **Increasing the temperature above 500ºC will result in the occurrence of reverse water-gas shift reaction,**
- **The addition of steam may suppress carbon formation in CO methanation, which explains why no carbon deposits are usually observed in CO_2 methanation reaction,**
- **The CO_2 conversion and selectivity to CH_4 are strongly dependent on the H_2/CO_2 ratio used for the reaction.**

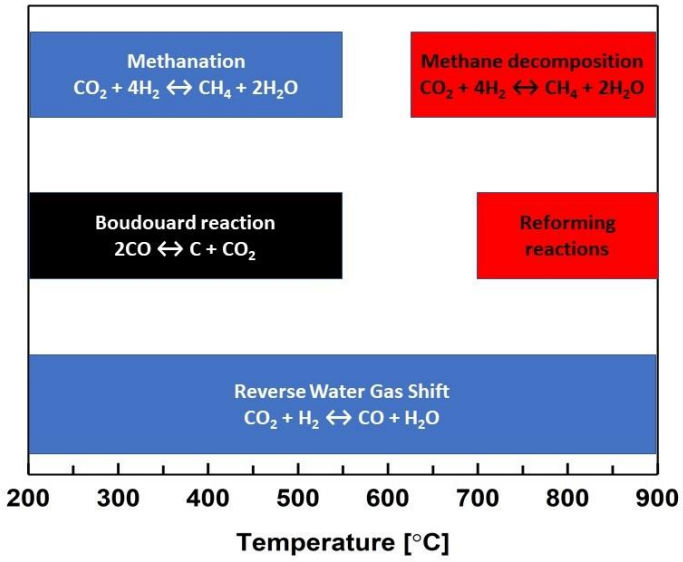

Figure 4.3 Main side reactions that may occur during CO_2 methanation

4.3. A review of CO_2 methanation catalysts

The reduction of fully oxidized carbon in carbon dioxide to methane is an eight-electron reaction, which results in considerable kinetic limitations. Thus, to apply this reaction on industrial scale, a highly active metal-based catalyst is required in order to

achieve acceptable reaction rates, appropriate methane selectivity and coke formation resistance. The performance of the catalysts is strongly dependent on the used active material and its particle size and shape, reduction conditions, preparation method, as well as an appropriate reactor.

Carbon dioxide methanation catalysts usually contain a supported metal, with Ni/Al_2O_3 most widely studied because of its low costs and availability as compared to other supports, such as e.g. zeolites. In general, it is accepted that the reaction occurs on the metal-support interface, where CO_2 is adsorbed and dissociated on the support and H_2 is adsorbed and dissociates on metal sites. Therefore, while designing a catalyst that would efficiently reduce CO_2 to CH_4 with low selectivity towards CO, two strategies can be considered: (i) the first one increasing the CO_2 adsorption capacity by choosing a basic support and (ii) the second where an additional metal is added to the main active component, which will increase dispersion of the latter, thus resulting in increased H_2 adsorption capacity. During last decades much effort have been devoted to develop highly active and selective CO_2 methanation catalysts. The following subchapter discusses the literature information on the influence of different supported metals, and the effect of the supports and/or promoters on the activity and selectivity of such materials in the reaction of CO_2 methanation. There are already some general reviews of catalysts for CO_2 methanation: Wei and Jinlong [82], Aziz *et al.* [83], Ghaib *et al.* [84], Su *et al.* [85], Rönsch *et al.* [54] and Frontera *et al.* [56], so the main focus here is on more recent literature findings, especially those not discussed in more detail in the mentioned reviews.

4.3.1. The role of active component

As reported in literature, transition metals of groups 8, 9 and 10, i.e. nickel, ruthenium, palladium, rhodium, platinum, copper, molybdenum, rhenium, silver, gold, iron and cobalt, are active for carbon dioxide methanation reaction. Table 4.3 lists different information on studies of supported transition metals in the reaction of CO_2 methanation. It has to be noted that the selection of the active phase for this reaction can affect, besides the activity, also the selectivity towards methane which is crucial from the industrial point of view.

Table 4.3 Literature data on active metals supported on the same material for CO_2 methanation

Catalyst	Metal loading [wt.%]	S_{BET} [m^2/g]	GHSV [ml/g*h]	Temperature [°C]	CO_2 conversion [%]	CH_4 Selectivity [%]	Ref
Rh/MSN		933			99.5	100.0	
Ru/MSN		1004			95.7	100.0	
Ni/MSN		879	50,000	350	85.4	99.9	[86]
Ir/MSN		976			9.5	83.0	
Fe/MSN		858			4.0	92.0	
Rh/TiO_2	0.5	nd	nd			100.0	
Ru/TiO_2	0.5	nd	total flow:			86.0	
Pt/TiO_2	0.5	nd	150	350	Rh >> Ru >Pt >Pd	1.0	[87]
Pd/TiO_2	0.5	nd	ml/min			0.0	
Pd/SiO_2	3	315					
Rh/SiO_2	3	310	60,000	350	Pd >Rh>Ni	Rh > Ni > Pd	[88]
Ni/SiO_2	3	311					

Ni/Al_2O_3	3	182					
Pd/Al_2O_3	3	187	60,000	350	Ni > Pd > Rh	Rh > Pd > Ni	[88]
Rh/Al_2O_3	3	180					
Pd/CeO_2	3	131					
Ni/CeO_2	3	128	60,000	350	Pd > Ni > Rh	Rh > Ni >> Pd	[88]
Rh/CeO_2	3	125					

Aziz *et al.* [86] prepared mesoporous silica nanoparticles (MSNs) doped with various metals, such as Rh, Ru, Ni, Fe, Ir, Cu, Zn, V, Cr, Mn, Al and Zr. The activity in CO_2 methanation at 350°C followed the sequence Rh > Ru > Ni > Ir > Fe > Cu. However, the authors indicate that on basis of specific surface area Ni doped MSN showed to be the most active and Ir/MSN the worst catalyst.

Panagiotopoulou [87] studied Rh, Ru, Pt and Pd supported on TiO_2. The catalytic activity expressed as TON followed the sequence: Rh > Ru > Pt > Pd, with Rh about 3 times more active than Pd. The selectivity towards methane was found to be much higher for Rh and Ru than Pt and Pd, both promoting mainly the formation of carbon monoxide via reverse water-gas shift (RWGS) reaction. The kinetic measurements showed that carbon dioxide hydrogenation reaction was structure sensitive i.e. the activity of the catalyst depended strongly on the metal crystallite size. The author claimed that small ruthenium crystallites influenced the formation of CO, which decreased with increasing Ru particle size (higher Ru loading).

Catalytic activity of Pd, Rh and Ni (3 wt.%) supported on Al_2O_3, CeO_2 and SiO_2 was compared by Martin *et al.* [88]. All catalysts were obtained using impregnation method. The catalytic performance was strongly dependent on the active material, as well as the used support. For Pd, Rh, Ni supported on SiO_2 the catalytic activity followed the

sequence Pd > Rh > Ni, while for Al_2O_3 it was Ni > Pd > Rh, for CeO_2 Pd > Ni > Rh. However, despite the fact that Rh based catalysts showed the worst performance the selectivity towards methane was higher than for Ni and Pd catalysts. It was also found that the mechanism of CO_2 methanation was different for Rh supported on Al_2O_3 and CeO_2.

Considering that Ni is much more available, as well as cheaper than noble metals, most research on CO_2 methanation is now focused on Ni-based catalysts.

4.3.2. Ni-based catalysts

Out of the studied transition metal-based catalysts Rh and Ni were found to have the best catalytic performance. However, in 2018 the prize of Rh was 500 times higher than that of Ni [89]. This is why Ni-based catalyst are more interesting from the industrial point of view. As nickel catalysts exhibit high selectivity towards methane, the main focus of the research on nickel-based catalysts is the improvement of the catalytic activity, especially at lower temperature region. To apply a catalyst on industrial scale, the CO_2 methanation activity at low operating temperatures ca. 250°C should be increased, thus decreasing the amount of energy input for the reaction initialization. In order to fulfil this goal several approaches have been proposed, such as:

- Modification of the method of nickel incorporation in order to change the nickel-support interaction, which may influence the metal dispersion, reducibility and metal crystallite size, this being crucial in achieving acceptable reaction rates;
- Enhancing basic properties by either incorporation of promoters or changing the support in order to increase CO_2 adsorption capacity;

- The addition of a second metal, e.g. a non-noble metal, which can enhance the catalytic activity;
- Changing reaction conditions, e.g. by using non-stoichiometric amounts of hydrogen.

In this subchapter an overview of the research on Ni-based catalysts carried out during last years is presented.

4.3.2.1. Ni-based catalysts – effect of support

The support plays a significant role in a catalyst. It determines the dispersion of the active metallic phase and resistance to sintering, as well as stabilization of active sites, provides high active surface area and, in some cases, such as CO_2 hydrogenation, can participate in the reaction. Catalysts containing nickel were tested on various supports, among them single oxides (Al_2O_3, SiO_2, MgO, CeO_2, ZrO_2, TiO_2, La_2O_3), mixed oxides (CeO_2/ZrO_2, ZrO_2-Sm_2O_3), meso-structured silica nanoparticles (MSN), mesoporous molecular sieves (MCM-41), zeolites (Y or USY) or metal-organic frameworks (MOFs) and carbon nano-tubes (CNTs). Selected information on the performance of such catalytic systems is presented in Table 4.4.

Table 4.4 Catalytic activity of selected Ni-based catalysts in CO_2 methanation. Effect of the support

Ni (wt.%)	Support	PM*	Reaction conditions				CO_2 Conv. [%]	CH_4 sel. [%]	Ref
			Temp. (°C)	H_2/CO_2 ratio	WHSV/GHSV	P [bar]			
10	γ-Al_2O_3	IMP	250	4	nd / 5,700	1	37.0	93.0	[90]
10	Al_2O_3	IMP	250	4	nd / 9,000	1	6.0	97.0	[91]
25	Al_2O_3	CP	235	4	2,400 / nd	9	99.0	99.7	[92]
40.4	Al_2O_3	SG	220	4	9,600 / nd	10	61.1	99.2	[93]
10	Al_2O_3	IMP	400	4	10,000 / nd	1	5.0	>99	[94]
15	Al_2O_3	IMP	300	4	15,000 / nd	1	45.0	>99	[95]
10	MgO	IMP		4	nd /10,000	1	ca.5.0	78.0	[96]
10	TiO_2	IMP		4	nd /10,000	1	ca.7.0	ca.100.0	[96]
12	CNT	IMP	350	4	nd / nd	1	ca.74% CH_4 yield		[97]
4.29	SiO_2	IMP	500	4	48,000 / nd	1	25.0	45.0	[98]
15	SiO_2-Al_2O_3	IMP	600	4	48,000 / nd	1	63.0	29.0	[99]
$LaNi_5$	-	CP	400	4	3,000 / nd	1	91.5.0	95.0	[100]
10	La_2O_3	IMP	280	4	nd / 30,000	1	76.6	ca.100.0	[101]
12	ZrO_2-Al_2O_3	IMP	360	4	nd / 8,100	1	42.0	nd	[102]
12	ZrO_2-Al_2O_3	CP	360	4	nd / 8,100	1	50.0	nd	[102]
3	MCM-41	IMP		4		1			[103]

59.9	Raney	-	300	4	nd / 38,000	1	87.0	ca.100.0	[104]
14.3	$Zr_{0.9}Ce_{0.1}$	IMP	350	4	nd / 5,400	1	78.0	ca.100.0	[105]
5	Ce-Zr	IMP	420	4	nd / 43,000	1	40.0	86.0	[58]
5	USY	IMP	400	4	nd / 40,000	1	24.7	61.4	[106]
10	CeO_2	IMP	300	4	nd /10,000	1	90.0	100.0	[96]
70at.%	Zr-Sm	MM	300	4	nd / 6,000	1	80.0	ca.100.0	[107]
$LaNiO_3$	perovskite	CM	300	4	nd / 7,500	1	77.7	99.4	[108]
10	MOF-5	IMP	280	4	nd / 2,000	1	47.2	ca.100.0	[109]

*PM-Preparation method – IMP - impregnation, CP - co-precipitation, Arc - Arc melting, SG - Sol-Gel, MM - mechanical mixture, CM - citrate method.
nd-no data

Alumina – Al_2O_3

Nickel supported on alumina is one of the most often studied catalytic systems for carbon dioxide methanation reaction. It is relatively cheap, has high specific surface area, basic character, thermal stability and shows good activity. However, because of high reaction temperatures used during methanation, such catalytic systems suffer from severe carbon deposition or poor stability. The activity is also strongly dependent on the catalysts structure, composition and calcination/reduction temperature.

Riani *et al.* [110] compared unsupported Ni nanoparticles with Ni supported on γ-Al_2O_3, proving that the latter had much higher activity in comparison to the former.

Rahmani *et al.* [91] prepared a series of nickel-impregnated mesoporous γ-Al_2O_3 with high specific surface area containing 10-25 wt.% Ni. CO_2 conversion increased with increasing Ni content from 10 to 20 wt.%, while the incorporation of higher amounts of Ni (25 wt.%) decreased both CO_2 conversion and CH_4 selectivity. This was explained by decreased Ni dispersion as a result of the formation of bigger crystallites. Additionally a

selected catalyst was calcined at various temperatures, the increasing calcination temperature had a negative influence on both CO_2 conversion and selectivity towards CH_4, because of increased NiO crystallite sizes, the decrease of the surface area and the growing fraction present as inactive $NiAl_2O_4$.

In order to obtain high dispersion of inorganic salts on the support Song *et al.* compared Ni(20wt.%)/Al_2O_3 catalyst prepared by microwave-assisted method and impregnation [111]. The former preparation procedure resulted in enhanced CO_2 adsorption capacity and increased Ni reducibility. The respective Ni dispersion calculated from H_2-TPR was 25.3 and 16.6%. As a result, enhanced activity and high selectivity towards methane of the former catalyst at low temperatures was registered. Moreover, the activity of the former remained almost unchanged during 72h stability tests [111].

Silica – SiO_2

Silica is used in catalysis as one of typical supports. Lu *et al.* [112] investigated SBA-15 with Ni particles grafted via ammonia complex ions ($Ni(NH_3)_x)^{2+}$) to form the chemical bond O-Ni-O-Si-O. As a reference material NiO supported on SBA-15 was obtained in a conventional post-synthesis method. The obtained results showed very high dispersion of grafted nickel, which resulted in much higher activity in CO_2 methanation in comparison to the conventional NiO/SBA-15 catalyst. Additionally, the results suggested that nickel was not fully reduced, thus Si-O-Ni could play an important role in CO_2 adsorption, which was, according to the authors, the explanation of much higher activity of grafted Ni-SBA-15.

Ni impregnated SiO_2 catalyst treated under glow discharge plasma (under nitrogen and hydrogen atmosphere) and the effect of such modification was studied by Zhang *et al.* [113]. High catalytic activity was obtained with CO_2 conversion of 90% at low

temperature (250℃), which was assigned to partial reduction of the catalyst under hydrogen plasma treatment. Both conversion of CO_2 and yield of CH_4 were higher than for the catalysts prepared by conventional impregnation and calcination method.

Magnesia – MgO

Magnesia is another commonly studied support for nickel-based catalysts because of its high Lewis basicity, which enhances CO_2 adsorption and thus is crucial for carbon dioxide methanation reaction. The most important advantage of magnesia as the support is the possibility to form a solid solution of NiO-MgO at any molar ratio due to similar ionic radii, of 0.065nm and 0.072nm for Mg^{2+} and Ni^{2+}, respectively[114]. This results in increased metal-support interaction preventing the sintering of the catalyst [115].

Yan *et al.* [116] prepared Ni_aMgO_x (a=0.5, 0.8, 1.0 and 1.2) catalysts for CO_2 methanation. NiO, MgO and Ni-impregnated MgO were studied as reference materials for comparison. The samples containing low amounts of nickel ($Ni_{0.5}MgO_x$ and $Ni_{0.8}MgO_x$) showed rather poor activity at temperatures below 300℃. The sequence of CO_2 conversion was $Ni_{1.0}MgO_x > Ni_{0.8}MgO_x > Ni_{1.2}MgO_x > Ni_{0.5}MgO_x >$ Ni/MgO (imp.). The reference samples NiO, MgO and Ni/MgO showed no activity in CO_2 methanation reaction at temperatures below 350℃. This was assigned to the essential role of synergetic interaction between nickel and magnesia for CO_2 methanation. The increased activity of Ni_aMgO_x catalysts was explained by improved dispersion of active Ni species on Ni-Mg mixed oxide. On the other hand, the decreased activity of the sample containing the highest amount of Ni was attributed to possible aggregation of surface Ni particles.

Ceria – CeO_2

Ceria is another interesting support that has been studied for Ni-based catalysts for CO_2 methanation because of its efficient heat exchange due to high conductivity. Ratchahat *et al.* [117] prepared structured Ni/CeO_2 catalysts (honeycomb-type structures – plain, stacked, segment and multi-stacked). Moderate hot spots were observed for multi-stacked catalyst which was examined for reboosting the catalytic activity. The 76h stability tests proved good stability of the catalysts, with initial CO_2 conversion of 92.7% at 300ºC dropping only by 0.6% and selectivity towards CH_4 remaining 99.9%.

Zirconia – ZrO_2

The effect of combustion media used during calcination of the materials on the catalytic activity of Ni/ZrO_2 catalysts in CO_2 methanation was investigated by Zhao *et al.* [118]. Ni/ZrO_2 materials containing 15 wt.% of Ni, were prepared by combustion method using different agents, such as urea, glycerol, glycol, ethanol and n-propanol. Reducibility, pore structure, Ni particle size and CO_2 adsorption capacity was strongly influenced by the combustion medium. The most active catalyst was the one prepared using urea, with the optimum nickel loading of Ni/ZrO_2 of 15 wt.%. This catalyst had much higher resistance to carbon deposition than the one prepared by impregnation method.

Ceria-Zirconia

Because of its high redox properties, good thermal stability and resistance to sintering Ceria-Zirconia is another widely studied support for catalysts. The addition of zirconia stabilizes ceria through the formation of a solid solution of ceria-zirconia in the whole composition range. In comparison to CeO_2 such support possesses much higher basicity

[119-121] and improved thermal and textural features [122]. It was also found that ceria-zirconia exhibit excellent catalytic activity and stability during 150h TOS, which was explained by high oxygen storage capacity and highly dispersed nickel [119].

Further studies of Ocampo *et al.* [120] on Ni-ceria-zirconia catalysts obtained by sol-gel and impregnation methods showed that the high activity of these materials in CO_2 methanation was related to interaction between Ni^{2+} and Ce-Zr support. The existance of Ni on both surface and inside ceria-zirconia structure improved the redox properties. Trovarelli *et al.* claimed that the presence of bulk oxygen vacancies was a driving force for carbon dioxide activation [123]. In contrast, Pan *et al.* [63] studied carbon dioxide methanation over Ni-ceria-zirconia and Ni-γ-Al_2O_3 catalysts using in-situ FTIR spectroscopy. The reaction mechanism for both catalysts was concluded to be the same but with different reactive basic sites. The assumption was that monodentate carbonates on medium-strength basic sites could be hydrogenated more rapidly than bidentate formates. Thus, it was proposed that medium-strength basic sites enhanced the activity of the catalyst in CO_2 methanation.

Titania – TiO_2

Another support, which was reported as showing good ability to suppress carbon deposition was titania. This was attributed to TiOx species, which are formed during reduction with hydrogen that can migrate to nickel particles and create Ni-O-Ti^{3+} species that can promote oxidation of deposited carbon to CO. Ni/TiO_2 materials prepared using incipient wetness impregnation method were used as catalysts for CO_2 methanation by Zhou *et al.* [124]. The obtained material was divided into two parts, one was calcined and the other one was decomposed under DBD plasma for 1h. The plasma-treated catalyst showed higher CO_2 conversion and selectivity towards methane when compared to the

conventionally calcined catalyst. This was explained by smaller metallic Ni crystallites, which were 14.4 nm (DBD) and 17.9 nm (calcined). The effect of nickel content on activity of 5-20 wt.% Ni/TiO_2 containing was studied by Liu *et al.* The optimal amount of nickel was found to be 15 wt.%, with higher amounts of nickel (20 wt.%) showing almost similar performance as the former catalyst [125].

Zeolites

Zeolites were studied as prospective catalysts for carbon dioxide methanation reaction by Graca et al, Wastermann *et al.* and Bacariza *et al.* [62, 106, 126]. Their acidic-basic properties can be tailored to some extent, depending on the applied chemical and physical treatment methods. The effect of preparation method and pre-reduction conditions on the performance of Ni containing ultra-stable Y zeolite (USY) was studied by Bacariza *et al.* [126]. The catalysts prepared via microwave method showed similar performance as those treated by calcination. The samples containing higher amount of nickel (14 wt.%) were more active and resistant to Ni sintering at higher temperatures (550℃) than the catalyst containing 5 wt.%.

Mixed oxides

$LaNiO_3$ perovskites as catalysts for CO_2 methanation were studied by Gao *et al.* [108]. Prior to the reaction the materials were reduced in-situ using reactant gases (CO_2+H_2) for 7h at different temperatures (400, 500, 600 and 700℃). The performance of the catalysts was compared to 5%Ni/$La_2O_2CO_3$ as reference sample. The catalytic performance followed the sequence: $LaNiO_3$ activated at 500 > 600 > 700 > 400 > 5%Ni/$La_2O_3CO_3$. The treatment temperature influenced the metal particle size, which was 7.1, 8.4, 10.3 and 13.2 for samples activated at 400, 500, 600 and 700℃, respectively. It was concluded

that the reason for enhanced catalytic activity was the activation leading to the formation of well dispersed metallic nickel particles covered by oxocarbonate species of $La_2O_2CO_3$.

Comparison of the supports

A direct comparison of the influence of different supports on the catalytic performance in carbon dioxide methanation is impossible, because the catalysts presented above were studied under different reaction conditions (temperature, flow, mass, GHSV). However, some general conclusions may be drawn. Different preparation methods influence strongly the metallic nickel particle size and the interaction between active phase and the support, both resulting in differences in catalytic performance. There are only a few articles comparing Ni catalysts on different supports tested under the same conditions in CO_2 methanation reaction, as reported below.

The effect of various nickel supports (ZSM-5, SBA15, MCM-41, Al_2O_3 and SiO_2) on the catalytic performance in CO_2 methanation reaction were studied by Guo *et al.* [127]. All the catalysts were prepared by impregnation method. At 250ºC the CO_2 conversion followed the sequence: Ni/ZSM-5 > Ni/SBA-15 > Ni/Al_2O_3 > Ni/SiO_2 > Ni/MCM-41. The catalytic activity was correlated with the amount of weak and medium-strength basic sites, which as suggested by CO_2 desorption behavior, have a positive effect on the methanation reaction and catalytic activities. The reduction of NiO species caused defects in the Ni/ZSM-5 catalyst, which was responsible for anchoring sites for active metallic Ni particles.

Tada *et al.* [96] studied the effect of CeO_2, α-Al_2O_3, TiO_2 and MgO. The CO_2 conversion followed the sequence: Ni/CeO_2 > Ni/α-Al_2O_3 > Ni/TiO_2 > Ni/MgO. Ni/CeO_2 showed the highest activity among all studied catalysts, with selectivity towards methane

very close to 100%. The high activity of Ni/CeO_2 was attributed to the surface coverage by CO_2-derived species on CeO_2, as well as a partial reduction of surface CeO_2.

Le *et al.* [128] studied Ni supported on TiO_2, γ-Al_2O_3, CeO_2, ZrO_2 and SiO_2 in both CO and CO_2 methanation. The catalytic performance of the catalysts in CO_2 methanation at 250ºC followed the sequence: $Ni/CeO_2 >> Ni/ZrO_2 > Ni/SiO_2 > Ni/TiO_2 > Ni/\gamma\text{-}Al_2O_3$. The superior activity of Ni supported on CeO_2 was attributed to high Ni dispersion and increased CO_2 adsorption capacity.

Ni-based catalysts supported on Al_2O_3, Y_2O_3, ZrO_2, La_2O_3, CeO_2 and Sm_2O_3 prepared by impregnation were compared in CO_2 methanation by Muroyama *et al.* [129]. The performance at 250ºC followed the sequence: $Ni/Y_2O_3 > Ni/Sm_2O_3 > Ni/ZrO_2 > Ni/CeO_2 > Ni/\gamma\text{-}Al_2O_3 > Ni/La_2O_3$.

Mixed oxide – Hydrotalcite-derived catalysts

Especially interesting materials for CO_2 methanation are hydrotalcite(HT)-derived catalysts. Such materials may form nano-oxides after thermal treatment at appropriate conditions. The advantage of such materials is that alumina and nickel may be introduced into their structure in close and strong contact, and there is a possibility of introduction of magnesia and few other additives, both on and into the structure. It has been reported that such materials show good catalytic properties e.g. in dry reforming of methane [130]. Several aspects were investigated in case of CO_2 methanation such as (i) the amount of Ni, (ii) the size of metallic Ni crystallites (iii) reducibility of Ni species and (iv) the basicity and distribution basic sites of hydrotalcite-derived materials.

Gabrovska *et al.* [131] studied the influence of Ni/Al molar ratio (between 0.5 and 3) and the reduction temperature on the performance of Ni-Al-HT-derived materials in

CO_2 methanation, with the removal of small amounts of CO_2 from a mixture containing low amounts of carbon dioxide, using considerable hydrogen excess.

He *et al.* studied Ni-Al hydrotalcites, with well dispersed stable nickel particles after thermal treatment. The authors claim that the enhanced activity was a result of both highly dispersed nickel particles and the presence of moderate and strong basic sites [6].

Fan *et al.* studied Ni-Mg-Al hydrotalcites containing nickel prepared by incipient wetness impregnation method of $MgAl_2O_4$ with Ni nitrate. One part of the impregnated material was calcined at 500°C, while the other was treated by DBD plasma in order to decompose the nickel precursor. The latter treatment resulted in higher Ni dispersion, which was 7.1%, as compared to 6.0% for the calcined sample. Additionally, the sample treated with plasma showed higher BET surface area. Basing on the results of catalytic tests the authors concluded that smaller Ni particles (for DBD treated sample) resulted in the enhanced hydrogenation of CO_2 to methane [132].

HT-derived Ni/Al catalysts obtained by co-precipitation at pH of 8.7 and 12 were studied by Abate *et al.* [133]. The Ni-HT catalyst obtained at pH=12 showed better catalytic performance than both the one obtained at pH=8.7 as well as the commercial reference catalyst. The authors claimed that the higher activity is related to higher Ni species reducibility and higher dispersion of nickel.

Long (50h)-catalytic tests over Ni (59 wt.%)/Mg/Al HT-derived catalysts were performed by Bette *et al.* and the catalysts remained stable [134].

Ni-Al HT-derived materials modified with Fe and Mg were prepared by Wang *et al.* [135]. Even low amounts of iron incorporated into Ni-Al hydrotalcites led to improved activity at low temperatures (200-250°C). The catalytic activity of the materials increased

from 16.4% at 206℃ for Ni-Al-HT to 80.8% and 81% for 0.05 Fe-Ni-Al-HT and 0.25 Fe-Ni-Al-HT, respectively. However, the incorporation of Fe increased also the selectivity towards ethane, while the incorporation of Mg to Ni-Al resulted in increased CO_2 adsorption capacity, thus accelerating carbon dioxide conversion. The positive effect of the addition of Mg and Fe on the catalytic activity was observed only at low temperatures (>300℃), with almost no difference at higher temperatures.

It should be mentioned, however, that the decrease in CH_4 selectivity was not observed by Mebrahtu *et al.* [136] who studied iron promoted nickel containing hydrotalcite catalysts. The incorporation of iron into Ni-HTs increased the dispersion of metallic Ni. This resulted in enhanced activity, as well as selectivity towards methane. This was explained by small-sized metal particles facilitating CO dissociation and increasing surface basicity.

The promoting effect of La addition to Ni-containing hydrotalcites was studied by Zhang *et al.* [137]. Various amounts of La (0, 2, 5 and 8 wt.%) were added to HT containing 15 wt.% of Ni, which improved the catalytic activity in CO_2 methanation. The optimum amount of La was found to be 5 wt.% and the improved performance was related to higher Ni dispersion, decreased Ni particles size and enhanced CO_2 adsorption capacity. Zhang *et al.* also compared the conventional method of HT synthesis with that using urea. (5wt.%) Ni dispersion as well as CO_2 adsorption capacity was improved for the catalyst obtained by the latter method as compared to the former one.

4.3.2.2. The effect of promoters

Promoters are added to catalytic systems in order to enhance their catalytic activity, selectivity and/or stability. The influence of a promoter on the activity may be explained by its modification of catalyst structure e.g. specific surface area, which is

crucial because of kinetic limitations of CO_2 methanation. Also basicity and size of Ni crystallites may be influenced. The most commonly studied promoters for CO_2 methanation reaction can be divided into three groups (i) alkali or alkaline earth metals e.g. Mg, Ca, Ba, (ii) rare earth elements e.g. La, Ce, Zr, Y and (iii) other metals e.g. Fe, Co, W. Table 4.5 lists the promoting effects of various promoters used in CO_2 methanation found in literature.

Table 4.5 Literature data of the promoting effect of various additives

Promoter	**Loading (wt.%)**	**Ni (wt.%)**	**Support**	**Effect of promoter addition**	**Ref.**
Mg	**1**	**10**	**SiO_2**	Increased interaction between Ni-Mg, resulting in increased Ni dispersion and small Ni particles	[138]
Mg	**2.5**	**3.7**	**USY zeolite**	Smaller Ni^0 particles, enhanced CO_2 molecule activation due to presence of defective surfaces containing low-coordinated protruded oxygen atoms	[139]
K	**0.3**	**78**	**γ-Al_2O_3**	Increased amount of basic sites	[6]
Ca	**8**	**10**	**γ-Al_2O_3**	intensified surface basicity	[140]
Ba	**4**	**10**	**SiO_2**	Enhanced catalytic activity	[141]
La				Increased amount of surface Ni species, enhanced basicity and stability	[137, 142-144]
Ce			**CNTs**	Increased activity and stability,	[97]

Ce	**2.5**	**10**	**γ-Al_2O_3**	Increased specific surface area, resistance to carbon deposition, lower reduction temperature, reduced particle size of NiO	[145]
Ce				Increased Ni dispersion, stabilization of β-type NiO species, that are reduced at lower temperatures	[146]
La, Ce, Fe or Co	**1**	**15**	**ZrO_2**	Increased NiO dispersion, enhanced thermal stability	[147]
Mo	**10**	**10**	**γ-Al_2O_3**	Enhanced activity due to increased CO_2 adsorption capacity	[148]
Y	**Y/(Y+Zr)=0.333**		**ZrO_2**	Enhanced catalytic performance	[149]
Mn	**-**		**-**	Improved Ni dispersion, increased amount of medium-strength basic sites and prevented agglomeration of metallic nickel during reaction	[150, 151]
Fe	**2.5**	**7.5**	**Al_2O_3, ZrO_2, TiO_2, SiO_2**	Strong electron-donating ability (Fe^{2+}), increased Ni dispersion	[152]

Li *et al.* [153] prepared NiO-MgO NPs (nanoparticles), containing various amounts of Ni and Mg, using surfactant-assisted chemical co-precipitation method, followed by thermal treatment and encapsulation by a porous silica shell (@SiO_2) by modified Stöber method. Additionally, pure Ni and MgO were used as reference catalysts. The obtained results showed that Ni@SiO_2 showed significant improvement in comparison to pure Ni at 350°C with CO_2 conversion reaching 78% and selectivity

towards methane of 98%. The addition of MgO to the catalytic system resulted in increased Ni dispersion, which influenced positively the catalytic activity. However, the increasing content of Mg resulted in higher selectivity towards CO. The catalyst with 6.3 wt.% of Mg showed the better catalytic activity than those containing 5, 7.7, 16.5 and 34.2 wt.%.

The effect of various impregnation methods on the catalytic performance in CO_2 methanation of MgO modified Ni/SiO_2 materials was studied by Guo et al [138]. Two strategies were considered (i) co-impregnation with a solution of $Ni(NO_3)_2$ and $Mg(NO_3)_2$ and (ii) first impregnation of SiO_2 with magnesium nitrate, followed by heat treatment, and further impregnation with nickel nitrate solution. The co-impregnated catalyst co-Ni/1Mg/Si (10 wt.% Ni and 1 wt.% Mg) showed superior activity with almost 100% CO_2 conversion at 350ºC. It remained stable during 50h, which was attributed to the synergistic effect of Ni and Mg species. On the other hand, the samples obtained by the second type of impregnation showed similar catalytic activies as the catalyst prepared using the first type of impregnation. In the case of the catalyst prepared using the first type of impregnation the catalytic activity decreased during 50h stability tests from ca. 93% to 91.2 and 89.9% at 350°C. The incorporation of higher amounts of Mg (2 and 4 wt.%) resulted in partial blockage of active sites, which resulted in decreased activity of the catalysts.

In contrary, Guo *et al.* [141]reported that the incorporation of 4 wt.% of MgO into Ni/SiO_2 catalyst lowered the reducibility of the nickel species compared to the non-promoted ones. However, the authors did not mention, which temperature was used for the in-situ reduction.

Potassium was also studied as prospective promoter of Ni-based catalysts. He *et al.* [6] prepared Ni/Al_2O_3 hydrotalcites impregnated with 0.3wt.% K. The obtained results proved that the incorporation of K led to increased number of basic sites, thus enhancing the catalytic activity of the sample in the CO_2 methanation reaction. This was explained by a higher number of basic sites after incorporation of potassium. However, no stability tests were performed for these catalysts.

The promoting effect of Ca incorporation into Ni-Al mesoporous composite oxides was studied by Xu *et al.* [140]. The obtained CO_2-TPD results proved that Ca doping resulted in intensified surface basicity, and a significant increase in the catalytic activity at low temperatures (<250°C). The optimal amount of Ca doping was found to be 8wt.%. On the contrary [141], the introduction of Ca into Ni/SiO_2 catalyst did not improve the catalytic activity. It should be mentioned, however, that the conditions of reduction were not specified.

Barium addition to Ni/SiO_2 catalyst, led to significant increase of the catalytic activity due to the increased number of basic sites [141]. However, during the stability tests significant sintering of metallic Ni phase was registered.

Lanthanum was another widely studied promoter to CO_2 methanation Ni-containing catalysts. Ni-La-promoted SiC catalysts prepared via impregnation method were studied by Zhi *et al.* [154]. The increased activity of La-promoted catalyst was assigned to the basic nature of lanthanum oxide, which favors dissociative adsorption of carbon dioxide and contributes to lowering the C-O bond strength and increased interaction between Ni-C. Qin *et al.* [142] reported that La-promoted (Ni-2La-Al) catalyst was highly stable in comparison to a reference catalyst (Ni-Al). This was attributed to the formation of Al_2O_3-La_2O_3 structure stabilizing and limiting sintering of metallic Ni [143].

Michalska *et al.* [144] studied similar materials and explained that the beneficial promoting effect of La was due to the creation of higher amount of Ni active surface sites and a synergistic effect between highly dispersed nickel particles and lanthanum oxide. Additionally, this article reported that the La-promoted catalyst showed much higher stability compared to NiO-Al_2O_3. Chen *et al.* [155] found that the incorporation of La into Ni/Al_2O_3 led to increased reducibility, higher Ni dispersion and smaller Ni particle size, which resulted in improved catalytic activity of CO_2 methanation.

Ceria promoted Ni-Al_2O_3 and Ni-CNTs, both obtained by impregnation, were studied by Feng *et al.* [97]. In both cases the incorporation of Ce resulted in enhanced activity in the reaction, with Ce-Ni-CNTs showing catalytic performance better than Ce-Ni-Al_2O_3. Sintering of Ni was decreased for the former as compared to the latter. Studies performed by Zhou *et al.* [145] for CeO_2 promoted Ni-containing mesoporous γ-Al_2O_3 showed that ceria incorporation increased the specific surface area, reduced the NiO particles size, increased resistance to carbon deposition, strengthened thermal stability and decreased the reduction temperature. Ni/MCM-41 catalysts promoted with various amounts of ceria were reported by Wang *et al.* [156]. It was found that the Ni dispersion was significantly influenced by the supports structure and the addition of CeO_2 could effectively stabilize nickel species. The catalytic activity of ceria-promoted catalysts was enhanced due to increased CO_2 capacity and higher activation of adsorbed CO_2.

Yttrium was also found to be a good promoter. Its effect on the performance of Ni/ZrO_2 catalyst was studied by Takano *et al.* [149]. Samples with yttrium showed much higher CO_2 conversion than Y-free catalyst, which was strongly dependent on the Y^{3+} concentration with higher activity obtained at the molar ratio Y/(Zr+Y) = 0.333.

The promoting effect of vanadium on Ni/Al_2O_3 catalyst was investigated by Liu et al [157]. The incorporation of V improved the H_2 uptake, resistance to coke formation, Ni dispersion and led to formation of small Ni particles, which influenced positively the activity in CO_2 methanation.

Zhao *et al.* [150] studied Mn-promoted Ni supported on Al_2O_3 catalysts. The incorporation of manganese inhibited the formation of $NiAl_2O_4$, thus improving the CO_2 conversion. It resulted also in increased reducibility because of the weakened interaction of Ni with the support, improved Ni dispersion, increased number of medium-strength basic sites and prevented agglomeration of metallic nickel during the reaction.

The effect of Fe incorporation into $Ni\text{-}Al_2O_3$, obtained by impregnation, was studied by Kang *et al.* [158]. The best catalyst with the highest CO_2 conversion and CH_4 selectivity was $Ni_{0.7}Fe_{0.3}/Al_2O_3$ (%mol). Further increase in Fe content resulted in decreased selectivity towards methane, enhanced the RWGS reaction and led to higher hydrocarbon selectivity. The crucial role of Fe on the dispersion of NiO nanoparticles, and, as a result, increased number of reduced active nickel species, was reported by Lu *et al.* [147] and Pandey *et al.* [152] studies for a series of Ni-Fe bimetallic catalysts supported on ZrO_2. TEM images confirmed that the average size of NiO particles on $Ni\text{-}ZrO_2$ catalyst was much bigger than those dispersed on $Ni\text{-}Fe/ZrO_2$. The catalyst doped with Fe showed superior activity in CO_2 methanation reaction. Optimum amount of iron was found to be 3 wt.% in Fe promoted Ni/ZrO_2 as reported by Ren *et al.* [159]. The enhanced CO_2 conversion was ascribed to the fact that Fe^{2+} (strong electron-donating ability) was present after reduction of the catalyst that can promote the reduction of both nickel and zirconia, which resulted in more reduced nickel species on the catalyst surface, as well as more oxygen vacancies produced by partial reduction of ZrO_2, thus improving the catalytic performance.

Hwang *et al.* [93] compared the influence of Fe, Zr, Ni, Y and Mg incorporation to Ni-Al_2O_3 xerogel materials (AX). The CO_2 conversion followed the sequence (the numbers in catalyst designation denote wt.% of metal): 35NiFe5AX > 35NiZr5AX > 35NiNi5AX >35NiY5AX > 35NiMg5AX, indicating the positive role of the second metal. the highest CO_2 conversion and yield of CH_4 was registered for Ni35Fe5AX, which was assigned the most optimal CO dissociation energy and weakened metal-support interaction.

The activity of Ni(12wt.%)/Al_2O_3 promoted with 5 wt.% of La,Ce, Pr, Eu or Gd at 250ºC followed the sequence: Pr-12%Ni-Al_2O_3 > Gd-12%Ni-Al_2O_3 > Ce-12%Ni-Al_2O_3 > Eu-12%Ni-Al_2O_3 ~ La-12%Ni-Al_2O_3 [160]. The increased activity of Pr-containing catalyst was attributed to inhibited crystal growth and higher surface area as compared to other lanthanide promoted catalysts.

4.3.2.3. The effect of Ni particle size

Nickel particle size and nickel dispersion are often discussed as a factor influencing the activity and selectivity of CO_2 methanation [103, 161, 162]. It has been reported that small nickel particles increase the rate of CO formation, which results in lower CH_4 selectivity [163, 164]. The mechanism of CO_2 hydrogenation is strongly dependent on the metallic Ni particle sizes, the key intermediate is HCOO formed from adsorbed CO_2 and H_2. On small metallic Ni particles this intermediate is decomposed to CO, which is hydrogenated to methane. However, the low amount of H_2 over small metallic Ni particles favors carbon monoxide formation. On the contrary, formate as intermediate on larger Ni metallic particles can be directly hydrogenated to methane due to higher amount of H_2 on the metallic surface and a higher methane production in comparison to CO may be observed.

Summary

The presented review on nickel and nickel-promoted catalysts shows that the catalytic performance in CO_2 methanation reaction depends strongly on a number of factors. The supports nature is crucial in high activity of carbon dioxide methanation. Single and mixed oxides, zeolites, clays or mesoporous materials showed good potential as supports for Ni. Due to the fact that most of the catalysts were prepared using different methods, contained various amounts of nickel and were tested under different conditions it is rather hard to establish the best support and promoter. However, some general trends in CO_2 methanation catalysts may be established.

As shown in the review, the main focus is on the preparation of materials characterized by high dispersion and small size of nickel particles, which can be achieved by increased interaction between Ni-support. However, strong interaction of Ni-support may significantly decrease the reducibility of nickel species, leading to a lower number of active metallic Ni species, negatively affecting the CO_2 conversion.

The addition of promoters can improve the properties of materials. A positive effect of addition of promoters with basic properties is stressed in literature. Another way to increase the activity, as well as stability of catalysts for CO_2 methanation, is the addition of a second metal, thus creating a synergetic effect between nickel and other metal species. It was found that the effect of the promoter addition was strongly dependent on the method of introduction, promoter loading, as well as the used support. It is also important to choose the right preparation method, which may affect the Ni dispersion, as well as metallic Ni particle sizes, influencing CO_2 methanation activity.

5. Double layered hydroxides – hydrotalcites-type compounds

Hydrotalcite is a naturally occurring mineral discovered in 1842 in Sweden, with a formula of $[Mg_6Al_2(OH)_{16}]CO_3 \bullet 4H_2O$. The structure is related to that of brucite ($Mg(OH)_2$), with 6 OH^- coordinated Mg^{2+} octahedra sharing the edges and forming an infinite sheet, with OH- ions located perpendicularly to the planes of the layers, as shown in Fig 5.1. The sheets are stacked one on another and form a 3D structure through weak interaction of hydrogen atoms. The sheets may be stacked on each other in different ways resulting in various possible polytypes. The two possible stackings that are most often found are rhombohedral (3R) and hexagonal (2H).

In hydrotalcites the Mg^{2+} ions are substituted by trivalent Al^{3+} cation, due to the fact of similar ionic radii of Mg^{2+} and Al^{3+}, which makes exchange possible. The positive charge of brucite layers is compensated by interlayer anions. The interlayer spaces of hydrotalcites are filled with randomly distributed water molecules and anions. The interaction between hydroxyl groups of the brucite layers and the interlayer anions is a combination of electrostatic effect and hydrogen bonds [165]. The arrangement of the layers influences the hydrotalcites structure, which may have rhombohedral or hexagonal symmetry, with unit cell build up of three or two hydrotalcite layers, respectively. The most common for natural and synthetic hydrotalcites is rhombohedral symmetry [3, 166-168].

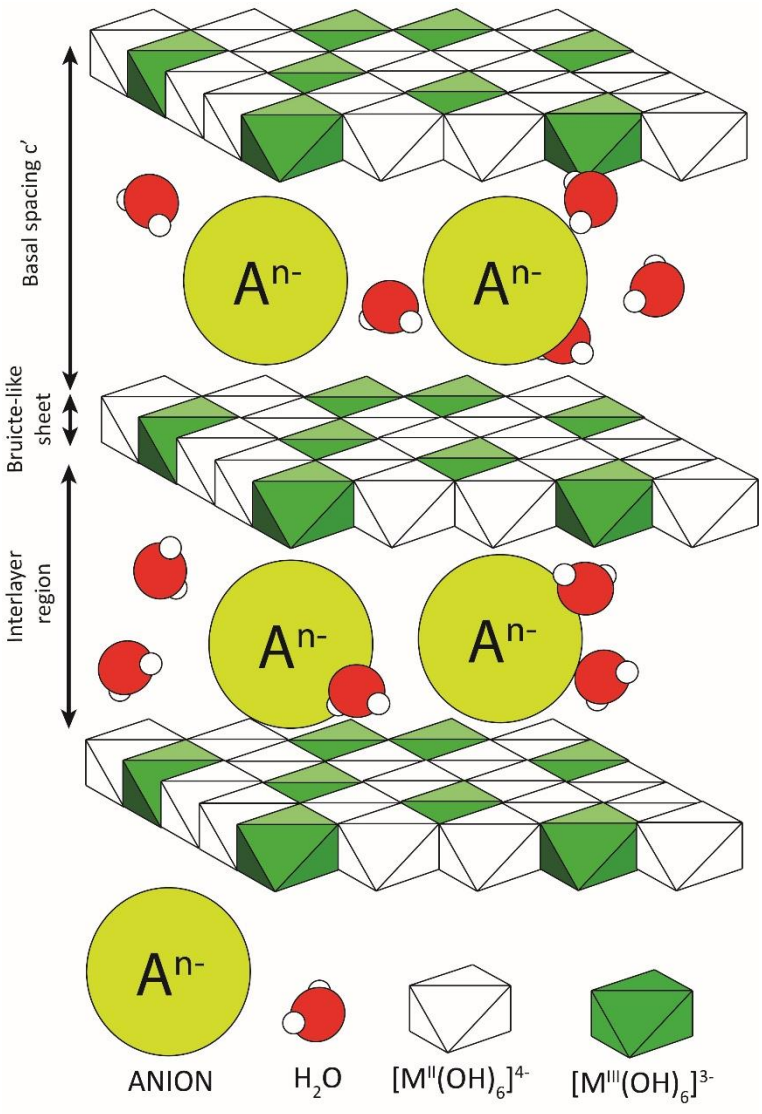

Figure 5.1 Scheme of the hydrotalcite structure

After the discovery of hydrotalcite, a large number of minerals with different composition, but a similar, hydrotalcite-like structure, have been discovered and/or developed. Nowadays, the name hydrotalcite, layered double hydroxides or hydrotalcite-like compounds, is used to describe a large group of minerals listed in Table 5.1. The main difference between these minerals is the replacement of cations in the brucite-like layers. The general formula of hydrotalcites can be represented as: $[M^{II+}_{1-x}M^{III+}_x(OH)_2][(A^{n-}_{x/n}) \bullet mH_2O]$, where: M^{II+} and M^{III+} are divalent and trivalent cations, A - anions present in the interlayer and x - the mole fraction of trivalent cations.

Table 5.1 Selected minerals from hydrotalcite and manasseite group (adapted from [169])

Mineral	Formula	Unit cell parameters		Symmetry
		a	***c***	
Hydrotalcite	$Mg_6Al_2(OH)_{16}CO_3•4H_2O$	3.054	22.81	3R
Manasseite	$Mg_6Al_2(OH)_{16}CO_3•4H_2O$	3.10	15.6	2H
Pyroaurite	$Mg_6Fe_2(OH)_{16}CO_3•4.5H_2O$	3.109	23.41	3R
Sjögrenite	$Mg_6Fe_2(OH)_{16}CO_3•4.5H_2O$	3.113	15.61	2H
Stichtite	$Mg_6Cr_2(OH)_{16}CO_3•4H_2O$	3.10	23.4	3R
Barbertonite	$Mg_6Cr_2(OH)_{16}CO_3•4H_2O$	3.10	15.6	2H
Takovite	$Ni_6Al_2(OH)_{16}CO_3,OH•4.5H_2O$	3.025	22.59	3R
Reevesite	$Ni_6Fe_2(OH)_{16}CO_3•4.5H_2O$	3.08	22.77	3R
Desautelsite	$Mg_6Mn_2(OH)_{16}CO_3•4H_2O$	3.114	23.39	3R

The synthesis of hydrotalcite-like materials can be easily carried out in a laboratory, however, in order to obtain materials of high purity, a few requirements have to be fulfilled. Divalent or trivalent cations that are introduced in place of Mg^{2+} and Al^{3+} need to have ionic radii similar to Mg and Al. The molar ratio of divalent to trivalent cations should be between 0.2 and 0.33 in order to obtain a HT-like structure. The introduced amount of cations is another important factor, which can affect the structure of the synthesized HTs. E.g. the introduction of high amounts of Cu^{2+} or Mn^{3+} may cause the formation of a separate phase of carbonate or hydroxide, as a result of Jahn-Teller effect, which involves the distortion of the octahedra. As reported in literature it is also possible to introduce monovalent and tetravalent cations to the brucite-like layers. Pavel *et al.* [170] reported the synthesis of Li/Al HTs, while Tichtit *et al.* [171] introduced Zr^{4+} and

Velu *et al.* [172]Sn^{4+}. On the other hand, the only limitation to the nature of the introduced anions is that they should not form complexes with the cations present in the brucite-like layers of the hydrotalcite. The type of anion present in the interlayer spaces influences also the distance between brucite-like layers and the parameter *c* of hydrotalcite unit cell. Carbonates and nitrates can be eliminated easily during calcination, whereas anions that form metal complexes can still be present in the material even after calcination [173]. The families of anions that can be found in hydrotalcites interlayer spaces are:

- Halides (F^-,Cl^-, Br^-, I^-)
- Non-metal oxoanions (CO_3^{2-}, NO_3^-, BO_3^{3-}, AsO_4^{3-}, SeO_4^{2-}, BrO_4^-, etc.)
- Oxometallate anions (VO_4^{3-}, CrO_4^{2-}, MnO_4^-, etc,
- Complexes of transition metals ($Fe(CN)_6^{2-}$, $[Metal(EDTA)]^{2-}$, etc,
- Volatile organic anions (CH_3COO^-, $C_6H_5COO^-$, $C_2O_4^{2-}$, etc,
- Anionic polymers.

Hydrotalcites properties

The physicochemical properties of hydrotalcites are strongly dependent on the chemical composition and preparation method. However, some features, such as basic character and memory effect, are common for LDHs regardless of the preparation method. One of the most important features of such materials is the formation of homogenous mixture of well-dispersed elements in the brucite-like and inter-layers [168]. Other very important features are:

(i) The thermal decomposition behavior of hydrotalcite-like materials is similar even though they may differ greatly in the composition. During the thermal decomposition four steps may be identified: (1) removal of physically adsorbed water from the external surface at temperatures below 100ºC, (2)

interlayer water removal up to 250ºC, (3) removal of hydroxyl groups from the layers and decomposition of interlayer anions and (4) formation of mixed nano-oxides of periclase-like structure;

(ii) High specific surface area of mixed oxides obtained after the thermal decomposition of hydrotalcite-like materials. Carbonates present in hydrotalcites leave the structure in the form of CO_2 during calcination, which results in the formation of porous structure (with mesopores of about 8 nm);

(iii) Hydrotalcites possess high anionic exchange capacity related to their lamellar structure, which allows to exchange anions present in the interlayer region. The exchange capacity of hydrotalcite-like materials is higher than that shown by cationic clays and is typically in the range of 200-400 cmol/kg.

(iv) Generally, HT-like materials are basic. The basic strength and the distribution of sites is dependent on the chemical composition of brucite-like layers. Thus, acid-base properties can be tailored to by substitution of cations present in the layers with other having stronger basic properties, as well as the introduction of some species with acidic properties into the interlayer spaces of HTs. Typically, mixed oxides derived from hydrotalcites obtained after thermal decomposition possess three types of surface basic sites as confirmed by CO_2 adsorption experiments [174] and presented in Fig. 5.2: (i) weak Brønsted basic sites – surface OH groups, (ii) medium-strength Lewis M-O pairs and (iii) strong basic sites related to low coordinated O^{2-} anions [174, 175].

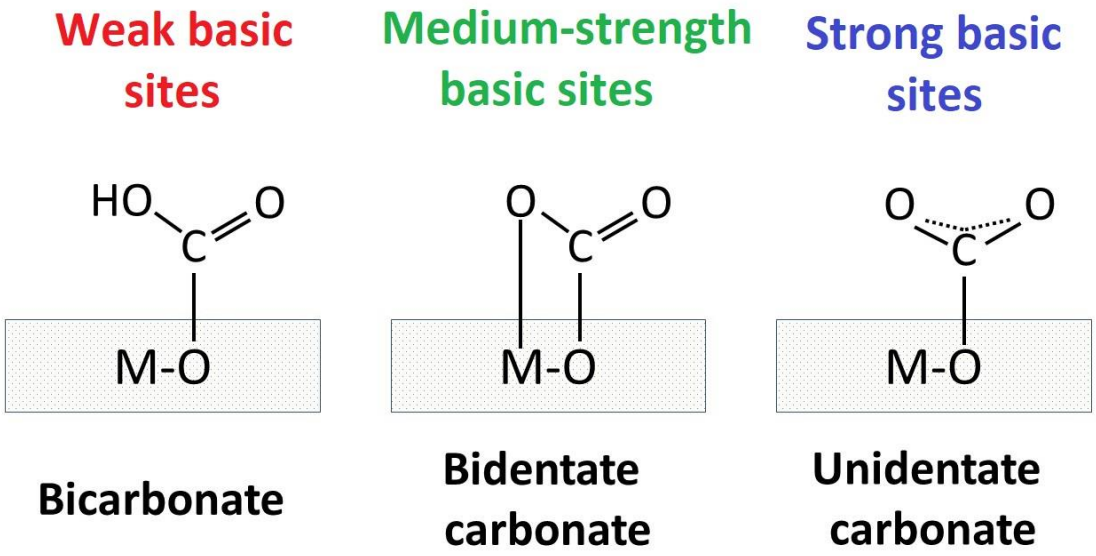

Figure 5.2 Hydrotalcites: types of basic sites - CO_2 species adsorbed (adapted from [174])

(v) HT-derived mixed oxides exhibit a so-called memory effect, which is the ability to recover layered structure after their thermal decomposition. It is possible if LDHs come into contact with a solution containing appropriate anions. This effect is, however, retained only if hydrotalcites were calcined at certain temperatures, usually lower than 500ºC.

As a result of their exceptional properties hydrotalcite-like and hydrotalcite-derived mixed oxides have found a large number of applications in various fields, as illustrated by Fig 5.3.

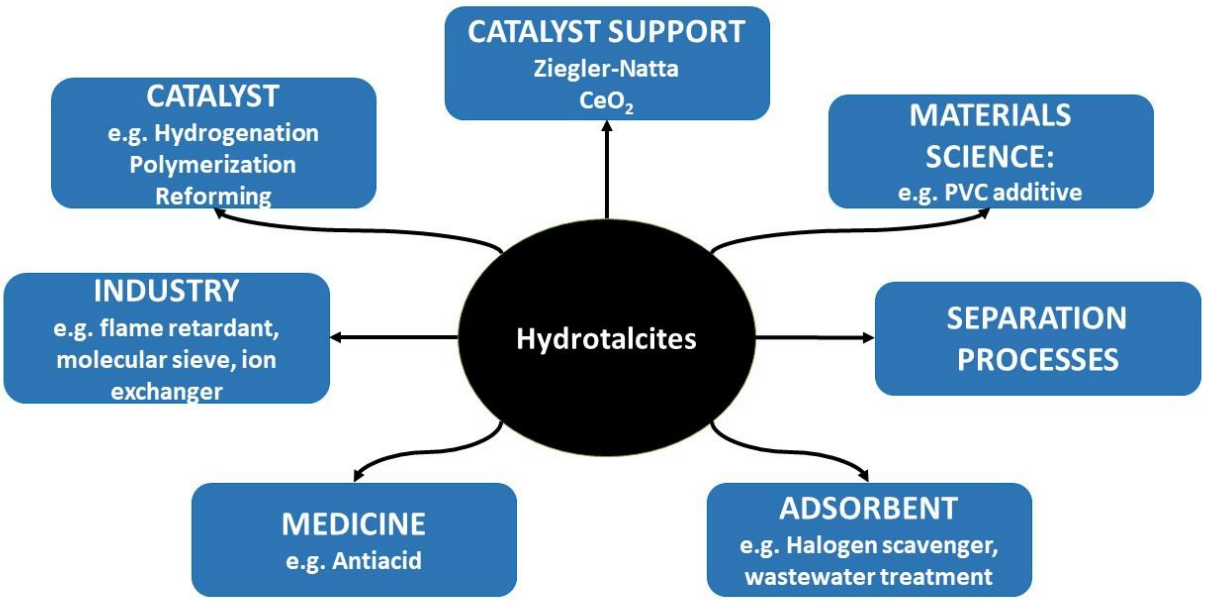

Figure 5.3 Existing and possible applications of hydrotalcite-like materials (adapted from [3])

Because of a wide range of possible cations present in the brucite-like layers, hydrotalcite-like materials are considered for a large number of applications in catalysis, among others:

- Methanation of CO [176] and CO_2 [177],
- Dry reforming of methane [178],
- Partial oxidation of methane [179],
- Ethanol steam reforming [180],
- Methanol [181] and higher alcohol [182] synthesis,
- Selective oxidation of alcohols to aldehydes [183],
- Reduction of aldehydes to alcohols [184],
- Epoxide ring opening [185],
- Epoxidation [186],

- Aldol condensation [187],
- Cyanoethylation [188],
- Michael reaction [189],
- Transesterification [190].

5.1. Hydrotalcites preparation methods

There are several methods of synthesis of hydrotalcite-like materials. The most often used are precipitation and urea method. The obtained materials may be further modified, among others by anion exchange, reconstruction method, microwave or hydrothermal treatment.

There are additionally several different synthesis methods, which are rarely used, such as hydrothermal synthesis [191], salt-oxide method [192], electrochemical synthesis [193], reverse microemulsion method [194], sol-gel method [195], separate nucleation and aging steps (SNAS) method [196], etc.

The three main routes for synthesis of hydrotalcite-like materials are schematically shown in Fig. 5.4: (i) the synthesis of hydrotalcite with metal cations incorporated into the brucite-like layers of hydrotalcite, (ii) the thermal treatment of obtained hydrotalcite, followed by impregnation of the obtained mixed oxide and (iii) ion-exchange of the anions present in the obtained hydrotalcite using anionic metal precursor with the desired metal.

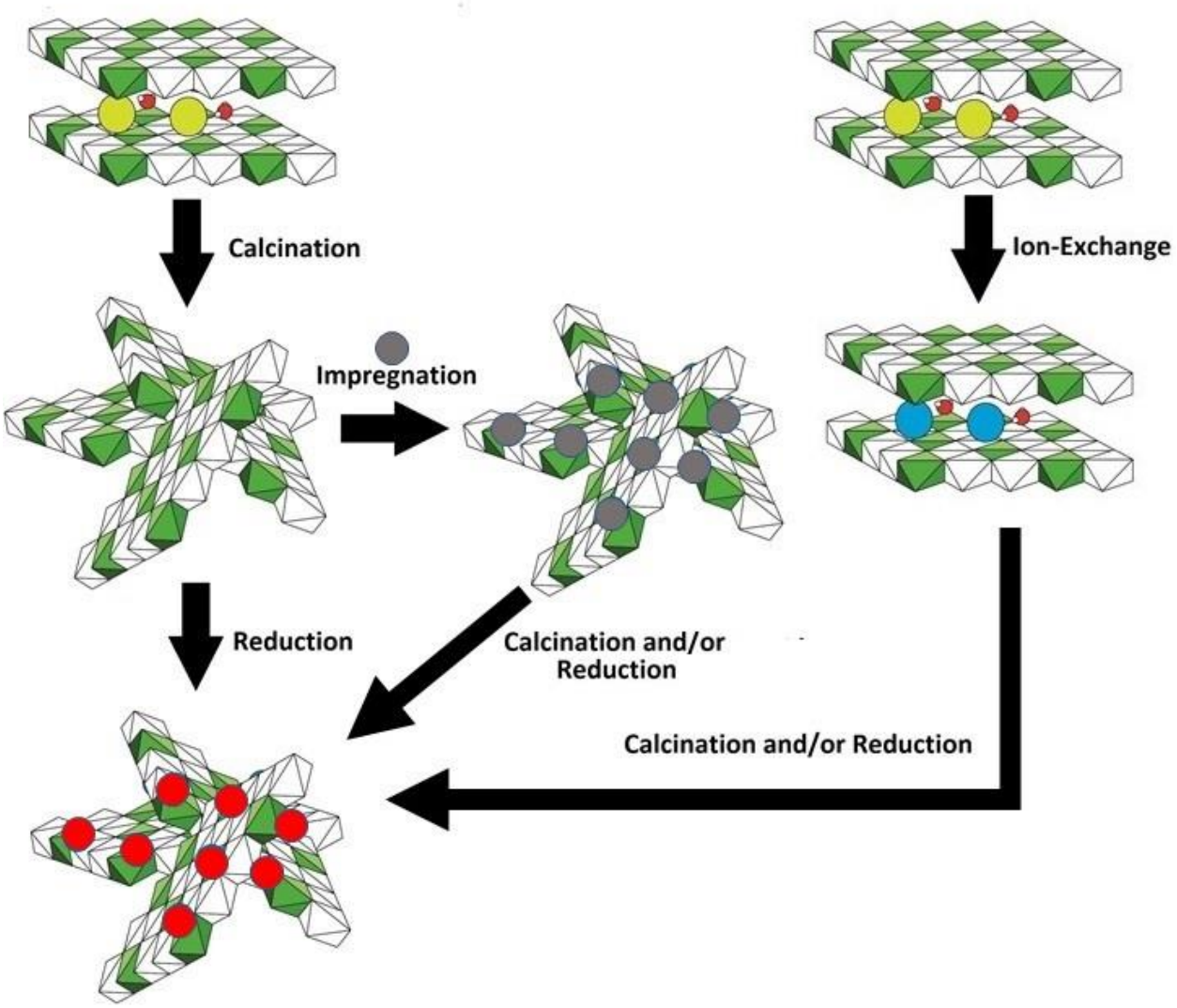

Figure 5.4 The main routes leading to HT-derived supported metal catalysts (adapted from [197])

The most commonly studied method of HTs synthesis is co-precipitation at constant pH, which involves a dropwise addition under vigorous stirring of a mixture containing divalent and trivalent metal salts into an alkaline solution. The co-precipitation can be carried out at variable or constant pH. The former results in the formation of hydroxides or hydrous oxides, followed by co-precipitation and formation of LDHs after addition of a base solution. The latter is recommended if high homogeneity is desirable. In order to maintain the pH at desired values the metal salt solution is added dropwise together with the base solution.

Co-precipitation mechanism is based on condensation of hexa-aqua complexes in a solution, forming brucite-like layers with metallic cations distributed homogenously, and solvated interlayer anions [198]. The XRD analysis of the precipitates showed the formation of both main layers and interlayers at an early stage, without observable delamination. The interlayer anions may origin from the metal salts used for precipitation. If the co-precipitation is performed at high pH, the interlayer anion may be OH^- originating from the alkaline solution. If sodium carbonate is used the interlayer anion will be CO_3^{2-} due to its high affinity.

In this way a wide range of hydrotalcites with various chemical compositions can be synthesized. They may be further modified using ion-exchange, dehydration-rehydration or hydrothermal treatment in order to tailor the properties for appropriate applications.

Urea hydrolysis method

This preparation method has the same principle as the co-precipitation described above, with the exception that in this case a urea solution is used. In the co-precipitation method supersaturation of the precipitating agent is reached rapidly, resulting in the nucleation of hydroxides and particle aggregation, resulting in a wide range of particle size distribution. On the contrary, using urea as precipitating agent leads to the separation of nucleation and aggregation, resulting in monodisperse particles. The particle size can be controlled by the hydrolysis rate, with larger particles formed at lower temperatures due to lower nucleation rates [199]. This method was reported to be suitable for obtaining Mg-Al hydrotalcites with high layer charge density [200] and HTs with well-defined hexagonal shape due to low supersaturation [201].

Anion exchange method

The goal of anion exchange method is to introduce different anions into the interlayer spaces of already formed hydrotalcites. It exploits the anion exchange properties of LDHs and is useful if the incorporation of metal cation or anion is impossible during co-precipitation method, because of e.g. the anion instability under alkaline conditions [202]. From the thermodynamic point of view the anion exchange depends on electrostatic interactions between the layers and the exchanging anions, hydrogen bonding and free energy associated with the hydration change [203]. The exchange is favoured for anions with high charge density. A comparative list of mono- and divalent anions selectivity was reported by Miyata *et al.* [204]:

$$CO_3^{2-} >> C_{10}H_4N_2O_8S^{2-} > SO_4^{2-} >> OH^- > F^- > Cl^- > Br^- > NO^{3-} > I^-$$

The selectivity of divalent oxoanions was determined by Yamaoka *et al.* [205]:

$$HPO_4^{2-} \sim HAsO_4^{2-} > CrO_4^{2-} > SO_4^{2-} > MoO_4^{2-}$$

In order to successfully exchange the anions, some aspects have to be considered. Because of the strongest bond with the layer, carbonate anions are almost impossible to exchange, thus CO_2 should be excluded from the system. Nitrates or chlorides should be chosen as anions if they should be easily exchanged.

From the kinetic viewpoint, the diffusion of the introduced anions within the layers is the rate-determining step of this reaction. Therefore, if the basal spacing of the hydrotalcite-like precursor is too small the diffusion of larger anions into the interlayers will be not possible. However, it is still possible to introduce bigger anions using intercalation via organic anion-pillared precursor, which is a two-step process: (i) the anions present in the interlayer spaces are exchanged by organic anion-pillars, which

results in an increased basal spacing (increase of interlayer spaces), and (ii) the introduction of the desired anion, which can enter because of the increased basal spacing. The anion-exchange possibility is dependent on factors such as: (i) exchange ability which increases with the increase of charge and decrease of ionic radius (ii) pH which should be larger than 4 in order to prevent the decomposition of LDH layered structure: low pH favors the introduction of weak basic anions, (iii) temperature which, if high, favours the anion exchange, and (iv) chemical composition of hydrotalcites.

Dehydration/Rehydration method

The dehydration/rehydration method exploits the memory effect of mixed oxides derived from hydrotalcites. As mentioned earlier the memory effect of HTs is the ability to reconstruct the layered structure of the precursor by addition of aqueous solution containing appropriate anions to the "collapsed" structure, Miyata was the first to describe this [206]. The first step of this method is the thermal treatment of hydrotalcite-like materials followed by addition of an aqueous solution of anions that will be intercalated.

However, the calcination followed by structure reconstruction cannot be repeated endlessly. Each cycle will result in a decreased content of the interlayer carbonates and enhances the extraction of Al^{3+} present in the brucite-like layers. Some hydrotalcite-like materials are not suitable for this method, among others those containing Fe^{3+}, because of the formation of spinel-like structure even at low temperatures.

6. Experimental

6.1. Thermodynamic analysis of CO_2 methanation reaction

The thermodynamic equilibrium analysis of CO_2 methanation reaction presented in this subchapter was performed using HSC Chemistry 5 software, by the method of Gibbs energy minimization. The main possible reactants, that were considered during the analysis of CO_2 methanation process were: $Ar_{(g)}$, $CO_{2(g)}$, $H_{2(g)}$, $CH_{4(g)}$, $C_2H_{2(g)}$, $C_2H_{4\,(g)}$, $C_2H_{6(g)}$, $H_2O_{(g)}$, $CH_3OH_{(g)}$, $HCOOH_{(g)}$, $C_{(s)}$. While $CO_{2(g)}$ and $H_{2(g)}$ were introduced into the system as substrates and $Ar_{(g)}$ as a diluting agent, the others are possible products of CO_2 methanation and side reactions.

The main goal of the analysis was to establish the influence of pressure, temperature and feed gas composition on the equilibrium concentrations of reactants. It has to be stressed that the presented results were obtained assuming a closed system. Catalysts, reaction kinetics and transport process were not considered in this study. The obtained results were used as a benchmark to compare with experimental data. The possible reactions involved in the methanation of carbon dioxide are summarized in Table 4.2 in Chapter 4.2.

CO_2 methanation at atmospheric pressure

The typical product fraction of CO_2 methanation at equilibrium is presented in Figure 6.1, for a feed gas composition of $H_2/CO_2 = 4$. The main products at low temperature (200-300°C) are CH_4 and H_2O. Increasing the temperature to 450°C results in increased fraction of a by-product, CO, due to the favoured water gas shift reaction. An increase in unreacted CO_2 and H_2 together with the decreased amount of product CH_4 is also observed at the same temperature. At 550°C the CO_2 fraction reaches its maximum and decreases with the further increase of temperature because RWGS reaction becomes dominant. Additionally, the calculations indicate that carbon deposition is negligible

under such conditions. As proposed in literature, CO_2 methanation may be a series of reactions that involve the reverse water gas shift reaction followed by CO methanation in the presence of steam. The addition of steam into CO methanation can effectively suppress carbon formation, which would explain the absence of carbon deposition [75].

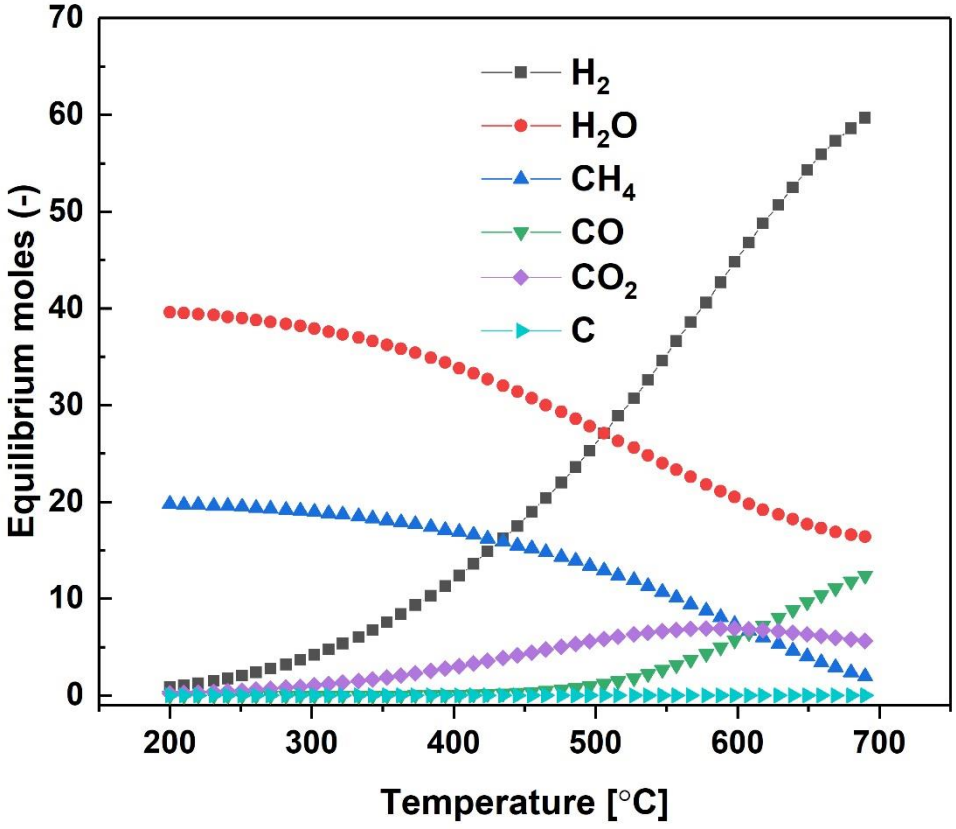

Figure 6.1 Product fraction of CO_2 methanation at equilibrium at atmospheric pressure

Fig 6.2 presents the effect of temperature on CO_2 methanation reaction for the conditions used in this study. CO_2 conversion in Fig 6.2 A shows that increasing the temperature up to 550°C results in the decreased CO_2 conversion, in good agreement with high exothermicity of the process. Thus, the temperature increase is unfavorable for this reaction. However, increasing the temperature above 550°C results in increased CO_2 conversion, which is caused by RWGS reaction which becomes dominant above 600°C, as illustrated by the results in Fig. 6.2 B and C. According to Fig. 6.2 D in order to obtain high CH_4 yield at atmospheric pressure the reaction temperature should not exceed ca.

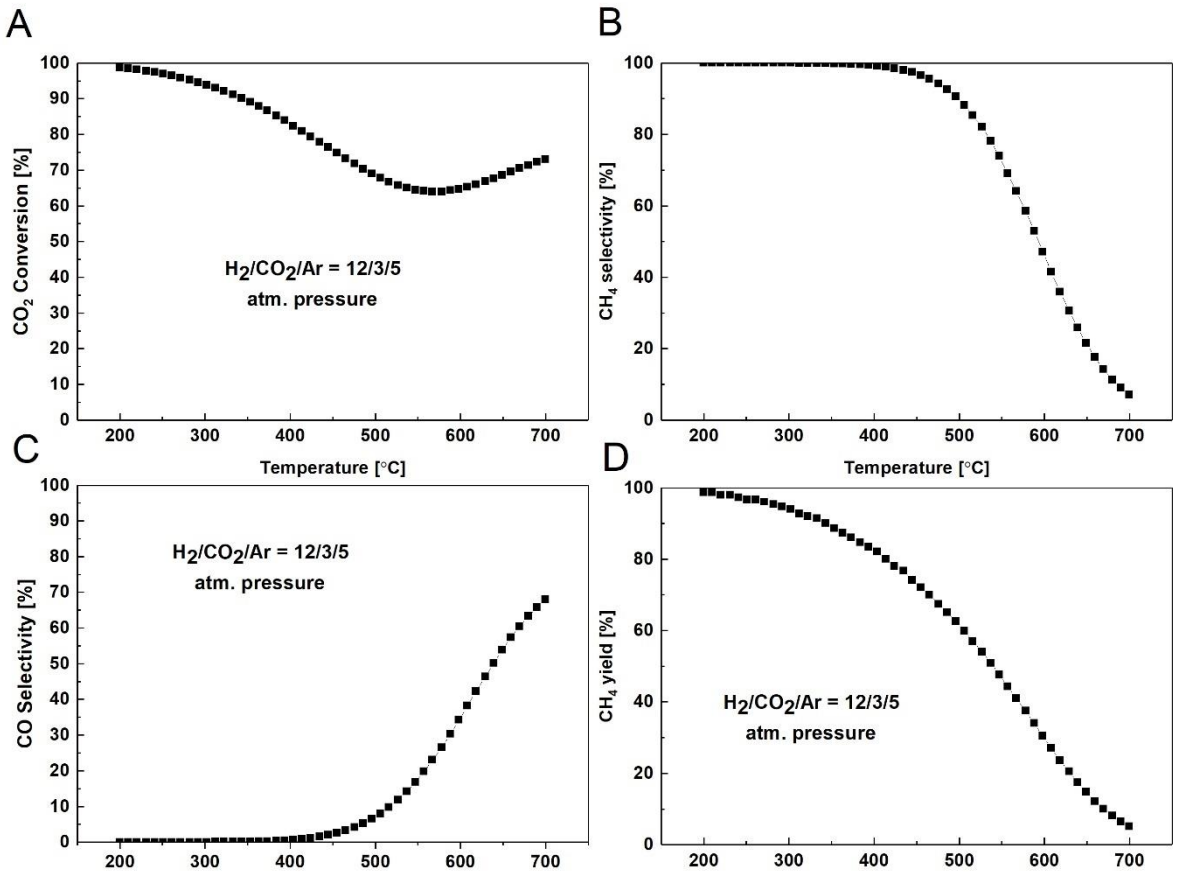

Figure 6.2 Effect of temperature on A – CO_2 conversion, B- CH_4 selectivity, C – CO selectivity and D – CH_4 yield at atmospheric pressure and conditions used in this study

300°C.

Figure 6.3. A, B, C and D presents the effect of both pressure and temperature on CO_2 methanation. The calculations were carried out for a mixture of 20%CO_2/80%H_2

from 1-15 bars (1bar step) and temperatures ranging from 200-700°C with a 50°C step. From Fig. 6.3 A it may be seen that CO_2 conversion increases with increasing pressure for the same temperatures in the whole temperature range of 200-700°C, with the most significant changes observed between 400 and 600°C. This is because CO_2 methanation beside being exothermic is also a volume-changing reaction. Increasing the pressure is effective up to a certain point, then being less effective. As shown in Fig 6.3 B and C, pressure has no influence on selectivity towards CH_4 and CO up to ca. 450°C. At temperatures higher than 450°C there is a significant influence of pressure, with CH_4 selectivity increasing and CO selectivity decreasing with increasing pressure. Figure 6.3 D presents the effect of temperature and pressure on CH_4 yield. Additionally it should be mentioned that no carbon generation was found under these conditions, which may be explained by the fact that water formed during the reaction can suppress carbon deposition as shown by Kopyscinski *et al.* [76].

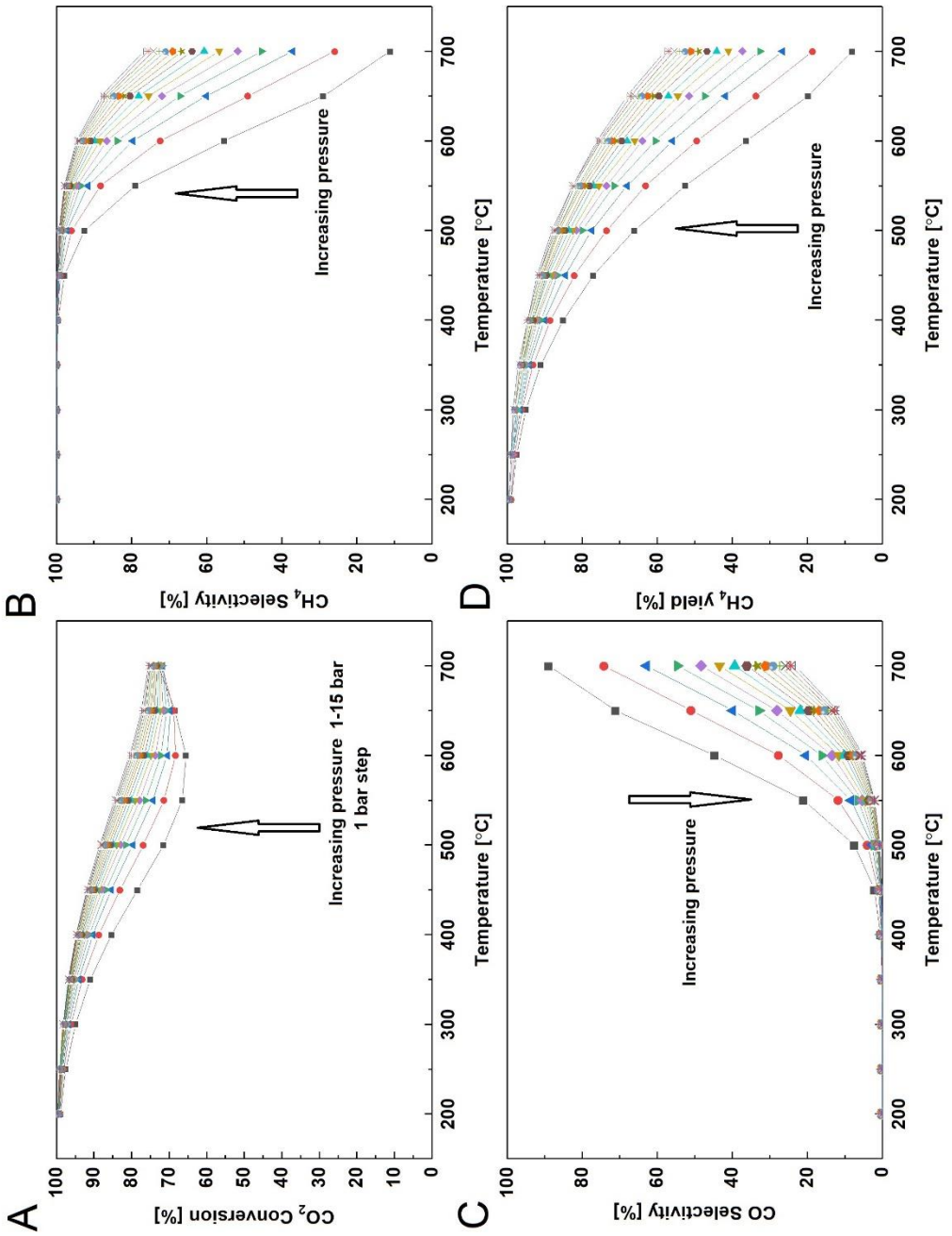

Figure 6.3 Effect of pressure and temperature on CO_2 methanation (A) CO_2 Conversion, (B) CH_4 Selectivity, (C) CO Selectivity and (D) CH_4 yield.

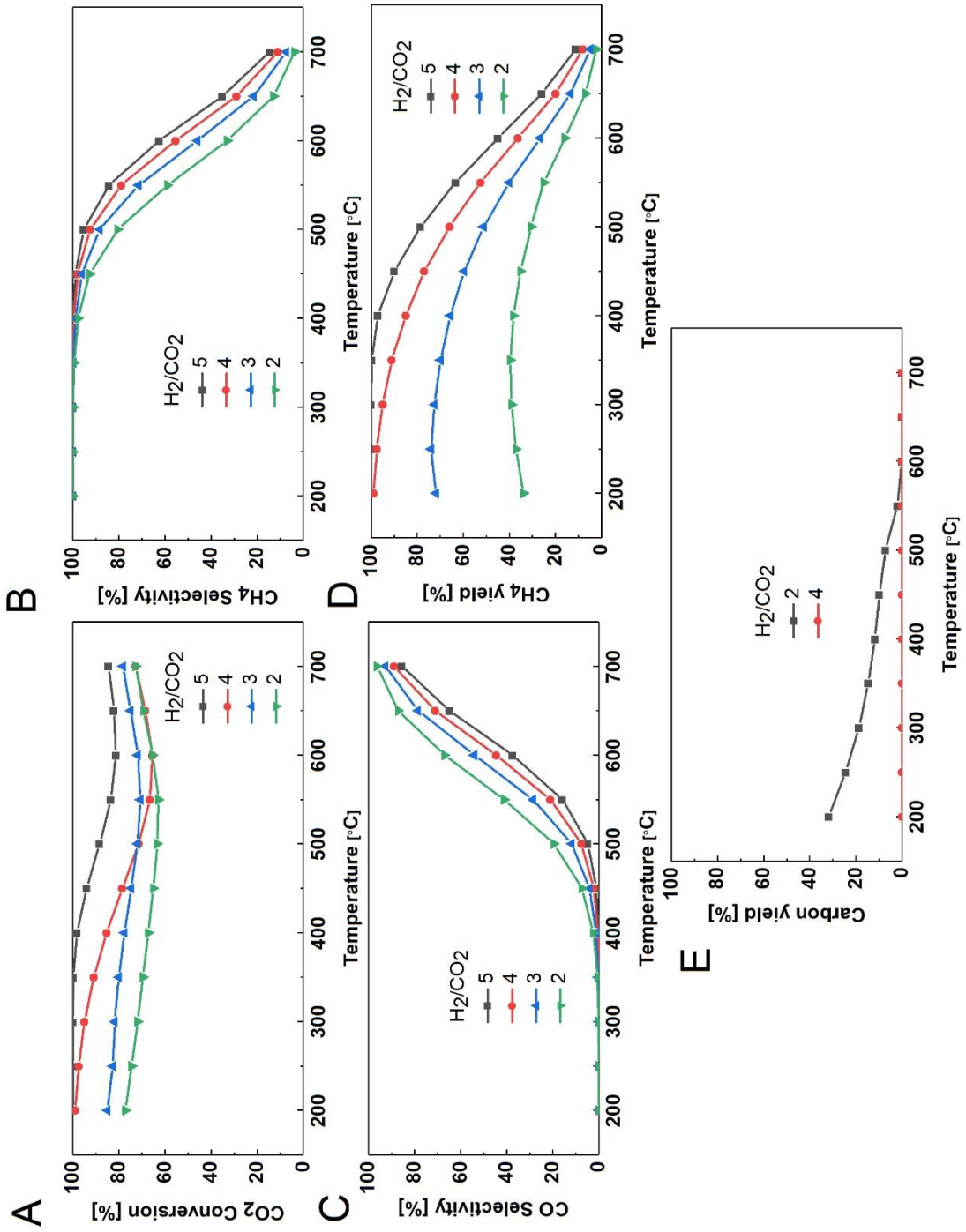

Figure 6.4 Effect of different H_2/CO_2 ratios on CO_2 methanation A – CO_2 Conversion, B – CH_4 selectivity, C – CO Selectivity, D – CH_4 yield and E - Carbon yield.

Figure 6.4 presents the effect of various H_2/CO_2 ratios on CO_2 methanation reaction. It can be observed that both CO_2 conversion (Fig 6.4 A) and CH_4 selectivity (Fig 6.4 B) are strongly dependent on H_2/CO_2 ratio. Stoichiometric and higher ratios of H_2/CO_2 lead to high CO_2 conversion and CH_4 selectivity. Decreasing the ratio from 4 to 2 results in the decrease in CO_2 conversion at 200°C from ca. 99% to ca. 77%, respectively. A remarkable difference in CH_4 yield (Fig 6.4 D) can be observed with H_2/CO_2 values changing from 4 and 2 from ca. 100% to ca. 33.9% at 200°C, respectively. On the other hand, increasing the ratio to 5 effectively increased the CH_4 yield to 100% up to the temperature of 350°C. It should be mentioned, additionally, that decreasing the ratio affects also the carbon deposition at temperatures ranging from 200-500°C as illustrated by Fig 6.4 E. No carbon deposition is found at ratios equal or higher than 4.

The thermodynamic analysis showed that the optimal conditions for CO_2 methanation are low temperature and moderately increased pressure. At low temperatures both the CO_2 conversion and CH_4 selectivity can reach almost 100%. However, at low temperatures the reaction rate is low. In order to suppress the kinetic limitations a highly active catalyst needs to be utilized.

6.1. Preparation of the catalysts

6.1.1. Hydrotalcite co-precipitation

Hydrotalcite-like materials were synthesized at controlled pH (9.5-10) by co-precipitation method using an aqueous solution of appropriate nitrates ($Mg(NO_3)_2 \cdot 6H_2O$, $Ni(NO_3)_2 \cdot 6H_2O$, $Al(NO_3)_3 \cdot 9H_2O$, $La(NO_3)_3 \cdot xH_2O$ and $Fe(NO_3)_3 \cdot 9H_2O$ (Sigma Aldrich). The precipitating agent used to control the pH was 1M NaOH. Both solutions were simultaneously added into a beaker containing a 0.05M Na_2CO_3. The flow of each solution was adjusted to maintain the pH in the range of 9.5-10. The co-precipitation was

carried out at 65ºC at constant stirring, followed by aging for 1h at 65ºC and filtration with warm distilled water. The synthesized materials were dried at 80ºC for 24h and milled to fine powder.

All the materials synthesized and tested in this work were based on hydrotalcites. The materials were obtained by co-precipitation, except selected samples which were additionally modified by adsorption of a promoter (La) species from aqueous solution of $[La(EDTA)]^-$ chelates, followed by calcination and final in-situ reduction in a stream of hydrogen in order to obtain metallic nickel supported catalyst. The preparation procedure is presented schematically in Fig. 6.5.

6.1.2. Influence of nickel content

Hydrotalcites containing various amounts of nickel were prepared by co-precipitation method. All the materials had a fixed M^{2+}/M^{3+} ratio equal to 3 with a varying ratio of Ni/Mg. The assumed amounts of introduced nickel for the fresh samples were 5, 10, 15, 25, 30 and 40 wt.%. The samples designated as Nix were prepared, where x stand for the wt.% of Ni introduced (theoretically) into the brucite-like layers of hydrotalcites.

6.1.3. Effect of promoter introduction

The effect of Fe or La introduction was also studied. Both promoters were incorporated into hydrotalcites using co-precipitation technique. Lanthanum as well as iron were added into hydrotalcites with a fixed amount of Ni (20 wt.%). The theoretical amounts of Fe or La incorporated were 1, 2 and 4 wt.% for the fresh material.

6.1.4. Effect of La incorporation method

The effect of three incorporation methods of lanthanum was examined. Lanthanum was incorporated using co-precipitation method, incipient wetness impregnation method (2 wt.% of La) and via adsorption method. The latter one was carried out using a solution of $La(EDTA)^-$ complexes, prepared by the addition of appropriate amount of lanthanum nitrate to a solution of EDTA disodium salt. The concentration of La was calculated to obtain the hydrotalcite (Ni-Mg-Al) with 1, 2 or 4 wt.% of La. The pH of the prepared solution was adjusted to 10 using a solution of NaOH. Such solution was then mixed with the hydrotalcite powder for 24h in a closed beaker. The synthesized hydrotalcites were filtered, washed with distilled water and dried at 80ºC for 24h.

6.1.5. Materials calcination

In order to obtain homogenous nano-oxides, the synthesized hydrotalcite-like materials were treated thermally. The calcination of the as-synthesized materials was performed from room temperature to 500ºC, with a temperature ramp of 10 ºC/min, in a flow of air for 5h at (500ºC). The samples were kept at this temperature for 5h and cooled to room temperature.

6.1.6. Catalyst activation

Prior to CO_2 methanation catalytic tests, the materials were reduced in-situ in a stream of 10%H_2/Ar, with a total flow of 100 cm^3/min. The materials were heated from room temperature to 900ºC and kept at this temperature for 1h, followed by cooling down to reaction temperature (250ºC).

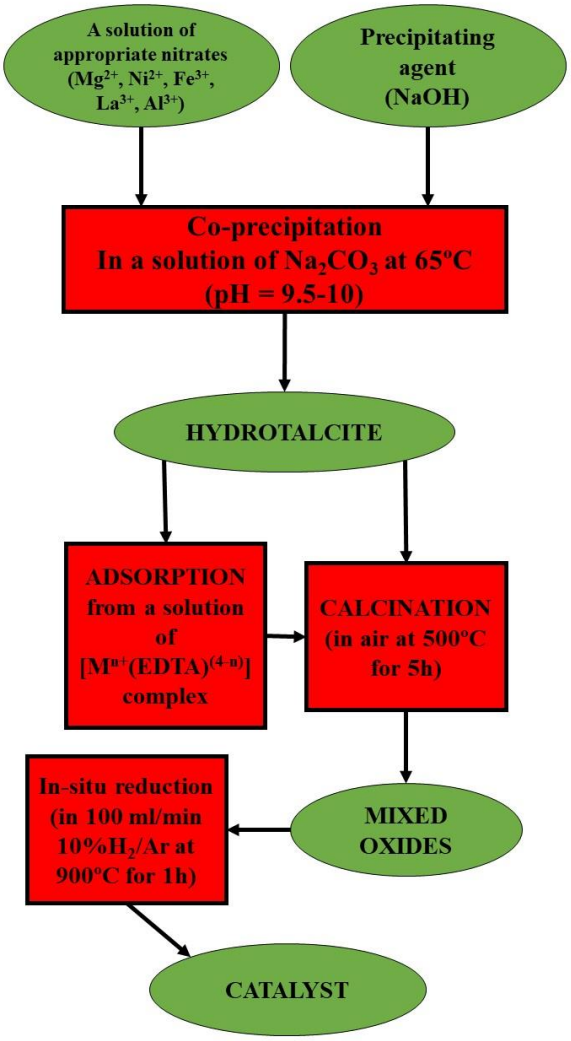

Figure 6.5 Scheme of material preparation/modification

The discussion of physico-chemical characterization and catalytic tests results is divided into five chapters:

(i) Influence of nickel content (Chapter 7),

(ii) The effect of promoter introduction (La or Fe) (Chapter 8.2 and 8.1, respectively),

(iii) The influence of lanthanum incorporation method (Chapter 8.3),

(iv) Optimization of the catalysts (Chapter 9)

(v) Operando X-ray absorption and emission spectroscopy investigation of Ni and Ni-La hydrotalcite-derived mixed oxides (Chapter 10)

All types of modification that the materials were submitted to are described in the respective chapters, while the designations and preparation details of the prepared materials are given in Table 6.1.

Table 6.1 Preparation details and nomenclature of the prepared catalysts

Material	Cations in brucite-like layers	M^{2+}/M^{3+} molar ratio	Method of promoter incorporation	Promoter content (wt.%)*
Influence of nickel content (Chapter 7)				
Ni5	Ni^{2+}, Mg^{2+}, Al^{3+}	3	-	-
Ni10	Ni^{2+}, Mg^{2+}, Al^{3+}	3	-	-
Ni15	Ni^{2+}, Mg^{2+}, Al^{3+}	3	-	-
Ni25	Ni^{2+}, Mg^{2+}, Al^{3+}	3	-	-
Ni30	Ni^{2+}, Mg^{2+}, Al^{3+}	3	-	-
Ni40	Ni^{2+}, Mg^{2+}, Al^{3+}	3	-	-
Effect of promoter incorporation (La or Fe) (Chapter 8.1 and 8.2)				
Ni15La1	Ni^{2+}, Mg^{2+}, Al^{3+}	3	Co-precipitation	1
Ni15La2	Ni^{2+}, Mg^{2+}, Al^{3+}	3	Co-precipitation	2
Ni15La4	Ni^{2+}, Mg^{2+}, Al^{3+}	3	Co-precipitation	4
Ni15Fe1	Ni^{2+}, Mg^{2+}, Fe^{3+}, Al^{3+}	3	Co-precipitation	1
Ni15Fe2	Ni^{2+}, Mg^{2+}, Fe^{3+}, Al^{3+}	3	Co-precipitation	2

Ni15Fe4	**Ni^{2+}, Mg^{2+}, Fe^{3+}, Al^{3+}**	**3**	**Co-precipitation**	**4**
Influence of lanthanum incorporation method (Chapter 8.3)				
$Ni15La1_{(ad)}$	**Ni^{2+}, Mg^{2+}, Al^{3+}**	**3**	**Adsorption of**	**1**
$Ni15La2_{(ad)}$	**Ni^{2+}, Mg^{2+}, Al^{3+}**	**3**	**$La(EDTA)^-$**	**2**
$Ni15La4_{(ad)}$	**Ni^{2+}, Mg^{2+}, Al^{3+}**	**3**	**solution**	**4**
Ni15La2	**Ni^{2+}, Mg^{2+}, Al^{3+}**	**3**	**Impregnation**	**2**
Optimization of the catalysts (Chapter 9)				
Ni40	**Ni^{2+}, Mg^{2+}, Al^{3+}**	**3**	**Co-precipitation**	**-**
Ni40La2	**Ni^{2+}, Mg^{2+}, Al^{3+}**	**3**	**Co-precipitation**	**1.8**

* - assumed content of the promoter for the fresh materials

6.2. Characterization of the catalysts

X-ray diffraction (XRD)

The as-synthesized hydrotalcites as well as the catalysts obtained upon their calcination, reduction and after reaction were characterized by XRD experiments. X-ray diffraction patterns were recorded on Empyrean (PANalytical) diffractometer equipped with a CuK_α (λ=1.54059Å) radiation source, within 2θ range from 8 to 90°.

For chosen hydrotalcites XRD diffractograms were recorded as a function of temperature. The sample was placed in a resistance oven and heated from room temperature to 900°C. The diffractograms were registered at 25°C and from 100 to 1000°C every 100°C.

The obtained XRD patterns gave information about the structure of the prepared samples. The diffractograms obtained in a function of temperature were used to examine the structural changes.

The average crystallite sizes of Ni^0 and periclase-like mixed oxides were calculated basing on Scherrer equation:

$$D_{hkl} = \frac{K\lambda}{\beta_{hkl} cos\theta}$$

Where: λ – is the radiation wavelength, β_{hkl} - is the half-width of the reflection and θ - is the Bragg diffraction angle

Low temperature nitrogen sorption

The textural properties: surface area and total pore volume were determined from N_2 adsorption isotherms obtained during low temperature nitrogen sorption experiments performed on BELsorp-MiniII apparatus (BEL Japan). Prior to N_2 adsorption the mixed oxides were outgassed at 110°C for 3h under vacuum.

The specific surface area of the obtained materials was calculated using Brunauer-Emmet-Teller (BET) method. The pore size distribution, volume of pores and mean pore diameter were examined by Barrett-Joyner-Halenda (BJH) analysis.

Elemental analysis

The composition of the obtained catalysts was determined by X-ray Fluorescence (XRF) or Inductively Coupled Plasma Optical Emission Spectroscopy (ICP-OES). The obtained results allowed to examine the chemical composition of the synthesized materials and to compare the nominal values of M^{II+}/M^{III+} molar ratios.

Temperature Programmed Reduction (H_2-TPR)

The reducibility of the prepared catalysts was evaluated by H_2-TPR carried out on BELCAT-M (BEL Japan). Prior to the measurement the calcined samples were outgassed at 100°C for 1h. The outgassed samples were subsequently reduced in a flow of 5%H_2/Ar from 100°C to 900°C with a heating ramp of 7.5 °C/min.

The results of the measurements allowed to examine the reducibility of the synthesized samples and to choose the appropriate reduction temperature of the catalyst prior to catalytic tests. Additional information i.e. the strength of metal-support interaction and the type of metal species present in the materials could be obtained from these experiments.

Temperature Programmed Desorption of CO_2 (CO_2-TPD)

The basicity of the studied materials was determined by CO_2-TPD on the same apparatus (BELCAT-M from BEL Japan) as H_2-TPR. The measurements were performed for the reduced samples. The material was cooled down after H_2-TPR to 80°C and a mixture of 10% (vol/vol) CO_2/He was introduced for 1h in order to adsorb carbon dioxide, followed by the desorption of weakly physically adsorbed CO_2 in a flow of He for 15 min. The evolution of desorbed CO_2 was measured with the aid of thermal conductivity detector (TCD) from 80°C to 800°C under He flow with a heating rate of 10°C/min. In order to calculate the number of basic sites of each strength (weak, medium-strength and strong) and total basicity, the TPD profiles were deconvoluted into three Gaussian peaks.

Transmission Electron Microscopy

The reduced and spent catalysts discussed in detail in Chapter 9 (Ni40 and Ni40La2) were additionally examined by Transmission Electron Microscopy (TEM). Based on the analysis of the obtained images, the distribution of nickel particle size was discussed. The

calculation of metallic nickel particle size and the distribution was analyzed using ImageJ software. The dispersion of Ni was determined by the methodology proposed in 'Handbook of heterogenous catalysis' Chapter 3.1.2 by G.Bergeret and P.Gallezot [207].

X-Ray absorption and X-Ray Emission Spectroscopy

Prior to the XAS and XES measurements the calcined hydrotalcites were reduced at 750ºC in stream of 5% H_2/Ar. The sample nomenclature used, depending on the applied treatment is listed in Table 6.2.

Table 6.2 Samples nomenclature for the materials discussed in Chapter 10 according to the applied treatment

Sample label	fresh	After calcination	reduced	operando conditions at 300ºC		
				H_2	CO_2	CO_2 + H_2
Ni40	✓					
Ni40La2	✓					
Ni40 calc	✓	✓				
Ni40La2 calc	✓	✓				
Ni40 red	✓	✓	✓			
Ni40La2 red	✓	✓	✓			
Ni40 H_2	✓	✓	✓	✓		
Ni40La2 H_2	✓	✓	✓	✓		
Ni40 CO_2	✓	✓	✓		✓	
Ni40La2 CO_2	✓	✓	✓		✓	
Ni40 CO_2+H_2	✓	✓	✓			✓
Ni40La2CO_2+H_2	✓	✓	✓			✓

The XAS and XES experiments were carried out at ID26 beamline of the European Synchrotron Radiation Facility (ESRF) in Grenoble, France. The energy of the first inflection point of the Ni K edge was set basing on the calibration results of Ni foil (at the energy of 8333 eV). The HERFD-XANES spectra were registered by scanning of the incident energy and the detection of the fluorescence at the maximum of $K\beta_{1,3}$ emission line. XES spectra were registered at 8.5 keV excitation energy (for both ctc- and vtc-XES). The reference spectra of nickel oxide and hydroxide were recorded on pellets containing 5 wt.% of the sample diluted with cellulose. Ni foil (4 μm) was used to collect the spectra of metallic nickel as reference.

The catalysts Ni40 and Ni40La2 (calcined) were pressed into thin wafers (0.5 mm) and placed inside Maxthal® (Figure 6.6) reactor cell. The Maxthal heating cell was developed at the Sample Environment unit of ESRF and is dedicated to in-situ measurements [208, 209]. The reactants ratio was $CO_2/H_2/He$ = 3/12/5, the total flow was 35 ml/min, the reaction products were analyzed using a micro-GC equipped with a TCD detector. The materials were reduced in-situ using a flow of 12.5%H_2 in He at 750°C. The analysis of the obtained HERFD-XANES data was performed using Athena software of IFEFFIT package.

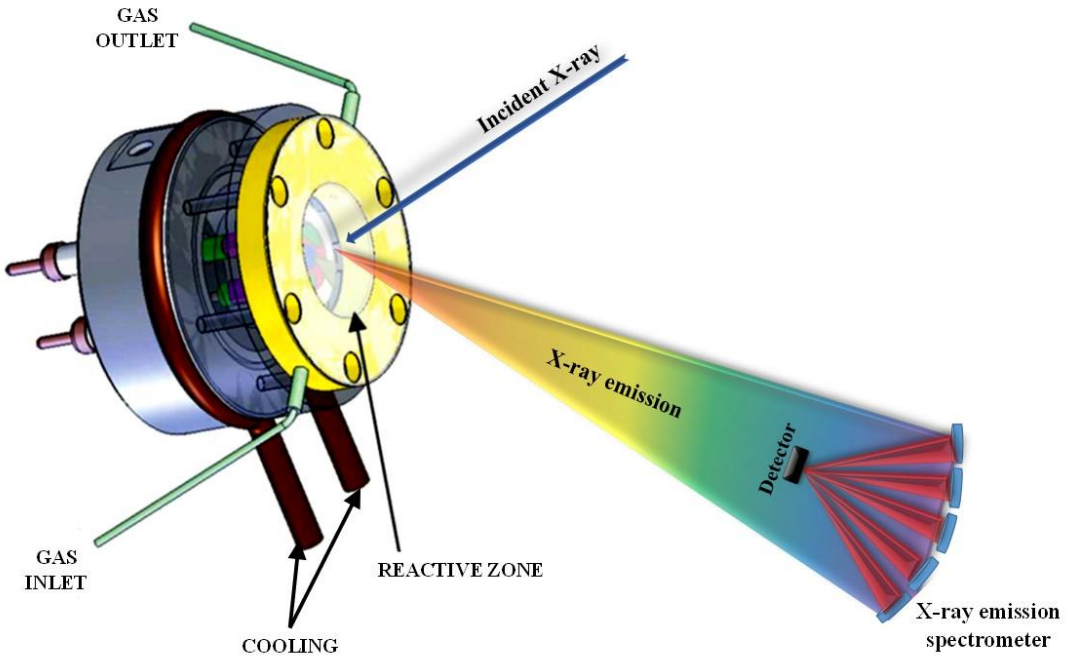

Figure 6.6 Maxthal reactor setup installed at ID26 beamline [208, 209]

6.3. Methanation of carbon dioxide catalytic tests

The activity of the studied catalysts towards methanation of carbon dioxide was evaluated in a fixed-bed reactor catalytic setup presented in Fig. 6.7. The catalyst was placed in a fixed-bed quartz U-type reactor. The ratio $CO_2/H_2/Ar$ was equal to 3/12/5 and the total flow of the mixture was 100 cm^3/min adjusted by several mass flow controllers (BROOKS). The mass of the catalysts was chosen basing on the bulk density measurement to work at constant value of gas hourly space velocity (GHSV) equal to 12000 h^{-1}. The temperature of the catalysts bed and the oven was controlled with the aid of K-type thermocouples and temperature programmer. In order to remove water (product of the reaction) the gaseous products were passed through a water trap and analyzed by a micro gas chromatograph (CPi 490 Varian) equipped with a COX column and a TCD.

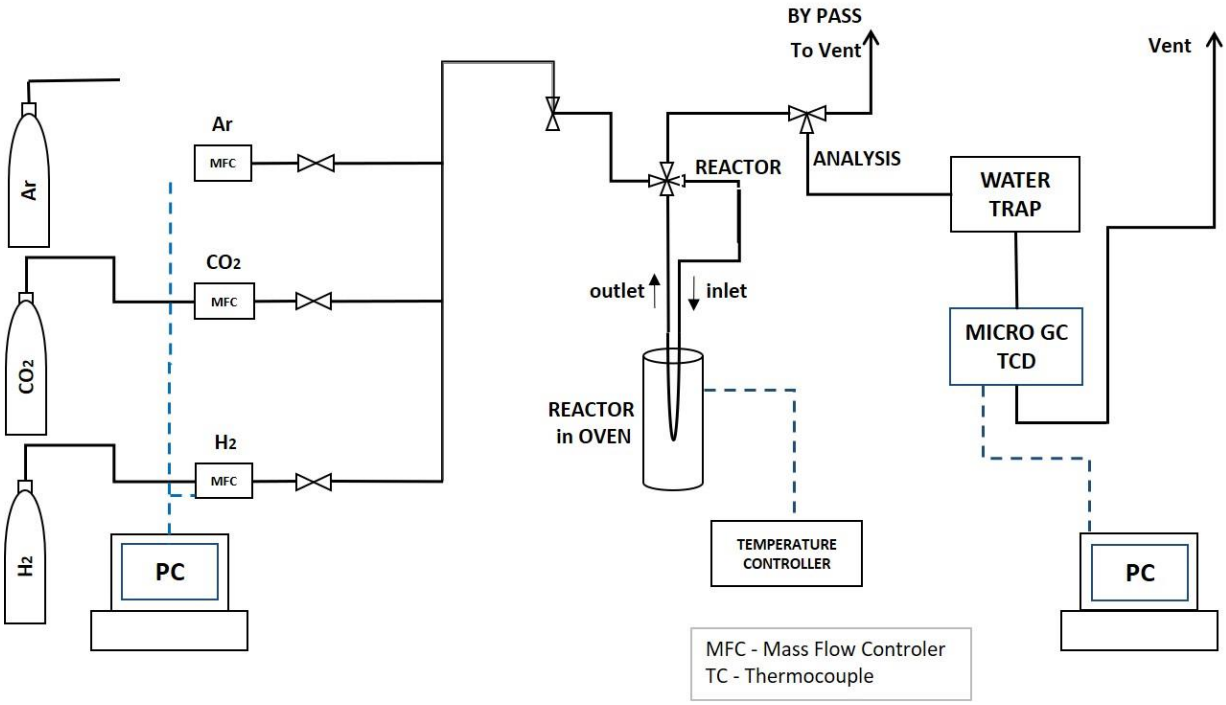

Figure 6.7 Scheme of the catalytic setup

The conversion of CO_2 and CH_4 selectivity were calculated as:

$$CO_2 \text{ conversion} = \frac{CO_{2,in} - CO_{2,out}}{CO_{2,in}} \times 100\% \qquad CH_4 \text{ selectivity} = \frac{CH_{4,out}}{CH_{4,out} + CO_{out}} \times 100\%$$

The catalytic CO_2 methanation tests were carried out as shown in Fig. 6.8. Prior to that the materials were reduced in-situ in a flow of 10%H_2/Ar. Then the catalyst bed was washed with Ar, while cooling down to 250ºC. The feed gas was then introduced into the reactor. The catalytic tests were carried out from 250 ºC to 450 ºC, every 50ºC for 30 minutes of steady state at each temperature.

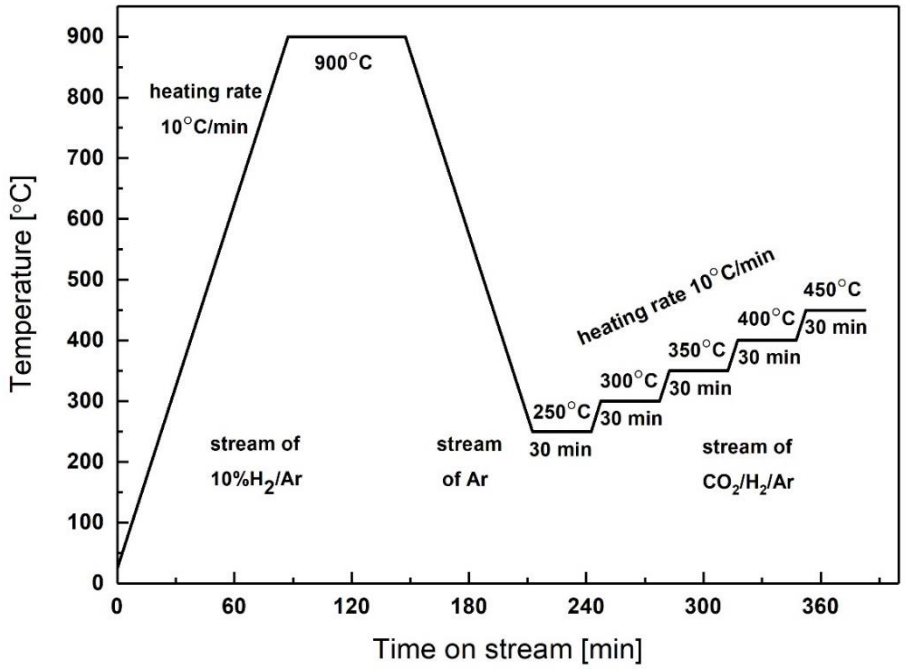

Figure 6.8 Temperature program of CO_2 methanation catalytic tests

TOF values were calculated assuming that the exposed nickel atoms participate in the methanation reaction.

$$\text{TOF} = \frac{nCH_4(mol)}{nNi\ (mol) * t(s)}$$

Results and Discussion

7. Effect of nickel content

No literature reports concerning the influence of nickel content on the catalytic activity of hydrotalcite-like materials in the reaction of CO_2 methanation were found in literature. Therefore, in this PhD thesis, hydrotalcite-like materials containing different amounts of nickel were synthesized by co-precipitation method at constant pH (9.5-10) at 65°C. The materials were characterized by XRD (fresh, calcined, reduced and spent), XRD as a function of temperature (fresh), low temperature nitrogen sorption (calcined), H_2-TPR (calcined), CO_2-TPD (reduced). Selected catalysts were additionally characterized by HERFD-XANES (calcined, reduced) and vtc-XES (calcined, reduced).

Physico-chemical characterization of fresh materials and hydrotalcite-derived mixed oxides

The diffractograms acquired for as-synthesized materials are shown in Figure 7.1. The XRD patterns of all synthesized materials exhibited reflections at 2θ = 11, 24 and 35°, originating from X-ray diffraction on (003), (006) and (009) planes, respectively, indicating the existence of layered hydrotalcite-like structure (3R rhombohedral layered structure, ICOD 00-014-0191). No additional reflections arising from other phases were observed, which suggests a successful incorporation of Ni into the brucite-like layers. As all samples exhibited rhombohedral symmetry, the parameter c of unit cell could be calculated from the position of the first three reflections (eq. 7.1.) or from the position of the first reflection (eq. 7.2.)

$$c = d_{(003)} + 2d_{(006)} + 3d_{(009)} \qquad \text{(eq 7.1.)}$$

$$c = 3d_{(003)} \qquad \text{(eq 7.2.)}$$

where: $d_{(hkl)}$ – basal spacing calculated from the position of the reflections. The values of unit cell parameter *c* were in the range of 23.31-23.46Å as listed in Table 7.1. The parameter c', which is related to the basal spacing between two neighbouring layers, could be calculated because the 3R symmetry of unit cell of hydrotalcite is built of three layers.

Table 7.1 Unit cell parameters values calculated basing on XRD diffractograms

Material	Unit cell parameter c (Å)	c'=c/3 (Å)	Unit cell parameter *a* (Å)	Anions present between brucite-like layers
Ni5	23.40	7.80	3.06	CO_3^{-2} and NO_3^-
Ni10	23.46	7.82	3.06	CO_3^{-2} and NO_3^-
Ni15	23.43	7.81	3.06	CO_3^{-2} and NO_3^-
Ni25	23.37	7.79	3.06	CO_3^{-2} and NO_3^-
Ni30	23.31	7.77	3.06	CO_3^{-2} and NO_3^-
Ni40	23.31	7.77	3.06	CO_3^{-2} and NO_3^-

As the values of parameter *c'* are strongly dependent on the types of anions in the interlayer spaces, the obtained results indicate the presence of carbonate anions and/or nitrates between hydrotalcite layers. The intensity of reflections arising from the hydrotalcite-like structure was decreasing with the increasing nickel content, which suggests a decrease of crystallinity.

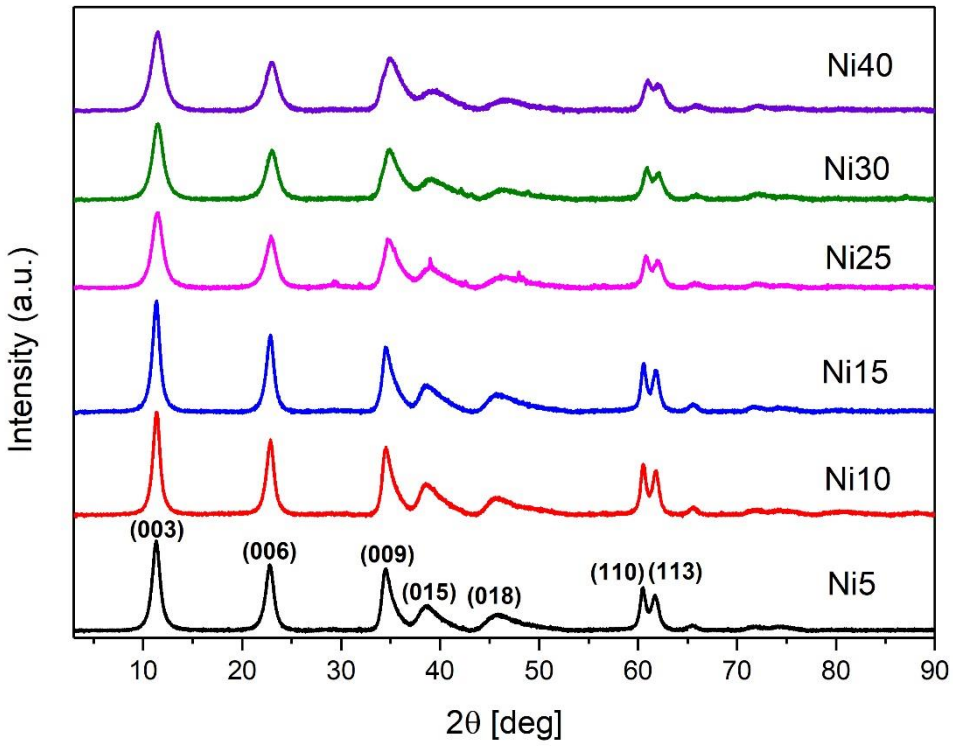

Figure 7.1 XRD diffractograms for as-synthesized hydrotalcite-like materials

The parameter *a* of the unit cell was calculated from the position of the doublet registered at 2θ close to 60º. This parameter describes the average cation-cation distance in the brucite-like layers of hydrotalcite. For all samples the value of parameter *a* was equal to ca. 3.06Å, suggesting no structural changes irrespective of the amount of introduced nickel.

The choice of calcination temperature was based on XRD experiments carried out as a function of temperature between 25°C and 900°C. The obtained diffractograms for Ni15 are shown as an example in Figure 7.2. Four structure types can be distinguished: from room temperature to ca. 200°C, at 200°C, from ca. 300°C to ca. 700°C and over 800°C. The XRD patterns reveal that the layered structure of hydrotalcite-like materials turned to almost amorphous one at around 200°C, followed by the formation of mixed oxides at temperature between 300 and 600°C, and then by spinel structure formation

over 800°C. Similar XRD diffractograms were obtained for other studied catalysts, in good agreement with [3] which reported that the thermal treatment of hydrotalcite-like materials results in the decomposition of the layered structure and the formation of amorphous oxides. The temperatures of calcination proposed in literature for such materials are in the range of 550-600°C. However, as no drastic changes between the structure of the catalysts at 500 and 600°C were observed, the former calcination temperature was chosen.

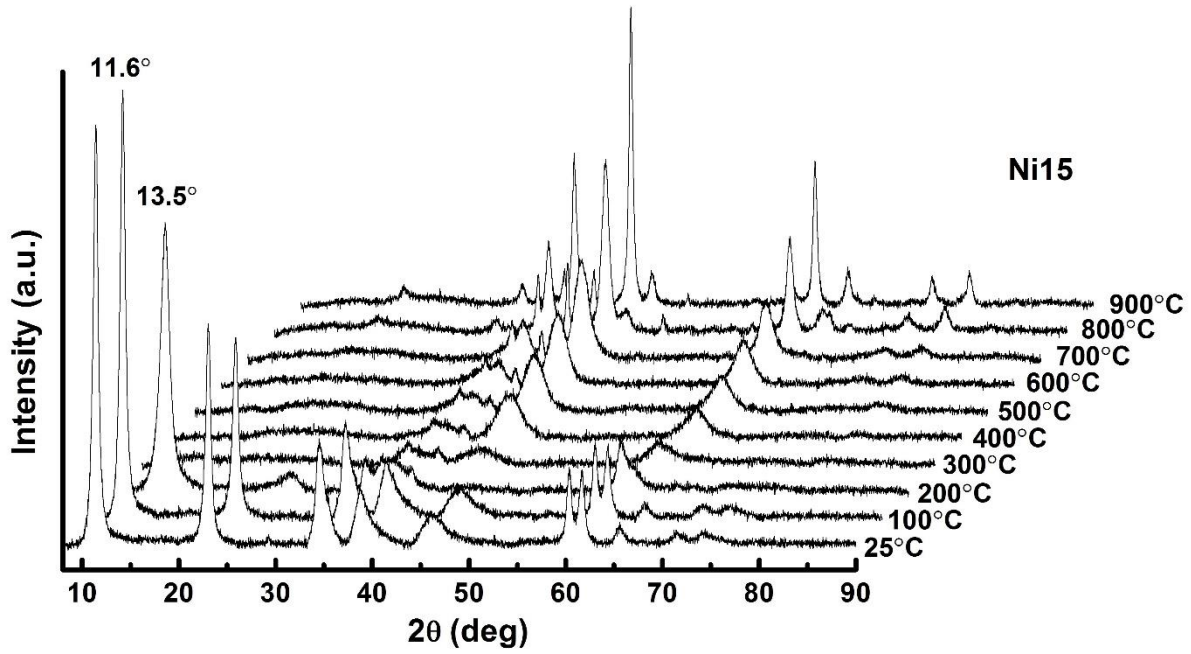

Figure 7.2 XRD as a function of temperature for a selected material (Ni15)

The XRD diffractograms acquired for the materials calcined in air for 5h at 500°C are shown in Figure 7.3. The patterns exhibit reflections typical for periclase-like structure (ICOD 00-045-0946) of Mg(Ni,Al)O mixed oxides obtained after thermal decomposition of hydrotalcite-like materials. The shift of the reflections at $2\theta = 35°$ to higher angles with increasing nickel content occurred because of the formation of NiO

structure with decreasing content of MgO. No other phases were observed for the calcined samples, suggesting that the chosen temperature was insufficient to cause the formation of $NiAl_2O_4$ spinel phase.

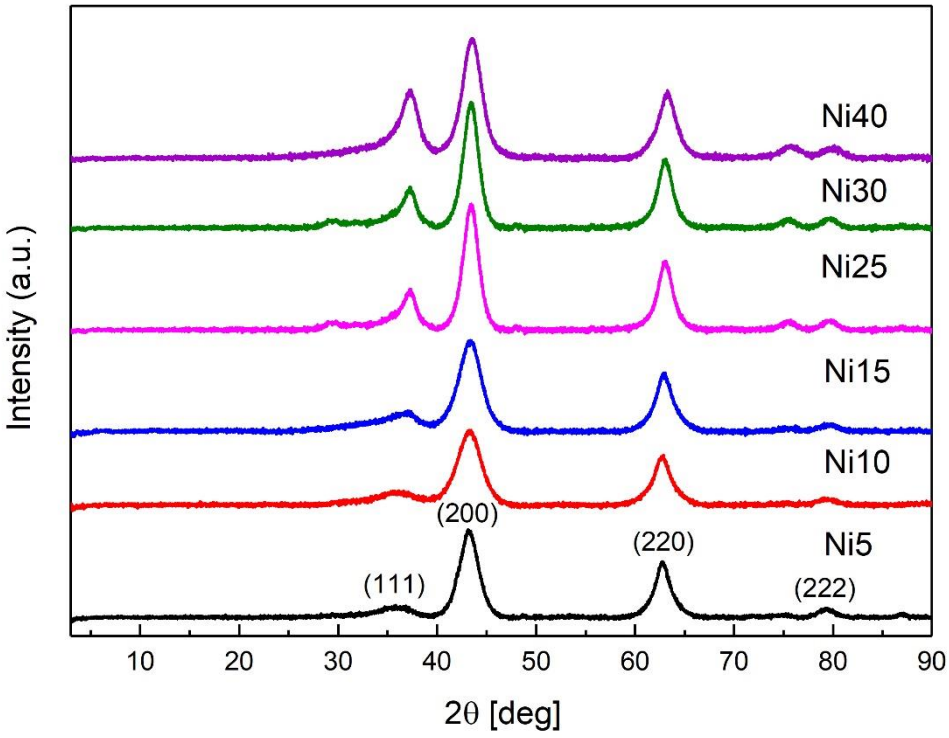

Figure 7.3 XRD diffractograms of HT-derived mixed oxides

The results of elemental analysis of the calcined samples obtained by XRF are presented in Table 7.2. The content of nickel varied from ca. 10.3 wt.% for sample Ni5 to 52.1 wt.% for sample Ni40.

Table 7.2 Theoretical content and elemental analysis results of the HT-derived mixed oxides catalysts

Catalyst	Molar content for fresh samples	Theoretical amount	Elemental analysis (calcined)
	Ni / Mg / Al	Ni wt.% (fresh)	Ni wt.%
Ni5	**0.067 / 0.683 / 0.25**	**5**	**10.3**
Ni10	**0.137 / 0.613 / 0.25**	**10**	**16.2**
Ni15	**0.212 / 0.538 / 0.25**	**15**	**20.1**
Ni25	**0.377 / 0.373 / 0.25**	**25**	**36.8**
Ni30	**0.478 / 0.272 / 0.25**	**30**	**42.5**
Ni40	**0.68 / 0.07 / 0.25**	**40**	**52.1**

Local environment of Ni in hydrotalcite-derived mixed oxides

The High-Energy Resolution Fluorescence Detected (HERFD) X-ray Adsorption Near Edge Spectroscopy (XANES) experiments were carried out to investigate the environment of nickel in selected calcined hydrotalcite-like samples. Figure 7.4 presents the obtained results of HERFD-XANES spectra of Ni5, Ni25 and Ni30, in comparison to Ni foil, NiO and $Ni(OH)_2$, which were used as reference. The spectra registered for the studied materials are almost the same, with features very similar as observed for the reference samples (nickel oxide and hydroxide) indicating that nickel is present in an octahedral coordination.

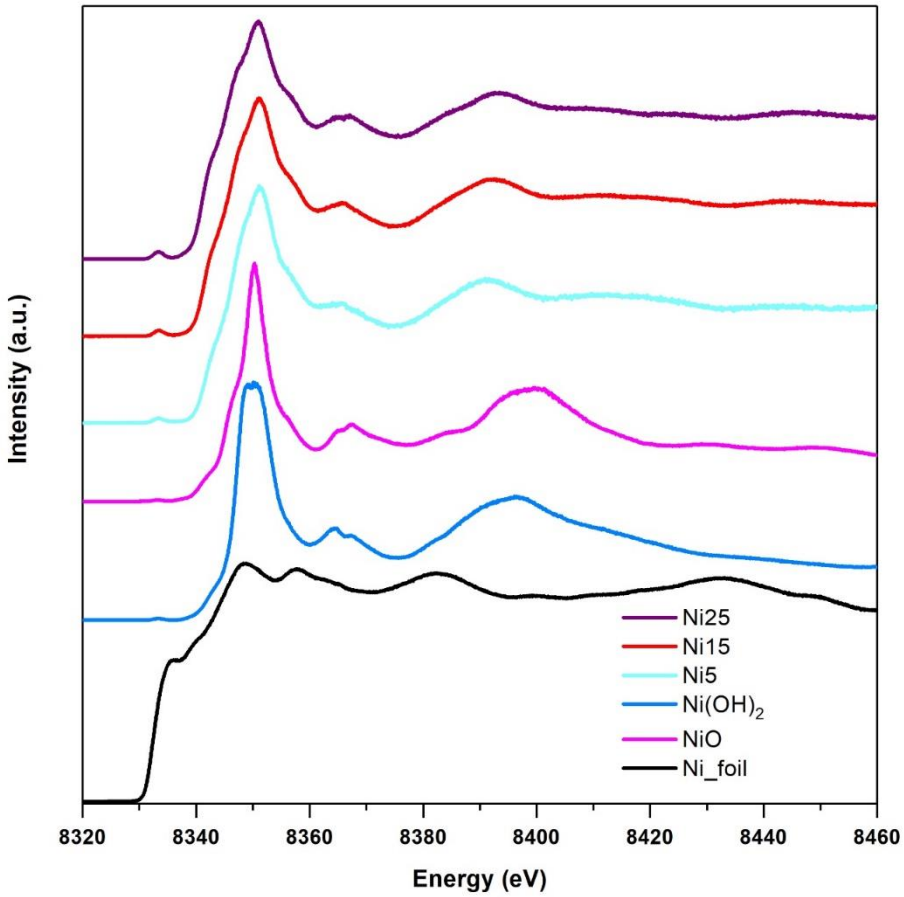

Figure 7.4 HERFD-XANES spectra of Ni5, Ni15 and Ni25, and Ni foil, NiO and $Ni(OH)_2$ as reference materials at room temperature at the Ni K edge

Figure 7.5 presents the valence-to-core (vtc) X-ray emission spectra. The differences between the catalysts in the $K\beta_{2,5}$ spectral shapes are negligible. The spectral features of the studied catalysts are similar to nickel oxide, which proves that Ni environment in the studied catalysts is almost identical to that of the reference. Basing on the obtained results it may be concluded that nickel in the studied catalysts, even with different nickel loading, is present in a similar coordination, and that changes in the Ni/Mg ratio did not influence the chemical finenvironment of NiO in the studied materials.

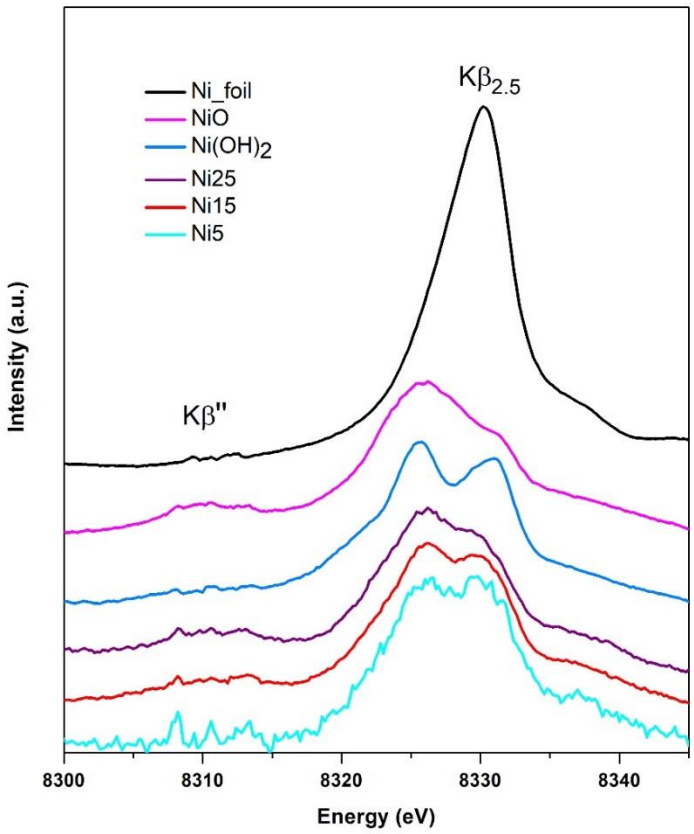

Figure 7.5 vtc-XES spectra recorded at room temperature of calcined Ni5, Ni15 and Ni25, and Ni foil, NiO and $Ni(OH)_2$ as reference materials

Reducibility and characterization of the reduced materials

The H_2-TPR profiles acquired for mixed oxides obtained after calcination of hydrotalcite-like materials are presented in Figure 7.6. All profiles of the studied materials exhibited a wide asymmetric reduction peak arising from the reduction of NiO. The most intense reduction peak for nickel containing mixed oxides derived from hydrotalcites was observed at temperatures of ca. 680-890°C and originated from the reduction of Ni^{2+} present in NiO-MgO solid solution. The maximum temperature of reduction was shifted to lower temperatures with the increasing content of nickel, suggesting decreasing interaction between NiO and other ex-hydrotalcite oxides.

As reported in literature the incorporation of higher amounts of nickel leads to the formation of NiO-MgO solid solution resulting in the decreased interaction between the active material and the support. As reported by Daza *et al.* [210] the reduction of Ni^{2+} in Ni-O-Mg species is not possible in contrast to Ni-O-Ni. Thus, as the increasing concentration of Ni leads to a higher probability of the formation of a higher number of Ni-O-Ni species, the reduction of NiO should then occur at lower temperatures. In order to reduce nickel oxide present in the framework of Mg(Ni,Al)O to metallic nickel it has to be extracted to the support's surface. Apart from the high-temperature TPR peak, an additional one was observed at lower temperatures of ca. 400°C for the samples containing low amounts of nickel (Ni5 and Ni10). It can be attributed to surface nickel oxide reduction, as according to literature the pure nickel oxide phase is reduced at the temperature range of 220-420℃. Li *et al.* [153] reported the reduction peak of bulk NiO at 220℃, while Mile *et al.* [211] found using TPR that bulk NiO reduction was represented by two peaks at ca. 250 and 400℃, corresponding to the reduction of Ni^{3+} and to the reduction of Ni^{2+} species, respectively. Thus, the observed reduction peaks at ca. 380 and 458℃ may arise from the reduction of bulk nickel oxide weakly interacting with the surface of the catalyst.

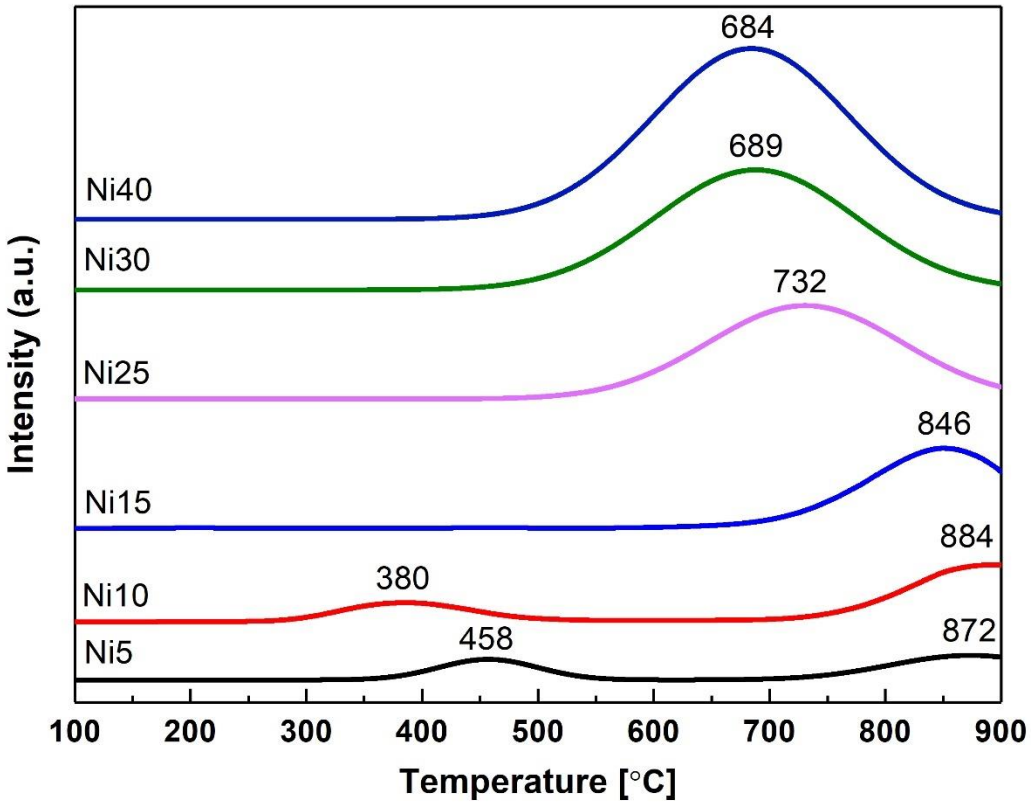

Figure 7.6 H_2-TPR results for the mixed oxides obtained after thermal treatment of hydrotalcite-like materials

XRD patterns of the reduced mixed oxide catalysts are presented in Figure 7.7. All catalysts showed reflections at 2θ of ca. 43, 51 and 76º, characteristic for the cubic structure of metallic nickel (ICOD 01-087-0712). The particle sizes ranged from 6-10 nm, in good agreement with values reported for similar materials. The lowest values were registered for the catalysts with higher Ni content.

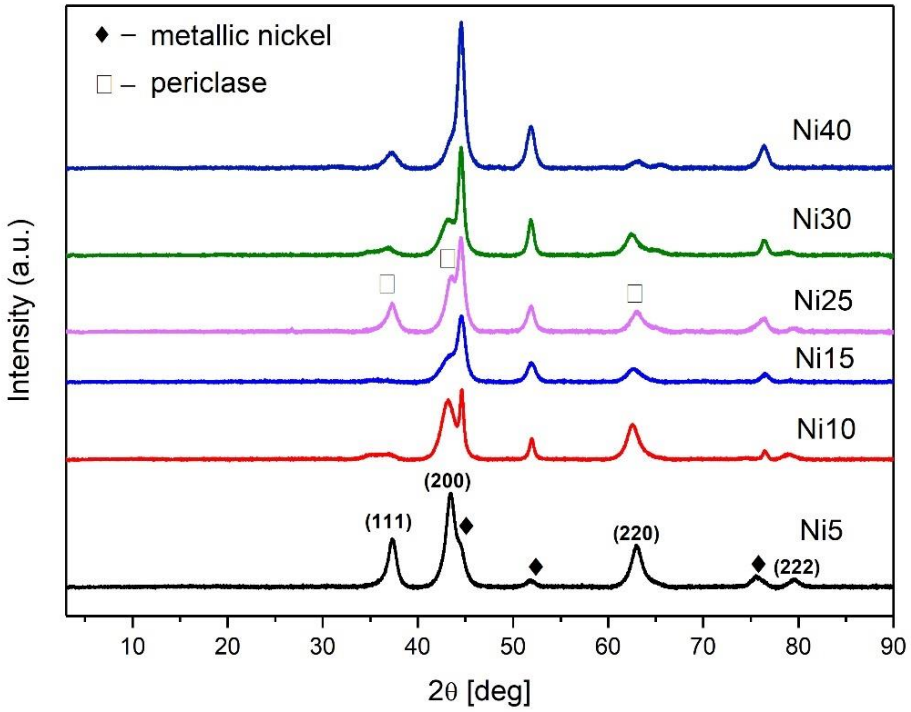

Figure 7.7 XRD patterns for reduced samples

It should be mentioned here that, according to Fan *et al.* [132], smaller particles of nickel enhance the hydrogenation of CO_2 to CH_4, so it may be expected that HT-derived catalysts with higher amount of Ni, which exhibit smaller crystallite sizes of Ni^0, will show better catalytic performance. Ni^0 crystallite sizes of both reduced and spent catalysts are summarized in Table 7.3. No metallic crystallite size changes were found for the catalysts after reaction when compared to the reduced ones.

Table 7.3 Ni crystallite size for the reduced and spent catalysts – based on XRD measurements

Catalyst	Ni particle size [nm]	
	Reduced	**Spent**
Ni5	10	11
Ni10	8	8
Ni15	7	6
Ni25	7	8
Ni30	6	6
Ni40	5	5

As the catalysts used in CO_2 methanation are reduced prior to reaction, the textural properties of the reduced mixed oxides are summarized in Table 7.4. Low temperature nitrogen sorption experiments performed for the reduced catalysts, which are presented in Fig. 7.8, showed that all samples exhibited type IV isotherms (IUPAC), characteristic for mesoporous materials. The reduced materials exhibited either H2 or H3 hysteresis loop, depending on the content of nickel. H3 hysteresis loop, which indicates the presence of slit shaped pores of nonuniform size and shape, was observed for samples Ni5, Ni10 and Ni15. On the other hand, samples Ni25, Ni30 and Ni40 exhibited H2 hysteresis loop, indicating the presence of cylindrical channel pores of nonuniform size and shape. Thus it may be concluded that the increasing content of nickel (with simultaneous decreasing content of Mg) influenced the textural properties of mixed oxides derived from hydrotalcites, where the character and distribution of pore size is concerned.

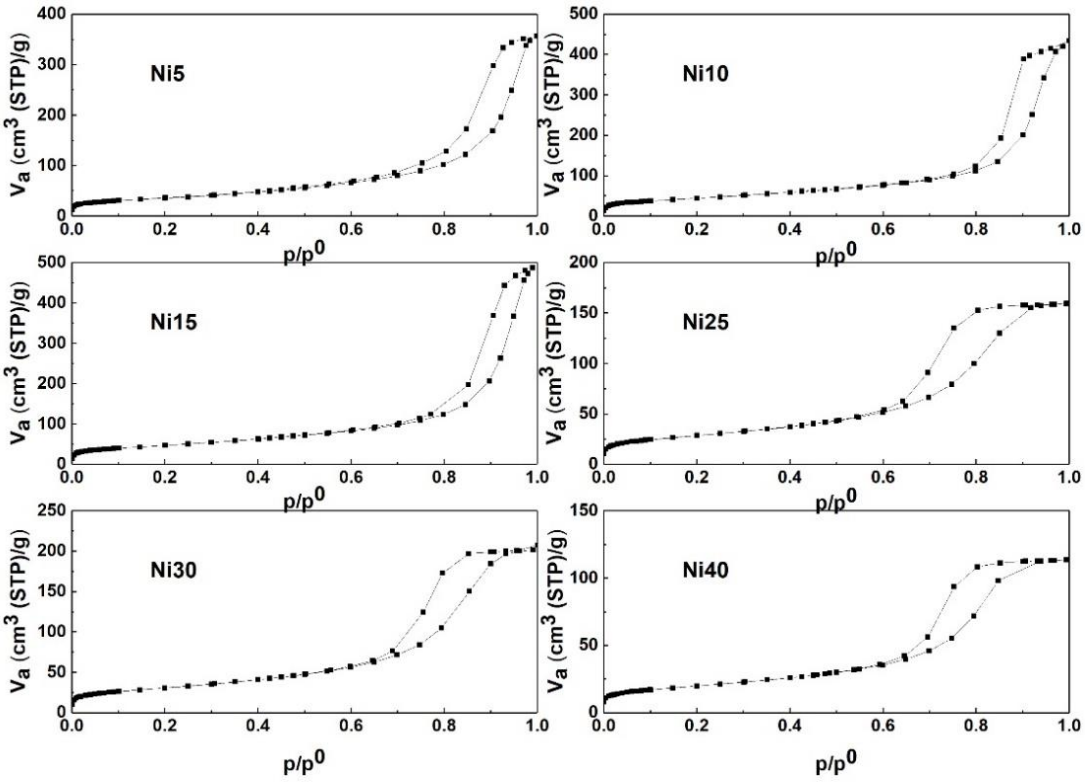

Figure 7.8 N_2 sorption isotherms of reduced samples

The specific surface areas were relatively high, ranging from 71 to 167 m^2/g. The values are in good agreement with literature reports for nickel containing hydrotalcite-derived mixed oxides. From Table 7.4 it may be observed that the introduction of Ni up to 15 wt.% led to the increase in specific surface area from 126 m^2/g for Ni5 to 145 and 167 m^2/g for Ni10 and Ni15, respectively. The increase of S_{BET} and V_{tot} observed for these samples can be explained by structural rearrangement, as confirmed by the shapes of hysteresis loops (Figure 7.8). On the contrary, the incorporation of higher amounts of nickel (samples Ni25, Ni30 and Ni40) led to a decrease in specific surface area from 167 m^2/g for Ni15 to 101, 109 and 71 m^2/g for Ni25, Ni30 and Ni40, respectively. The same observations were made for the total pore volume, with values of 0.52, 0.62 and 0.73

cm^3/g for Ni5, Ni10 and Ni15, respectively, as compared to 0.24, 0.3 and 0.27 cm^3/g for Ni25, Ni30 and Ni40.

Table 7.4 Specific surface area, total pore volume and the mean pore diameter of the reduced HT-derived catalysts

Catalyst	S_{BET} $[m^2/g]$[a]	Total pore volume $[cm^3/g]$	Average pore diameter (nm)
Ni5	126	0.52	17
Ni10	145	0.62	17
Ni15	167	0.73	18
Ni25	101	0.24	9
Ni30	109	0.30	11
Ni40	71	0.27	9

[a]The accuracy of S_{BET} determination is usually assumed to be ca. ± 5 %

The average pore diameter was ca. 17 nm for Ni5, Ni10 and Ni15 and much smaller (9-11 nm) for Ni25, Ni30 and Ni40.

The obtained CO_2-TPD profiles of the hydrotalcite-derived mixed oxides after reduction by 10% H_2/Ar at 900°C are presented in Figure 7.9. The basicity calculated from the obtained profiles is presented in Table 7.5. The literature indicates that it is strongly dependent on the layer's composition, the presence of promoters and type of anions between interlayer species. The obtained CO_2-TPD profiles after reduction of hydrotalcite-derived materials studied in this PhD exhibit one wide asymmetric desorption peak at the temperature range of 125-442°C with three shoulders at 125-171°C, 207-321°C and 321-442°C, similarly as reported in literature [175]. According to Di Cosimo *et al.* [175] the first, second and third desorption peak may be attributed to the

desorption of CO_2, respectively from weak Brønsted OH^- groups, from bidentate carbonates formed on metal-oxygen pairs and to carbon dioxide bonded with low coordination oxygen anions.

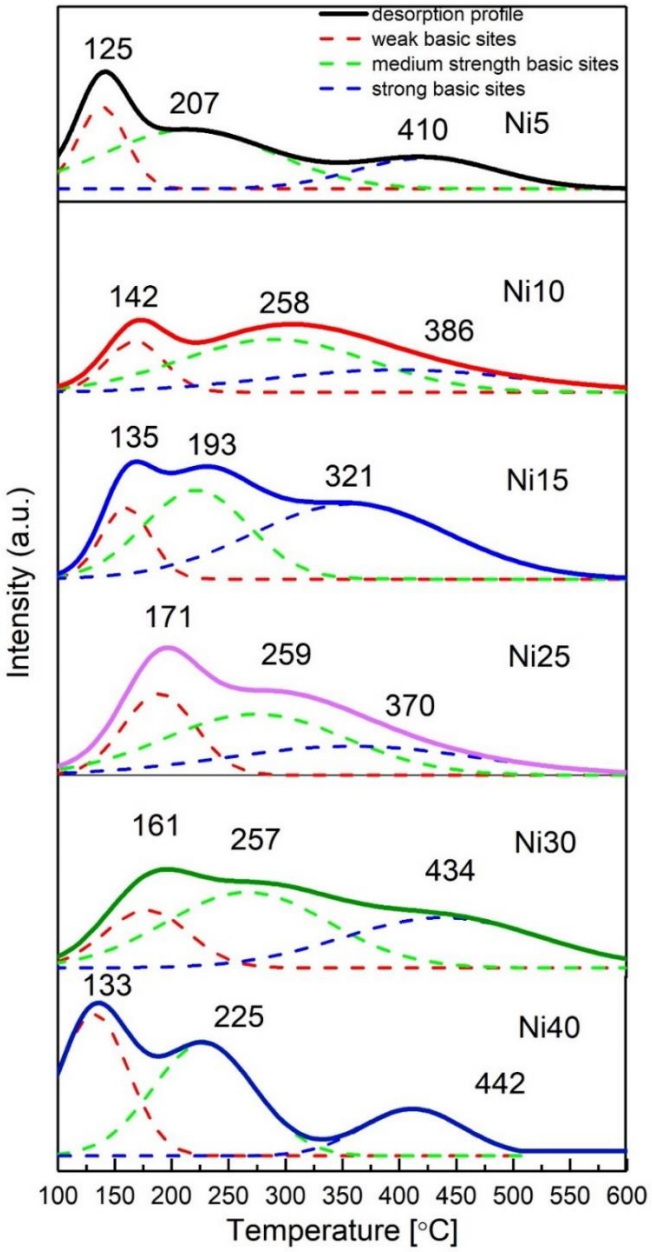

Figure 7.9 CO_2-TPD profiles for the reduced HT-derived catalysts

The total basicity increased with the increasing content of nickel from 52 μmol/g for Ni5 to 60, 81, 113, 134 and 130 μmol/g for the samples Ni10, Ni15, Ni25, Ni30 and Ni40, respectively. Similar results were reported in literature [212]. The number

of moderate basic sites increased with increasing molar ratio of Ni/Mg almost linearly, with the exception of Ni40, indicating a strong influence of the content of nickel on this parameter. The number of weak sites increased only slightly. In case of strong basic sites the changes were almost negligible, except for Ni40 where the number of strong basic sites was almost doubled in comparison to Ni30.

Table 7.5 Basicity of the reduced samples calculated from CO_2-TPD

Sample	Total basicity [µmol/g][a]	The number of basic sites		
		Weak [µmol/g][a]	Medium [µmol/g][a]	Strong [µmol/g][a]
Ni5	52	13	27	12
Ni10	60	15	33	12
Ni15	81	12	46	23
Ni25	113	25	71	17
Ni30	134	34	80	20
Ni40	130	32	59	39

[a] The residual error of the measurement is in the range of 10 µmol/g

Catalytic performance

The conversion of carbon dioxide in the methanation reaction is plotted versus temperature in Fig. 7.10 for all nickel-containing hydrotalcite-derived catalysts.

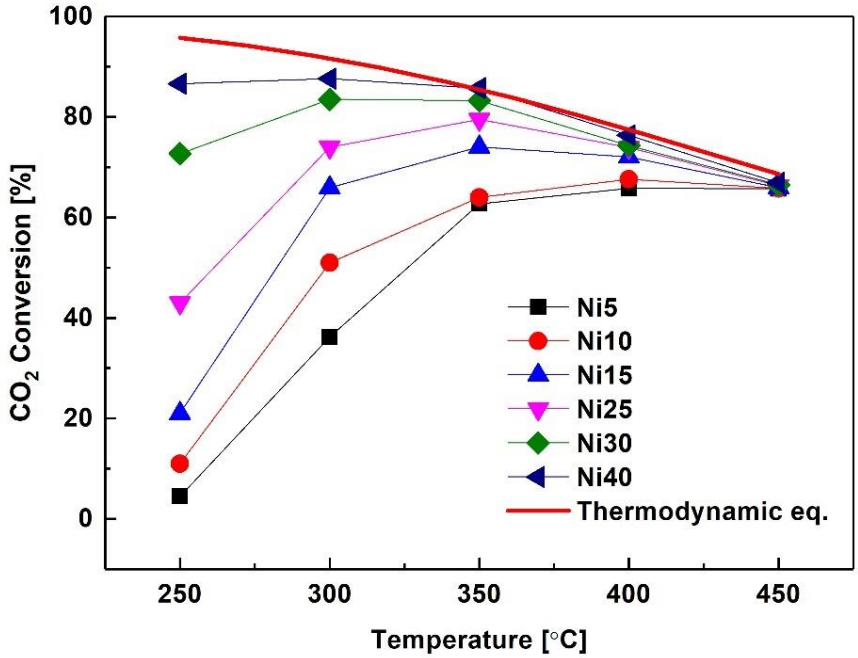

Figure 7.10 CO_2 conversion versus temperature for the obtained catalysts (reduced at 900°C in 10%H_2/Ar, total flow of 100 cm^3/min, GHSV=12 000 h^{-1})

The red continuous line represents the thermodynamic limitation of CO_2 conversion for the reaction carried out under the used conditions. The thermodynamic calculations predict almost complete CO_2 conversion at low temperatures (ca. 250°C) and due to the competing reaction routes - reforming reaction or reverse water gas shift - the decrease in CO_2 conversion at higher temperatures, the latter being the reason of CO formation. All nickel-containing HT-derived catalysts were active in of CO_2 methanation. At 250 and 300°C the conversion for all catalysts was below the thermodynamic limit. The CO_2 conversion values at 250°C were: 5, 11, 21, 43, 73 and 87% for catalysts Ni5, Ni10, Ni15, Ni25, Ni30 and Ni40, respectively, while for 300°C the appropriate numbers were: 36, 51, 66, 74, 79 and 84%, respectively. This proves a strong influence of Ni content on CO_2 conversion. The activity data for all temperatures are summarized in Table 7.6.

Table 7.6 CO_2 Conversion vs temperature for the tested HT-derived catalysts

Catalyst	CO_2 Conversion [%]				
	250°C	300°C	350°C	400°C	450°C
Ni5	5	36	63	66	66
Ni10	11	51	64	66	66
Ni15	21	66	74	72	66
Ni25	43	74	80	74	66
Ni30	73	79	83	74	66
Ni40	87	84	86	76	67

The enhanced activity of catalysts containing higher amount of Ni seems to be a complicated function of crystallite size, the number of moderate basic sites and specific surface area. The number of moderate basic sites seems to be a dominating factor as indicated by Fig. 7.11. Figure 7.12 presents almost linear linear correlation between the specific basicity expressed in μmol/m^2 and CO_2 conversion. As reported by Zhang, higher dispersion of Ni enhanced the activity towards methane as a product, thus the importance of small metallic nickel crystallites should not be neglected. This may have been one of the reasons for the deviations from straight line in Fig. 7.11, especially for Ni40, characterized by the smallest size of Ni^0 crystallites. Another reason could have been differences in specific surface area S_{BET}, as suggested by Fig. 7.12.

To estimate the stability of the catalysts, additional 24h-tests were performed at 250°C. All studied catalysts showed satisfactory stability, with no remarkable change in CO_2 conversion with time-on-stream.

XRD characterization of the catalysts after the catalytic experiments confirmed no variations in of Ni crystal size (cp. Table 7.4). Additionally, no reflections

corresponding to graphitic carbon were observed in the XRD diffractograms at 2θ of ca. 26º.

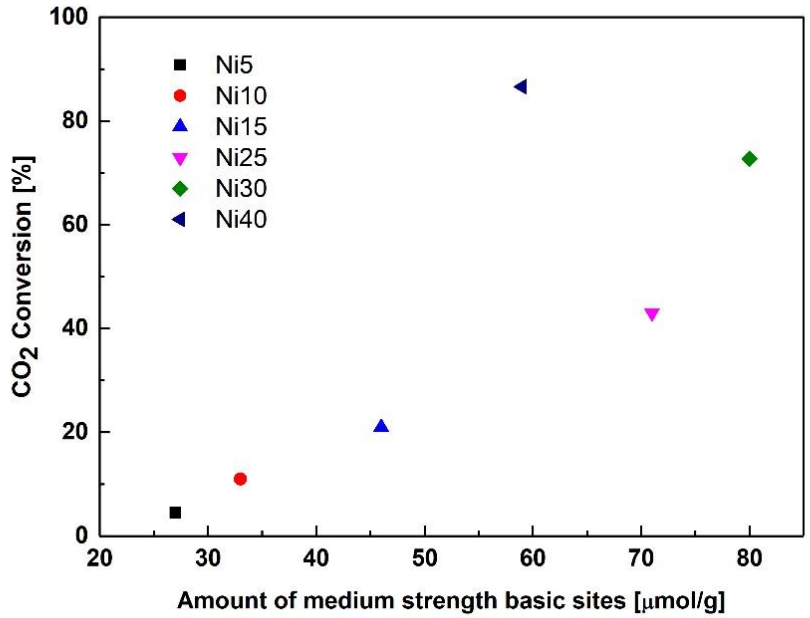

Figure 7.11 CO_2 conversion at 250°C vs number of basic sites μmol/g

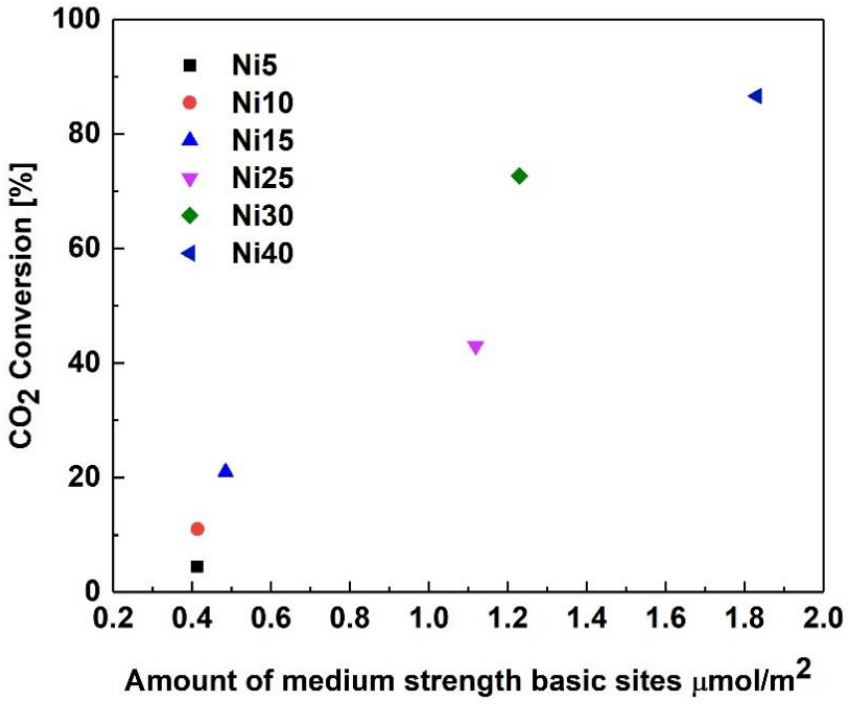

Figure 7.12 CO_2 conversion at 250°C vs number of medium-strength basic sites μmol/m^2

The selectivity towards CH_4 and CO is presented as a function of temperature in Fig. 7.13. At temperatures ranging from 250 to 350°C almost complete selectivity towards methane was recorded, with the exception of Ni5 catalyst. The latter catalyst showed CH_4 selectivity of 97%-98.3% at 250-350°C. At 400-450ºC the selectivity towards methane decreased for all catalysts and low amounts of side reaction product (CO) up to 2.5% were recorded, in good agreement with thermodynamics, which forecasts CO formation via the RWGS reaction.

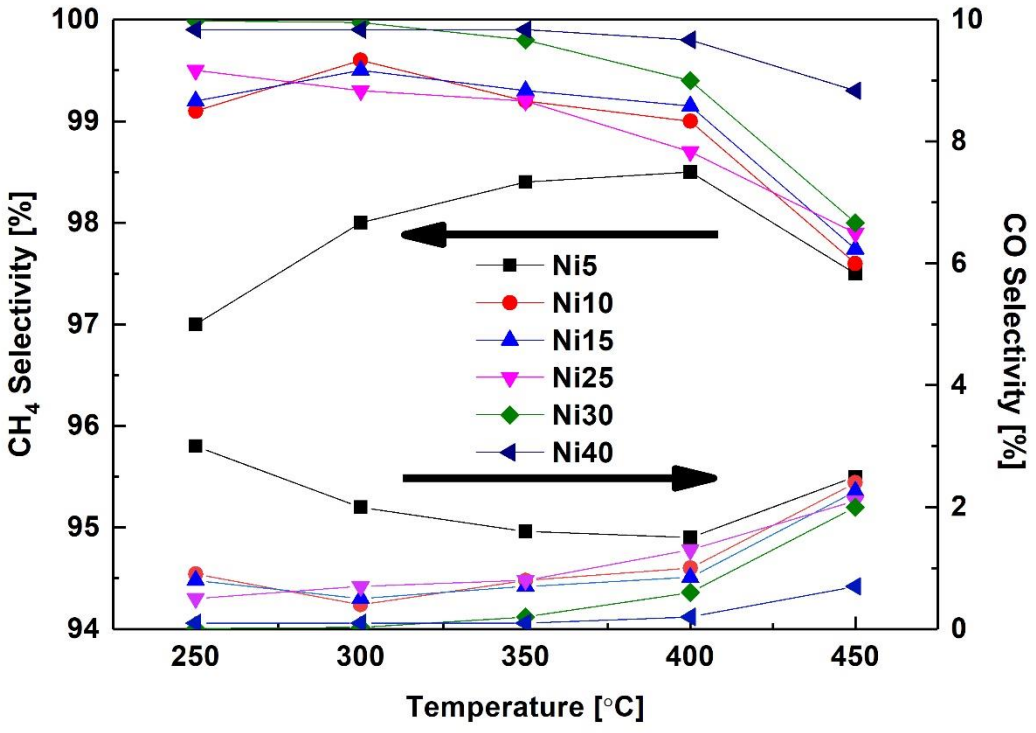

Figure 7.13 CH_4 Selectivity versus temperature for obtained mixed oxides

Effect of Gas Hourly Space Velocity (GHSV)

Figure 7.14 shows the effect of gas hourly space velocity (GHSV) on the methanation performance of a chosen catalyst (Ni40) at temperatures from 250 to 450℃. It may be observed that the CO_2 conversion decreased with increasing GHSV in the whole studied temperature range, as expected because of the reaction operation below thermodynamic equilibrium where a higher GHSV results in lower carbon dioxide conversions. A somewhat higher selectivity towards CO was observed for the catalyst operating at increased GHSV, which can be explained by the reduced contact time of the reactants with the catalyst resulting in decreased chance of CO hydrogenation.

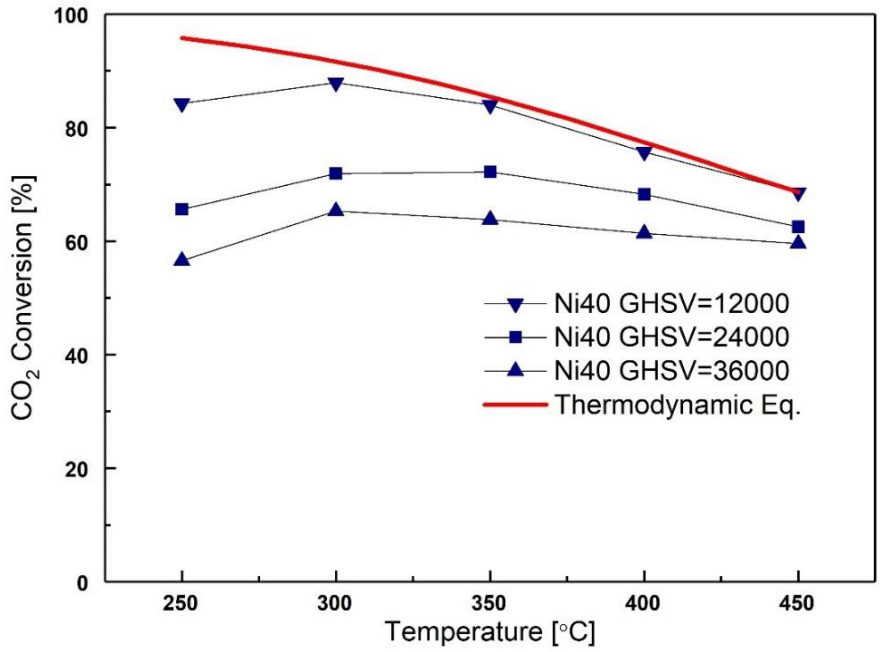

Figure 7.14 Effect of GHSV on the catalytic performance of Ni40 catalyst

Conclusions

Hydrotalcite-like materials containing different amounts of nickel (for the calcined samples from 10.3 to 52.1wt.%Ni) were synthesized by co-precipitation method. The characterization of the fresh samples showed that Ni was introduced into hydrotalcite structure. For the calcined material NiO was present in octahedral environment as confirmed by HERFD-XANES and was not influenced by variations of the ratio of Ni/Mg.

A weakened interaction between Ni and the supports matrix for the materials containing higher amounts of Ni was proven by H_2-TPR. XRD indicated the formation of highly dispersed Ni with Ni^0 particle size ranging between 5-9 nm. The higher amounts of introduced nickel:

- led to smaller Ni^0 crystallites,
- affected the reducibility of the catalysts – reducibility increased with increasing Ni content, and
- influenced the materials CO_2 adsorption capacity.

The distribution of weak basic sites changed only slightly while the number of medium-strength basic sites was strongly affected. The latter had the dominating influence on catalytic performance in methanation of CO_2.

The activity at 250°C increased with increasing nickel content and, almost linearly, with the increase in the number of moderate basic sites. At 250°C CO_2 conversion increased from 4% for Ni5 to 10, 21, 43, 72 and 88.3% for Ni10, Ni15, Ni25, Ni30 and Ni40, respectively. At the same temperature, high selectivity towards CH_4 formation of ca. 99% were registered for all studied catalysts, except Ni5.

The catalytic performance of the studied catalysts in CO_2 methanation at low temperatures (250-300°C) was strongly dependent on the Ni/Mg molar ratio, which varied, 300°C) and resulted in a highly efficient CO_2 methanation catalyst.

8. The influence of promoters on catalytic performance of Ni-hydrotalcites

As reported in the previous Chapter, Ni/Mg/Al hydrotalcite-derived materials showed very good catalytic performance in CO_2 methanation. In this section the work was focused on the investigation of the effect of either iron or lanthanum promotion on the physicochemical properties and catalytic activity in carbon dioxide methanation.

8.1. Influence of Fe incorporation

Recently Ni-Fe catalytic systems found renewed interest because of the possibility of exploiting CO_2 for obtaining methane, as well as in Fischer-Tropsch synthesis. Such catalytic systems showed very high activity in the reaction of carbon dioxide methanation and have a great advantage over rhodium- or palladium-based catalytic systems, because of much lower price of active material.

Hydrotalcite-like materials containing Ni/Mg/Fe/Al were synthesized by co-precipitation at constant pH. All synthesized materials had a fixed M^{2+}/M^{3+} molar ratio with a varying Fe^{3+}/Al^{3+} ratio. The theoretical amount of iron introduced into brucite-like layers was 1, 2 and 4 wt.%. This chapter presents their physico-chemical characterization and the catalytic performance in the reaction of carbon dioxide methanation.

Physicochemical properties of Fe-promoted Ni-containing HT-precursors and the derived catalysts

The results of elemental analysis performed by ICP-OES technique and textural properties are presented in Table 8.1 for the calcined samples.

Table 8.1 Elemental analysis and texture of calcined Ni-Fe-hydrotalcites

Sample	S_{BET} $[m^2/g]^1$	Total pore volume $[cm^3/g]$	Elemental Analysis [wt.%]		
			Ni	Fe	Mg
Ni15	162	0.54	20.1	-	21.7
Ni15Fe1	169	0.34	20.0	1.5	21.4
Ni15Fe2	113	0.26	20.0	2.8	21.3
Ni15Fe4	106	0.22	20.0	5.6	21.0

[1]The accuracy of S_{BET} determination is usually assumed to be ca. ± 5 %

Specific surface area S_{BET} ranged from 106 to 169 m^2/g. From Table 8.1, it may be seen that the incorporation of 1.5 wt.% of iron did not change S_{BET}, while higher amounts of Fe resulted in its decrease by ca. 30-34%. The total pore volume decreased from 0.54 for Ni15 to 0.34, 0.26 and 0.22 cm^3/g, for Ni15Fe1, Ni15Fe2 and Ni15Fe4, respectively.

Figures 8.1 and 8.2 present the XRD patterns for the fresh and calcined catalysts, respectively. The patterns for the fresh hydrotalcite catalysts show typical reflections and as mentioned in the previous chapter, indicate the existence of a multilayer hydrotalcite-like structure. The unit cell parameters values calculated basing on XRD diffractograms according to the method proposed by Rives *et al.* [213] were in the range of 23.02 – 23.48Å for *c*, while the values of *a* were 3.04Å for all samples indicating the absence of any influence of introduced Fe on the parent hydrotalcite structure. Since no other nickel or iron species were observed as separate phases, the results point to a successful incorporation of these metals into the structure of hydrotalcite.

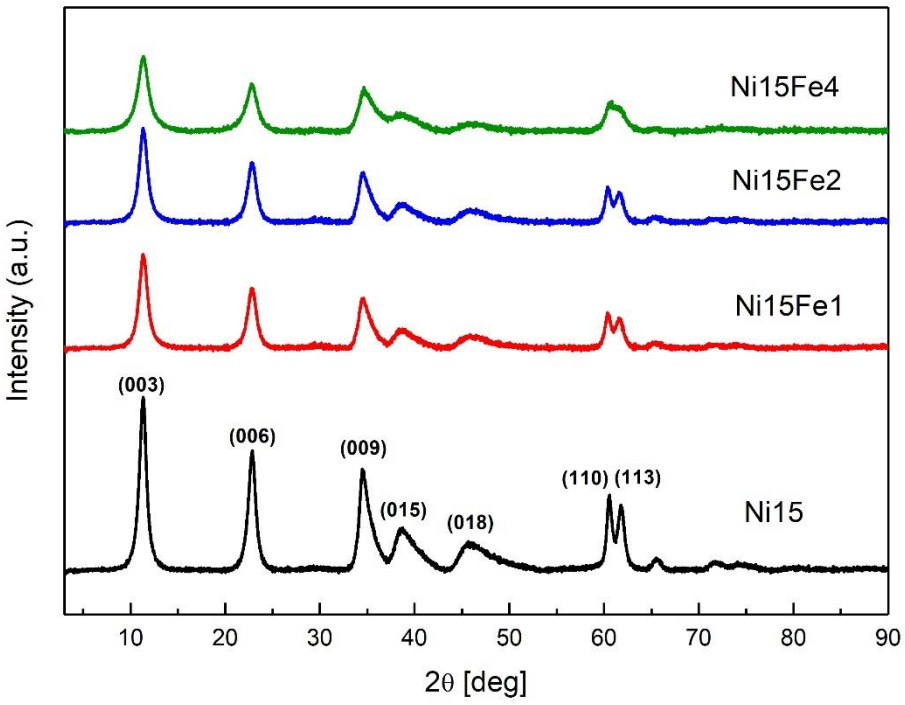

Figure 8.1 XRD patterns of as-synthesized Ni and Ni-Fe hydrotalcite-like materials

The XRD diffractograms of the catalysts after calcination at 500°C for 5h presented in Fig. 8.2 show reflections typical for periclase-like structure at 2θ = 43.5° and 63.0°, as expected for the samples derived from hydrotalcite materials after thermal treatment at this temperature. However, as reported in literature, iron containing HTs materials may form spinel-like structure even at temperatures lower than used in this work [214, 215]. It should be stressed that no such phases or any other Ni- or Fe-containing phases were registered for the studied samples, which again confirms the incorporation of Ni and Fe into the periclase-like structure. Additionally, it is worth noting that the increasing content of Fe affected the amount of NiO phase formed, as indicated by the shift of the reflection at 2θ from ca. 35° to higher values.

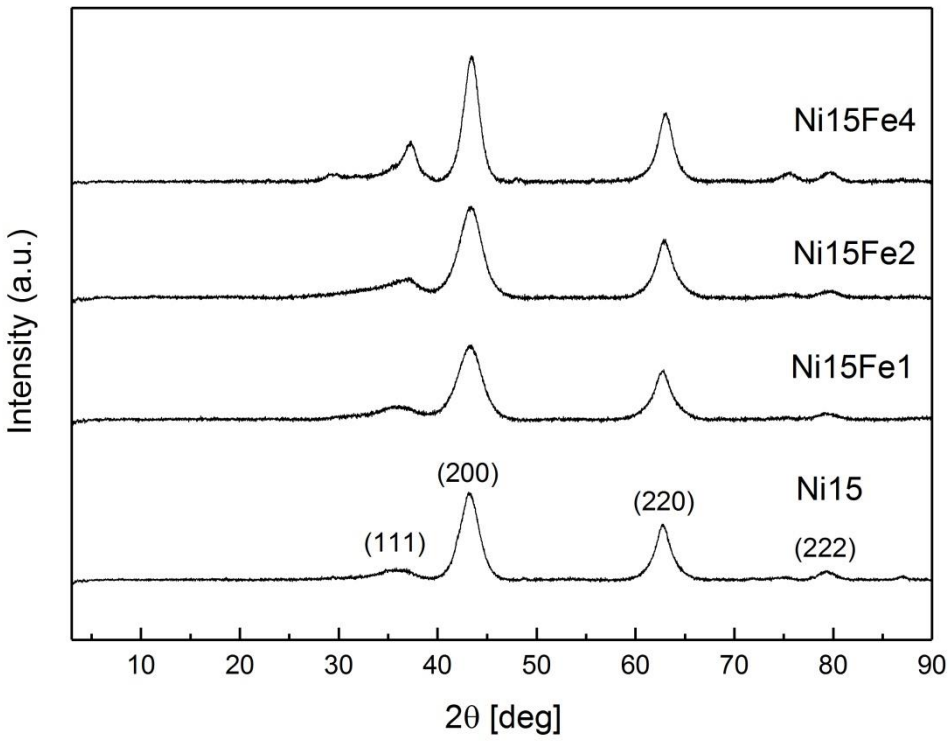

Figure 8.2 XRD patterns of mixed oxides obtained after thermal treatment of Ni and Ni-Fe hydrotalcite-like materials

Reducibility and basic properties of Fe-promoted Ni-containing hydrotalcite-derived mixed oxides

In order to examine the metal-support interactions and the reducibility of the catalysts TPR measurements were carried out. Figure 8.3 shows H_2-TPR profiles for the calcined catalysts. All profiles, except that for Ni15 catalyst, exhibit two wide asymmetric peaks with a maximum at temperatures between 346 and 380°C, and from 709 to 850°C. The first hydrogen consumption peak may be assigned to the reduction of iron oxide weakly interacting with Mg(Al)O [215]. As Fe^{2+} cannot be completely reduced to metallic iron below 800°C it can be attributed to the reduction of Fe^{3+} to Fe^{2+}. The second peak was registered at much higher temperature and may be assigned to nickel oxide which

strongly interacts with its surroundings, as a result of the existence of a thermally stable solid phase solution of mixed oxides Mg(Ni,Al)O [212]. As reported in literature, the reduction of Fe^{2+} to Fe^{0} takes place at higher temperatures (500-900°C), but it is impossible to distinguish between the peaks originating from the reduction of Fe^{2+} and Ni^{2+} [215]. The obtained results point to homogenous dispersion of cations, which resulted in a strong interaction between the active phase and supports matrix. It can be also observed that the incorporation of Fe increased the reducibility of NiO species, as indicated by the high temperature H_2 consumption peak shifting from 850 for Ni15 to 798, 752 and 709°C for Ni15Fe1, Ni15Fe2 and Ni15Fe4, respectively. The XRD patterns acquired for the catalysts reduced at 900°C confirmed the existence of metallic nickel and periclase structure, and suggest that either iron oxide species were not, or not fully, reduced to metallic iron, or Fe entities formed were of the size under detection level of XRD.

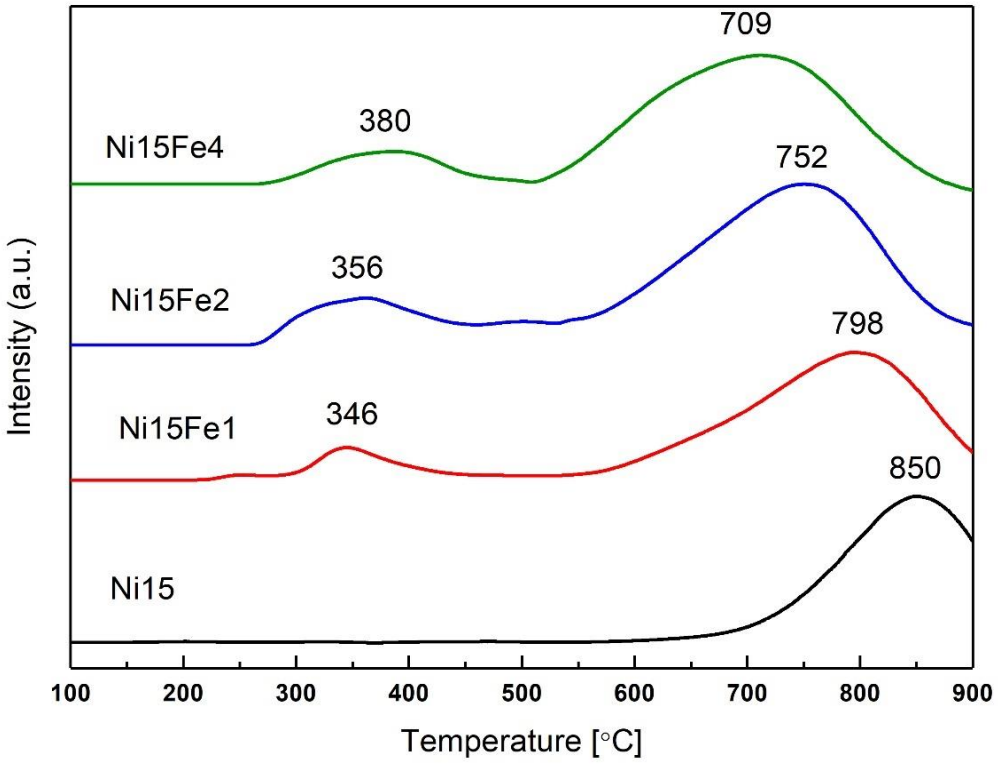

Figure 8.3 TPR profiles obtained for calcined Ni and Ni-Fe materials

The XRD diffractograms of the reduced Ni-Fe HT-derived mixed oxide catalysts compared to Ni-hydrotalcite in Fig 8.4 reveal the existence of periclase-like structure (MgO) and metallic nickel phase (Ni^0), the latter with particle sizes ranging from 6-10 nm in good agreement with values reported in literature [214]. The crystallite sizes increased somewhat with the increasing amount of incorporated iron, from 7 nm for Ni15 to 7, 8 and 9 nm for Ni20Fe1, Ni20Fe2 and Ni20Fe4, respectively (cp. appropriate data further in the text - Table 8.3). The reflections corresponding to metallic nickel shifted to

smaller 2θ values with increasing Fe content, indicating the formation of Ni-Fe alloy, as registered previously in literature [216, 217].

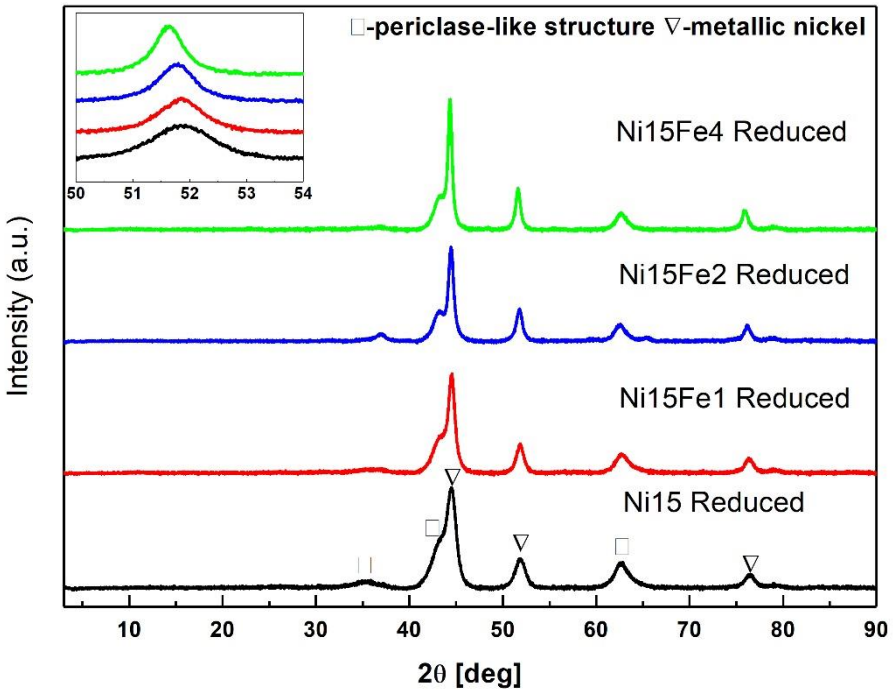

Figure 8.4 XRD patterns of reduced Ni and Ni-Fe mixed oxides reduced at 900°C

Figure 8.5 compares the CO_2-TPD profiles obtained for the Ni-Fe HT-derived materials after reduction by 10% H_2/Ar at 900°C with that for Ni hydrotalcite similarly treated. The basicity data are summarized in Table 8.2.

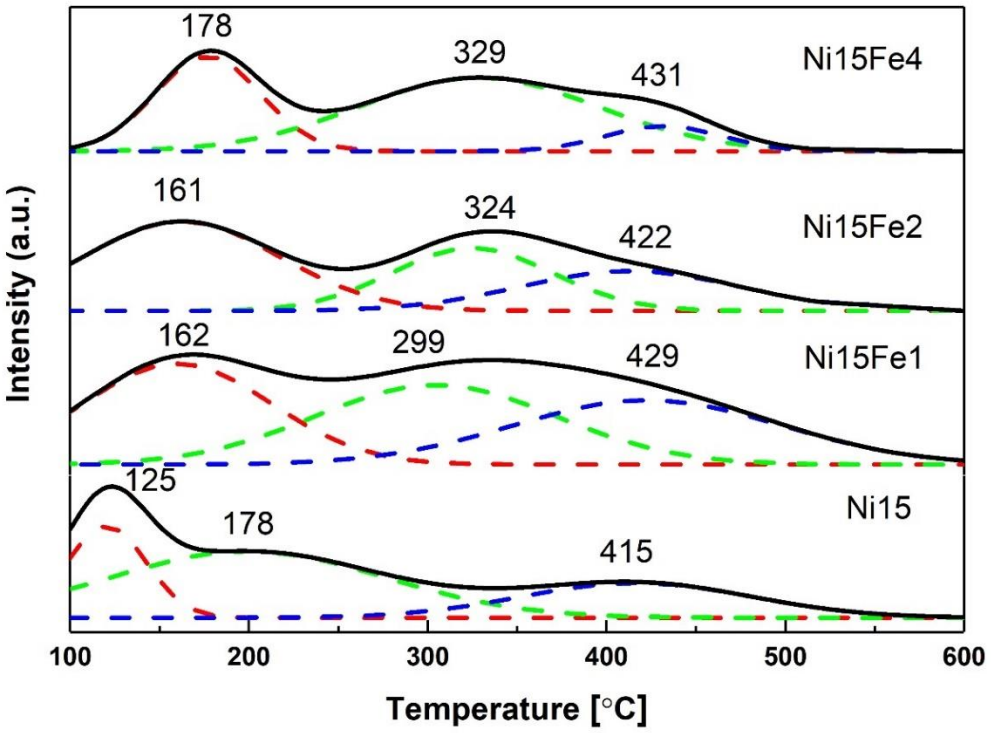

Figure 8.5 CO_2-TPD profiles of Ni and Ni-Fe-HT reduced samples

The total basicity increased slightly after the addition of 1.5 wt.% of iron from 81 for Ni15 to 101 μmol/g for Ni15Fe1. However, after incorporation of 2.8 and 5.6 wt.% of iron the basicity decreased somewhat from 81 for Ni15 to 73 and 72 for Ni15Fe2 and Ni15Fe4, respectively. The incorporation of iron into the nickel containing hydrotalcites influenced, additionally, the distribution of basic sites in a way depending on Fe content. There was: (i) a slightly increased number of weak sites for all Fe-promoted catalysts when compared to Ni15, (ii) an increase in the number of moderate sites for Ni15Fe1 and a slight decrease for Ni15Fe2 and Ni15Fe4, and (iii) a slight decrease of the number of strong sites after incorporation of Fe.

Table 8.2 Basicity (CO_2-TPD) and crystallite sized of Ni^0 particles (XRD) of reduced Ni and Ni-Fe samples

Sample	Total basicity [μmol/g][a]	Weak sites [μmol/g][a]	Medium sites [μmol/g][a]	Strong sites [μmol/g][a]
Ni15	**81**	**12**	**46**	**23**
Ni15Fe1	**101**	**38**	**60**	**13**
Ni15Fe2	**73**	**27**	**32**	**14**
Ni15Fe4	**72**	**31**	**23**	**18**

[a] The residual error of the measurement is in the range of 10 μmol/g

Activity and selectivity in CO_2 methanation

Fig. 8.6 shows carbon dioxide conversion as a function of reaction temperature for nickel-containing catalysts with and without iron promotion. All tested catalysts were active in the reaction of carbon dioxide methanation. Although the CO_2 conversion at 250˚C was lower than the thermodynamic limit, an improvement, strongly influenced by the amount of incorporated iron, could be observed. Low amounts of introduced iron (1 and 2 wt.% for fresh samples) resulted in a significant increase in activity of the catalysts as compared to Ni15, which at 250°C showed 21% CO_2 conversion as compared to 42% and 76% for Ni15Fe2 and Ni15Fe1, respectively. On the other hand, the addition of higher amount of Fe (5.6 wt.%) significantly decreased the activity to 7%. It is also worth noting that the activity of the catalyst containing 2.8 wt.% Fe (calcined sample) was higher at 250˚C than that for Ni15 catalyst but lower at higher temperatures. The enhanced activity of the sample containing 1.5 wt.% of iron (calcined sample) as compared to Ni15 may have its origin in the simultaneous improvement of the following properties: (i) the

highest S_{BET} of the catalysts, (ii) the increased reducibility of nickel species and (iii) the highest content of basic sites of medium strength of all strength, which, as proposed by Pan *et al.* [218] are involved in the reaction of CO_2 methanation. The latter may have been the dominating effect, as shown for the unpromoted Ni-hydrotalcite in the previous Chapter. The decreased activity of the catalysts containing highest amount of iron (5.6 wt.% for calcined sample), on the other hand, may be explained by a drastic decrease in specific surface area, which suggests partial coverage of the catalysts surface by iron species. This resulted in a strong decrease in the number of basic sites of medium strength and this effect could not be compensated by higher reducibility of this catalyst. At higher temperature applied in our experiments (350 and 400°C), Ni15Fe1 catalyst showed CO_2 conversion values at or almost at thermodynamic limit. At 400°C all samples, except Ni15Fe4 reached thermodynamic equilibrium. The incorporation of Fe into Ni-hydrotalcites did not have any major influence on either Ni-sintering or carbonaceous deposits formation.

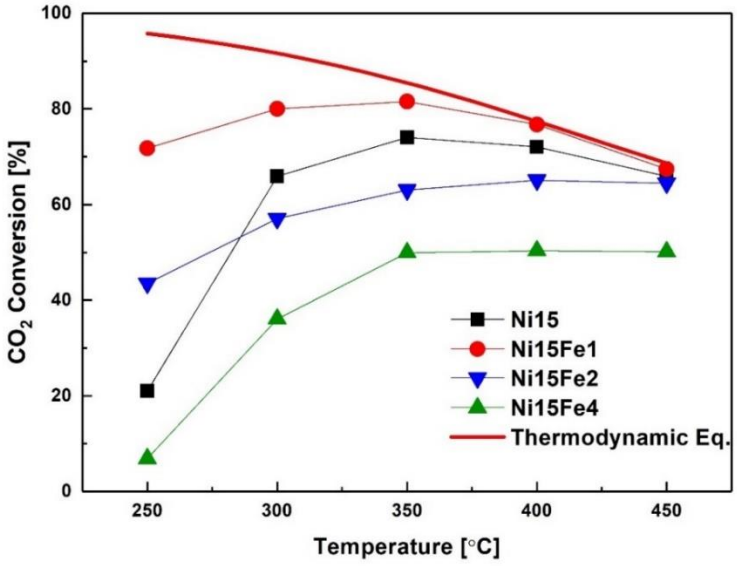

Figure 8.6 CO_2 conversion versus temperature for Fe-promoted Ni-containing HT-derived catalysts

As shown in Table 8.3, the metallic nickel crystallite sizes for the spent catalysts did not change when compared to the reduced ones. No reflections arising from graphite at 2θ = 26° were observed for the spent catalysts. Thus, extensive coking with graphite formation may be excluded, in agreement with the results obtained by Abate *et al.* [133] who reported that carbon deposition was absent on Ni/Al-HT catalysts in carbon dioxide methanation.

Table 8.3 Crystallite size of Ni^0 for the reduced and spent Ni-containing Fe-promoted HT-derived catalysts

Sample	Crystallite size [nm][b]	
	Reduced	Spent
Ni15	7	6
Ni15Fe1	7	8
Ni15Fe2	8	8
Ni15Fe4	9	9

Fig. 8.7 depicts the selectivity towards methane in a function of temperature. The incorporation of Fe did not decrease the high selectivity to methane, except for Ni15Fe4 and, to a smaller extent, the results at 450°C for the other Fe-promoted catalysts. At low temperature range of 250-300˚C almost total selectivity towards methane was recorded, except the sample containing 5.6 wt.% Fe. The Ni15Fe4 catalyst showed CH_4 selectivity of 97% at 250°C. For Ni15, Ni15Fe1 and Ni15Fe2 the selectivity towards methane was almost the same at the temperature range of 250-350˚C, and at 450˚C only 2-4 % of side reaction product (carbon monoxide) were recorded for Ni15, Ni15Fe1 and Ni15Fe2, while 21% selectivity towards CO was registered at 450°C for Ni15Fe4. The formation

of this by-product at higher temperatures originates, according to the thermodynamic predictions, from reverse water gas shift reaction. No other products, except CH_4 and CO, were registered during the catalytic tests.

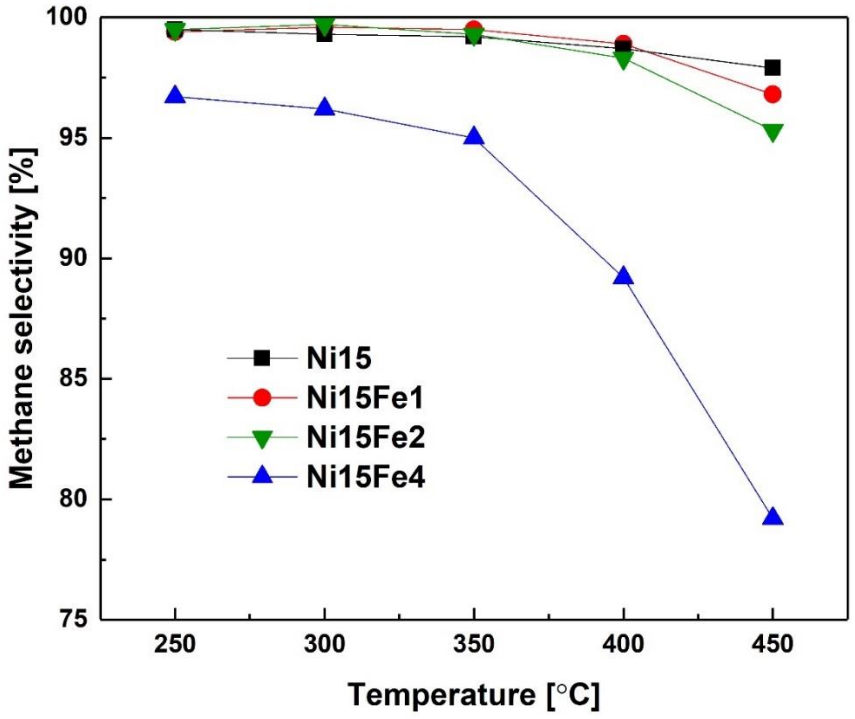

Figure 8.7 CH_4 selectivity vs temperature for Fe-promoted Ni-HT catalysts

Conclusions

Iron-promoted Ni-HT-derived materials were prepared by co-precipitation method. All obtained catalysts were characterized by low temperature N_2 sorption, ICP-OES, XRD, H_2-TPR and CO_2-TPD and tested in the reaction of carbon dioxide methanation at GHSV = 12000h^{-1} using a mixture of CO_2/H_2/Ar with molar ratio of 3/12/5.

The XRD results suggest the successful incorporation of both nickel and iron into the structure of hydrotalcite. The introduction of iron into the nickel-containing hydrotalcite

resulted in increased reducibility of the samples due to the weakened Ni-MgO interaction. The specific surface area was not changed when low amount (1.5 wt.%) of Fe was added while higher amounts (2.8 or 5.6 wt.%) led to the S_{BET} decrease by ca. 30%. The XRD experiments suggest the formation of highly dispersed metallic nickel phase with particle size ranging from 7-9 nm. No crystallite size changes were observed for the catalysts after reaction as compared to the reduced ones. The incorporation of iron affected the CO_2 adsorption capacity of the catalysts only to a small extent. However, it influenced the distribution of basic sites and in this case the amount of Fe was the determining factor. There was a slight increase of the number of weak sites, a strong increase in the number of medium-strength sites and a decrease when higher amounts of Fe were introduced. The number of strong sites was decreased after incorporation of Fe. The activity of the catalysts at low temperature (250˚C) increased after the incorporation of 1.5 and 2.8 wt.% of Fe when compared to the sample containing only Ni (Ni15). However, after incorporation of 5.6 wt.% Fe the activity decreased. The dominant influence on activity may be assigned to changes in basicity, with some additional influence of S_{BET} and reducibility. However, the first two effects, if negative, dominated over the reducibility improvements, as observed for the catalyst with the highest amount of iron (Ni15Fe4).

8.2. The influence of La promotion

The choice of La as promoter was based on literature studies. Zhi *et al.* indicated that Ni-containing SiC catalyst promoted with lanthanum showed higher activity in comparison to the non-promoted one [154]. However, lanthanum was not considered as promoter of Ni-hydrotalcites in their function as CO_2 methanation catalysts.

Lanthanum-promoted Ni-HT-like materials were synthesized by co-precipitation method at controlled pH. All prepared materials had a fixed molar ratio of M^{2+}/M^{3+}, and the varying parameter was Al^{3+}/La^{3+}. This Chapter presents the results of physicochemical characterization of the prepared Ni-containing La-promoted materials and their catalytic evaluation towards CO_2 methanation reaction. As it will be described in this Chapter, lanthanum was not successfully incorporated into the brucite-like layers of hydrotalcite via co-precipitation, therefore this Chapter was divided into two subchapters, which were focused on influence of, respectively, lanthanum introduction via co-precipitation and adsorption or impregnation.

Influence of lanthanum promotion using co-precipitation method

Physico-chemical properties of the catalysts

The elemental analysis of the calcined samples was determined by XRF and is presented in Table 8.4. La addition to the preparation mixture had almost no effect on the content of nickel in the calcined samples, thus, XRF analysis has proving that the composition of mixed oxide materials derived from hydrotalcites may be strictly controlled during the synthesis, even in the presence of La as promoter.

Table 8.4 The results of elemental analysis of the obtained lanthanum-promoted mixed oxides

Material	Molar content for the samples (fresh) Ni / Mg / La / Al	Metal content [%][1]	
		Ni	La
Ni15	0.212 / 0.54 / - / 0.25	21.4	-
Ni15La1	0.215 / 0.535 / 0.006 / 0.244	21.3	0.9
Ni15La2	0.215 / 0.535 / 0.0122 / 0.2378	21.2	1.8
Ni15La4	0.22 / 0.53 / 0.025 / 0.225	21.2	3.6

[1] Determined by XRF analysis

XRD analysis of fresh and calcined HT-derived La-promoted mixed oxides

The XRD diffractograms obtained for fresh and calcined Ni/Mg/La/Al hydrotalcites are shown in Fig. 8.8 and 8.9, respectively. All XRD patterns exhibited reflections at 2θ = 11, 24 and 35°, originating from X-ray diffraction on (003), (006) and (009) planes, respectively. For Lanthanum-promoted hydrotalcites additionally two separate phases arising from La compounds were found in the diffractograms, $La_2(CO_3)_2(OH)_2$ and $La_2O_2CO_3$. No changes in the interlayer spacing (parameter *c*) and average cation-cation distance (parameter *a*) were observed, which suggests that no La was introduced into the brucite-like layers of hydrotalcite, in good agreement with Serrano-Lotina *et al.* and Kalai *et al.* who studied similar materials [130, 219].

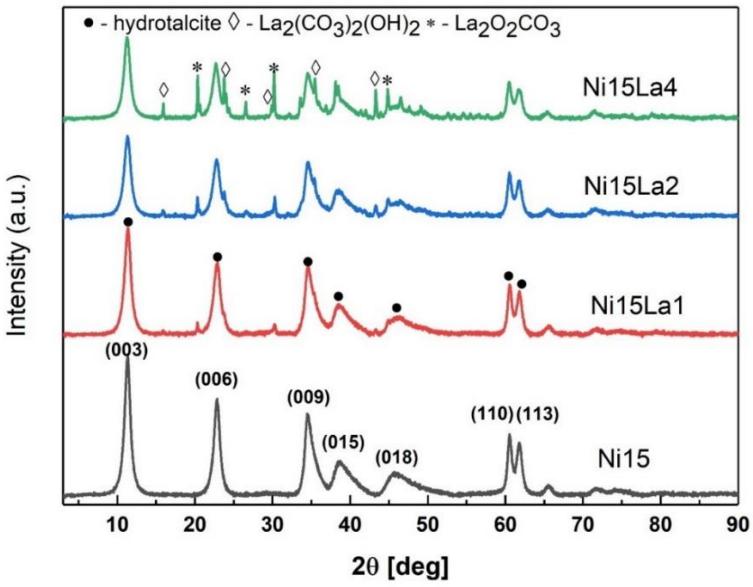

Figure 8.8 XRD patterns of the as-synthesized hydrotalcite-like materials

The unit cell parameters calculated for the obtained hydrotalcites are shown in Table 8.5. The *c* and *c'* parameters are in the range typical for CO_3^{2-} (7.65 Å) and NO_3^- (8.79Å) anions present in interlayer spaces [3]. The values of parameter *a* of the unit cell, which describes the average cation-cation distance, did not change for the lanthanum-promoted samples, again confirming that La was not introduced into hydrotalcites brucite-like layers.

Table 8.5 Unit cell parameters of the obtained hydrotalcite-like materials

Material	parameter c (Å)	c'=c/3 (Å)	Parameter *a* (Å)	Anions present between brucite-like layers
Ni15	23.46	7.82	3.06	CO_3^{-2} and NO_3^-
Ni15La1	23.43	7.81	3.06	CO_3^{-2} and NO_3^-
Ni15La2	23.49	7.83	3.06	CO_3^{-2} and NO_3^-
Ni15La4	23.52	7.84	3.06	CO_3^{-2} and NO_3^-

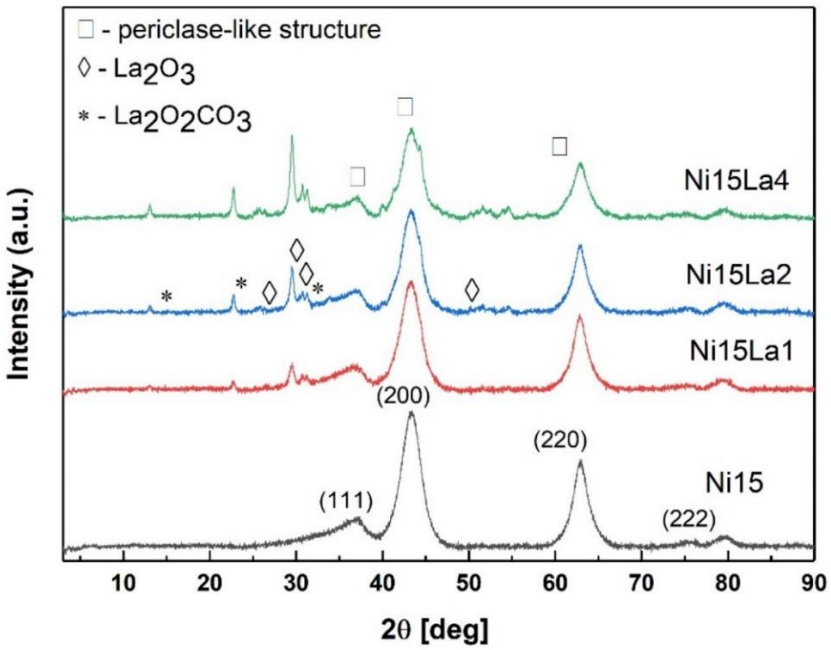

Figure 8.9 The XRD diffractograms obtained for lanthanum promoted HT-derived mixed oxides obtained upon thermal decomposition

Figure 8.9 for the calcined samples proves, by the two main reflections at 2θ = 43 and 64º, the formation of periclase-like structure of Mg(Ni,Al)O mixed oxides, typically obtained upon thermal decomposition of hydrotalcite-like materials [3]. Additionally, two phases of La compounds can be observed assigned to La_2O_3 and $La_2O_2CO_3$. The presence of La promoter did not influence the structure of Ni-hydrotalcite to any significant extent.

Reducibility of La-promoted Ni-containing hydrotalcite-derived catalysts and characterization of reduced samples

The H_2-TPR profiles for the catalysts promoted with lanthanum are presented in Fig. 8.10. The profiles of all catalysts exhibit one wide asymmetric peak at temperatures in the range of 814-846°C, which corresponds to the reduction of NiO species to metallic nickel (Ni^0). The high reduction temperature points to the existence of thermally stable solid phase solution in the form of mixed oxides Mg(Ni,Al)O [220,

221], as also suggested by other literature reports [210, 222]. The addition of lanthanum shifted the reduction temperatures of Ni species to lower temperatures, from 846°C for Ni15 to 821°C, 814°C and 814°C for Ni15La1, Ni15La2 and Ni15La4, respectively. At lower temperature of ca. 695°C a weak shoulder for La-promoted hydrotalcites may be observed, which may correspond to isolated and weakly bonded NiO species. This is in contrast to Lucredio *et al.* [30] who reported that the promotion with low amount of La resulted in the stabilization of Ni phase and thus increased reduction temperatures of Ni-HTs.

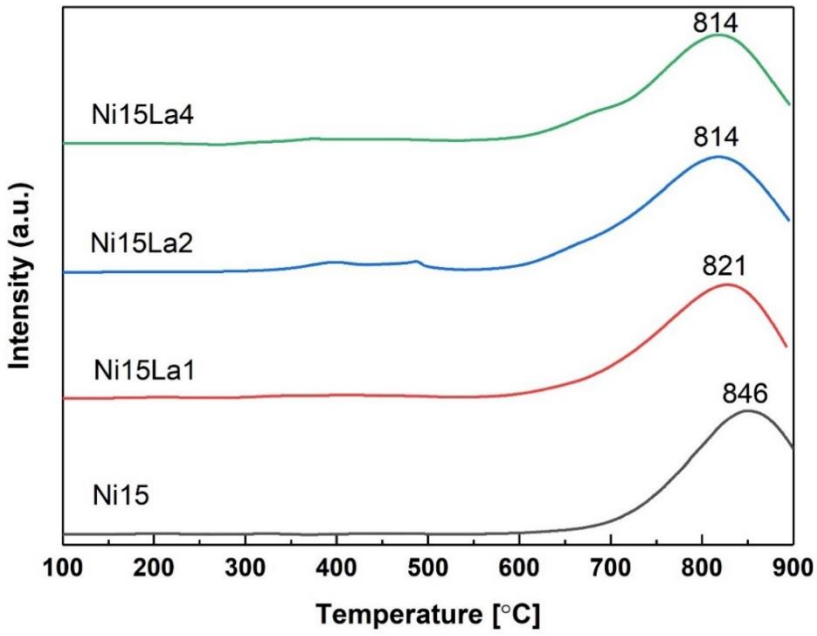

Figure 8.10 H_2-TPR profiles of HT-derived mixed oxides

The specific surface areas of the reduced materials ranged from 145 to 167 m^2/g (cp. Table 8.6), in good agreement with literature reports for similar mixed oxides derived from hydrotalcites [179, 223]. The incorporation of low amount of La (1 wt.%) decreased somewhat the specific surface area, which points to a partial blockage of the surface. On

the other hand, the values of S_{BET} for the samples promoted with 2 and 4 wt.% of La are close to the non-promoted parental sample Ni15, this possibly due to some additional area provided by the La-oxide deposited on the surface, as discussed in more detail together with XRD results for the reduced samples.

Table 8.6 S_{BET}, total pore volume and average pore diameter of the reduced HT-derived mixed oxide

Catalyst	S_{BET} [m^2/g][a]	Total pore volume [cm^3/g]	Average pore diameter (nm)
Ni15	167	0.73	17
Ni15La1	145	0.31	13
Ni15La2	165	0.37	16
Ni15La4	161	0.35	15

The XRD diffractograms registered for the materials reduced in the stream of 10%H_2/Ar are shown in Fig. 8.11. All diffractograms showed reflections at 2θ = 44.5, 51 and 76º arising from cubic metallic nickel (ICOD 01-087-0712) with the second reflection overlapped with the one arising from periclase-like structure.

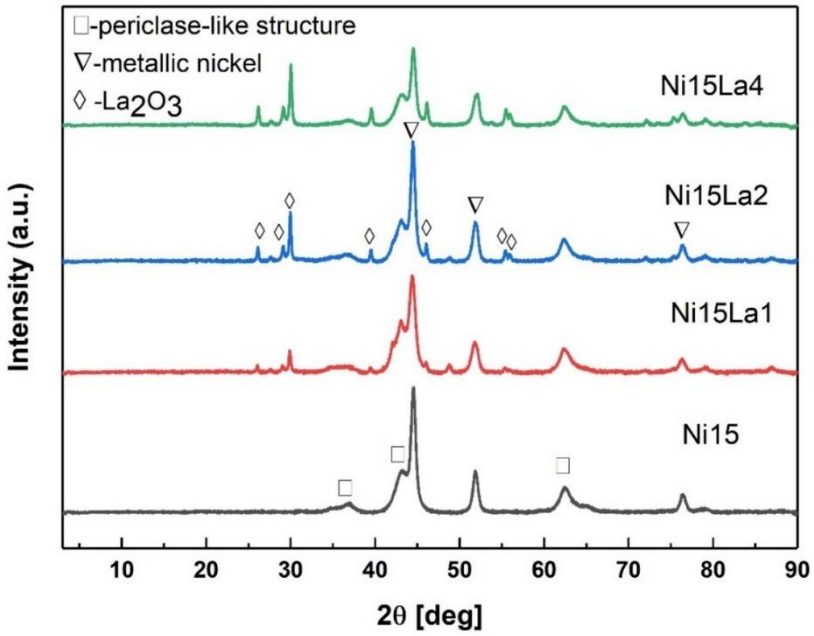

Figure 8.11 The XRD diffractograms obtained for lanthanum-promoted HT-derived mixed oxides after activation in a stream of 10%H_2/Ar for 1h at 900°C

The estimated values of Ni crystallite size, which were calculated using the position of Ni(200) reflection and Scherrer equation, are presented in Table 8.7.

Table 8.7 Metallic nickel crystallite size for HT-derived reduced catalysts after reduction and reaction

Material	Ni^0 Crystallite size [nm]	
	Reduced	Spent
Ni15	8	8
Ni15La1	9	8
Ni15La2	9	9
Ni15La4	9	10

Figure 8.12 shows the CO_2-TPD profiles obtained for the mixed oxide materials derived from hydrotalcites after reduction by 10% H_2/Ar. Three peaks may be observed on the profiles corresponding to weak (138-150°C), medium-strength (232-251°C) and strong basic sites (349-374°C). The number of respective sites is presented in Table 8.8.

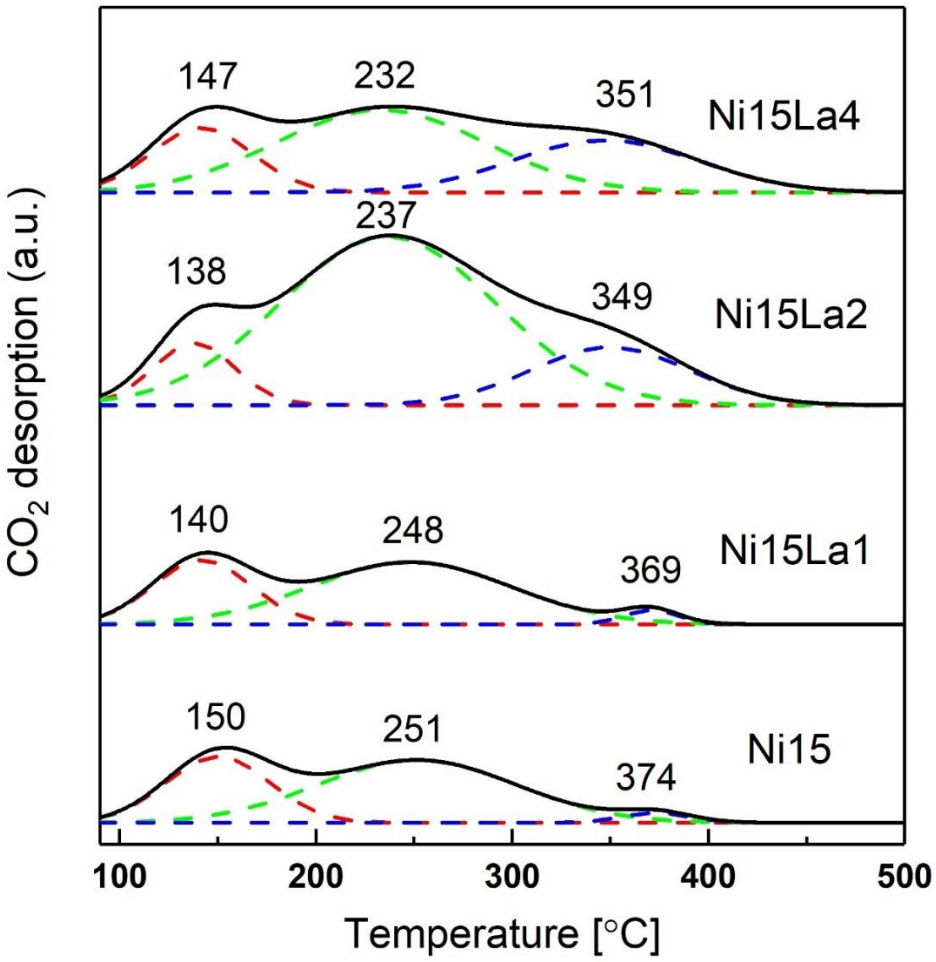

Figure 8.12 CO_2-TPD profiles of reduced La-promoted HT-derived mixed oxides in comparison to unpromoted catalyst

As presented in Table 8.8 the introduction of 0.9 wt.% of lanthanum led to a small decrease in total basicity from 82 for Ni15 to 55 μmol/g for Ni15La1. On the other hand, the total number of basic sites increased for La-loading of 1.8 and 3.6 wt.%, respectively, to 139 and 122 μmol/g. Moreover, for the latter samples the main increase in basicity was connected with the increase in the number of medium-strength basic sites. Similar results were reported by Wang *et al.* [223]. The lack of direct correlation between basicity for Ni-HT containing 0.9 wt.% as compared to 1.8 and 3.6 wt.% of La may have been caused by a summary effect of a partial blocking of the basic sites (as suggested by decreased

S_{BET} for Ni15La1) and the formation of new basic sites by lanthanum oxides for Ni15La2 and Ni15La4 compensating to certain extent the blocking effect. It should be mentioned that the increase of basicity for Ni15La2 is in good agreement with Zhang *et al.* who studied similar materials obtained by urea synthesis method [137].

Table 8.8 Total basicity and distribution of basic sites for the reduced Ni-containing La-promoted HT-derived catalysts (CO_2-TPD).

Sample	Total basicity [µmol/g]	Weak sites [µmol/g]	Medium sites [µmol/g]	Strong sites [µmol/g]
Ni15	**82**	**7**	**60**	**15**
Ni15La1	**55**	**21**	**30**	**4**
Ni15La2	**139**	**12**	**113**	**14**
Ni15La4	**122**	**21**	**87**	**14**

Catalytic performance in CO_2 methanation

The CO_2 conversion registered during the methanation experiments (Fig. 8.13) is plotted as a function of temperature for the studied La-promoted catalysts derived from hydrotalcite obtained by co-precipitation method. Complete CO_2 conversion is predicted at low reaction temperatures, decreasing with increasing temperature. At 250°C, the CO_2 conversions were much lower than the calculated maximal thermodynamic conversion limit.

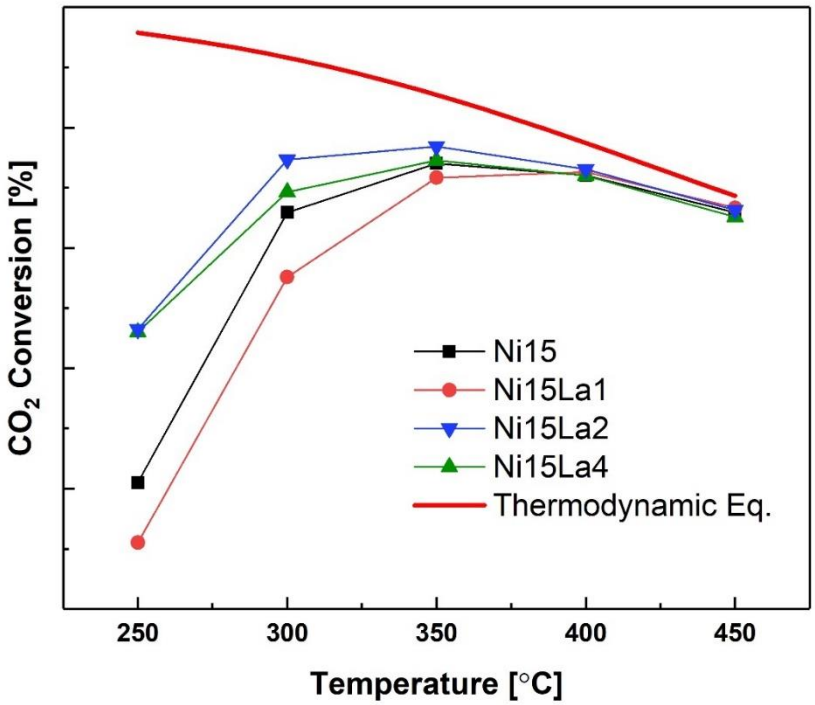

Figure 8.13 The results of catalytic tests carried out in the temperature range of 250-450°C, total flow 100 cm^3/min, $CO_2/H_2/Ar$ = 3/12/5, GHSV = 12000 h^{-1}

However, as compared to non-promoted Ni15, a considerable improvement was registered for Ni15La2 and Ni15La4, in contrast to Ni15La1, which showed decreased activity. The highest carbon dioxide conversions were registered for the catalysts promoted with 1.8 and 3.6 wt.% of La and were 46.5% and 46% of CO_2, respectively. Their increased activity as compared to Ni15 and Ni15La1 may be explained by both increased basicity of the Ni15La2 and Ni15La4, especially where the number of moderate basic sites is concerned, and increased reducibility resulting from the weakened interaction of Ni species with the support matrix. As proven by XRD, La forms separate phases and is not introduced into the hydrotalcite-like structure. For the catalyst with 0.9% La the decrease in the catalytic performance is well correlated with the lowest number of basic sites. As reported by Pan *et al.* [63] the reaction of CO_2 methanation on Ni-

containing catalysts involves the dissociative adsorption of H_2 on metallic nickel and adsorption of CO_2 on the basic sites, thus an optimum catalyst composition needs to be found.

At higher reaction temperatures the CO_2 conversion converges to similar values for all studied catalysts. At temperatures higher than 400°C, a loss in reaction selectivity can be expected as suggested by the thermodynamic calculations.

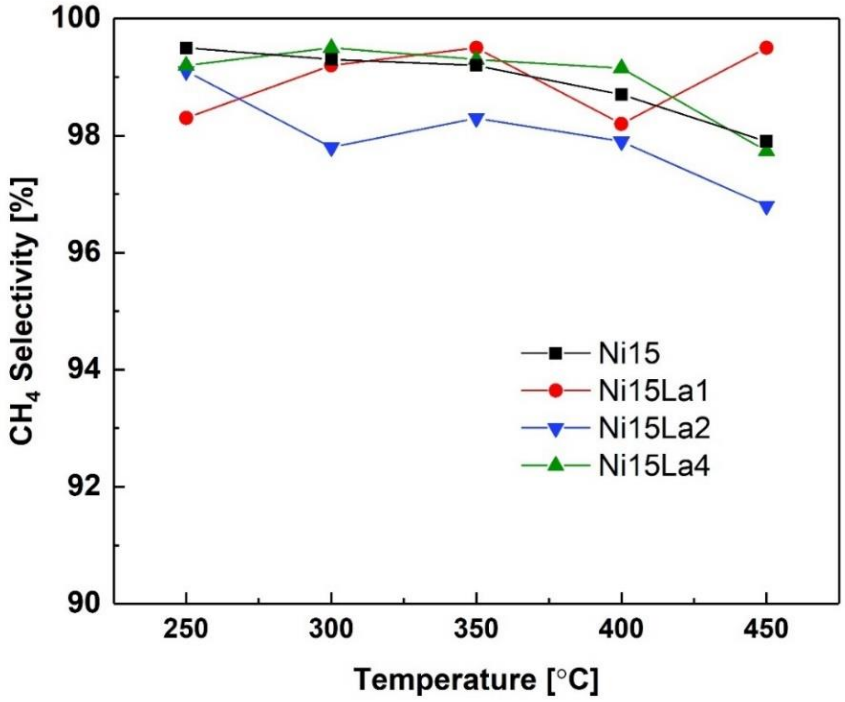

Figure 8.14 Selectivity towards CH_4 versus temperature for the studied La-promoted Ni-containing HT-derived mixed oxides

Figure 8.14 shows the methane selectivity as a function of temperature measured for the studied catalysts during the activity tests. Almost complete selectivity to methane at 250°C was registered for all the studied catalysts and was between 98-99%. The same tendency was observed at 300 and 350°C, with the exception of Ni15La2, with selectivity slightly lower. As predicted by thermodynamics, the selectivity decreased slightly with

increasing temperature for all samples except Ni15La1, where the selectivity towards methane increased from 400°C to 450°C. No other product except carbon monoxide and methane were registered during the catalytic tests. The selectivity towards CO was in the range of 1- 3% (highest for the most active Ni15La2 at 450ºC). As the amounts of CO were low, it is difficult to find a correlation between the selectivity towards carbon monoxide formation and the properties of the studied catalysts. The catalysts activity was not changed during 24h tests, without further evolution of basicity and no modification of Ni^0 crystallite size on the spent catalysts (cp. Table 8.7).

Conclusions

La-promoted Ni-containing catalysts derived from hydrotalcites were synthesized using co-precipitation at constant pH, with a fixed M^{2+}/M^{3+} molar ratio equal to 3.

The theoretical amount of La introduced into fresh as-synthesized HTs were 1, 2 and 4 wt.%. The calcined catalysts revealed similar contents of La, of 0.9, 1.8 and 3.6%, respectively. However, as proven by XRD, La species were not incorporated into the brucite-like layers of hydrotalcites, but were present as separate phases of La_2O_3 and $La_2O_2CO_3$ on the materials surface. H_2 temperature programmed reduction of the materials derived from hydrotalcites showed that the introduction of lanthanum resulted in the increased reducibility of Ni-species due to the weakened interaction with the HTs matrix. CO_2 temperature programmed desorption tests of reduced HT-derived mixed oxides showed that the introduction of La influenced strongly the CO_2 adsorption capacity of the catalysts via the formation of medium-strength basic sites, although the final effect was superposition of the effect of blocking of parent Ni-HT sites by the deposited La species and the formation of new basic sites arising from La-phases. Both increased basicity, especially that connected with medium-strength basic sites, and increased Ni-

reducibility, resulted in increased activity at low temperatures for La-promoted HT-derived catalysts. This was the case when appropriate amount of the promoter (2 or 4 wt.%) was introduced. For Ni15La1, the blockage of basic sites by La-compounds deposited on the surface could not be compensated by new La-originating sites and thus, due to overall decreased number of basic sites, activity was lower than that of Ni15. The selectivity towards methane in the low temperature region was in the range of 98-99% for all the catalysts. During 24h stability tests activity and selectivity of all catalysts remained almost unchanged.

8.3. The comparison of La-promoted catalysts prepared by different methods

As discussed in the Chapter 8.2, lanthanum was not introduced into the brucite-like layers of HT materials during co-precipitation procedure. Thus, this chapter was focused on other, alternative, methods of lanthanum introduction into Ni-hydrotalcites in order to assess the effect of such methods on physicochemical properties and their influence on the catalytic performance in CO_2 methanation reaction. Lanthanum was introduced via impregnation or adsorption from a solution of La-EDTA complex and the obtained catalysts were compared to a selected catalyst prepared by co-precipitation and discussed in the previous Chapter. For this comparison the best performing Ni15La2 catalyst was chosen and for the sake of clarity of discussion, renamed in this Chapter by adding the preparation procedure (CP) to the former designation. In case of adsorption, additionally $Ni15L4_{(ADS)}$ and $Ni15La1_{(ADS)}$ were prepared.

Physicochemical features of La-promoted Ni-containing HT-derived catalysts

Figure 8.15 and 8.16 compare diffraction patterns of fresh hydrotalcites and mixed oxides obtained upon thermal treatment of La-promoted hydrotalcite-like materials, where La was introduced either by co-precipitation of La, Ni, Mg and Al nitrates or by adsorption of $La(EDTA)^-$ complex or impregnation (of calcined material). The patterns obtained for all as-synthesized materials confirmed the existence of a multilayer hydrotalcite-like structure [224]. When lanthanum was introduced by adsorption from aqueous La-EDTA complex solution no additional reflections arising from a separate phase were observed, suggesting either the presence of non-crystalline deposits or of crystallites of very small size, under the detection limit of XRD.

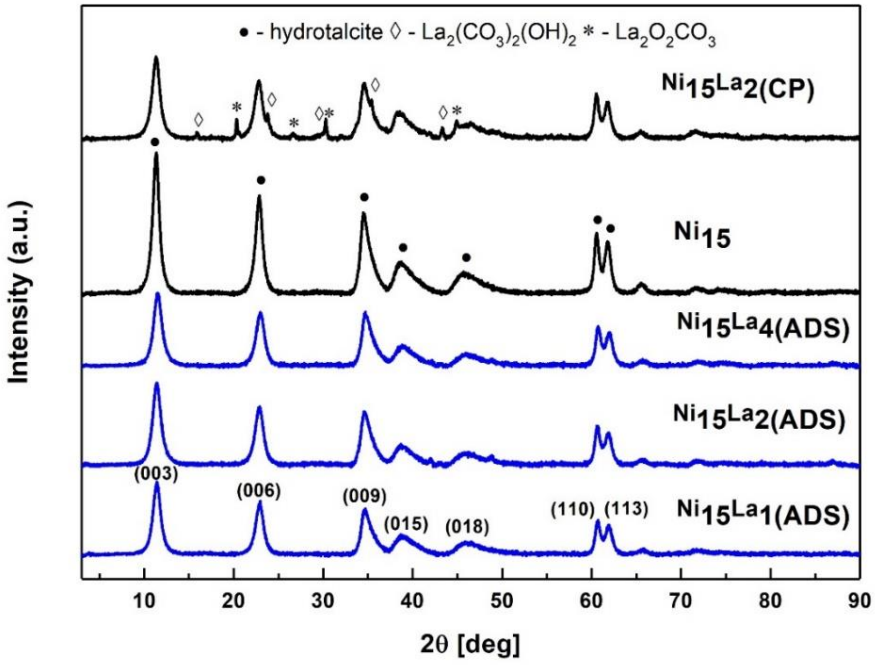

Figure 8.15 XRD patterns for as-synthesized materials. CP – denotes the catalyst with La introduced during co-precipitation of all components, ADS – denotes catalysts with Ni-hydrotalcite promoted via adsorption with $La(EDTA)^-$ complex

The values of parameter c, summarized in Table 8.9, calculated from the position of the first reflection are 23.04Å-23.49Å [213]. Average distance between cations (parameter *a*) was 3.06Å for all materials. As discussed in Chapter 8.2, the XRD patterns confirmed that La was not incorporated into hydrotalcite layers for co-precipitated catalysts, as no variation in the unit cell c parameter could be observed. There is no proof of La introduction also for the samples promoted with La by adsorption. On the other hand, an absorption band at 1604 cm^{-1} arising from COO^- present in EDTA (Appendix A1) was observed in the FTIR spectra acquired for these materials, which suggests that the $La(EDTA)^-$ complex was deposited on the materials surface.

Table 8.9 Unit cell parameters of La-promoted Ni-containing hydrotalcite-like materials

Material	Unit cell parameter c (Å)	c'=c/3 (Å)	Unit cell parameter *a* (Å)	Anions present between brucite-like layers
Ni15	23.46	7.82	3.06	CO_3^{-2} and NO_3^-
Ni15La(ADS)	23.23	7.76	3.06	CO_3^{-2} and NO_3^-
Ni15La2(ADS)	23.26	7.76	3.06	CO_3^{-2} and NO_3^-
Ni15La4(ADS)	23.04	7.68	3.06	CO_3^{-2} and NO_3^-
Ni15La2(CP)	23.49	7.83	3.06	CO_3^{-2} and NO_3^-

XRD patterns of the calcined hydrotalcites are shown in Fig 8.16. Typical reflections were observed at $2\theta = 42.5$ and 63° confirming that mixed oxides of periclase-like structure were obtained. No additional phase was observed for the samples where La was incorporated using adsorption method, in contrast to the samples obtained by co-precipitation and impregnation method, with separate phases of La_2O_3 and $La_2O_2CO_3$.

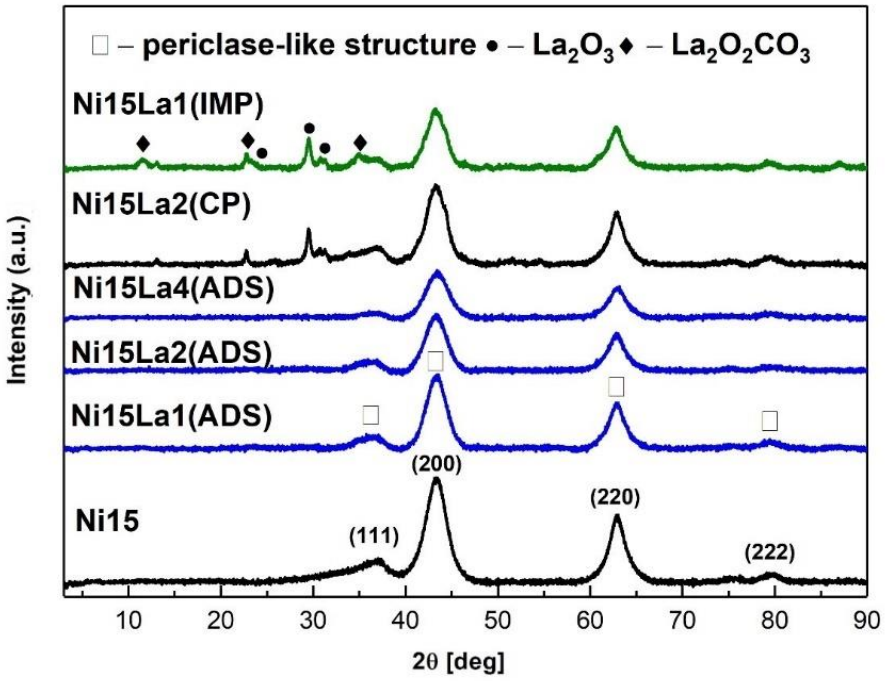

Figure 8.16 XRD patterns for the calcined materials

Reducibility and physico-chemical characterization of reduced catalysts

The H_2-TPR profiles obtained for the calcined catalysts derived from hydrotalcites are shown in Figure 8.17. All profiles obtained for the studied materials show one wide asymmetric peak originating from the reduction of NiO species to metallic nickel (Ni°) with a maximum at 818-850°C. The introduction of La shifted the reduction peaks of Ni species to lower temperatures i.e. from 850°C for Ni15 to 818°C, 824°C, 832°C, 836°C and 836°C for $Ni15La4_{(ADS)}$, $Ni15La2_{(ADS)}$, $Ni15La2_{(CP)}$, $Ni15La1_{(ADS)}$ and $Ni15La1_{(IMP.)}$, respectively. At lower temperatures of ca. 700°C an additional shoulder appears, which may arise from the reduction of weaker bonded NiO species.

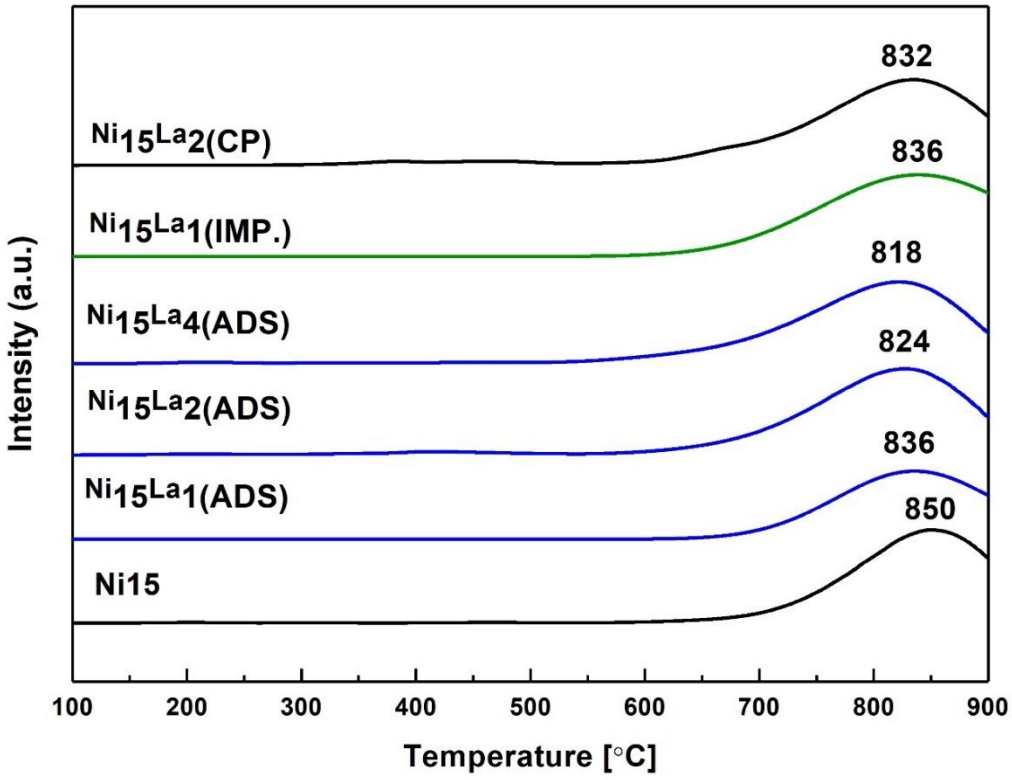

Figure 8.17 H_2-TPR profiles of La-promoted Ni-containing hydrotalcites with La introduced by different methods

The H_2-TPR profiles obtained for the studied catalysts are in good agreement with literature reports [6].

Table 8.10 summarizes the textural properties and elemental analysis (XRF) of the reduced catalysts. The specific surface area, which ranged from 157 to 167 m^2/g, was not influenced after introduction of lanthanum by adsorption method, in good agreement with results obtained for similar materials [178]. On the other hand, total pore volumes decreased after introduction of La from 0.71 to 0.33-0.37 cm^3/g, and were similar for all materials containing La, irrespective of the method of La introduction. This confirms that La was deposited on the surface of hydrotalcite materials, most probably at the inlet to the porous system. The content of nickel and lanthanum ranged from 21.0-21.4 wt.% and

0.4-1.8 wt.%, respectively. Thus, it may be observed that the amount of introduced La was dependent on the introduction method.

Table 8.10 Specific surface area (S_{BET}), total pore volume and elemental analysis for reduced hydrotalcite catalysts

Catalyst	S_{BET} [m^2/g][1]	Total pore volume [cm^3/g][1]	Elemental analysis[1]	
			Ni wt.%	La wt.%
Ni15	**167**	**0.73**	**21.4**	**-**
Ni15La2$_{(CP)}$	**165**	**0.37**	**21.2**	**1.8**
Ni15La1$_{(ADS)}$	**167**	**0.35**	**21.3**	**0.4**
Ni15La2$_{(ADS)}$	**161**	**0.37**	**21.0**	**0.9**
Ni15La4$_{(ADS)}$	**163**	**0.36**	**21.1**	**1.4**
Ni15La1$_{(IMP.)}$	**157**	**0.33**	**21.2**	**1.1**

[1]Low temperature N_2 sorption and XRF analysis performed for the reduced catalysts

The XRD patterns acquired for the reduced mixed oxides, shown in Fig. 8.18, show a separate phase of metallic Ni [179]. For the catalysts with lanthanum added via adsorption of La-EDTA complex no additional reflections arising from separate lanthanum phases were registered, in contrast to the catalysts with La added via co-precipitation or impregnation, where a separate phase of La_2O_3 may be observed.

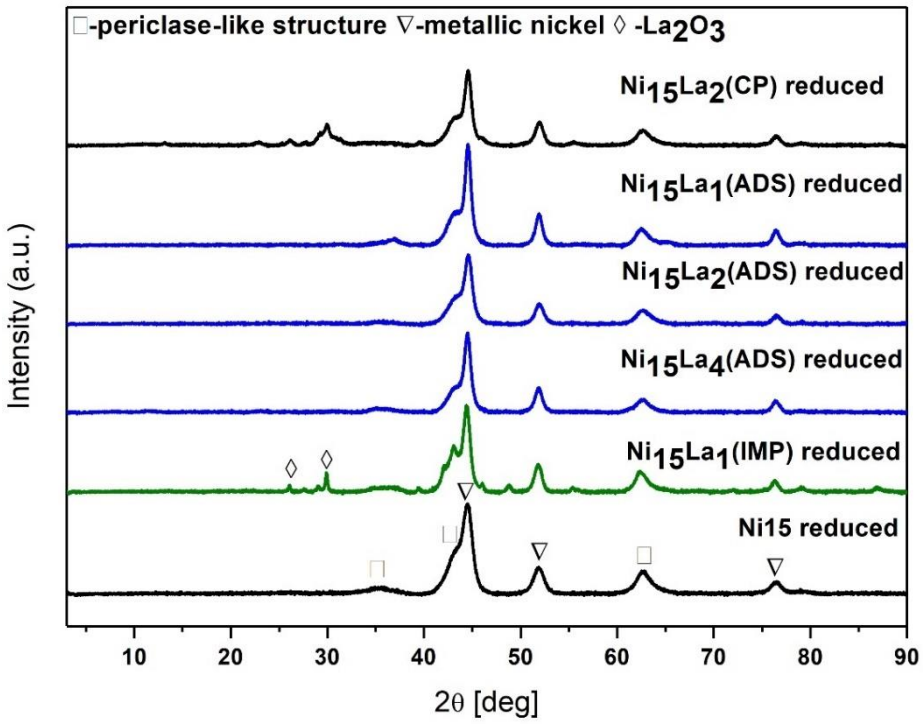

Figure 8.18 XRD patterns for the reduced catalysts, reduction conditions: 900°C for 1h in 100ml/min of 10%H_2/Ar

The Ni crystallite sizes for the reduced catalysts, summarized in Table 8.11, were in the range of 5-10 nm. The introduction of lower amounts of La by adsorption (0.4 wt.% for $Ni15La1_{(ADS)}$ and 0.9 wt.% for $Ni15La2_{(ADS)}$) led to an enhanced dispersion of Ni, with nickel particle size decreasing from 9 nm for Ni15 to 5 and 7 nm for $Ni15La1_{(ADS)}$ and $Ni15La2_{(ADS)}$, respectively. This should be of advantage where catalytic performance in CO_2 methanation is concerned, as according to Fan *et al.* nickel particles of small size faciliate the CO_2 hydrogenation to methane [132]. However, when higher amounts of La were deposited on the catalysts, crystallite size increased to 10 and 11 nm for $Ni15La2_{(ADS)}$ and $Ni15La4_{(ADS)}$, respectively. Thus, a higher dispersion can be obtained when low amounts of lanthanum are introduced by adsorption method, which results in a limited growth of nickel crystallites size, as discussed later.

Table 8.11 Crystallite sizes of metallic nickel (Ni^0) calculated for the reduced and spent catalysts

Catalyst	La content [wt.%]	Crystallite size [nm]	
		Reduced	Spent
Ni15	**-**	**9**	**8**
$Ni15La2_{(CP)}$	**1.8**	**8**	**9**
$Ni15La1_{(ADS)}$	**0.4**	**5**	**5**
$Ni15La2_{(ADS)}$	**0.9**	**7**	**7**
$Ni15La4_{(ADS)}$	**1.8**	**11**	**11**
$Ni15La1_{(IMP.)}$	**1.1**	**10**	**10**

The CO_2-TPD profiles obtained for the materials derived from hydrotalcites after reduction by 10% H_2/Ar shown in Fig. 8.19 were deconvoluted into three Gaussian peaks corresponding to weak, medium-strength and strong basic sites, with the appropriate numbers summarized in Table 8.12.

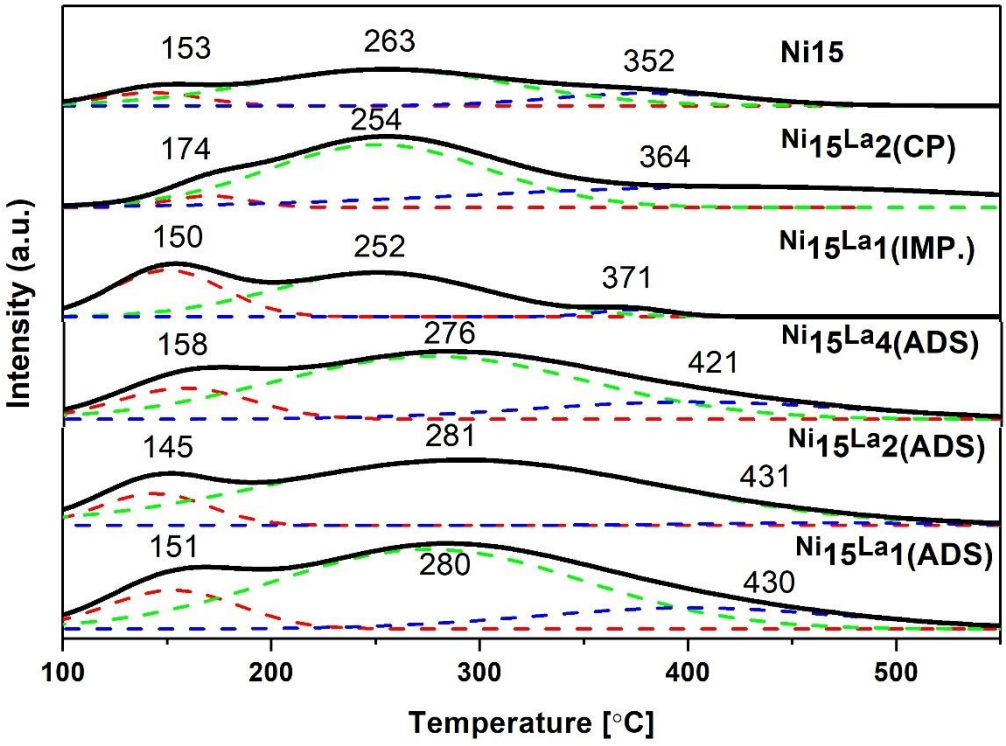

Figure 8.19 CO_2-TPD profiles for the reduced HT-derived catalysts.

The promotion with lanthanum increased the basicity of the catalysts, with the exception of $Ni15La1_{(IMP)}$ sample. The increase could have its origin not only in the amount of introduced La but also its dispersion on the surface arising from different methods of introduction. Lanthanum changed not only the total number of basic sites, but also their distribution by increasing the number of medium-strength sites, and barely affecting the number of weak and only slightly that of strong basic species.

The total basicity for samples obtained by adsorption method followed the sequence: $Ni15La1_{(ADS)} \sim Ni15La2_{(ADS)} > Ni15La4_{(ADS)}$, while the appropriate sequence for medium-strength basic sites was $Ni15La1_{(ADS)} > Ni15La2_{(ADS)} \sim Ni15La4_{(ADS)}$. Simultaneously, the data in Table 8.12 prove that adsorption of La complex led to higher basicity, as well as higher number of basic sites of medium-strength than both co-

precipitation and impregnation methods. This may have arisen from better dispersion of La (and thus possibly better contact between Ni and La species). The former is backed by two observations: (i) XRD patterns, showing no La-crystallites for the catalysts obtained by adsorption in contrast to impregnated and co-precipitated samples, and (ii) basicity decreasing slightly with the amount of La introduced by adsorption, which suggests the simultaneous formation of larger La-entities.

Table 8.12 Basicity of the reduced La-promoted Ni-HTs (CO_2-TPD) promoted with La by different methods.

Catalyst	Total basicity [µmol/g]	Weak sites [µmol/g]	Medium sites [µmol/g]	Strong sites [µmol/g]
Ni15	**82**	**7**	**60**	**15**
$Ni15La2_{(CP)}$	**139**	**12**	**103**	**24**
$Ni15La1_{(ADS)}$	**202**	**18**	**141**	**43**
$Ni15La2_{(ADS)}$	**198**	**27**	**127**	**48**
$Ni15La4_{(ADS)}$	**185**	**29**	**120**	**41**
$Ni15La1_{(IMP.)}$	**86**	**42**	**33**	**11**

Activity and selectivity in CO_2 methanation

The CO_2 conversion in CO_2 methanation versus temperature is shown for all studied catalysts in Fig. 8.20. All catalysts were active, with results strongly depending on the method of La introduction, especially at the lowest studied temperature of 250°C.

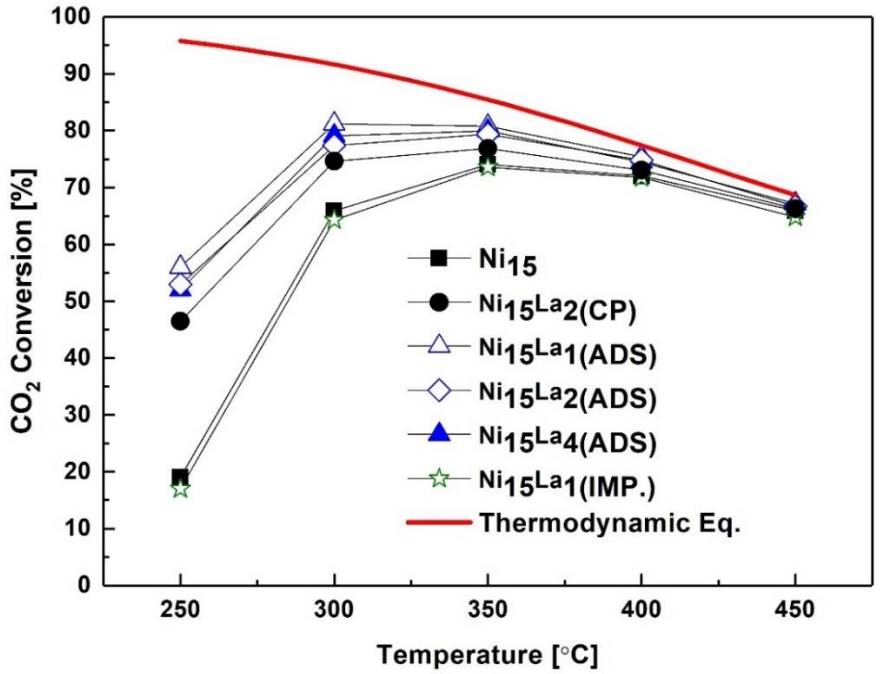

Figure 8.20 CO_2 conversion for Ni-hydrotalcites promoted with La by different methods. Reaction conditions: $CO_2/H_2/Ar$ = 3/12/5, GHSV = 12 000 h^{-1}, temperature range from 250 to 450°C

Although at this temperature CO_2 conversion was far from the thermodynamic limit, CO_2 conversion was significantly improved by La promotion (with the exception of the samples prepared by La-impregnation) and formed a sequence: $Ni_{15}La_{1(ADS)}$ > $Ni_{15}La_{4(ADS)}$ > $Ni_{15}La_{2(ADS)}$ > $Ni_{15}La_{2(CP)}$ > Ni_{15} ~ $Ni_{15}La_{1(IMP)}$. This indicates that appropriate La introduction method may lead to considerable activity improvements. On the other hand, only slight dependence of CO_2 conversion on La content was observed for the most active catalysts. The appropriate number for the samples prepared via La introduction by adsorption were 56%, 53% and 52% for $Ni_{15}La_{1(ADS)}$, $Ni_{15}La_{2(ADS)}$ and $Ni_{15}La_{4(ADS)}$, respectively.

The enhanced activity towards CO_2 methanation for the catalysts promoted with lanthanum may have resulted from both (i) increased basicity and (ii) the weakened interaction of NiO species with the supports matrix, the latter leading to smaller and better dispersed Ni crystallites. Figure 8.21 a) shows CO_2 conversion plotted versus total number of basic sites and Figure 8.21 b versus the number of moderate sites, respectively. From Fig. 8.21 a) it may be observed that the increase in number of basic sites leads to increased CO_2 conversion. On the other hand, Fig. 8.21 b) shows an almost linear relationship between CO_2 and the number of moderate sites, as discussed in the Chapter 7 in connection to the improvements in catalytic performance of Ni-hydrotalcites.

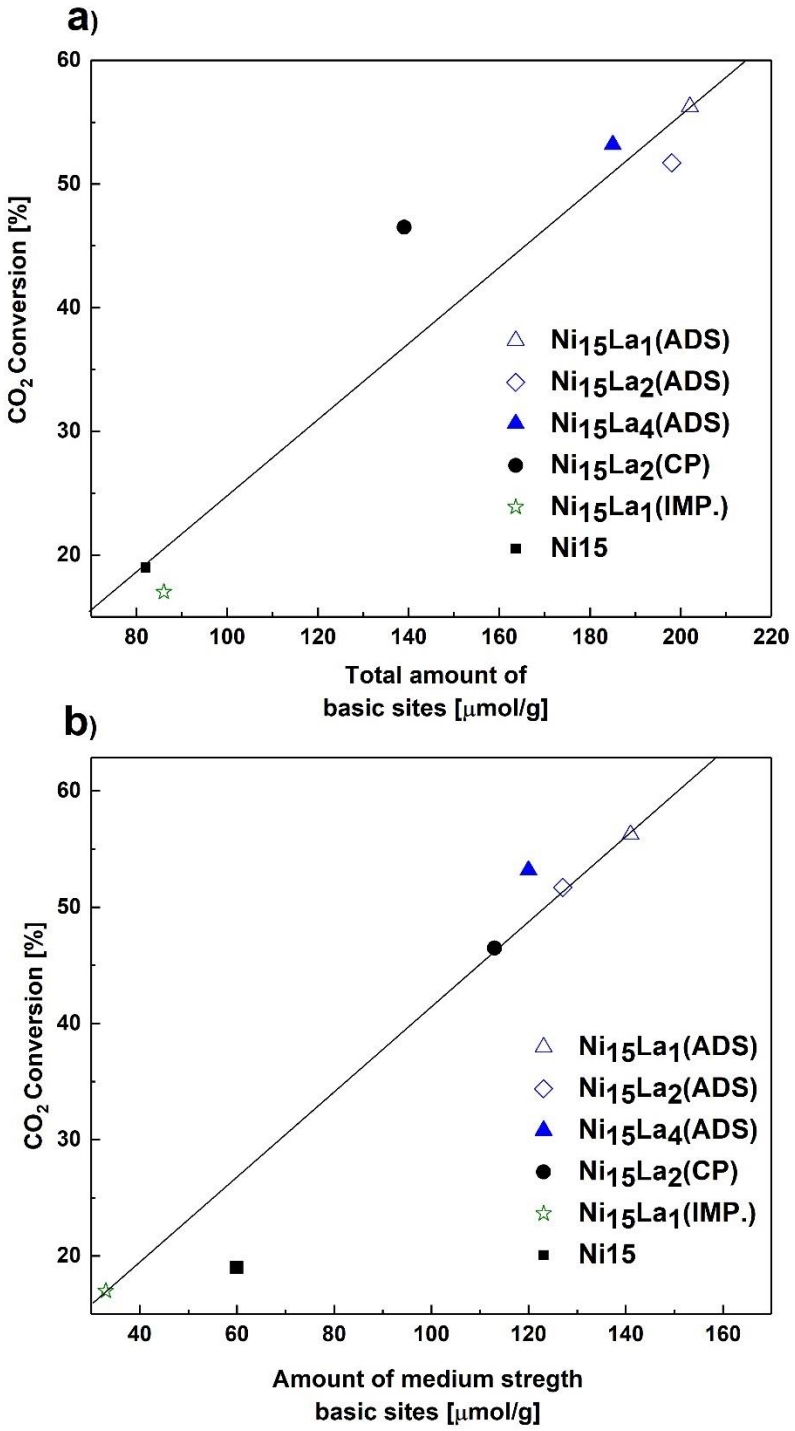

Figure 8.21 CO_2 conversion vs (a) total of amount basic sites, and (b) the number of moderate basic sites

The selectivity towards CH_4 formation is plotted as a function of temperature in Fig. 8.22 for the studied catalysts. Almost complete selectivity towards methane at 250°C (99-99.8%) was registered. As expected, the CH_4 selectivity decreased with increasing temperature and trace amounts of side reaction product (carbon monoxide) were found. However, the registered amounts of CO were relatively low. No other products except CH_4 and CO were registered.

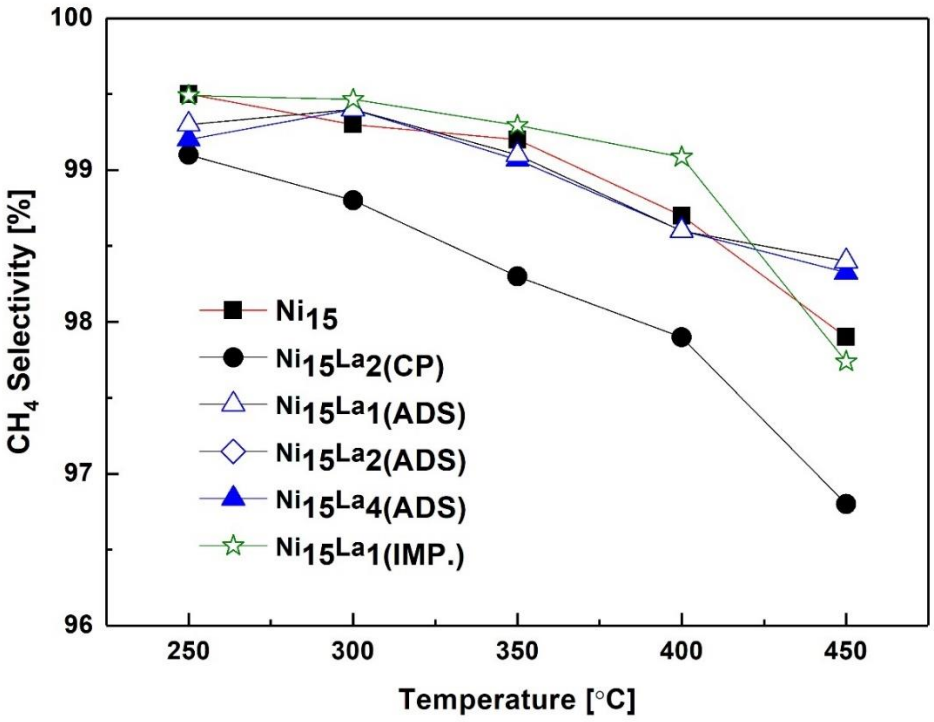

Figure 8.22 CH_4 Selectivity for lanthanum promoted Ni-containing hydrotalcites

The stability tests performed at 250°C for 24h for the selected samples are shown in Fig. 8.23. A slight decrease can be observed after 2.5h TOS followed by stabilization. After this first period, the catalysts remained stable till the end of the 24h-catalytic tests.

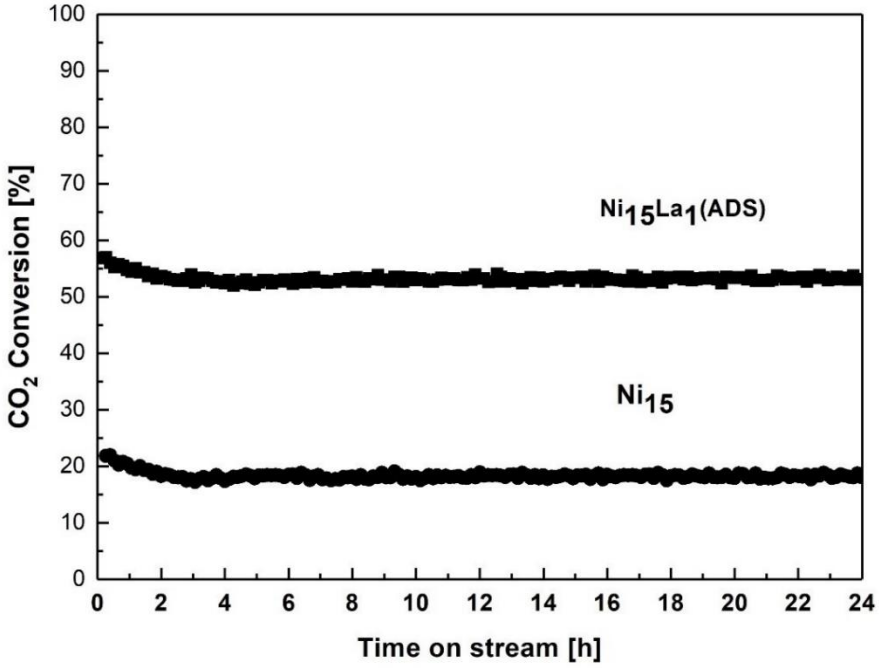

Figure 8.23 Stability tests for selected catalysts at 250°C for 24h, reaction conditions: GHSV = 12 000 h^{-1}, total flow = 100 cm^3/min, $CO_2/H_2/Ar$ = 3/12/5

Characterization of the spent catalysts

Figure 8.24 shows XRD patterns of the spent samples. As shown in Table 8.11 the crystallite sizes of Ni did not change after reaction in comparison to the reduced samples. No reflections arising from graphite (at $2\theta = 26^{\circ}$) could be observed in the diffractograms of the spent samples.

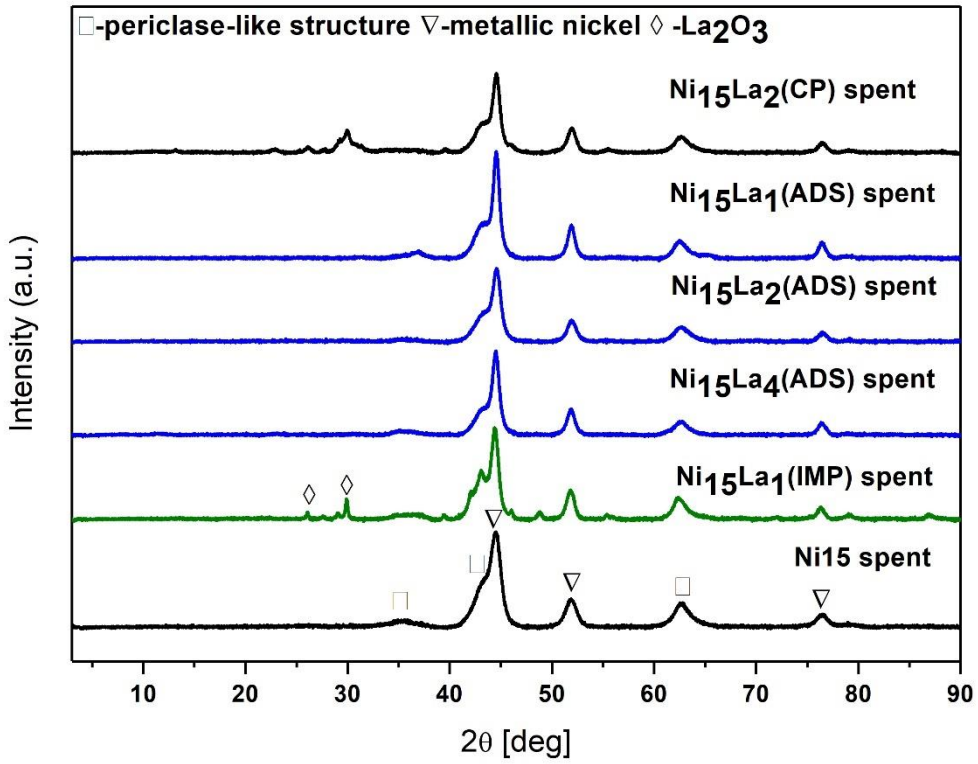

Figure 8.24 XRD patterns of the spent La-promoted Ni-containing HT-derived catalysts

Conclusions

The hydrotalcite-like materials were promoted by La using different methods (i) co-precipitation of hydrotalcites in the solution of sodium carbonate, (ii) adsorption of La-EDTA complex on Ni-hydrotalcite and (iii) impregnation of Ni-hydrotalcite with a solution of lanthanum nitrate, and tested as catalysts in CO_2 methanation. The physico-chemical characterization of the obtained materials showed that La was not incorporated into the structure of hydrotalcite-like materials, but was present on the surface, either well dispersed (in case of adsorption) or in the form of La-species (co-precipitation or impregnation).

As proven by CO_2-TPD performed for the reduced materials, the introduction of lanthanum affected the CO_2 adsorption capacity by influencing the number of medium-

strength basic sites. The changes in the number of basic sites and their distribution were dependent on the method of La introduction, the most efficient method to increase the number of moderate basic sites being the adsorption. On the other hand, impregnation led to the decrease of the number of such sites. H_2-TPR indicated that the promotion with La resulted in the weakened interaction between Ni and HT-derived matrix, where Ni-species are commonly present in the form of solid oxide solutions NiO-MgO. The activity of the catalysts in carbon dioxide methanation was found to be almost linearly dependent to the number of moderate basic sites. The crystal size of Ni particles in the reduced catalysts, which was lower for the samples with small amounts of La, could have also contributed to an enhancement of the catalytic activity in the hydrogenation of carbon dioxide to methane, even at the lowest studied temperature of 250°C. Catalytic tests carried out at 250°C for 24h for the unpromoted (Ni15) and La-promoted catalyst ($Ni15La1_{(ADS)}$) proved high stability of both during CO_2 methanation.

9. Optimization of the catalysts

Chapter 7 showed that CO_2 conversion of Ni-hydrotalcite depends on Ni content. Ni40 was found to be the best performing catalyst. Chapter 8.2 showed that the promoting effect depended on the amount of introduced La, with 2 wt.% resulting in the best performance. Promotion with La increased the catalytic activity of Ni15, especially at 250°C and 300°C – temperatures, which are of most interest for CO_2 methanation. This is why in order to optimize the Ni-hydrotalcite catalyst, Ni40 was promoted with 2wt.% of La by co-precipitation method. The same catalysts were then studied by operando XAS and XES (Chapter 10) in order to elucidate the role of promoter.

Physico-chemical properties of the optimized catalysts

The contents of Ni and La determined by XRF are close to the calculated before synthesis (cp Table 9.1). The specific surface areas (S_{BET}) were 71-72 m^2 g^{-1} and total pore volumes (V_{tot}) are 0.25 – 0.27 cm^3 g^{-1} (cp. Table 9.1). Thus, he textural properties were not significantly affected after introduction of 2.6 wt. % of La.

The XRD patterns obtained for as-synthesized Ni40La2 hydrotalcite (compared to Ni40 in Appendix, Fig. A2) show reflections typical for hydrotalcite-like material. In case of the studied Ni40La2 sample the *c* parameter value was in 23.34Å and parameter *a* value was ca. 3.04 Å.

Typical reflections arising from periclase-like structure were observed (Appendix, Fig. A3) after calcination of the as-synthesized hydrotalcite-like materials. No other phases were observed on the XRD diffractograms, similarly, as discussed in Chapter 7 for Ni-containing samples and in contrary to the results presented in Chapter 8.2 for La-

promoted materials, where separate phases of La compounds were observed on XRD diffractograms for calcined samples.

Table 9.1 Specific surface area S_{BET}, total pore volume V_{tot} and elemental analysis results for the reduced Ni and Ni/La HT-derived catalysts

Catalyst	Textural properties		Chemical analysis					
	Specific surface area (S_{BET}) [m^2/g][a]	Total pore volume [cm^3/g]			Ni	Mg	La	Al
Ni40	-	-	fresh	wt.%	40	1.9	-	6.8
				mol%	0.67	0.08	-	0.25
	71	0.27	reduced	wt.%	52.1	2.5	-	8.6
Ni40La2	-	-	fresh	wt.%	40	1.5	2	6.3
				mol%	0.68	0.067	0.015	0.235
	72	0.25	reduced	wt.%	51.6	1.8	2.6	7.7

[a]**The accuracy of S_{BET} determination is usually assumed to be ca. ± 5 %**

The active sites and reducibility are in good agreement with general tendencies registered for other Ni-hydrotalcites studied in this PhD thesis, as discussed in Chapters 7, 8.2 and 8.3. Appropriate H_2-TPR and CO_2-TPD profiles are given in Appendix (Fig. A4 and A6). All H_2-TPR profiles obtained for the calcined catalysts showed an asymmetric peak at temperature ranging from 676 to 686°C, originating from the reduction of NiO species to Ni^0, confirming a strong interaction of NiO and the supports matrix and thus suggesting high Ni dispersion. Similarly, as found in the Chapter 8.2 and

8.3, the reducibility of La-promoted sample increased, resulting in a shift of the reduction peak from 686°C Ni40 to 676°C for Ni40La2.

The XRD diffractograms obtained for the reduced materials (Appendix, Fig. A5) revealed the existence of periclase-like structure (MgO) and metallic nickel (Ni^0) phase, the latter with crystallite sizes ranging from 8-9 nm. In contrary to the studied presented in Chapter 8.2 and 8.3 no other reflections originating from separate lanthanum phases were registered for the La-promoted sample.

From the CO_2-TPD profiles obtained for the HT-derived mixed oxides after reduction at 900°C in 10%H_2/Ar, the number of basic sites was calculated (cp. Table 9.2). Similarly, as for the samples discussed in Chapter 8.2, the distribution of basic sites changed and the total number of basic sites increased with La introduction, especially those of medium-strength.

Table 9.2 Basicity of reduced materials (CO_2-TPD) and crystallite sizes of Ni^0 particles (XRD), TOF and Ni dispersion

Material	Total basicity [µmol/g][a]	Weak basic sites [µmol/g]	Medium strength basic sites [µmol/g]	Strong basic sites [µmol/g]	Crystallite size [nm][b]		Ni dispersion [%] reduced /spent	TOF [s^{-1}][d]
					Reduced	Spent		
Ni40	130	32	59	39	8	8	7.6 / 9.1	$3.1x10^{-2}$
Ni40La2	211	55	97	49	9	8	8.0 / 7.5	$3.4x10^{-2}$

[a] The residual error of the measurement is in the range of 10 µmol/g

[b] The weighted residual error is in the range from 3 to 6% for the crystallite size

[d] GHSV= 12000h^{-1} at 250ºC

Catalytic performance

The carbon dioxide conversion measured during catalytic CO_2 methanation experiments are plotted in Figure 9.1. Both catalysts were active in the reaction of CO_2 methanation. As for Ni15, the promotion of Ni40 with 2wt.% La increased at 250°C the CO_2 conversion, from 84.3% for Ni40 to 88.2 % for Ni40La2. Increasing the temperature to 350, 450 and 450°C resulted in quite similar CO_2 conversion, reaching thermodynamic equilibrium for both. The TOF values at GHSV = 12000 h^{-1} and 250°C (Table 9.2) were $3.1x10^{-2}$ and $3.4x10^{-2}$ for Ni40 and Ni40La2, respectively.

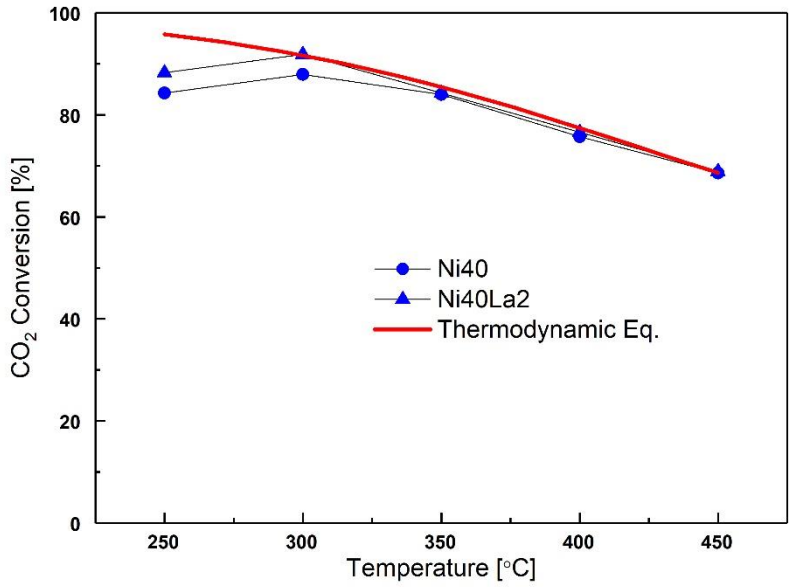

Figure 9.1 CO_2 conversion versus temperature for the studied catalysts

The selectivity towards methane as a function of temperature is plotted in Figure 9.2. Almost complete selectivity towards CH_4 of ca. 99.0 and ca. 99.6% for Ni40 and Ni40La2, respectively, was registered for the catalysts at 250°C. Only negligible amounts of carbon monoxide as side-product were recorded at higher temperatures.

24h catalytic tests were performed to study the stability of the catalysts at 250°C at GHSV = 12000h^{-1} (Figure 9.3). The 24h tests proved that the catalysts remained stable., after the first (ca.) 2 hours TOS.

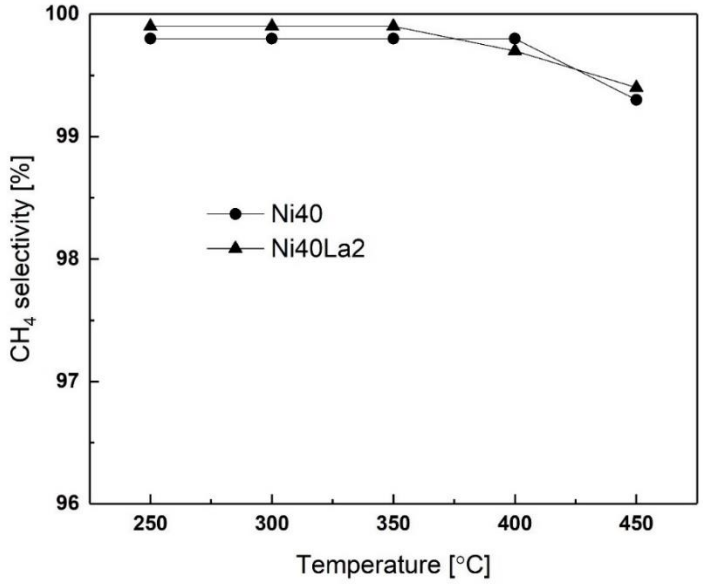

Figure 9.2 CH_4 selectivity vs function of temperature for the studied catalysts

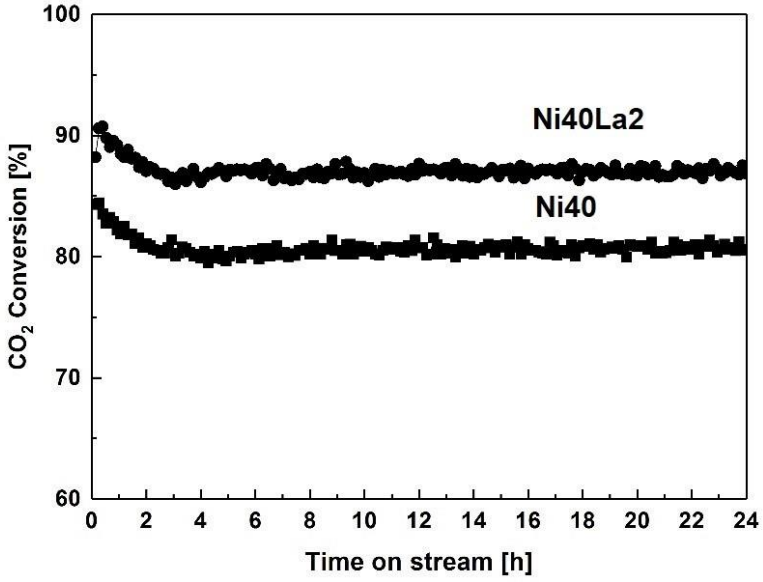

Figure 9.3 CO_2 methanation reaction performed for 24h at 250°C and GHSV = 12000h^{-1}

Characterization of the spent catalysts

Ni40 and Ni40La2 samples were characterized by XRD (Appendix, Fig. A7) and TEM (Fig. 9.4) after methanation reaction carried out at constant GHSV = 12000h^{-1}. To examine the structural changes of materials the obtained results were compared with the ones registered for samples after reduction.

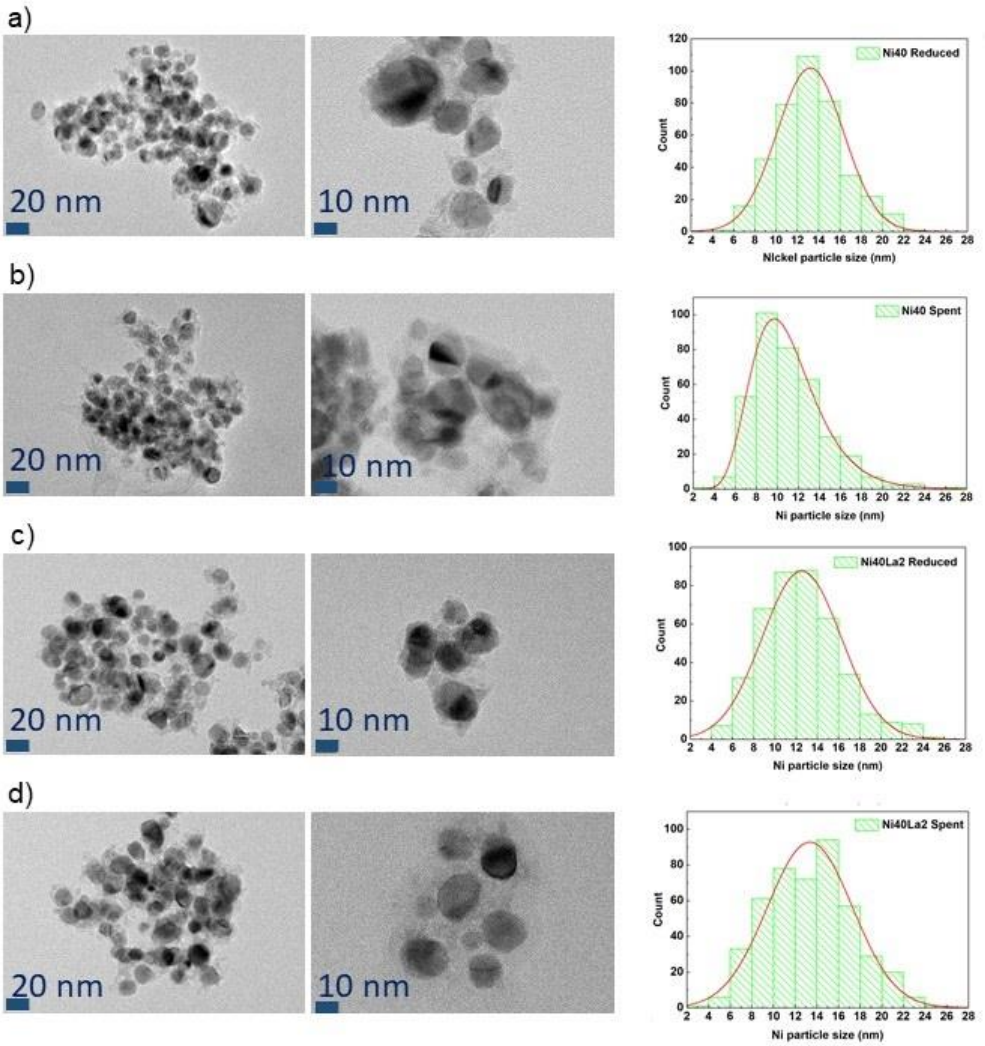

Figure 9.4 TEM images and Ni particle size distribution of: a) reduced Ni40, b) spent Ni40, c) reduced Ni40La2 and d) spent Ni40La2

XRD analysis showed no changes in crystallite sizes for the spent (cp. Appendix, Fig. A7) catalysts then compared to the reduced ones. No reflections originating from graphite phase were registered on the diffractograms of the spent catalysts.

The Ni particle mean size of calculated from TEM are in the same range as the values calculated from XRD diffractograms (Table 9.2). The reduced Ni40 catalyst showed larger metallic Ni crystallite size compared to the spent catalyst, which points to reorganization of Ni crystallites during CO_2 methanation reaction.

10. Examination of the promoting role of lanthanum – in-situ XAS and XES studies

Despite new findings both, the reaction path and the role of promoters in Ni-catalysts, still need to be elucidated. Recently, both theoretical Density Functional Theory (DFT) calculations and experimental Fourier Transform Infrared Spectroscopy (FTIR) and X-ray absorption fine structure (XAFS) have been used to describe the chemical activity of the surface of Ni-based catalyst in the CO_2 methanation process [7, 82, 225, 226]. The mechanisms proposed by literature are either an associative [58] or a dissociative one [66] as discussed in Chapter 4.1. The associative mechanism proposes the formation of oxygenate intermediates, which are subsequently hydrogenated to CH_4, while the dissociative mechanism involves the dissociation of CO_2 to adsorbed CO and O with the subsequent hydrogenation of CO to CH_4. However, in most of the publications, CO is accepted as the main intermediate in CO_2 methanation. Literature reports confirm that the synchrotron-based techniques are efficient tools for the study of active species local coordination and the behaviour of the catalysts under various conditions [11, 227]. This is why in order to examine the promoting effect of La on CO_2 methanation reaction operando XAS and XES techniques were chosen. Such techniques as HERFD-XANES or X-ray emission spectroscopy - XES may help to identify the adsorbed species, determine the chemical information and calculate the bond distances. These techniques were used to determine the local coordination and oxidation state of nickel in the studied catalysts in both reduction step and carbon dioxide methanation reaction. Valence-to-core X-ray emission spectroscopy (vtc-XES) was used to study the ligand environment of Ni species during pre-treatment and CO_2 methanation.

High Energy Resolution Fluorescence Detection – X-ray Absorption Near Edge Spectroscopy

The local coordination and oxidation state of Ni was examined using XANES. The spectra were collected during the reduction step and CO_2 methanation reaction. The XANES spectra of Ni K edge arise from symmetry allowed transitions of 1s electron to the excited vacant bound states, while the pre-edge features originiate from the transitions of 1s electron to unoccupied 3d orbital. The main absorption edge features originate from the dipole allowed transition of 1s -> 4p [228, 229]. The reference spectra (Ni foil and NiO) are plotted in Figure 10.1 together with the spectra of the Ni40 catalyst after preparation steps - fresh, calcined and reduced. The higher pre-peak intensity for the calcined Ni40 material suggests higher distortion of Ni octahedral sites in the catalyst [230]. X-ray absorption spectra of the reduced Ni40 catalyst are similar to Ni foil, thus indicating that all Ni^{2+} in Ni40 was totally reduced to Ni^0 and the Ni^0 nanoparticles are without long-range structure ordering.

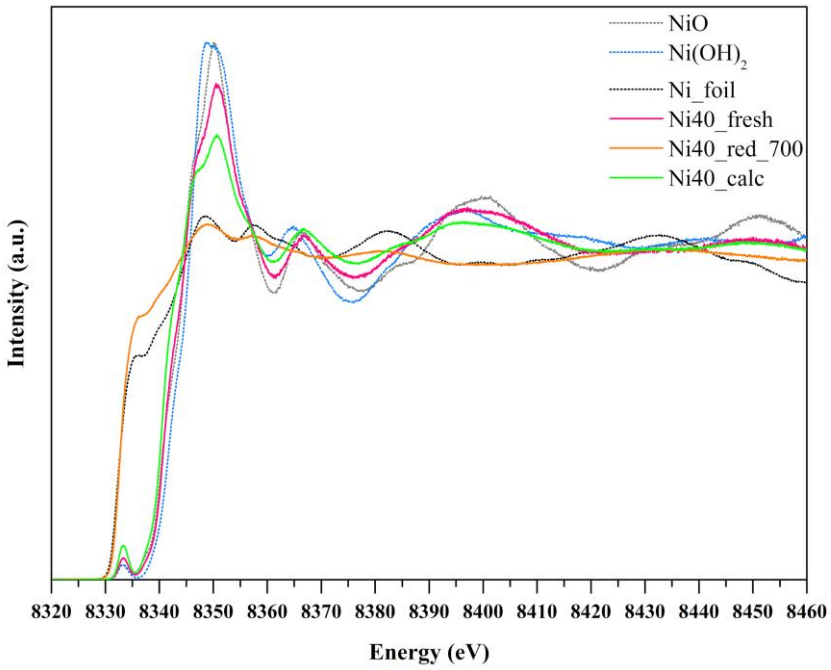

Figure 10.1 HERFD-XANES spectra of fresh, calcined and reduced Ni40 catalyst compared to reference spectra of Ni foil, Ni oxide and Ni hydroxide

Additionally, in order to follow the local environment changes of Ni the XANES spectra were recorded in-situ during reduction carried out at 400, 500, 600 and 700°C for Ni40 and Ni40La2. Before the reduction both catalysts were calcined at 500°C for 1h in air. The reduction was performed in H_2/He from room temperature to 750°C, and the spectra recorded for both catalysts during reduction are presented in Figure 10.2. From Fig. 10.2 it may be seen that the white line intensity decreased with increasing temperature of reduction. Simultaneously the pre-peak grew in intensity, reflecting a transition of nickel oxide to metallic Ni nanocrystallites. After 30 minutes treatment in H_2/He flow at 750^{o}C, no spectral features of oxide phase were registered, proving the full reduction.

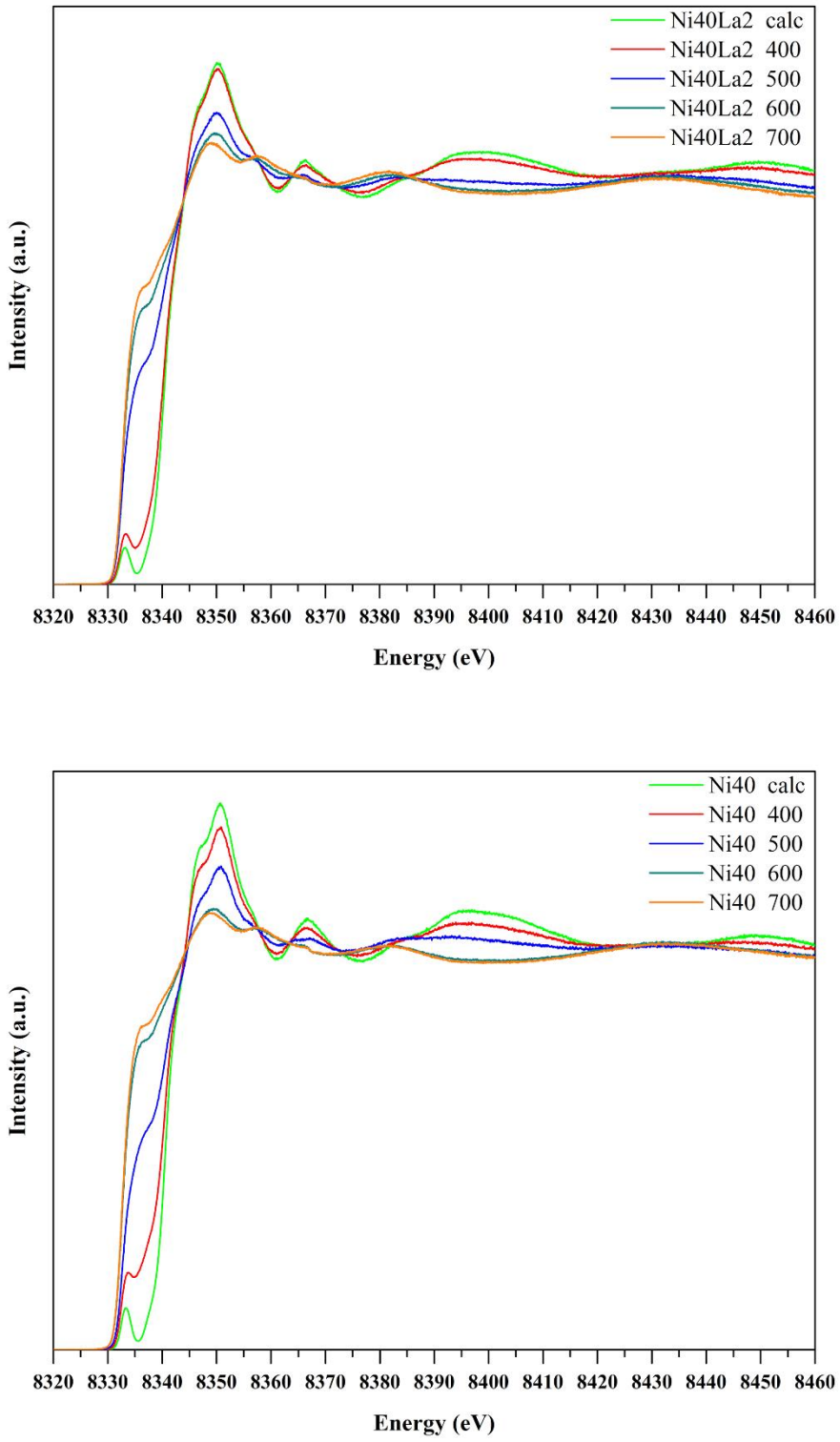

Figure 10.2 HERFD-XANES spectra evolution of both studied catalyst during in-situ reduction, calc – calcined, 400, 500, 600 and 700 – reduction temperature

The changes of Ni state were studied by changing the sequence of introduction of the reaction reagents. The catalysts, after reduction procedure mentioned above, were

exposed separately to a stream of H_2 or CO_2, as well as a mixture of both. The reactor was cooled down after the reduction at 750°C to 300°C and a mixture of 30%H_2/He was introduced. The XANES spectra collected at these conditions are almost identical to those recorded after reduction at 750°C. Subsequently, the flow of H_2/He was switched to 12% CO_2/He at the same temperature of 300°C. Only small changes were registered in the spectral features of Ni40 CO_2 catalyst in comparison to the Ni40 H_2 spectrum shown in Figure 10.3. In contrary, a considerable pre-edge peak intensity decrease may be clearly observed for Ni40La2 CO_2 as shown in Fig. 10.4. The obtained results prove that nickel in the La-promoted Ni40La2 catalyst reacts more easily with CO_2 influencing strongly Ni chemical state. While the Ni state did not change after introduction of the reaction mixture (CO_2 + H_2) for Ni40 catalyst, an intermediate state in between reduction (H_2) and oxidation (CO_2) conditions was observed for the Ni40La2 catalyst. These results show the crucial role of lanthanum introduction in the enhancement of the activity in CO_2 methanation of HT-derived catalysts.

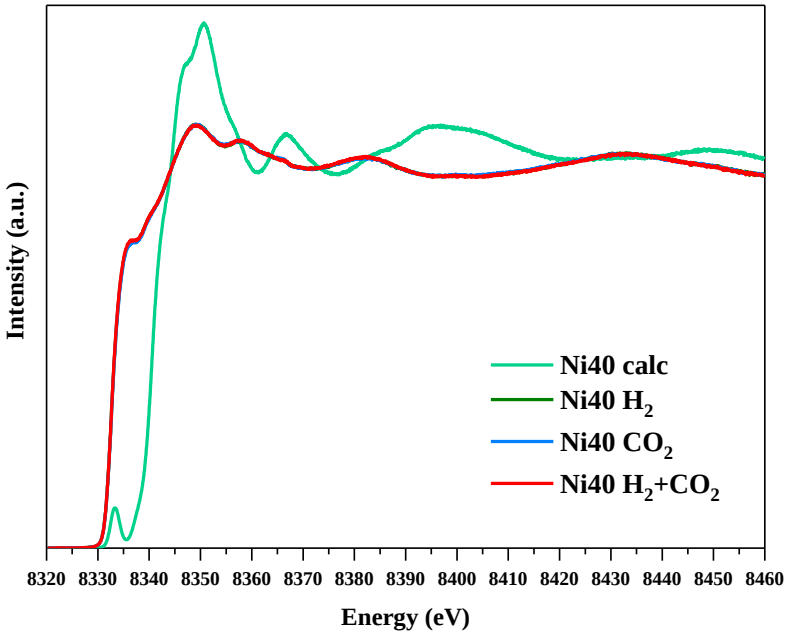

Figure 10.3 The XANES spectra of Ni40 catalyst registered under various conditions (H_2(reduction), CO_2 and CO_2+H_2).

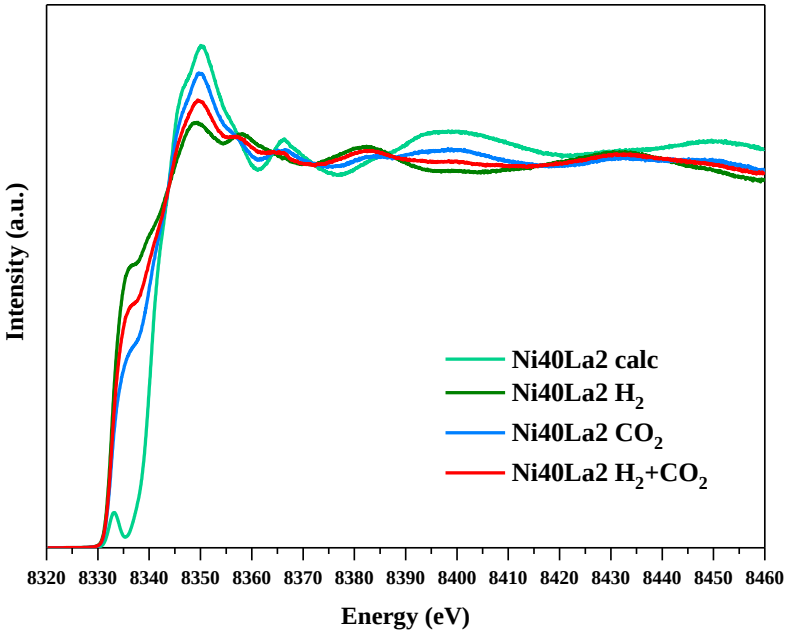

Figure 10.4 The XANES spectra of Ni40La2 catalyst registered under various conditions (H_2(reduction), CO_2 and CO_2+H_2).

The linear combination fitting (LCF) was applied to the studied XANES spectra in order to estimate the fraction of oxidized Ni and the results are summarized in Table 10.1.

Table 10.1 The fraction of Ni oxidized calculated from LC fitting of XANES spectra

Catalyst	Atmosphere	fraction of Ni oxidized
Ni40	CO_2	0.006
	$CO_2 + H_2$	0
Ni40La2	CO_2	0.37
	$CO_2 + H_2$	0.18

As shown in Table 10.1, La promotion resulted in strong Ni oxidation during the exposure to both CO_2 and CO_2+H_2 mixture. For Ni40 catalysts only 0.6% of Ni has undergone oxidation to NiO after treatment with CO_2, while for the La-promoted catalyst almost 40% of Ni was found to be oxidized to NiO. The addition of H_2 to CO_2 flow resulted in a decrease in fraction of NiO to 19% for Ni40La2, while Ni40 catalyst showed no oxidized Ni under the same conditions.

ctc-XES

The Kβ (3p → 1s) emission has a high chemical sensitivity originating from the interaction between the unpaired 3p and 3d electron spins, which leads to the arise of Kβ features – Kβ' and $K\beta_{1,3}$, which may provide information on local spin moment [231]. The variation in the local spin moment originate from a change in the metal oxidation state, the covalency degree or a spin configuration transition [232-234]. The Kβ emission spectroscopy was used as a supplementary technique to X-ray absorption spectroscopy in order to follow the changes of nickel state at various conditions and compare the results

with the LCF analysis of XANES spectra. In Figure 10.5 the spectra of both catalysts recorded during operando experiments under various conditions (H_2, CO_2 or CO_2+H_2) are presented together with those for nickel foil and nickel oxide used as reference samples. The spectra of the catalysts recorded at various conditions are between the ones of NiO and Ni foil, which indicates changes of the spin state, which may be connected with the changes in the oxidation state. The integrated absolute difference (IAD) method was applied to quantitatively present the fractions of two phases. IAD analysis considers the value of absolute difference between material's spectrum and the reference spectrum, and was described by Vanko *et al.* [235, 236]. The appropriate calcined samples Ni40 and Ni40La2 were used as reference for the respective catalyst groups. Figure 10.6 compares the fraction of NiO phase calculated by IAD analysis with the results obtained with the linear combination fitting (LCF) analysis of XANES measurements. The results of these two methods followed the same trend, though differed in values of NiO content, especially for Ni40La2 catalyst under CO_2 atmosphere. This may have arisen from different sensivity of both methods. XANES spectroscopy is very sensitive to the local chemical state of the probed element, which allows to distinguish between similar compounds. Kβ X-ray emission spectroscopy in comparison to XANES probes global chemical environment, which leads to almost similar spectra for compounds that have the same spin state.

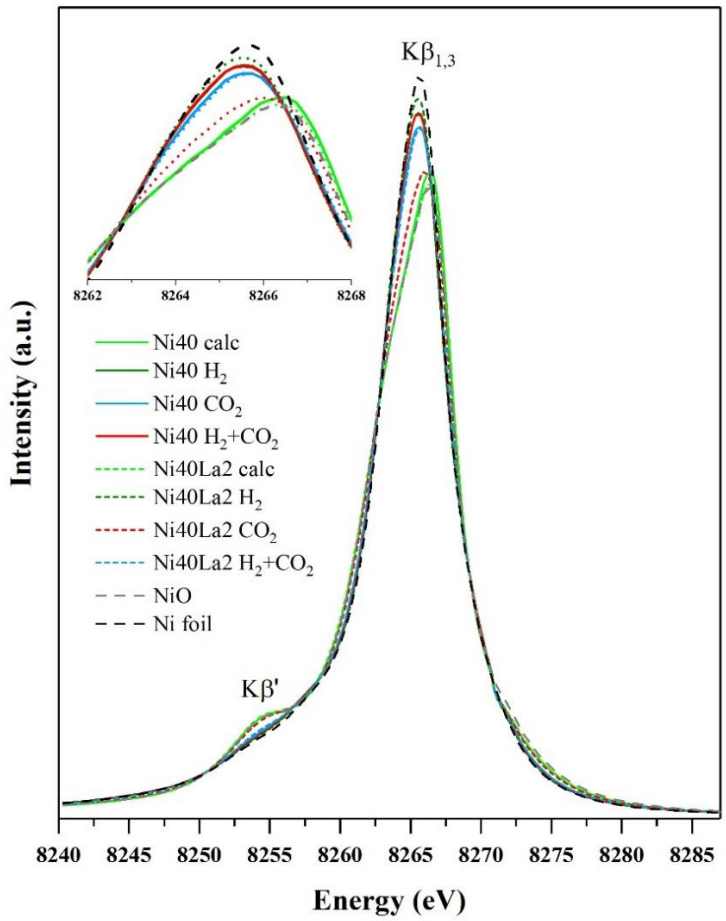

Figure 10.5 Ni Kβ core-to-core XES spectra of both catalysts under various conditions together with NiO and Ni foil as standards.

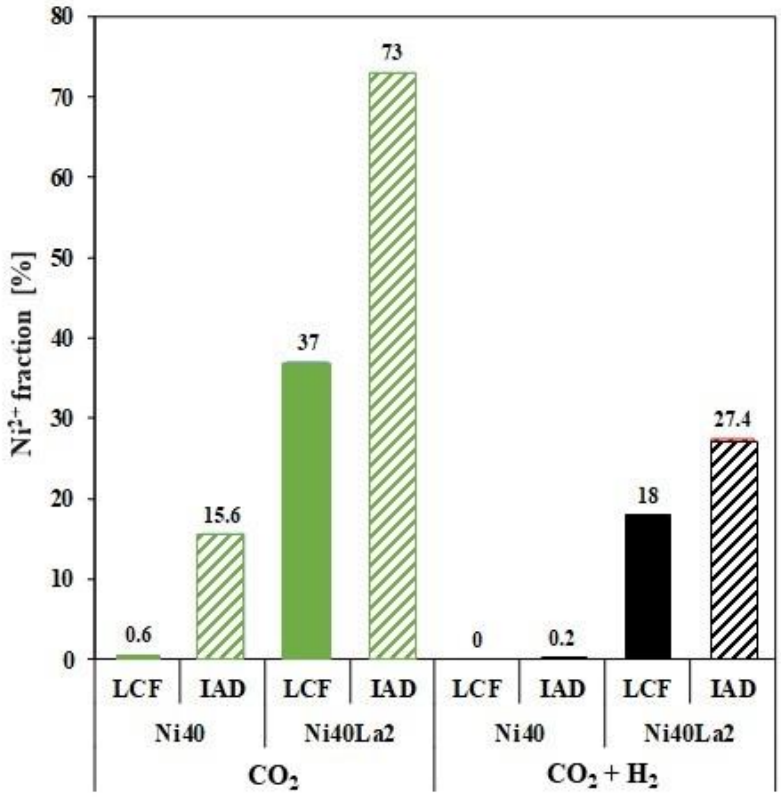

Figure 10.6 NiO fraction for both studied catalysts under (i) CO_2 and (ii) CO_2+H_2 treatments analyzed using LCF and IAD methods; the spectra of calcined materials were used as reference for the Integrated Absoluted Different analysis [237].

vtc-XES

To get an insight of atoms surrounding Ni, vtc-XES was applied, as this technique may distinguish ligands with similar atomic number [238]. The Kβ" and $K\beta_{2,5}$ features originate from the electron transition between filled ligand orbitals and 1s core hole. The Ni environment was studied using vtc-XES at similar preparation steps and in-situ conditions as for the previously mentioned techniques. The spectra of calcined Ni40 and Ni40La2 are similar to the spectrum of NiO (cp. Figure 10.7), with two intense peaks of $K\beta_{2,5}$ at ca. 8326 and ca. 8331 eV, and a broad Kβ" feature at lower energies.

After the reduction of the materials the NiO nanoparticles (present in calcined materials) were converted into nano-metallic Ni species, which finds confirmation in the merge of the $K\beta_{2,5}$ features into one peak at ca. 8329 eV and almost total disappearance of Kβ" signal, similar as for Ni foil. The introduction of CO_2 flow after reduction changed significantly the XES spectra. The decrease in intensity, which was a result of change of nickel oxidation state, of the peak at ca. 8329eV and the appearance of the peak at ca. 8326eV suggest the coverage of surface of Ni present in Ni40 by oxygen atoms after introduction of CO_2. On the other hand, the shape of vtc-XES spectrum obtained after CO_2 treatment of La-promoted sample (Ni40La2 CO_2) suggests that deep oxidation of Ni^0 species took place, resulting in formation of NiO nanoparticles. After the introduction of CO_2+H_2 mixture oxidized Ni species turned back totally to the metallic phase for Ni40 CO_2+H_2 catalysts while the formation of mixed Ni^{2+}/Ni^0 nanoparticles were registered on the surface of Ni40La2 (CO_2+H_2). This indicates that the introduction of La increased significantly the CO_2 chemisorption on the Ni particles. According to literature [79, 239, 240] CO_2 undergoes dissociative adsorption in the methanation process to adsorbed CO and atomic O species, followed by further dissociation of CO to a C intermediate. However, the results show the domination of CO_2 adsorption and that adsorbed C and CH_X species were not observed using XES technique.

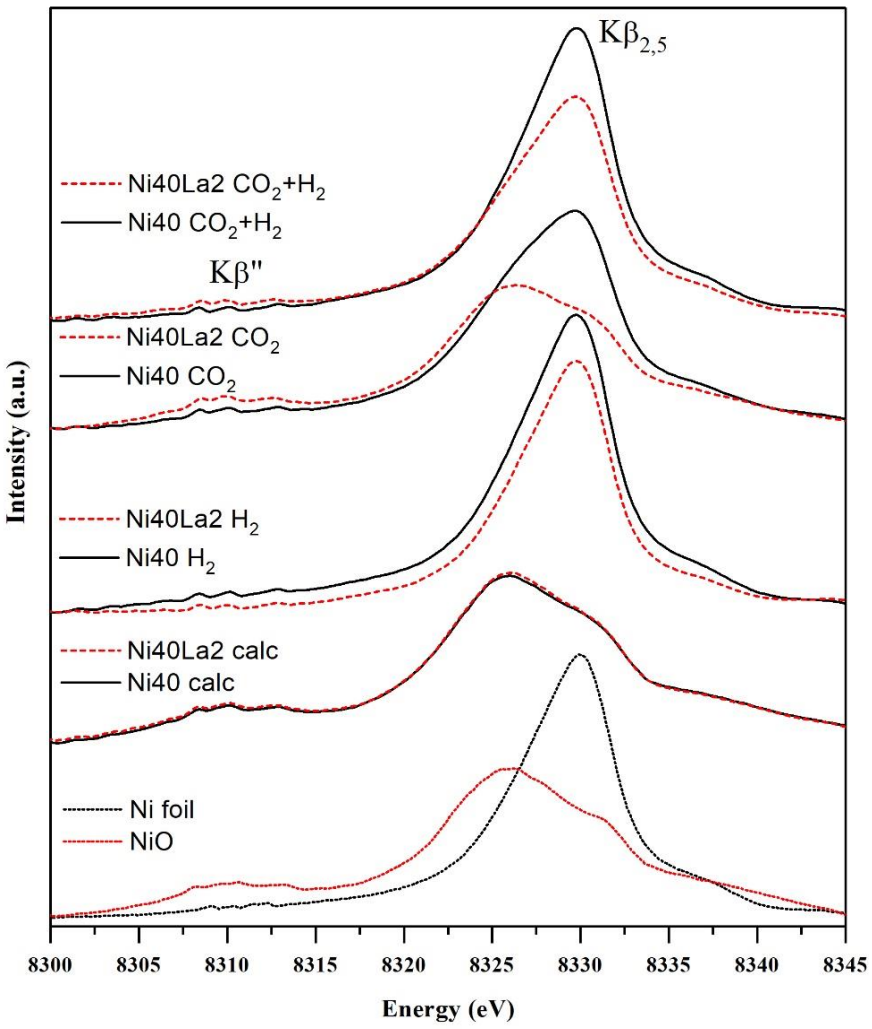

Figure 10.7 Ni Kβ vtc-XES spectra evolution of both catalysts under various conditions.

Conclusions

The promoting role of lanthanum was studied by operando HERFD-XANES, valence-to-core XES and core-to-core XES. The XANES experiments under various conditions revealed that La present in Ni-containing hydrotalcites influenced significantly the oxidation state of nickel under various conditions. Due to increased CO_2 chemisorption nickel was oxidized more easily in the La-promoted catalyst. On the other

hand, in case of the unpromoted catalyst only a small fraction of Ni was transformed from metallic to oxide state.

Integrated Absolute Difference (IAD) analysis, which was performed for the Kβ mainline allowed to determine the content of Ni oxide under various conditions and confirmed the possibility of using this analysis for in-situ experiments.

The results of vtc-XES point that the CO_2 adsorption step is not a limiting step in CO_2 methanation process. However, the formation of adsorbed C and CH_X could not be observed under the conditions applied in the experiments.

11. General conclusions

The research presented in this PhD Thesis was focused on the application of hydrotalcite-derived catalysts for CO_2 methanation reaction as one of the prospective methods of chemical utilization of CO_2. The literature analysis concerning the utilization of carbon dioxide presented in Chapter 3 proves that CO_2 methanation may become an important process for the storage of excess energy in the form of methane.

As presented in Chapter 4, a wide range of different materials has been studied as catalysts for CO_2 methanation. Currently the most intensive studies are focused on Ni-based materials supported on single oxides e.g. Al_2O_3, MgO, SiO_2, TiO_2, mixed oxides e.g. Al_2O_3-MgO, CeO_2-ZrO_2, zeolites etc. Ni-supported catalysts proved to be effective in this reaction. Some of properties of such materials affect positively the catalytic performance, e.g. increased basicity, which is a crucial factor in CO_2 activation, or the formation of small Ni^0 crystallites, which facilitate the hydrogenation reaction. Mixed oxides of alumina and magnesia possess these beneficial properties.

Hydrotalcite materials proved to be an appropriate precursor to give materials with desired properties for CO_2 methanation such as relatively high specific surface area, high basicity and homogeneous distribution of nickel. Additionally, the composition of such materials may be strictly controlled at the synthesis stage and it was also proven that they can be modified after the synthesis through e.g. adsorption method. However, the amount of studies regarding such materials as catalysts for CO_2 methanation reaction is limited. Thus, the aim of presented studies was focused on the preparation of Ni/Mg/Al hydrotalcites-like materials with different amounts of introduced nickel and to study the promoting effect of Fe and La introduction.

The prepared materials were characterized by X-ray flurorescence (XRF) or Inductively Coupled Plasma Mass Spectroscopy (ICP-MS), low temperature N_2 sorption,

X-ray diffraction (XRD), temperature-programmed reduction (H_2-TPR) and temperature-programmed desorption (CO_2-TPD). The catalysts were tested in CO_2 methanation reaction. The optimized catalysts (Chapter 9) were also characterized using transmission electron microscopy (TEM). The promoting effect of lanthanum was studied using in-situ X-ray absorption near edge structure spectroscopy and X-ray emission spectroscopy.

The research was divided into four main parts: (i) the investigation of the effect of nickel content on physicochemical properties and catalytic performance in CO_2 methanation, (ii) the effect of iron or lanthanum introduction on the catalytic properties of nickel-containing hydrotalcites (iii) investigation of the effect of lanthanum incorporation method on catalytic properties of Ni-HTs, and (iv) elucidation of the role of promotion of Ni-hydrotalcites with lanthanum in CO_2 methanation, using in-situ XANES and XES techniques.

The following conclusions may be drawn from the physico-chemical characterization of the materials:

- XRD analysis of the as-synthesized materials confirmed successful synthesis of hydrotalcite-like materials. No separate phase of Ni and Fe species were found in the diffractograms suggesting successful incorporation of these elements into the structure. Only for lanthanum-promoted samples additional phases of $La_2O_2CO_3$ and La_2O_3 were registered.
- FTIR spectra confirmed the presence of $La(EDTA)^-$ species in the materials modified using adsorption method,
- XRD analysis of the calcined materials showed that the layered structure was destroyed and Mg(Ni,Al)O and Mg(Ni,Fe,Al)O mixed nano-oxides with periclase-like structure were formed,

- Elemental analysis of the HT-derived materials proved that the desired compositions of mixed oxides were obtained, confirming that the preparation of such materials may be strictly controlled,
- H_2-TPR profiles of calcined materials showed that nickel introduced into the structure of HT-derived material interacts strongly with the support. The temperature of NiO reduction was above 600°C, and was strongly dependent on the amount of introduced nickel, as well as the addition of Fe or La,
- XRD analysis of the reduced materials revealed a separate phase of metallic nickel, and thus successful reduction of NiO, with crystallite size dependent on the amount of introduced nickel, as well as the introduction of promoter,
- CO_2-TPD profiles obtained for all reduced materials showed the presence of three types of basic sites: (i) weak Brønsted basic sites – surface OH groups, (ii) medium-strength Lewis M-O pairs and (iii) strong basic sites related to low coordinated O^{2-} anions. The total number of basic sites and their distribution was strongly dependent on both the amount of introduced nickel and the introduction of promoters.

The dependence of catalytic pefromance on the nickel content was studied for the materials materials containing 5, 10, 15, 25, 30 and 40 wt.% of Ni (fresh samples). These materials were evaluated in CO_2 methanation at the temperature range from 250 to 450°C. From these experiments the following conclusions may be drawn:

- The CO_2 conversion at 250°C increased with the increasing content of nickel. For the most active catalyst the conversion reached almost the thermodynamic equilibrium at 350°C. No differences were observed in the CO_2 conversion between all catalysts at 450°C, all of them showing values corresponding to

thermodynamic equilibrium. The higher activity of the catalysts with higher nickel content could be correlated with the increasing number of basic sites, especially those of medium-strength,

- The selectivity towards methane at 250°C was ranging from 99 to 99.9% for all catalysts except Ni5 (CH_4 selectivity of 97%). With increasing temperature CH_4 selectivity decreased, in good agreement with the thermodynamic predictions.
- The 24h-tests carried out for the worst and best catalyst (Ni5 and Ni40, respectively) proved that the CO_2 conversion remained stable,
- The XRD characterization of the catalysts after reaction showed no reflections arising from graphite,

The effect of Fe or La promoter introduction was investigated by the promotion of the material containing 15 wt.% of Ni (fresh samples) introduced into the brucite-like layers. Fe species were introduced, as confirmed by XRD, into the brucite-like layers of hydrotalcite-like materials at the co-precipitation stage. Lanthanum species added during the co-precipitation were present as a separate phase of $La_2O_2CO_3$ and La_2O_3. Alternative ways of La promotion studied were wet impregnation or adsorption from the solution of $La(EDTA)^-$.

The conclusions from this part of the studies are:

- Promotion with Fe influenced the properties of the materials, such as the number of basic sites and their distribution, texture, reducibility and the size of metallic nickel crystallites. The influence on these parameters was strongly dependent on the amount of introduced Fe (1, 2 and 4 wt.% for the fresh materials),

- The introduction of low amounts of Fe (1 or 2 wt.%) effectively increased the activity in CO_2 methanation at 250°C, while the introduction of 4 wt.% of Fe resulted in decreased activity in comparison to the unpromoted catalyst (Ni15). The decreased activity may be explained by the drastic decrease in specific surface area and, as suggested by H_2-TPR, a partial coverage of the catalysts surface with iron species. Additionally, XRD analysis of reduced materials suggests the formation of Ni-Fe alloy, which may also explain the decrease in activity,
- The metallic nickel crystallite sizes for the reduced materials decreased after the introduction of 1 wt.% of Fe and increased for the materials containing 2 and 4 wt.% of Fe. XRD analysis of catalysts after the reaction showed no reflections arising from carbon.
- The introduction of lanthanum by co-precipitation method resulted in somewhat increased reducibility, and affected strongly CO_2 adsorption capacity of the catalysts. In case of the materials promoted with small amount of La (1 wt.%) a partial blockage of existing basic sites was observed. On the other hand, 2 and 4 wt.% La promotion resulted in the increased number of new basic sites, especially those of medium-strength, which may explain the increased activity in CO_2 methanation reaction,
- The comparison of the catalysts promoted with La on the co-precipitation stage with those obtained using impregnation and adsorption methods showed the crucial importance of the choice of preparation technique. The application of impregnation method resulted in a partial blockage of the catalysts surface, resulting in the decreased number of basic sites and lower specific surface area in comparison to the unpromoted catalyst, while adsorption method led to

a significantly higher number of basic sites, especially those of medium-strength. The latter may be correlated with the enhanced activity of these catalysts in CO_2 methanation at 250°C. The highest CO_2 conversion was found for the catalysts promoted with the lowest amount of La using adsorption method. CO_2 methanation activity decreased somewhat with the increasing content of La.

In order to optimize the catalytic properties of Ni-containing hydrotalcite, the Ni-catalyst that showed the best CO_2 conversion (Ni40) was promoted with 2 wt.% of La using co-precipitation method. The general conclusions on physicochemical properties – structure, texture, reducibility and basicity could be confirmed. The catalytic performance of Ni40 could be additionally improved by 2wt.% La promotion, reaching equilibrium conversion values already at 250°C. The role of La promotion was investigated by operando XAS and XES.

The conclusions from this part of the studies are:

- Operando XANES studies revealed that La introduction influenced strongly the nickel state under various conditions. In the presence of La, nickel underwent oxidation due to the increased CO_2 chemisorption, while for the unpromoted Ni-containing sample only a small fraction of metallic nickel was transformed into oxide state.
- Valence-to-core X-ray emission spectroscopy measurements suggest that carbon dioxide adsorption is not the limiting step in the CO_2 methanation mechanism. However, the formation of $C_{(ads)}$ and $CH_{x(ads)}$ could not be observed.

Summarizing the results presented in the PhD thesis, it was proven that the catalytic properties of Ni-containing HT-derived catalysts can be tailored by:

- appropriate nickel content in the brucite-like layers of hydrotalcites,
- introduction of promoter Fe or La, and
- appropriate method of promoter introduction.

The obtained catalysts exhibited very good catalytic properties in the CO_2 methanation process. Higher nickel contents and the introduction of Fe or La as promoters effectively increased the activity. As derived from the 24h tests for the selected catalysts their stability was high and no carbon formation was found.

References

[1] M. Aresta; "Carbon Dioxide as Chemical Feedstock",2010:1-414, doi:

[2] Y.P. Patil, P.J. Tambade, S.R. Jagtap, B.M. Bhanage; "Carbon dioxide: a renewable feedstock for the synthesis of fine and bulk chemicals",Frontiers of Chemical Engineering in China, 2010;4:213-235, doi: 10.1007/s11705-009-0227-0

[3] F. Cavani, F. Trifirò, A. Vaccari; "Hydrotalcite-type anionic clays: Preparation, properties and applications",Catalysis Today, 1991;11:173-301, doi: https://doi.org/10.1016/0920-5861(91)80068-K

[4] G.A. Somorjai; "Modern Surface Science and Surface Technologies: An Introduction",Chemical Reviews, 1996;96:1223-1236, doi: 10.1021/cr950234e

[5] "U.S. Energy Information Administration, International Energy Statistics, (http://www.eia.gov/cfapps/ipdbproject/IEDIndex3.cfm), Accessed: 05.08.2018",doi:

[6] L. He, Q. Lin, Y. Liu, Y. Huang; "Unique catalysis of Ni-Al hydrotalcite derived catalyst in CO_2 methanation: cooperative effect between Ni nanoparticles and a basic support",Journal of Energy Chemistry, 2014;23:587-592, doi: https://doi.org/10.1016/S2095-4956(14)60144-3

[7] B. Mutz, H.W.P. Carvalho, S. Mangold, W. Kleist, J.-D. Grunwaldt; "Methanation of CO_2: Structural response of a Ni-based catalyst under fluctuating reaction conditions unraveled by operando spectroscopy",Journal of Catalysis, 2015;327:48-53, doi: https://doi.org/10.1016/j.jcat.2015.04.006

[8] A. Samanta, A. Zhao, G.K.H. Shimizu, P. Sarkar, R. Gupta; "Post-Combustion CO2 Capture Using Solid Sorbents: A Review",Industrial & Engineering Chemistry Research, 2012;51:1438-1463, doi: 10.1021/ie200686q

[9] A. Padurean, C.-C. Cormos, P.-S. Agachi; "Pre-combustion carbon dioxide capture by gas–liquid absorption for Integrated Gasification Combined Cycle power plants",International Journal of Greenhouse Gas Control, 2012;7:1-11, doi: https://doi.org/10.1016/j.ijggc.2011.12.007

[10] C. Kunze, H. Spliethoff; "Assessment of oxy-fuel, pre- and post-combustion-based carbon capture for future IGCC plants",Applied Energy, 2012;94:109-116, doi: https://doi.org/10.1016/j.apenergy.2012.01.013

[11] T. Gunter, H.W.P. Carvalho, D.E. Doronkin, T. Sheppard, P. Glatzel, A.J. Atkins, J. Rudolph, C.R. Jacob, M. Casapu, J.-D. Grunwaldt; "Structural snapshots of the SCR reaction mechanism on Cu-SSZ-13",Chemical Communications, 2015;51:9227-9230, doi: 10.1039/C5CC01758K

[12] H.A. J., S.E.H. K., M. Ray, C.J. H.; "Generation, Capture, and Utilization of Industrial Carbon Dioxide",ChemSusChem, 2010;3:306-322, doi: doi:10.1002/cssc.200900169

[13] G.T. Rochelle; "Amine Scrubbing for CO_2 Capture",Science, 2009;325:1652-1654, doi: 10.1126/science.1176731

[14] D.Y.C. Leung, G. Caramanna, M.M. Maroto-Valer; "An overview of current status of carbon dioxide capture and storage technologies",Renewable and Sustainable Energy Reviews, 2014;39:426-443, doi: https://doi.org/10.1016/j.rser.2014.07.093

[15] L. Dubois, D. Thomas; "Screening of Aqueous Amine-Based Solvents for Postcombustion CO_2 Capture by Chemical Absorption",Chemical Engineering & Technology, 2012;35:513-524, doi: 10.1002/ceat.201100523

[16] J.C.M. Pires, F.G. Martins, M.C.M. Alvim-Ferraz, M. Simões; "Recent developments on carbon capture and storage: An overview",Chemical Engineering Research and Design, 2011;89:1446-1460, doi: https://doi.org/10.1016/j.cherd.2011.01.028

[17] "IEA Greenhouse Gas R&D Programme (IEA GHG), "CO_2 capture ready plants", 2007/4, May 2007. Chapter 7.2",

[18] J.A. Mason, K. Sumida, Z.R. Herm, R. Krishna, J.R. Long; "Evaluating metal-organic frameworks for post-combustion carbon dioxide capture via temperature swing adsorption",Energy & Environmental Science, 2011;4:3030-3040, doi: 10.1039/C1EE01720A

[19] H. Li, K. Wang, D. Feng, Y.-P. Chen, W. Verdegaal, H.-C. Zhou; "Incorporation of Alkylamine into Metal–Organic Frameworks through a Brønsted Acid–Base Reaction for CO2 Capture",ChemSusChem, 2016;9:2832-2840, doi: 10.1002/cssc.201600768

[20] C. Preston, M. Monea, W. Jazrawi, K. Brown, S. Whittaker, D. White, D. Law, R. Chalaturnyk, B. Rostron; "IEA GHG Weyburn CO_2 monitoring and storage project",Fuel Processing Technology, 2005;86:1547-1568, doi: https://doi.org/10.1016/j.fuproc.2005.01.019

[21] T.A. Torp, J. Gale; "Demonstrating storage of CO_2 in geological reservoirs: The Sleipner and SACS projects",Energy, 2004;29:1361-1369, doi: https://doi.org/10.1016/j.energy.2004.03.104

[22] R.M. Enick, D.K. Olsen, J.R. Ammer, W. Schuller, Mobility and Conformance Control for CO2 EOR via Thickeners, Foams, and Gels -- A Literature Review of 40 Years of Research and Pilot Tests, Society of Petroleum Engineers.

[23] Z. Dai, R. Middleton, H. Viswanathan, J. Fessenden-Rahn, J. Bauman, R. Pawar, S.-Y. Lee, B. McPherson; "An Integrated Framework for Optimizing CO_2 Sequestration and Enhanced Oil Recovery",Environmental Science & Technology Letters, 2014;1:49-54, doi: 10.1021/ez4001033

[24] D.P. Schrag; "Preparing to Capture Carbon",Science, 2007;315:812-813, doi: 10.1126/science.1137632

[25] T.F. Faisal, S. Chevalier, Y. Bernabe, R. Juanes, M. Sassi; "Quantitative and qualitative study of density driven CO_2 mass transfer in a vertical Hele-Shaw

cell",International Journal of Heat and Mass Transfer, 2015;81:901-914, doi: https://doi.org/10.1016/j.ijheatmasstransfer.2014.11.017

[26] H.d. Coninck, S.M. Benson; "Carbon Dioxide Capture and Storage: Issues and Prospects",Annual Review of Environment and Resources, 2014;39:243-270, doi: 10.1146/annurev-environ-032112-095222

[27] S. Dołęgowska, A. Gałuszka, Z.M. Migaszewski; "Assessing soil sampling uncertainty in heterogeneous historic metal ore mining sites",Accreditation and Quality Assurance, 2015;20:163-170, doi: 10.1007/s00769-015-1109-4

[28] G. Centi, S. Perathoner; "Opportunities and prospects in the chemical recycling of carbon dioxide to fuels",Catalysis Today, 2009;148:191-205, doi: https://doi.org/10.1016/j.cattod.2009.07.075

[29] E.A. Quadrelli, G. Centi, J.-L. Duplan, S. Perathoner; "Carbon Dioxide Recycling: Emerging Large-Scale Technologies with Industrial Potential",ChemSusChem, 2011;4:1194-1215, doi: 10.1002/cssc.201100473

[30] P.N.E. Chris Hendriks, Paul Zakkour and Greg Cook (Carbon Counts); "Final Report: Implications of the Reuse of Captured CO2 for European Climate Action Policies, Project number: CLIMA.C.1/SER/2011/0033",2013;

[31] P.F.M.D.M. BOCIN DUMITRIU Andrei, TZIMAS Evangelos; "Carbon Capture and Utilisation Workshop: Background and proceedings",Publications Office of the European Union, 2013;doi:

[32] M.d.M.P.F. Andrei Bocin-Dumitriu, Evangelos Tzimas, Thea Sveen; "JRC Scientific and Policy Reports, Carbon Capture and Utilisation Workshop Background and proceedings",Luxembourg: Publications Office of the European Union, 2013;doi: doi:10.2790/11560

[33] "Parsons & Brinckerhoff, Accelerating The Uptake Of CCS: Industrial Use of Captured Carbon Dioxide, March 2011, Global CCS Institute",doi:

[34] E. Alper, O. Yuksel Orhan; "CO2 utilization: Developments in conversion processes",Petroleum, 2017;3:109-126, doi: https://doi.org/10.1016/j.petlm.2016.11.003

[35] K.S. Lackner, D.P. Butt, C.H. Wendt; "Progress on binding CO_2 in mineral substrates",Energy Conversion and Management, 1997;38:S259-S264, doi: https://doi.org/10.1016/S0196-8904(96)00279-8

[36] K.S. Lackner, C.H. Wendt, D.P. Butt, E.L. Joyce, D.H. Sharp; "Carbon dioxide disposal in carbonate minerals",Energy, 1995;20:1153-1170, doi: https://doi.org/10.1016/0360-5442(95)00071-N

[37] P.B. Kelemen, J. Matter; "In situ carbonation of peridotite for CO_2 storage",Proceedings of the National Academy of Sciences, 2008;105:17295-17300, doi: 10.1073/pnas.0805794105

[38] E.M. Mervine, S.E. Humphris, K.W.W. Sims, P.B. Kelemen, W.J. Jenkins; "Carbonation rates of peridotite in the Samail Ophiolite, Sultanate of Oman, constrained

through 14C dating and stable isotopes",Geochimica et Cosmochimica Acta, 2014;126:371-397, doi: https://doi.org/10.1016/j.gca.2013.11.007

[39] M. Pérez-Fortes, A. Bocin-Dumitriu, E. Tzimas; "CO_2 Utilization Pathways: Techno-Economic Assessment and Market Opportunities",Energy Procedia, 2014;63:7968-7975, doi: https://doi.org/10.1016/j.egypro.2014.11.834

[40] S. Porada, G. Czerski, T. Dziok, P. Grzywacz, D. Makowska; "Kinetics of steam gasification of bituminous coals in terms of their use for underground coal gasification",Fuel Processing Technology, 2015;130:282-291, doi: https://doi.org/10.1016/j.fuproc.2014.10.015

[41] "A. Strugała, Czerski, G., Studies on coal gasification in Poland, Przemysł Chemiczny, 91 (2012) 2181-2185.",doi:

[42] W. Wang, S. Wang, X. Ma, J. Gong; "Recent advances in catalytic hydrogenation of carbon dioxide",Chemical Society Reviews, 2011;40:3703-3727, doi: 10.1039/C1CS15008A

[43] M. Peters, B. Köhler, W. Kuckshinrichs, W. Leitner, P. Markewitz, T.E. Müller; "Chemical Technologies for Exploiting and Recycling Carbon Dioxide into the Value Chain",ChemSusChem, 2011;4:1216-1240, doi: doi:10.1002/cssc.201000447

[44] T. Maihom, S. Wannakao, B. Boekfa, J. Limtrakul; "Production of Formic Acid via Hydrogenation of CO_2 over a Copper-Alkoxide-Functionalized MOF: A Mechanistic Study",The Journal of Physical Chemistry C, 2013;117:17650-17658, doi: 10.1021/jp405178p

[45] G. Peng, S.J. Sibener, G.C. Schatz, S.T. Ceyer, M. Mavrikakis; "CO_2 Hydrogenation to Formic Acid on Ni(111)",The Journal of Physical Chemistry C, 2012;116:3001-3006, doi: 10.1021/jp210408x

[46] Y. Himeda, S. Miyazawa, T. Hirose; "Interconversion between Formic Acid and H2/CO2 using Rhodium and Ruthenium Catalysts for CO_2 Fixation and H_2 Storage",ChemSusChem, 2011;4:487-493, doi: 10.1002/cssc.201000327

[47] R. Tanaka, M. Yamashita, K. Nozaki; "Catalytic Hydrogenation of Carbon Dioxide Using Ir(III)−Pincer Complexes",Journal of the American Chemical Society, 2009;131:14168-14169, doi: 10.1021/ja903574e

[48] C.-L. Chiang, K.-S. Lin, H.-W. Chuang, C.-M. Wu; "Conversion of hydrogen/carbon dioxide into formic acid and methanol over Cu/$CuCr_2O_4$ catalyst",International Journal of Hydrogen Energy, 2017;42:23647-23663, doi: https://doi.org/10.1016/j.ijhydene.2017.04.226

[49] C. Federsel, A. Boddien, R. Jackstell, R. Jennerjahn, P.J. Dyson, R. Scopelliti, G. Laurenczy, M. Beller; "A Well-Defined Iron Catalyst for the Reduction of Bicarbonates and Carbon Dioxide to Formates, Alkyl Formates, and Formamides",Angewandte Chemie International Edition, 2010;49:9777-9780, doi: 10.1002/anie.201004263

[50] G.H. Gunasekar, K. Park, K.-D. Jung, S. Yoon; "Recent developments in the catalytic hydrogenation of CO2 to formic acid/formate using heterogeneous catalysts",Inorganic Chemistry Frontiers, 2016;3:882-895, doi: 10.1039/C5QI00231A

[51] S. Moret, P.J. Dyson, G. Laurenczy; "Direct synthesis of formic acid from carbon dioxide by hydrogenation in acidic media",Nature Communications, 2014;5:4017, doi: 10.1038/ncomms5017

https://www.nature.com/articles/ncomms5017#supplementary-information

[52] Y.-y. Ohnishi, Y. Nakao, H. Sato, S. Sakaki; "Ruthenium(II)-Catalyzed Hydrogenation of Carbon Dioxide to Formic Acid. Theoretical Study of Significant Acceleration by Water Molecules",Organometallics, 2006;25:3352-3363, doi: 10.1021/om060307s

[53] "Green Carbon Dioxide: Advances in CO_2 Utilization, Editors: G. Centi and S. Perathoner, John Wiley & Sons, Hoboken, NJ, Mar 2014."

[54] S. Rönsch, J. Schneider, S. Matthischke, M. Schlüter, M. Götz, J. Lefebvre, P. Prabhakaran, S. Bajohr; "Review on methanation – From fundamentals to current projects",Fuel, 2016;166:276-296, doi: https://doi.org/10.1016/j.fuel.2015.10.111

[55] ""Un démonstrateur Power to gas en service à Nantes". Le Moniteur (in French). 2018.",doi:

[56] P. Frontera, A. Macario, M. Ferraro, P. Antonucci; "Supported Catalysts for CO_2 Methanation: A Review",Catalysts, 2017;7:59, doi:

[57] B. Miao, S. Ma, X. Wang, H. Su, S.H. Chan, Catalysis Mechanisms of CO_2 and CO Methanation, 2016.

[58] P.A.U. Aldana, F. Ocampo, K. Kobl, B. Louis, F. Thibault-Starzyk, M. Daturi, P. Bazin, S. Thomas, A.C. Roger; "Catalytic CO_2 valorization into CH_4 on Ni-based ceria-zirconia. Reaction mechanism by operando IR spectroscopy",Catalysis Today, 2013;215:201-207, doi: https://doi.org/10.1016/j.cattod.2013.02.019

[59] C. Schild, A. Wokaun, R.A. Koeppel, A. Baiker; "Carbon dioxide hydrogenation over nickel/zirconia catalysts from amorphous precursors: on the mechanism of methane formation",The Journal of Physical Chemistry, 1991;95:6341-6346, doi: 10.1021/j100169a049

[60] M.R. Prairie, A. Renken, J.G. Highfield, K. Ravindranathan Thampi, M. Grätzel; "A fourier transform infrared spectroscopic study of CO_2 methanation on supported ruthenium",Journal of Catalysis, 1991;129:130-144, doi: https://doi.org/10.1016/0021-9517(91)90017-X

[61] D.C. Upham, A.R. Derk, S. Sharma, H. Metiu, E.W. McFarland; "CO_2 methanation by Ru-doped ceria: the role of the oxidation state of the surface",Catalysis Science & Technology, 2015;5:1783-1791, doi: 10.1039/C4CY01106F

[62] A. Westermann, B. Azambre, M.C. Bacariza, I. Graça, M.F. Ribeiro, J.M. Lopes, C. Henriques; "Insight into CO_2 methantion mechanism over Ni USY zeolite: operando

IR study",Applied Catalysis B: Environmental, 2015;174-175:120-125, doi: https://doi.org/10.1016/j.apcatb.2015.02.026

[63] Q. Pan, J. Peng, S. Wang, S. Wang; "In situ FTIR spectroscopic study of the CO_2 methanation mechanism on $Ni/Ce_{0.5}Zr_{0.5}O_2$",Catalysis Science & Technology, 2014;4:502-509, doi: 10.1039/C3CY00868A

[64] J. Barrault, A. Alouche; "Isotopic exchange measurements of the rate of interconversion of carbon monoxide and carbon dioxide over nickel supported on rare earth oxides",Applied Catalysis, 1990;58:255-267, doi: https://doi.org/10.1016/S0166-9834(00)82294-0

[65] A. Borgschulte, N. Gallandat, B. Probst, R. Suter, E. Callini, D. Ferri, Y. Arroyo, R. Erni, H. Geerlings, A. Zuttel; "Sorption enhanced CO_2 methanation",Physical Chemistry Chemical Physics, 2013;15:9620-9625, doi: 10.1039/C3CP51408K

[66] G.D. Weatherbee, C.H. Bartholomew; "Hydrogenation of CO2 on group VIII metals: II. Kinetics and mechanism of CO2 hydrogenation on nickel",Journal of Catalysis, 1982;77:460-472, doi: https://doi.org/10.1016/0021-9517(82)90186-5

[67] J.W.E. Coenen, P.F.M.T. van Nisselrooy, M.H.J.M. de Croon, P.F.H.A. van Dooren, R.Z.C. van Meerten; "The dynamics of methanation of carbon monoxide on nickel catalysts",Applied Catalysis, 1986;25:1-8, doi: https://doi.org/10.1016/S0166-9834(00)81215-4

[68] M.P. Andersson, F. Abild-Pedersen, I.N. Remediakis, T. Bligaard, G. Jones, J. Engbæk, O. Lytken, S. Horch, J.H. Nielsen, J. Sehested, J.R. Rostrup-Nielsen, J.K. Nørskov, I. Chorkendorff; "Structure sensitivity of the methanation reaction: H_2-induced CO dissociation on nickel surfaces",Journal of Catalysis, 2008;255:6-19, doi: https://doi.org/10.1016/j.jcat.2007.12.016

[69] M. Jacquemin, A. Beuls, P. Ruiz; "Catalytic production of methane from CO_2 and H_2 at low temperature: Insight on the reaction mechanism",Catalysis Today, 2010;157:462-466, doi: https://doi.org/10.1016/j.cattod.2010.06.016

[70] A. Beuls, C. Swalus, M. Jacquemin, G. Heyen, A. Karelovic, P. Ruiz; "Methanation of CO_2: Further insight into the mechanism over $Rh/\gamma\text{-}Al_2O_3$ catalyst",Applied Catalysis B: Environmental, 2012;113-114:2-10, doi: https://doi.org/10.1016/j.apcatb.2011.02.033

[71] S. Eckle, H.-G. Anfang, R.J. Behm; "Reaction Intermediates and Side Products in the Methanation of CO and CO_2 over Supported Ru Catalysts in H_2-Rich Reformate Gases",The Journal of Physical Chemistry C, 2011;115:1361-1367, doi: 10.1021/jp108106t

[72] M. Marwood, R. Doepper, A. Renken; "In-situ surface and gas phase analysis for kinetic studies under transient conditions The catalytic hydrogenation of CO_2",Applied Catalysis A: General, 1997;151:223-246, doi: https://doi.org/10.1016/S0926-860X(96)00267-0

[73] F. Solymosi, A. Erdöhelyi, T. Bánsági; "Methanation of CO_2 on supported rhodium catalyst",Journal of Catalysis, 1981;68:371-382, doi: https://doi.org/10.1016/0021-9517(81)90106-8

[74] F. Solymosi, A. Erdohelyi, M. Kocsis; "Methanation of CO_2 on supported Ru catalysts",Journal of the Chemical Society, Faraday Transactions 1: Physical Chemistry in Condensed Phases, 1981;77:1003-1012, doi: 10.1039/F19817701003

[75] J. Gao, Y. Wang, Y. Ping, D. Hu, G. Xu, F. Gu, F. Su; "A thermodynamic analysis of methanation reactions of carbon oxides for the production of synthetic natural gas",RSC Advances, 2012;2:2358-2368, doi: 10.1039/C2RA00632D

[76] J. Kopyscinski, T.J. Schildhauer, S.M.A. Biollaz; "Production of synthetic natural gas (SNG) from coal and dry biomass – A technology review from 1950 to 2009",Fuel, 2010;89:1763-1783, doi: https://doi.org/10.1016/j.fuel.2010.01.027

[77] G.A. Mills, F.W. Steffgen; "Catalytic Methanation",Catalysis Reviews, 1974;8:159-210, doi: 10.1080/01614947408071860

[78] V. Ponec; "Some Aspects of the Mechanism of Methanation and Fischer-Tropsch Synthesis",Catalysis Reviews, 1978;18:151-171, doi: 10.1080/03602457808067530

[79] J.G. Wei WANG; "Methanation of carbon dioxide: an overview",Front. Chem. Sci. Eng., 2011;5:2-10, doi: 10.1007/s11705-010-0528-3

[80] R.W. Dorner, D.R. Hardy, F.W. Williams, H.D. Willauer; "Heterogeneous catalytic CO_2 conversion to value-added hydrocarbons",Energy & Environmental Science, 2010;3:884-890, doi: 10.1039/C001514H

[81] K. Stangeland, D. Kalai, H. Li, Z. Yu, CO_2 Methanation: The Effect of Catalysts and Reaction Conditions, 2017.

[82] W. Wei, G. Jinlong; "Methanation of carbon dioxide: an overview",Frontiers of Chemical Science and Engineering, 2011;5:2-10, doi: 10.1007/s11705-010-0528-3

[83] M.A.A. Aziz, A.A. Jalil, S. Triwahyono, A. Ahmad; "CO_2 methanation over heterogeneous catalysts: recent progress and future prospects",Green Chemistry, 2015;17:2647-2663, doi: 10.1039/C5GC00119F

[84] K. Ghaib, K. Nitz, F.-Z. Ben-Fares; "Chemical Methanation of CO_2: A Review",ChemBioEng Reviews, 2016;3:266-275, doi: 10.1002/cben.201600022

[85] X. Su, J. Xu, B. Liang, H. Duan, B. Hou, Y. Huang; "Catalytic carbon dioxide hydrogenation to methane: A review of recent studies",Journal of Energy Chemistry, 2016;25:553-565, doi: https://doi.org/10.1016/j.jechem.2016.03.009

[86] M.A.A. Aziz, A.A. Jalil, S. Triwahyono, S.M. Sidik; "Methanation of carbon dioxide on metal-promoted mesostructured silica nanoparticles",Applied Catalysis A: General, 2014;486:115-122, doi: https://doi.org/10.1016/j.apcata.2014.08.022

[87] P. Panagiotopoulou; "Hydrogenation of CO_2 over supported noble metal catalysts",Applied Catalysis A: General, 2017;542:63-70, doi: https://doi.org/10.1016/j.apcata.2017.05.026

[88] N.M. Martin, P. Velin, M. Skoglundh, M. Bauer, P.-A. Carlsson; "Catalytic hydrogenation of CO_2 to methane over supported Pd, Rh and Ni catalysts",Catalysis Science & Technology, 2017;7:1086-1094, doi: 10.1039/C6CY02536F

[89] "InfoMine: Mining Intelligence & Technology. <http://www.infomine.com/investment/nickel/> <http://www.infomine.com/investment/ruthenium/> [download 23.01.2018]",doi:

[90] M. Mihet, M.D. Lazar; "Methanation of CO_2 on Ni/γ-Al_2O_3: Influence of Pt, Pd or Rh promotion",Catalysis Today, 2016;doi: https://doi.org/10.1016/j.cattod.2016.12.001

[91] S. Rahmani, M. Rezaei, F. Meshkani; "Preparation of highly active nickel catalysts supported on mesoporous nanocrystalline γ-Al_2O_3 for CO_2 methanation",Journal of Industrial and Engineering Chemistry, 2014;20:1346-1352, doi: https://doi.org/10.1016/j.jiec.2013.07.017

[92] A. Erhan Aksoylu, Z. İlsenÖnsan; "Hydrogenation of carbon oxides using coprecipitated and impregnated Ni/Al_2O_3 catalysts",Applied Catalysis A: General, 1997;164:1-11, doi: https://doi.org/10.1016/S0926-860X(97)00151-8

[93] S. Hwang, U.G. Hong, J. Lee, J.H. Baik, D.J. Koh, H. Lim, I.K. Song; "Methanation of Carbon Dioxide Over Mesoporous Nickel-M/Alumina (M=Fe, Zr, Ni, Y and Mg) Xerogel Catalysts: Effect of Second Metal",Catalysis Letters, 2012;142:860-868, doi: 10.1007/s10562-012-0842-0

[94] C. Jia, J. Gao, J. Li, F. Gu, G. Xu, Z. Zhong, F. Su; "Nickel catalysts supported on calcium titanate for enhanced CO methanation",Catalysis Science & Technology, 2013;3:490-499, doi: 10.1039/C2CY20542D

[95] H. Liu, X. Zou, X. Wang, X. Lu, W. Ding; "Effect of CeO_2 addition on Ni/Al_2O_3 catalysts for methanation of carbon dioxide with hydrogen",Journal of Natural Gas Chemistry, 2012;21:703-707, doi: https://doi.org/10.1016/S1003-9953(11)60422-2

[96] S. Tada, T. Shimizu, H. Kameyama, T. Haneda, R. Kikuchi; "Ni/CeO_2 catalysts with high CO_2 methanation activity and high CH_4 selectivity at low temperatures",International Journal of Hydrogen Energy, 2012;37:5527-5531, doi: https://doi.org/10.1016/j.ijhydene.2011.12.122

[97] Y. Feng, W. Yang, S. Chen, W. Chu; "Cerium Promoted Nano Nickel Catalysts Ni-Ce/CNTs and Ni-Ce/Al_2O_3 for CO_2 Methanation",Integrated Ferroelectrics, 2014;151:116-125, doi: 10.1080/10584587.2014.901141

[98] F.-W. Chang, M.-T. Tsay, S.-P. Liang; "Hydrogenation of CO_2 over nickel catalysts supported on rice husk ash prepared by ion exchange",Applied Catalysis A: General, 2001;209:217-227, doi: https://doi.org/10.1016/S0926-860X(00)00772-9

[99] F.-W. Chang, M.-S. Kuo, M.-T. Tsay, M.-C. Hsieh; "Hydrogenation of CO_2 over nickel catalysts on rice husk ash-alumina prepared by incipient wetness impregnation",Applied Catalysis A: General, 2003;247:309-320, doi: https://doi.org/10.1016/S0926-860X(03)00181-9

[100] H. Ando, M. Fujiwara, Y. Matsumura, H. Miyamura, Y. Souma; "Methanation of carbon dioxide over LaNi4X type catalysts",Energy Conversion and Management, 1995;36:653-656, doi: https://doi.org/10.1016/0196-8904(95)00090-Z

[101] H. Song, J. Yang, J. Zhao, L. Chou; "Methanation of Carbon Dioxide over Highly Dispersed Ni/La_2O_3 Catalyst",Chinese Journal of Catalysis, 2010;31:21-23, doi: https://doi.org/10.1016/S1872-2067(09)60036-X

[102] M. Cai, J. Wen, W. Chu, X. Cheng, Z. Li; "Methanation of carbon dioxide on Ni/ZrO2-Al2O3 catalysts: Effects of ZrO_2 promoter and preparation method of novel ZrO2-Al2O3 carrier",Journal of Natural Gas Chemistry, 2011;20:318-324, doi: https://doi.org/10.1016/S1003-9953(10)60187-9

[103] G. Du, S. Lim, Y. Yang, C. Wang, L. Pfefferle, G.L. Haller; "Methanation of carbon dioxide on Ni-incorporated MCM-41 catalysts: The influence of catalyst pretreatment and study of steady-state reaction",Journal of Catalysis, 2007;249:370-379, doi: https://doi.org/10.1016/j.jcat.2007.03.029

[104] G.D. Lee, M.J. Moon, J.H. Park, S.S. Park, S.S. Hong; "Raney Ni catalysts derived from different alloy precursors Part II. CO and CO_2 methanation activity",Korean Journal of Chemical Engineering, 2005;22:541-546, doi: 10.1007/bf02706639

[105] N. Perkas, G. Amirian, Z. Zhong, J. Teo, Y. Gofer, A. Gedanken; "Methanation of Carbon Dioxide on Ni Catalysts on Mesoporous ZrO_2 Doped with Rare Earth Oxides",Catalysis Letters, 2009;130:455-462, doi: 10.1007/s10562-009-9952-8

[106] I. Graça, L.V. González, M.C. Bacariza, A. Fernandes, C. Henriques, J.M. Lopes, M.F. Ribeiro; "CO_2 hydrogenation to CH_4 on NiHNaUSY zeolites",Applied Catalysis B: Environmental, 2014;147:101-110, doi: https://doi.org/10.1016/j.apcatb.2013.08.010

[107] H. Takano, K. Izumiya, N. Kumagai, K. Hashimoto; "The effect of heat treatment on the performance of the Ni/(Zr-Sm oxide) catalysts for carbon dioxide methanation",Applied Surface Science, 2011;257:8171-8176, doi: https://doi.org/10.1016/j.apsusc.2011.01.141

[108] J. Gao, L.-s. Jia, W.-p. Fang, Q.-b. Li, H. Song; "Methanation of carbon dioxide over the $LaNiO_3$ perovskite catalysts activated under the reactant stream",Journal of Fuel Chemistry and Technology, 2009;37:573-577, doi: https://doi.org/10.1016/S1872-5813(10)60008-4

[109] W. Zhen, B. Li, J. Ma, G. Lu, Enhancing catalytic activity and stability for CO_2 methanation on Ni@MOF-5 via control of active species dispersion, 2014.

[110] P. Riani, G. Garbarino, M.A. Lucchini, F. Canepa, G. Busca; "Unsupported versus alumina-supported Ni nanoparticles as catalysts for steam/ethanol conversion

and CO_2 methanation",Journal of Molecular Catalysis A: Chemical, 2014;383-384:10-16, doi: https://doi.org/10.1016/j.molcata.2013.11.006

[111] F. Song, Q. Zhong, Y. Yu, M. Shi, Y. Wu, J. Hu, Y. Song; "Obtaining well-dispersed Ni/Al_2O_3 catalyst for CO_2 methanation with a microwave-assisted method",International Journal of Hydrogen Energy, 2017;42:4174-4183, doi: https://doi.org/10.1016/j.ijhydene.2016.10.141

[112] B. Lu, Y. Ju, T. Abe, K. Kawamoto; "Grafting Ni particles onto SBA-15, and their enhanced performance for CO_2 methanation",RSC Advances, 2015;5:56444-56454, doi: 10.1039/C5RA07461D

[113] X. Zhang, W.-j. Sun, W. Chu; "Effect of glow discharge plasma treatment on the performance of Ni/SiO2 catalyst in CO2 methanation",Journal of Fuel Chemistry and Technology, 2013;41:96-101, doi: https://doi.org/10.1016/S1872-5813(13)60012-2

[114] X. Li, Y. Huang, Q. Zhang, C. Luan, V.A. Vinokurov, W. Huang; "Highly stable and anti-coking Ni/MoCeZr/$MgAl_2O_4$-MgO complex support catalysts for CO_2 reforming of CH_4: Effect of the calcination temperature",Energy Conversion and Management, 2019;179:166-177, doi: https://doi.org/10.1016/j.enconman.2018.10.067

[115] M. Jafarbegloo, A. Tarlani, A.W. Mesbah, S. Sahebdelfar; "One-pot synthesis of NiO–MgO nanocatalysts for CO_2 reforming of methane: The influence of active metal content on catalytic performance",Journal of Natural Gas Science and Engineering, 2015;27:1165-1173, doi: https://doi.org/10.1016/j.jngse.2015.09.065

[116] Y. Yan, Y. Dai, H. He, Y. Yu, Y. Yang; "A novel W-doped Ni-Mg mixed oxide catalyst for CO_2 methanation",Applied Catalysis B: Environmental, 2016;196:108-116, doi: https://doi.org/10.1016/j.apcatb.2016.05.016

[117] S. Ratchahat, M. Sudoh, Y. Suzuki, W. Kawasaki, R. Watanabe, C. Fukuhara; "Development of a powerful CO_2 methanation process using a structured Ni/CeO_2 catalyst",Journal of CO_2 Utilization, 2018;24:210-219, doi: https://doi.org/10.1016/j.jcou.2018.01.004

[118] K. Zhao, W. Wang, Z. Li; "Highly efficient Ni/ZrO_2 catalysts prepared via combustion method for CO_2 methanation",Journal of CO_2 Utilization, 2016;16:236-244, doi: https://doi.org/10.1016/j.jcou.2016.07.010

[119] F. Ocampo, B. Louis, A.-C. Roger; "Methanation of carbon dioxide over nickel-based $Ce_{0.72}Zr_{0.28}O_2$ mixed oxide catalysts prepared by sol–gel method",Applied Catalysis A: General, 2009;369:90-96, doi: https://doi.org/10.1016/j.apcata.2009.09.005

[120] F. Ocampo, B. Louis, A. Kiennemann, A.C. Roger; "CO_2 methanation over Ni-Ceria-Zirconia catalysts: effect of preparation and operating conditions",IOP Conference Series: Materials Science and Engineering, 2011;19:012007, doi:

[121] F. Ocampo, B. Louis, L. Kiwi-Minsker, A.-C. Roger; "Effect of Ce/Zr composition and noble metal promotion on nickel based $Ce_xZr_{1-x}O_2$ catalysts for carbon dioxide methanation",Applied Catalysis A: General, 2011;392:36-44, doi: https://doi.org/10.1016/j.apcata.2010.10.025

[122] A. Kambolis, H. Matralis, A. Trovarelli, C. Papadopoulou; "Ni/CeO_2-ZrO_2 catalysts for the dry reforming of methane",Applied Catalysis A: General, 2010;377:16-26, doi: https://doi.org/10.1016/j.apcata.2010.01.013

[123] A. Trovarelli, C. Deleitenburg, G. Dolcetti, J.L. Lorca; "CO_2 Methanation Under Transient and Steady-State Conditions over Rh/CeO_2 and CeO_2-Promoted Rh/SiO_2: The Role of Surface and Bulk Ceria",Journal of Catalysis, 1995;151:111-124, doi: https://doi.org/10.1006/jcat.1995.1014

[124] R. Zhou, N. Rui, Z. Fan, C.-j. Liu; "Effect of the structure of Ni/TiO_2 catalyst on CO_2 methanation",International Journal of Hydrogen Energy, 2016;41:22017-22025, doi: https://doi.org/10.1016/j.ijhydene.2016.08.093

[125] J. Liu, C. Li, F. Wang, S. He, H. Chen, Y. Zhao, M. Wei, D.G. Evans, X. Duan; "Enhanced low-temperature activity of CO_2 methanation over highly-dispersed Ni/TiO_2 catalyst",Catalysis Science & Technology, 2013;3:2627-2633, doi: 10.1039/C3CY00355H

[126] M.C. Bacariza, I. Graça, A. Westermann, M.F. Ribeiro, J.M. Lopes, C. Henriques; "CO_2 Hydrogenation Over Ni-Based Zeolites: Effect of Catalysts Preparation and Pre-reduction Conditions on Methanation Performance",Topics in Catalysis, 2016;59:314-325, doi: 10.1007/s11244-015-0435-4

[127] X. Guo, A. Traitangwong, M. Hu, C. Zuo, V. Meeyoo, Z. Peng, C. Li; "Carbon Dioxide Methanation over Nickel-Based Catalysts Supported on Various Mesoporous Material",Energy & Fuels, 2018;doi: 10.1021/acs.energyfuels.7b03826

[128] T.A. Le, M.S. Kim, S.H. Lee, T.W. Kim, E.D. Park; "CO and CO_2 methanation over supported Ni catalysts",Catalysis Today, 2017;293-294:89-96, doi: https://doi.org/10.1016/j.cattod.2016.12.036

[129] H. Muroyama, Y. Tsuda, T. Asakoshi, H. Masitah, T. Okanishi, T. Matsui, K. Eguchi; "Carbon dioxide methanation over Ni catalysts supported on various metal oxides",Journal of Catalysis, 2016;343:178-184, doi: https://doi.org/10.1016/j.jcat.2016.07.018

[130] A. Serrano-Lotina, L. Rodríguez, G. Muñoz, L. Daza; "Biogas reforming over La promoted NiMgAl catalysts derived from hydrotalcites-like precursors",Journal of Power Sources, 2011;196:4404-4410, doi: https://doi.org/10.1016/j.jpowsour.2010.10.107

[131] M. Gabrovska, R. Edreva-Kardjieva, D. Crişan, P. Tzvetkov, M. Shopska, I. Shtereva; "Ni–Al LDHs as catalyst precursors for CO_2 removal by methanation",Reaction Kinetics, Mechanisms and Catalysis, 2012;105:79-99, doi: 10.1007/s11144-011-0378-0

[132] Z. Fan, K. Sun, N. Rui, B. Zhao, C.-j. Liu; "Improved activity of Ni/$MgAl_2O_4$ for CO_2 methanation by the plasma decomposition",Journal of Energy Chemistry, 2015;24:655-659, doi: http://dx.doi.org/10.1016/j.jechem.2015.09.004

[133] S. Abate, K. Barbera, E. Giglio, F. Deorsola, S. Bensaid, S. Perathoner, R. Pirone, G. Centi; "Synthesis Characterization and Activity Patterns of Ni/Al Hydrotalcite Catalyts in CO_2 Methanation",Industrial & Engineering Chemistry Research, 2016;55:8299-8308, doi: 10.1021/acs.iecr.6b01581

[134] N. Bette, J. Thielemann, M. Schreiner, F. Mertens; "Methanation of CO_2 on a (Mg, Al)Ox Supported Nickel Catalyst Derived from (Ni,Mg,Al) Hydrotalcite-like Precursor",ChemCatChem, 2016;8:2903-2906, doi: 10.1002/cctc.201600469

[135] X. Wang, T. Zhen, C. Yu; "Application of Ni–Al-hydrotalcite-derived catalyst modified with Fe or Mg in CO_2 methanation",Applied Petrochemical Research, 2016;6:217-223, doi: 10.1007/s13203-016-0154-1

[136] C. Mebrahtu, F. Krebs, S. Perathoner, S. Abate, G. Centi, R. Palkovits; "Hydrotalcite based Ni-Fe/(Mg, Al)Ox catalysts for CO_2 methanation - tailoring Fe content for improved CO dissociation, basicity, and particle size",Catalysis Science & Technology, 2018;doi: 10.1039/C7CY02099F

[137] L. Zhang, L. Bian, Z. Zhu, Z. Li; "La-promoted Ni/Mg-Al catalysts with highly enhanced low-temperature CO_2 methanation performance",International Journal of Hydrogen Energy, 2018;43:2197-2206, doi: https://doi.org/10.1016/j.ijhydene.2017.12.082

[138] M. Guo, G. Lu; "The effect of impregnation strategy on structural characters and CO2 methanation properties over MgO modified Ni/SiO_2 catalysts",Catalysis Communications, 2014;54:55-60, doi: https://doi.org/10.1016/j.catcom.2014.05.022

[139] M.C. Bacariza, I. Graça, S.S. Bebiano, J.M. Lopes, C. Henriques; "Magnesium as Promoter of CO_2 Methanation on Ni-Based USY Zeolites",Energy & Fuels, 2017;31:9776-9789, doi: 10.1021/acs.energyfuels.7b01553

[140] L. Xu, H. Yang, M. Chen, F. Wang, D. Nie, L. Qi, X. Lian, H. Chen, M. Wu; "CO_2 methanation over Ca doped ordered mesoporous Ni-Al composite oxide catalysts: The promoting effect of basic modifier",Journal of CO_2 Utilization, 2017;21:200-210, doi: https://doi.org/10.1016/j.jcou.2017.07.014

[141] M. Guo, G. Lu; "The difference of roles of alkaline-earth metal oxides on silica-supported nickel catalysts for CO_2 methanation",RSC Advances, 2014;4:58171-58177, doi: 10.1039/C4RA06202G

[142] H. Qin, C. Guo, Y. Wu, J. Zhang; "Effect of La2O3 promoter on NiO/Al_2O_3 catalyst in CO methanation",Korean Journal of Chemical Engineering, 2014;31:1168-1173, doi: 10.1007/s11814-014-0013-7

[143] K.H. Song, X. Yan, D.J. Koh, T. Kim, J.-S. Chung; "La effect on the long-term durability of Ni-Mg-Al_2O_3 catalysts for syngas methanation",Applied Catalysis A: General, 2017;530:184-192, doi: https://doi.org/10.1016/j.apcata.2016.11.002

[144] K. Michalska, P. Kowalik, W. Próchniak, T. Borowiecki; "The Effect of La_2O_3 on Ni/Al_2O_3 Catalyst for Methanation at Very Low COx/H_2 Ratio",Catalysis Letters, 2018;148:972-978, doi: 10.1007/s10562-018-2302-y

[145] L. Zhou, Q. Wang, L. Ma, J. Chen, J. Ma, Z. Zi; "CeO_2 Promoted Mesoporous Ni/γ-Al_2O_3 Catalyst and its Reaction Conditions For CO_2 Methanation",Catalysis Letters, 2015;145:612-619, doi: 10.1007/s10562-014-1426-y

[146] C. Mebrahtu, S. Abate, S. Perathoner, S. Chen, G. Centi; "CO_2 methanation over Ni catalysts based on ternary and quaternary mixed oxide: A comparison and analysis of the structure-activity relationships",Catalysis Today, 2018;304:181-189, doi: https://doi.org/10.1016/j.cattod.2017.08.060

[147] H. Lu, X. Yang, G. Gao, J. Wang, C. Han, X. Liang, C. Li, Y. Li, W. Zhang, X. Chen; "Metal (Fe, Co, Ce or La) doped nickel catalyst supported on ZrO_2 modified mesoporous clays for CO and CO_2 methanation",Fuel, 2016;183:335-344, doi: https://doi.org/10.1016/j.fuel.2016.06.084

[148] L. Yao, Y. Wang, M.E. Galvez, C. Hu, P.d. Costa; "Alumina-Supported Ni-Mo Carbides as Promising Catalysts for CO_2 Methanation",Modern Research in Catalysis, 2017;Vol.06No.04:11, doi: 10.4236/mrc.2017.64010

[149] H. Takano, Y. Kirihata, K. Izumiya, N. Kumagai, H. Habazaki, K. Hashimoto; "Highly active Ni/Y-doped ZrO_2 catalysts for CO_2 methanation",Applied Surface Science, 2016;388:653-663, doi: https://doi.org/10.1016/j.apsusc.2015.11.187

[150] K. Zhao, Z. Li, L. Bian; "CO2 methanation and co-methanation of CO and CO_2 over Mn-promoted Ni/Al_2O_3 catalysts",Frontiers of Chemical Science and Engineering, 2016;10:273-280, doi: 10.1007/s11705-016-1563-5

[151] T. Burger, F. Koschany, O. Thomys, K. Köhler, O. Hinrichsen; "CO_2 methanation over Fe- and Mn-promoted co-precipitated Ni-Al catalysts: Synthesis, characterization and catalysis study",Applied Catalysis A: General, 2018;558:44-54, doi: https://doi.org/10.1016/j.apcata.2018.03.021

[152] D. Pandey, G. Deo; "Effect of support on the catalytic activity of supported Ni–Fe catalysts for the CO_2 methanation reaction",Journal of Industrial and Engineering Chemistry, 2016;33:99-107, doi: https://doi.org/10.1016/j.jiec.2015.09.019

[153] Y. Li, G. Lu, J. Ma; "Highly active and stable nano NiO-MgO catalyst encapsulated by silica with a core-shell structure for CO_2 methanation",RSC Advances, 2014;4:17420-17428, doi: 10.1039/C3RA46569A

[154] G. Zhi, X. Guo, Y. Wang, G. Jin, X. Guo; "Effect of La_2O_3 modification on the catalytic performance of Ni/SiC for methanation of carbon dioxide",Catalysis Communications, 2011;16:56-59, doi: https://doi.org/10.1016/j.catcom.2011.08.037

[155] W.C. Chen, W. Yang, J.D. Xing, L. Liu, H.L. Sun, Z.X. Xu, S.Z. Luo, W. Chu; "Promotion Effects of La_2O_3 on Ni/Al_2O_3 Catalysts for CO_2 Methanation",Advanced Materials Research, 2015;1118:205-210, doi: 10.4028/www.scientific.net/AMR.1118.205

[156] X. Wang, L. Zhu, Y. Liu, S. Wang; "CO_2 methanation on the catalyst of Ni/MCM-41 promoted with CeO_2",Science of The Total Environment, 2018;625:686-695, doi: https://doi.org/10.1016/j.scitotenv.2017.12.308

[157] Q. Liu, F. Gu, X. Lu, Y. Liu, H. Li, Z. Zhong, G. Xu, F. Su; "Enhanced catalytic performances of Ni/Al_2O_3 catalyst via addition of V_2O_3 for CO methanation",Applied Catalysis A: General, 2014;488:37-47, doi: https://doi.org/10.1016/j.apcata.2014.09.028

[158] S.-H. Kang, J.-H. Ryu, J.-H. Kim, S.-J. Seo, Y.-D. Yoo, P.S. Sai Prasad, H.-J. Lim, C.-D. Byun; "Co-methanation of CO and CO_2 on the Ni X -Fe1−X /Al_2O_3 catalysts; effect of Fe contents",Korean Journal of Chemical Engineering, 2011;28:2282-2286, doi: 10.1007/s11814-011-0125-2

[159] J. Ren, X. Qin, J.-Z. Yang, Z.-F. Qin, H.-L. Guo, J.-Y. Lin, Z. Li; "Methanation of carbon dioxide over Ni–M/ZrO2 (M=Fe, Co, Cu) catalysts: Effect of addition of a second metal",Fuel Processing Technology, 2015;137:204-211, doi: https://doi.org/10.1016/j.fuproc.2015.04.022

[160] W. Ahmad, M.N. Younis, R. Shawabkeh, S. Ahmed; "Synthesis of lanthanide series (La, Ce, Pr, Eu & Gd) promoted Ni/γ-Al2O3 catalysts for methanation of CO2 at low temperature under atmospheric pressure",Catalysis Communications, 2017;100:121-126, doi: https://doi.org/10.1016/j.catcom.2017.06.044

[161] H.C. Wu, Y.C. Chang, J.H. Wu, J.H. Lin, I.K. Lin, C.S. Chen; "Methanation of CO2 and reverse water gas shift reactions on Ni/SiO_2 catalysts: the influence of particle size on selectivity and reaction pathway",Catalysis Science & Technology, 2015;5:4154-4163, doi: 10.1039/C5CY00667H

[162] S. He, C. Li, H. Chen, D. Su, B. Zhang, X. Cao, B. Wang, M. Wei, D.G. Evans, X. Duan; "A Surface Defect-Promoted Ni Nanocatalyst with Simultaneously Enhanced Activity and Stability",Chemistry of Materials, 2013;25:1040-1046, doi: 10.1021/cm303517z

[163] J.H. Kwak, L. Kovarik, J. Szanyi; "CO_2 Reduction on Supported Ru/Al_2O_3 Catalysts: Cluster Size Dependence of Product Selectivity",ACS Catalysis, 2013;3:2449-2455, doi: 10.1021/cs400381f

[164] J.K. Kesavan, I. Luisetto, S. Tuti, C. Meneghini, C. Battocchio, G. Iucci; "Ni supported on YSZ: XAS and XPS characterization and catalytic activity for CO_2 methanation",Journal of Materials Science, 2017;52:10331-10340, doi: 10.1007/s10853-017-1179-2

[165] J. Pérez-Ramírez, G. Mul, J.A. Moulijn; "In situ Fourier transform infrared and laser Raman spectroscopic study of the thermal decomposition of Co–Al and Ni–Al hydrotalcites",Vibrational Spectroscopy, 2001;27:75-88, doi: https://doi.org/10.1016/S0924-2031(01)00119-9

[166] Faıza Bergaya, Gerhard Lagaly Editors. Handbook of Clay Science, Elsevier Amsterdam, The Netherlands, Volume 5 Techniques and Applications Chapter 14.1, 745-782., 2013.

[167] S.R.C.T. Evans D.G., Structural Aspects of Layered Double Hydroxides. In: Duan X., Evans D.G. (eds) Layered Double Hydroxides. Structure and Bonding, vol 119. Springer, Berlin, Heidelberg.

[168] "Rives V., Carriazo D., Martín C. (2010) Heterogeneous Catalysis by Polyoxometalate-Intercalated Layered Double Hydroxides. In: Gil A., Korili S., Trujillano R., Vicente M. (eds) Pillared Clays and Related Catalysts. Springer, New York, NY",doi:

[169] C. Forano, U. Costantino, V. Prévot, C. Taviot-Gueho, Layered Double Hydroxides (LDH), in: G.L.E. Faıza Bergaya (Ed.) Handbook of Clay Science, Elsevier Amsterdam, The Netherlands2013, pp. Volume 5 Techniques and Applications Chapter 14.11, 745-782.

[170] O.D. Pavel, R. Zăvoianu, R. Bîrjega, E. Angelescu; "Impact of the memory effect on the catalytic activity of Li–Al hydrotalcite-like compounds for the cyanoethylation reaction",Materials Research Bulletin, 2010;45:1106-1111, doi: https://doi.org/10.1016/j.materresbull.2010.06.003

[171] D. Tichit, N. Das, B. Coq, R. Durand; "Preparation of Zr-Containing Layered Double Hydroxides and Characterization of the Acido-Basic Properties of Their Mixed Oxides",Chemistry of Materials, 2002;14:1530-1538, doi: 10.1021/cm011125l

[172] S. Velu, K. Suzuki, M. Okazaki, T. Osaki, S. Tomura, F. Ohashi; "Synthesis of New Sn-Incorporated Layered Double Hydroxides and Their Thermal Evolution to Mixed Oxides",Chemistry of Materials, 1999;11:2163-2172, doi: 10.1021/cm990067p

[173] J. Carpentier, J.F. Lamonier, S. Siffert, E.A. Zhilinskaya, A. Aboukaïs; "Characterisation of Mg/Al hydrotalcite with interlayer palladium complex for catalytic oxidation of toluene",Applied Catalysis A: General, 2002;234:91-101, doi: https://doi.org/10.1016/S0926-860X(02)00201-6

[174] D.P. Debecker, E.M. Gaigneaux, G. Busca; "Exploring, Tuning, and Exploiting the Basicity of Hydrotalcites for Applications in Heterogeneous Catalysis",Chemistry – A European Journal, 2009;15:3920-3935, doi: doi:10.1002/chem.200900060

[175] J.I. Di Cosimo, V.K. Díez, M. Xu, E. Iglesia, C.R. Apesteguía; "Structure and Surface and Catalytic Properties of Mg-Al Basic Oxides",Journal of Catalysis, 1998;178:499-510, doi: https://doi.org/10.1006/jcat.1998.2161

[176] L. Bian, W. Wang, R. Xia, Z. Li; "Ni-based catalyst derived from Ni/Al hydrotalcite-like compounds by the urea hydrolysis method for CO methanation",RSC Advances, 2016;6:677-686, doi: 10.1039/C5RA19748A

[177] P. Marocco, E.A. Morosanu, E. Giglio, D. Ferrero, C. Mebrahtu, A. Lanzini, S. Abate, S. Bensaid, S. Perathoner, M. Santarelli, R. Pirone, G. Centi; "CO_2 methanation over Ni/Al hydrotalcite-derived catalyst: Experimental characterization and kinetic study",Fuel, 2018;225:230-242, doi: https://doi.org/10.1016/j.fuel.2018.03.137

[178] A. Serrano-Lotina, A.J. Martin, M.A. Folgado, L. Daza; "Dry reforming of methane to syngas over La-promoted hydrotalcite clay-derived catalysts",International Journal of Hydrogen Energy, 2012;37:12342-12350, doi: https://doi.org/10.1016/j.ijhydene.2012.06.041

[179] J. Zhang, N. Zhao, W. Wei, Y. Sun; "Partial oxidation of methane over Ni/Mg/Al/La mixed oxides prepared from layered double hydrotalcites",International Journal of Hydrogen Energy, 2010;35:11776-11786, doi: https://doi.org/10.1016/j.ijhydene.2010.08.025

[180] S. Bepari, S. Basu, N.C. Pradhan, A.K. Dalai; "Steam reforming of ethanol over cerium-promoted Ni-Mg-Al hydrotalcite catalysts",Catalysis Today, 2017;291:47-57, doi: https://doi.org/10.1016/j.cattod.2017.01.027

[181] C. Busetto, G. Del Piero, G. Manara, F. Trifirò, A. Vaccari; "Catalysts for low-temperature methanol synthesis. Preparation of Cu-Zn-Al mixed oxides via hydrotalcite-like precursors",Journal of Catalysis, 1984;85:260-266, doi: https://doi.org/10.1016/0021-9517(84)90130-1

[182] P. Liao, C. Zhang, L. Zhang, Y. Yang, L. Zhong, H. Wang, Y. Sun; "Higher alcohol synthesis via syngas over CoMn catalysts derived from hydrotalcite-like precursors",Catalysis Today, 2017;doi: https://doi.org/10.1016/j.cattod.2017.09.022

[183] N. Kakiuchi, Y. Maeda, T. Nishimura, S. Uemura; "Pd(II)−Hydrotalcite-Catalyzed Oxidation of Alcohols to Aldehydes and Ketones Using Atmospheric Pressure of Air",The Journal of Organic Chemistry, 2001;66:6620-6625, doi: 10.1021/jo010338r

[184] B.M. Choudary, M.L. Kantam, A. Rahman, C.R. Venkat Reddy; "Selective reduction of aldehydes to alcohols by calcined Ni-Al hydrotalcite",Journal of Molecular Catalysis A: Chemical, 2003;206:145-151, doi: https://doi.org/10.1016/S1381-1169(03)00413-8

[185] G. Fogassy, P. Ke, F. Figueras, P. Cassagnau, S. Rouzeau, V. Courault, G. Gelbard, C. Pinel; "Catalyzed ring opening of epoxides: Application to bioplasticizers synthesis",Applied Catalysis A: General, 2011;393:1-8, doi: 10.1016/j.apcata.2010.11.020

[186] I. Kirm, F. Medina, X. Rodríguez, Y. Cesteros, P. Salagre, J. Sueiras; "Epoxidation of styrene with hydrogen peroxide using hydrotalcites as heterogeneous catalysts",Applied Catalysis A: General, 2004;272:175-185, doi: https://doi.org/10.1016/j.apcata.2004.05.039

[187] D. Tichit, D. Lutic, B. Coq, R. Durand, R. Teissier; "The aldol condensation of acetaldehyde and heptanal on hydrotalcite-type catalysts",Journal of Catalysis, 2003;219:167-175, doi: https://doi.org/10.1016/S0021-9517(03)00192-1

[188] P. S. Kumbhar; "Modified Mg-Al hydrotalcite: a highly active heterogeneous base catalyst for cyanoethylation of alcohols",Chemical Communications, 1998:1091-1092, doi: 10.1039/A801872C

[189] B.M. Choudary, M. Lakshmi Kantam, C.R. Venkat Reddy, K. Koteswara Rao, F. Figueras; "The first example of Michael addition catalysed by modified Mg–Al hydrotalcite",Journal of Molecular Catalysis A: Chemical, 1999;146:279-284, doi: https://doi.org/10.1016/S1381-1169(99)00099-0

[190] H.-y. Zeng, Z. Feng, X. Deng, Y.-q. Li; "Activation of Mg–Al hydrotalcite catalysts for transesterification of rape oil",Fuel, 2008;87:3071-3076, doi: https://doi.org/10.1016/j.fuel.2008.04.001

[191] M. Ogawa, S. Asai; "Hydrothermal Synthesis of Layered Double Hydroxide−Deoxycholate Intercalation Compounds",Chemistry of Materials, 2000;12:3253-3255, doi: 10.1021/cm000455n

[192] H.P. Boehm, J. Steinle, C. Vieweger; "$[Zn_2Cr(OH)_6]X\cdot 2H_2O$, New Layer Compounds Capable of Anion Exchange and Intracrystalline Swelling",Angewandte Chemie International Edition in English, 1977;16:265-266, doi: doi:10.1002/anie.197702651

[193] L. Indira, M. Dixit, P.V. Kamath; "Electrosynthesis of layered double hydroxides of nickel with trivalent cations",Journal of Power Sources, 1994;52:93-97, doi: https://doi.org/10.1016/0378-7753(94)01939-8

[194] G. Hu, D. O'Hare; "Unique Layered Double Hydroxide Morphologies Using Reverse Microemulsion Synthesis",Journal of the American Chemical Society, 2005;127:17808-17813, doi: 10.1021/ja0549392

[195] Aramendı, x, M. a, x, A. a, V. Borau, C. Jiménez, J.M. Marinas, J.R. Ruiz, F.J. Urbano; "Comparative Study of Mg/M(III) (M=Al, Ga, In) Layered Double Hydroxides Obtained by Coprecipitation and the Sol–Gel Method",Journal of Solid State Chemistry, 2002;168:156-161, doi: https://doi.org/10.1006/jssc.2002.9655

[196] Y. Zhao, F. Li, R. Zhang, D.G. Evans, X. Duan; "Preparation of Layered Double-Hydroxide Nanomaterials with a Uniform Crystallite Size Using a New Method Involving Separate Nucleation and Aging Steps",Chemistry of Materials, 2002;14:4286-4291, doi: 10.1021/cm020370h

[197] D. Tichit, B. Coq; "Catalysis by Hydrotalcites and Related Materials",CATTECH, 2003;7:206-217, doi: 10.1023/b:catt.0000007166.65577.34

[198] L. Mohapatra, K. Parida; "A review on the recent progress, challenges and perspective of layered double hydroxides as promising photocatalysts",Journal of Materials Chemistry A, 2016;4:10744-10766, doi: 10.1039/C6TA01668E

[199] M. Ogawa, H. Kaiho; "Homogeneous Precipitation of Uniform Hydrotalcite Particles",Langmuir, 2002;18:4240-4242, doi: 10.1021/la0117045

[200] J.J. Bravo-Suárez, E.A. Páez-Mozo, S.T. Oyama; "Review of the synthesis of layered double hydroxides: a thermodynamic approach",Química Nova, 2004;27:601-614, doi:

[201] M. Adachi-Pagano, C. Forano, J.-P. Besse; "Synthesis of Al-rich hydrotalcite-like compounds by using the urea hydrolysis reaction-control of size and morphology",Journal of Materials Chemistry, 2003;13:1988-1993, doi: 10.1039/B302747N

[202] N. Morel-Desrosiers, J. Pisson, Y. Israeli, C. Taviot-Gueho, J.-P. Besse, J.-P. Morel; "Intercalation of dicarboxylate anions into a Zn-Al-Cl layered double hydroxide: microcalorimetric determination of the enthalpies of anion exchange",Journal of Materials Chemistry, 2003;13:2582-2585, doi: 10.1039/B303953F

[203] Y. Israeli, C. Taviot-Gueho, J.-P. Besse, J.-P. Morel, N. Morel-Desrosiers; "Thermodynamics of anion exchange on a chloride-intercalated zinc-aluminum layered double hydroxide: a microcalorimetric study",Journal of the Chemical Society, Dalton Transactions, 2000:791-796, doi: 10.1039/A906346C

[204] S. Miyata; "Anion exchange properties of hydrotalcite-like compounds",Clays and Clay Minerals, 1983;31:305-311, doi:

[205] T. Yamaoka, M. Abe, M. Tsuji; "Synthesis of Cu-Al hydrotalcite like compound and its ion exchange property",Materials Research Bulletin, 1989;24:1183-1199, doi: https://doi.org/10.1016/0025-5408(89)90193-1

[206] S. Miyata; "Physico-Chemical Properties of Synthetic Hydrotalcites in Relation to Composition ",Clays and Clay Minerals 1980;28:50-56, doi:

[207] H.K. G. Ertl, F. Schüth, J. Weitkamp, Handbook of Heterogenous Catalysis, 2008.

[208] G. Guilera, B. Gorges, S. Pascarelli, H. Vitoux, M.A. Newton, C. Prestipino, Y. Nagai, N. Hara; "Novel high-temperature reactors for in situ studies of three-way catalysts using turbo-XAS",Journal of Synchrotron Radiation, 2009;16:628-634, doi: doi:10.1107/S0909049509026521

[209] B. Gorges, H. Vitoux, P. Redondo, G. Carbone, C. Mocouta, G. Guilera; "A Miniature Maxthal Furnace for X-ray Spectroscopy and Scattering Experiments up to 1200 degrees C",AIP Conference Proceedings, 2010;1234:572-594, doi: 10.1063/1.3463269

[210] C.E. Daza, J. Gallego, J.A. Moreno, F. Mondragón, S. Moreno, R. Molina; "CO_2 reforming of methane over Ni/Mg/Al/Ce mixed oxides",Catalysis Today, 2008;133-135:357-366, doi: https://doi.org/10.1016/j.cattod.2007.12.081

[211] B. Mile, D. Stirling, M.A. Zammitt, A. Lovell, M. Webb; "The location of nickel oxide and nickel in silica-supported catalysts: Two forms of “NiO” and the assignment of temperature-programmed reduction profiles",Journal of Catalysis, 1988;114:217-229, doi: https://doi.org/10.1016/0021-9517(88)90026-7

[212] R. Dębek, K. Zubek, M. Motak, M.E. Galvez, P. Da Costa, T. Grzybek; "Ni–Al hydrotalcite-like material as the catalyst precursors for the dry reforming of methane at low temperature",Comptes Rendus Chimie, 2015;18:1205-1210, doi: http://dx.doi.org/10.1016/j.crci.2015.04.005

[213] V. Rives; "Characterisation of layered double hydroxides and their decomposition products",Materials Chemistry and Physics, 2002;75:19-25, doi: http://dx.doi.org/10.1016/S0254-0584(02)00024-X

[214] S. Hwang, J. Lee, U.G. Hong, J.H. Baik, D.J. Koh, H. Lim, I.K. Song; "Methanation of carbon dioxide over mesoporous Ni–Fe–Ru–Al_2O_3 xerogel catalysts: Effect of ruthenium content",Journal of Industrial and Engineering Chemistry, 2013;19:698-703, doi: http://dx.doi.org/10.1016/j.jiec.2012.10.007

[215] T.J. Vulic, A.F.K. Reitzmann, K. Lázár; "Thermally activated iron containing layered double hydroxides as potential catalyst for N_2O abatement",Chemical Engineering Journal, 2012;207:913-922, doi: http://dx.doi.org/10.1016/j.cej.2012.06.152

[216] L. Dalin, K. Mitsuru, W. Lei, N. Yoshinao, X. Ya, T. Keiichi; "Regenerability of Hydrotalcite-Derived Nickel–Iron Alloy Nanoparticles for Syngas Production from Biomass Tar",ChemSusChem, 2014;7:510-522, doi: doi:10.1002/cssc.201300855

[217] S. Hwang, J. Lee, U. Gi Hong, J. Seo, J. Chul Jung, D. Koh, H. Lim, C. Byun, I. Kyu Song; "Methane production from carbon monoxide and hydrogen over nickel–alumina xerogel catalyst: Effect of nickel content",Journal of Industrial and Engineering Chemistry, 2011;17:154–157, doi: 10.1016/j.jiec.2010.12.015

[218] Q. Pan, J. Peng, T. Sun, D. Gao, S. Wang, S. Wang; "CO_2 methanation on Ni/Ce0.5Zr0.5O2 catalysts for the production of synthetic natural gas",Fuel Processing Technology, 2014;123:166-171, doi: http://dx.doi.org/10.1016/j.fuproc.2014.01.004

[219] D.Y. Kalai, K. Stangeland, H. Li, Z. Yu; "The effect of La on the hydrotalcite derived Ni catalysts for dry reforming of methane",Energy Procedia, 2017;142:3721-3726, doi: https://doi.org/10.1016/j.egypro.2017.12.267

[220] O. Clause, M. Goncalves Coelho, M. Gazzano, D. Matteuzzi, F. Trifirò, A. Vaccari; "Synthesis and thermal reactivity of nickel-containing anionic clays",Applied Clay Science, 1993;8:169-186, doi: https://doi.org/10.1016/0169-1317(93)90035-Y

[221] A.F. Lucrédio, G. Jerkiewickz, E.M. Assaf; "Nickel catalysts promoted with cerium and lanthanum to reduce carbon formation in partial oxidation of methane reactions",Applied Catalysis A: General, 2007;333:90-95, doi: https://doi.org/10.1016/j.apcata.2007.09.009

[222] K. Takehira, T. Shishido, P. Wang, T. Kosaka, K. Takaki; "Autothermal reforming of CH_4 over supported Ni catalysts prepared from Mg–Al hydrotalcite-like anionic clay",Journal of Catalysis, 2004;221:43-54, doi: https://doi.org/10.1016/j.jcat.2003.07.001

[223] D. Wang, X. Zhang, J. Ma, H. Yu, J. Shen, W. Wei; "La-modified mesoporous Mg-Al mixed oxides: effective and stable base catalysts for the synthesis of dimethyl carbonate from methyl carbamate and methanol",Catalysis Science & Technology, 2016;6:1530-1545, doi: 10.1039/C5CY01712B

[224] A. Węgrzyn, A. Rafalska-Łasocha, D. Majda, R. Dziembaj, H. Papp; "The influence of mixed anionic composition of Mg–Al hydrotalcites on the thermal decomposition mechanism based on in situ study",Journal of Thermal Analysis and Calorimetry, 2010;99:443-457, doi: 10.1007/s10973-009-0190-5

[225] H.Y. Kim, H.M. Lee, J.-N. Park; "Bifunctional Mechanism of CO_2 Methanation on Pd-MgO/SiO_2 Catalyst: Independent Roles of MgO and Pd on CO_2 Methanation",The Journal of Physical Chemistry C, 2010;114:7128-7131, doi: 10.1021/jp100938v

[226] J.K. Nørskov, T. Bligaard, J. Rossmeisl, C.H. Christensen; "Towards the computational design of solid catalysts",Nature Chemistry, 2009;1:37, doi: 10.1038/nchem.121

[227] I. Lezcano-González, R. Oord, M. Rovezzi, P. Glatzel, S.W. Botchway, B.M. Weckhuysen, A.M. Beale; "Molybdenum Speciation and its Impact on Catalytic Activity during Methane Dehydroaromatization in Zeolite ZSM-5 as Revealed by Operando X-Ray Methods",Angewandte Chemie International Edition, 2016;55:5215-5219, doi: 10.1002/anie.201601357

[228] A.N. Mansour, C.A. Melendres; "Analysis of X-ray Absorption Spectra of Some Nickel Oxycompounds Using Theoretical Standards",The Journal of Physical Chemistry A, 1998;102:65-81, doi: 10.1021/jp9619853

[229] M. Lenglet, A. D'Huysser, J.P. Bonelle, J. Dürr, C.K. Jørgensen; "Analysis of x-ray Ni Kβ emission, xanes, xps, Ni 2p, and optical spectra of nickel(II) spinels and structure inference",Chemical Physics Letters, 1987;136:478-482, doi: https://doi.org/10.1016/0009-2614(87)80291-9

[230] L. Soriano, M. Abbate, J. Vogel, J.C. Fuggle, A. Fernández, A.R. González-Elipe, M. Sacchi, J.M. Sanz; "The electronic structure of mesoscopic NiO particles",Chemical Physics Letters, 1993;208:460-464, doi: https://doi.org/10.1016/0009-2614(93)87173-Z

[231] S. Lafuerza, J. García, G. Subías, J. Blasco, P. Glatzel; "High-resolution Mn K-edge x-ray emission and absorption spectroscopy study of the electronic and local structure of the three different phases in $Nd_{0.5}Sr_{0.5}MnO_3$",Physical Review B, 2016;93:205108, doi:

[232] S. Ceppi, A. Mesquita, F. Pomiro, E.V. Pannunzio Miner, G. Tirao; "Study of Kβ X-ray emission spectroscopy applied to Mn(2−x)V(1+x)O4 (x=0 and 1/3) oxyspinel and comparison with XANES",Journal of Physics and Chemistry of Solids, 2014;75:366-373, doi: https://doi.org/10.1016/j.jpcs.2013.11.002

[233] F. Pomiro, S. Ceppi, J.M. De Paoli, R.D. Sánchez, A. Mesquita, G. Tirao, E.V. Pannunzio Miner; "Magnetocrystalline interactions and oxidation state determination of Mn(2−x)V(1+x)O4 (x=0, 1/3 and 1) magnetorresistive spinel family",Journal of Solid State Chemistry, 2013;205:57-63, doi: https://doi.org/10.1016/j.jssc.2013.06.025

[234] C.J. Pollock, M.U. Delgado-Jaime, M. Atanasov, F. Neese, S. DeBeer; Journal of the American Chemical Society, 2014;136:9453-9463, doi: 10.1021/ja504182n

[235] G. Vankó, T. Neisius, G. Molnár, F. Renz, S. Kárpáti, A. Shukla, F.M.F. de Groot; The Journal of Physical Chemistry B, 2006;110:11647-11653, doi: 10.1021/jp0615961

[236] G. Vankó, J.-P. Rueff, A. Mattila, Z. Németh, A. Shukla; "Temperature- and pressure-induced spin-state transitions in $LaCoO_3$",Physical Review B, 2006;73:024424,

[237] D. Wierzbicki, R. Baran, R. Dębek, M. Motak, M.E. Gálvez, T. Grzybek, P. Da Costa, P. Glatzel; Applied Catalysis B: Environmental, 2018;232:409-419, doi: https://doi.org/10.1016/j.apcatb.2018.03.089

[238] E. Borfecchia, K.A. Lomachenko, F. Giordanino, H. Falsig, P. Beato, A.V. Soldatov, S. Bordiga, C. Lamberti; "Revisiting the nature of Cu sites in the activated Cu-SSZ-13 catalyst for SCR reaction",Chemical Science, 2015;6:548-563, doi: 10.1039/C4SC02907K

[239] S. Fujita, H. Terunuma, M. Nakamura, N. Takezawa, Industrial & Engineering Chemistry Research, 1991;30:1146-1151, doi: 10.1021/ie00054a012

[240] A.L. Lapidus, N.A. Gaidai, N.V. Nekrasov, L.A. Tishkova, Y.A. Agafonov, T.N. Myshenkova; "The mechanism of carbon dioxide hydrogenation on copper and nickel catalysts",Petroleum Chemistry, 2007;47:75-82, doi: 10.1134/s0965544107020028

Summary

The increasing concentration of CO_2 in the atmosphere, which is considered to be one of the anthropogenic sources of global warming, increased concerns and social awareness about the climate change. The strategies for CO_2 emissions reduction may be divided into (i) carbon capture and storage (CCS) and (ii) carbon capture and utilization (CCU) groups. In comparison to CCS, the CCU technologies allow to convert carbon dioxide into a valuable product. Thus, CCU methods are treating CO_2 as raw material and not as pollutant. Among the processes that convert CO_2 into a valuable compound is carbon dioxide methanation. In this process carbon dioxide is hydrogenated to methane with hydrogen supplied via water electrolysis using e.g. excess energy. It should be mentioned that some industrial scale installation already exists (up to 10MW).

The literature study suggests that the most appropriate active metal in this process is nickel due to (i) very good catalytic activity (comparable to noble metals), (ii) low cost and (iii) availability. As reported in literature, different strategies were implemented in order to increase the activity of Ni-based catalysts in CO_2 methanation. The most common ones include using various supports, changing the content of nickel or introduction of promoters. These strategies change the physicochemical properties, such as interaction of nickel active phase with the support, which inhibits sintering and increases the CO_2 adsorption capacity. The latter property , as well as stability towards sintering, are crucial in order to obtain an active, selective and stable catalyst for CO_2 methanation reaction. The application of mixed oxides of magnesia and alumina allows to introduce these properties, as MgO possesses basic character and is strongly bonded with NiO due to the formation of a solid solution of NiO-MgO.

Hydrotalcites seem to be the highly promising materials for such application, because NiO, MgO and Al_2O_3 may be easily introduced into such materials. Literature studies confirmed that Ni-containing hydrotalcites are very active in CO2 methanation. Therefore, **the goal of this PhD thesis was to evaluate the catalytic properties of Ni-containing hydrotalcite-derived mixed oxide materials in CO_2 methanation**. As the literature review showed that there are not many studies focused on such materials in the mentioned field, this work was focused on filling these gaps. The work was divided into four parts: (i) evaluation of catalytic properties of hydrotalcites containing various amounts of nickel in brucite-like layers, (ii) evaluation of catalytic properties of nickel-containing hydrotalcites promoted with Fe or La, (iii) evaluation of the effect of different methods of introduction of La on catalytic properties of Ni-hydrotalcites, and (iv) optimization of the catalysts and examination of promoting effect of La. In order to correlate the changes of physico-chemical properties, of the materials prepared by co-precipitation, the catalysts were characterized by means of elemental analysis (ICP-MS or XRF), XRD, FTIR, low temperature nitrogen sorption, H_2-TPR and CO_2-TPD. Additionally, selected catalysts were characterized using TEM, XANES and XES. The catalytic tests were carried out in the temperature range from 250°C to 450°C. In order to elucidate the promoting effect of lanthanum introduction operando XANES and XES under various reaction conditions were implemented.

The effect of nickel content was evaluated by the comparison of the physico-chemical properties and catalytic activity of hydrotalcites containing 5, 10, 15, 25, 30 and 40 wt.% of Ni (fresh) prepared by co-precipitation in a solution of Na_2CO_3. The characterization of the so-prepared materials confirmed that hydrotalcite-like materials were successfully synthesized. Calcination and reduction temperature was chosen basing on XRD and TPR-H_2 studies. The highest catalytic activity in CO_2 methanation was

found for the Ni40 catalyst, which showed CO_2 conversion of ca. 88% at 250°C.The higher activity was attributed to increased reducibility and much higher CO_2 adsorption capacity in comparison to samples containing lower amounts of Ni.

The influence of promoters introduction was evaluated by the preparation of Ni-containing (15 wt.% - fresh) materials promoted with Fe or La (1, 2 or 4 wt.%), at the stage of co-precipitation. It was proven that iron was successfully incorporated into the brucite-like layers, while lanthanum was deposited on the surface of the material as a separate phase. The introduction of iron or lanthanum increased the reducibility of material. However, the incorporation of higher amounts of Fe resulted in increased metallic nickel crystallite size, while the incorporation of La decreased somewhat the particle size. In general, the incorporation of the promoters, 1wt.% of Fe and 2wt.% of La, resulted in increased CO_2 adsorption capacity, which positively influenced the catalytic performance of the catalysts. The increased activity in CO_2 methanation was attributed to the increased reducibility and enhanced CO_2 adsorption capacity. Especially the number of medium-strength basic sites was positively influenced. The 24h tests proved that the catalysts remained stable.

Additionally, the influence of three lanthanum incorporation methods were studied: co-precipitation, adsorption from $La(EDTA)^-$ solution and impregnation. It was found that the introduction of lanthanum using impregnation method led to decreased CO_2 adsorption capacity through partial blockage of the existing basic sites, which negatively influenced the performance of the catalyst. However, the introduction of La using adsorption method (1wt.% of La) led to a significant increase in the number of moderate basic sites, which had a positive effect on the catalytic performance. However,

the incorporation of 2 and 4 wt.% of La using this technique did not further influence the catalytic activity. The 24h tests proved that the catalysts remained stable.

Additionally, the most active nickel-containing catalyst Ni40 was promoted with 2wt.% of La in order to optimize the catalytic properties. The optimized catalyst Ni40La2 and Ni40 were examined using operando XANES and XES techniques. XANES studies revealed that lanthanum strongly influenced the oxidation state of nickel under various reaction conditions, which resulted in enhanced CO_2 chemisorption. The Intergrated Absolute Difference method employed for for the analysis of Kβ line was found to be an appropriate method to determine the Ni oxidation state in in-situ reactions. The results of vtc XES measurements suggests that the adsorption of CO_2 is not the rate determining step of methanation reaction.

The best catalytic performance, in comparison to all studied materials, was found for the Ni-containing HT-derived catalysts promoted with 1 wt.% of La introduced using the adsorption method.

Streszczenie pracy

Rosnąca koncentracja CO_2 w atmosferze, który jest uważana za jedno z antropogenicznych źródeł globalnego ocieplenia, zwiększyła obawy i świadomość społeczną na temat zachodzących zmian klimatycznych. Strategie redukcji emisji CO_2 można podzielić na dwie grupy: (i) wychwytywanie i składowanie (Carbon Capture and Storage – CCS) oraz wychwytywanie i chemiczna utylizacja ditlenku węgla (Carbon Capture and Utilization – CCU). W przeciwieństwie do CCS, technologie CCU umożliwiają przekształcenie ditlenku węgla w wartościowy produkt. Do procesów przekształcających CO_2 w cenne związki zalicza się metanizację ditlenku węgla. W procesie tym ditlenek węgla uwodarniany jest do metanu za pomocą wodoru dostarczanego do procesu przez elektrolizę wody, do której można użyć np. nadmiarowej energii ze źródeł odnawialnych. Należy zaznaczyć, że istnieją już instalacje przemysłowe o mocy do 10MW.

Badania literaturowe sugerują, że najodpowiedniejszym metalem aktywnym w tym procesie jest nikiel ze względu na: (i) bardzo dobrą aktywność katalityczną (porównywalną z metalami szlachetnymi), (ii) niski koszt oraz (iii) ogólną dostępność. W literaturze zaproponowano różne strategie mające na celu zwiększenie aktywności katalizatorów niklowych w metanizacji CO_2. Najczęstsze z nich to zastosowanie różnych nośników, zmiana zawartości niklu lub wprowadzenie promotorów. Odpowiedni dobór strategii pozwala na zmianę właściwości fizykochemicznych, takich jak oddziaływanie pomiędzy faza aktywną niklu a nośnikiem, co skutkuje spowolnieniem lub wykluczeniem procesu spiekania, oraz zwiększoną zdolnością adsorpcji CO_2. Obie właściwości mają kluczowe znaczenie dla uzyskania aktywnego, selektywnego i stabilnego katalizatora reakcji metanizacji CO_2. Zastosowanie mieszanych tlenków magnezu i glinu pozwala na wprowadzenie tych właściwości do katalizatora, ponieważ MgO wykazuje charakter

zasadowy, i równocześnie jest silnie związany z NiO na skutek tworzenia stałego roztworu NiO-MgO.

Hydrotalkity są obiecującymi materiałami do zastosowania jako katalizatory reakcji metanizacji CO_2 ze względu na łatwość wprowadzenia NiO, MgO oraz Al_2O_3 do struktury. Badania literaturowe potwierdziły, że hydrotalkity zawierające nikiel są bardzo aktywne w tej reakcji. Z tego względu celem moich badań była ocena właściwości katalitycznych materiałów hydrotalkitowych zawierających nikiel w reakcji metanizacji. Ponieważ przegląd literaturowy wykazał niewielką ilość opracowań poświęconych hydrotalkitom niklowym jako katalizatorom do tej reakcji, moje badania skupiły się na wypełnieniu szeregu luk. Przeprowadzone przeze mnie badania można podzielić na 4 części: (a) ocena właściwości katalitycznych hydrotalkitów zawierających różne ilości niklu w warstwach brucytowych, (b) poprawa właściwości katalitycznych hydrotalkitów niklowych poprzez promowanie żelazem lub lantanem, (c) ocena wpływu metody wprowadzenia lantanu na właściwości katalityczne hydrotalkitów niklowych oraz (d) optymalizacja katalizatorów niklowo-lantanowych i badanie roli lantanu jako promotora. W celu skorelowania zmian właściwości fizykochemicznych materiałów otrzymanych za pomocą metody współstrącania, otrzymane katalizatory scharakteryzowałem za pomocą analizy elementarnej (XRF lub ICP-MS), dyfrakcji promieni rentgenowskich (XRD), niskotemperaturowej sorpcji azotu, termoprogramowanej redukcji wodorem (H_2-TPR) oraz termoprogramowanej desorpcji CO_2 (CO_2-TPD). Dodatkowo zoptymalizowane katalizatory zostały zbadane za pomocą transmisyjnej mikroskopii elektronowej (TEM), oraz rentgenowskiej spektroskopii absorpcyjnej i emisyjnej. Testy katalityczne w reakcji metanizacji CO_2 prowadzone były w zakresie temperatur od 250 do 450°C na katalizatorach zredukowanych in-situ w 900°C w przepływie 100 ml/min 10%H_2/Ar. W

celu wyjaśnienia promującego efektu lantanu, katalizatory przebadane za pomocą operando XANES oraz XES w dynamicznych warunkach reakcji.

W celu określenia efektu zawartości niklu porównałem właściwości fizykochemiczne oraz aktywność katalityczną hydrotalkitów zawierających 5, 10, 15, 25, 30 lub 40%wag. niklu (materiały świeże), które otrzymałem za pomocą metody współstrącania przy stałym pH. Charakterastyka otrzymanych katalizatorów potwierdziła, że otrzymane materiały mają strukturę podobną do hydrotalkitów. Temperatury kalcynacji oraz redukcji zostały dobrane na podstawie wyników XRD oraz H_2-TPR. Najwyższą aktywność katalityczną w reakcji metanizacji, ze stopniem konwersji CO_2 równym 88% w 250°C, wykazał katalizator zawierający 40%wag. Ni. Wzrost aktywności można powiązać ze zwiększoną redukowalnością oraz ze znacznym zwiększeniem zdolności adsorpcji CO_2 w porównaniu do materiałów zawierających mniejsze ilości Ni.

W celu określenia wpływu promotorów na właściwości katalityczne hydrotalkitów niklowych, do materiału zawierającego 15%wag. Ni wprowadziłem za pomocą metody współstrącania żelazo (1, 2 lub 4%wag.) lub lantan (1, 2 lub 4%wag.). Charakterystyka otrzymanych materiałów potwierdziła wprowadzenie żelaza do struktury hydrotalkitowej, podczas gdy lantan został osadzony na powierzchni materiału jako oddzielna faza. Wprowadzenie żelaza lub lantanu zwiększyło redukowalność materiałów. Równocześnie wprowadzenie większych ilości żelaza (2 oraz 4%wag.) skutkowało zwiększeniem wielkości krystalitów metalicznego niklu, podczas gdy wprowadzenie lantanu zmniejszyło nieco rozmiar krystalitów Ni^0. Wprowadzenie 1%wag. Fe oraz 2 i 4 %wag. La spowodowało zwiększenie zdolności adsorpcji CO_2, co pozytywnie wpłynęło na aktywność katalityczną. Zwiększoną aktywność w metanizacji

CO_2 przypisałem zwiększonej redukowalności oraz zwiększonej zdolności adsorpcji CO_2, a w szczególności zwiększonej liczbie centrów zasadowych średniej mocy.

Dodatkowo oceniłem wpływ trzech różnych metod wprowadzenia lantanu, takich jak współstrącanie (najaktywniejsza próbka z badań wymienionych wyżej – zawierająca 2%wag. La), adsorpcji z roztworu $La(EDTA)^-$ oraz impregnacji. Wprowadzenie lantanu za pomocą metody impregnacji spowodowało zmniejszenie zdolności adsorpcji CO_2 poprzez częściowe zablokowanie już istniejących centrów zasadowych, co negatywnie wpłynęło na właściwości katalityczne. Natomiast wprowadzenie lantanu za pomocą metody adsorpcji (1%wag. La) spowodowało znaczny wzrost ilości centrów zasadowych średniej mocy, co miało pozytywny wpływ na wydajność katalityczną.

Przeprowadziłem ponadto optymalizację składu katalizatora, promując najbardziej aktywny katalizator niklowy Ni40 2%wag. lantanu. Dla zoptymalizowanego katalizatora oraz najlepszej niepromowanej próbki Ni40 przeprowadziłem badania operando spektroskopii emisyjnej oraz absorpcyjnej promieniowania X. Badania XANES wykazały, że wprowadzenie lantanu miało silny wpływ na stopień utlenienia niklu w badanych próbkach w dynamicznych warunkach reakcji, co wiązało się ze zwiększoną chemisorpcją CO_2. Wykazałem, że metoda analizy różnic bezwzględnych (IAD – Integrated Absolute Difference) dla linii głównych Kβ nadaje się do określenia zawartości tlenku niklu w różnych warunkach reakcji in-situ. Wyniki pomiarów emisyjnej spektroskopii typu valence-to-core sugerują ponadto, iż adsorpcja ditlenku węgla nie jest etapem ograniczającym metanizację CO_2.

Résumé de Thèse

L'augmentation de la concentration de CO_2 dans l'atmosphère, considérée comme l'une des sources anthropiques du réchauffement de la planète, suscite de plus en plus d'inquiétudes et une prise de conscience sociale face au changement climatique. Les stratégies de réduction des émissions de CO_2 peuvent être divisées en deux groupes (i) capture et stockage du carbone (CCS) et (ii) capture et utilisation du carbone (CCU). En comparaison avec le CCS, les technologies CCU permettent de convertir le dioxyde de carbone en un produit valorisé. Ainsi, les méthodes CCU traitent le CO_2 en tant que matière première et non en tant que polluant. Parmi les processus convertissant le CO_2 en un composé valorisé, on trouve la méthanation du dioxyde de carbone. Dans ce processus, le dioxyde de carbone est hydrogéné en méthane à l'aide de l'hydrogène provenant de l'électrolyse de l'eau en utilisant par exemple des excès d'énergie. Il convient de mentionner qu'une installation à l'échelle industrielle existe déjà (jusqu'à 10 MW).

La littérature suggère que le nickel est le métal actif le plus approprié dans ce procédé en raison de (i) sa très bonne activité catalytique (comparable aux métaux nobles), (ii) un faible coût et (iii) une grande disponibilité. Dans la littérature, différentes stratégies ont déjà été mises en œuvre afin d'accroître l'activité des catalyseurs à base de Ni lors de la méthanation du CO_2. Les plus courants incluent l'utilisation de divers supports, la modification de la teneur en nickel ou l'introduction de promoteurs. De telles stratégies modifient les propriétés physicochimiques telles que l'interaction entre la phase active au nickel et le support, ce qui inhibe le frittage et augmente la capacité d'adsorption du CO_2. Ces deux propriétés sont essentielles afin d'obtenir un catalyseur à la fois actif et sélectif pour la méthanation du CO_2. L'application d'oxydes mixtes de magnésie et d'alumine permet d'introduire ces propriétés car le MgO possède un caractère basique et est fortement lié au NiO en raison de la formation d'une solution solide de NiO-MgO.

Les hydrotalcites semblent être les matériaux les plus prometteurs pour une telle application car NiO, MgO et Al_2O_3 peuvent être facilement introduits dans ceux-ci. La littérature a confirmé que les hydrotalcites contenant du Ni sont très actifs dans cette réaction. L'objectif de cette thèse était donc d'évaluer les propriétés catalytiques d'oxydes mixtes dérivés d'hydrotalcite contenant du Ni lors de la méthanation du CO_2. Comme la revue de littérature a montré qu'il y avait peu d'études sur de tels matériaux pour cette réaction, ces travaux ont servi à combler ces lacunes. Ces travaux peuvent être divisé en quatre parties : (i) évaluation des propriétés catalytiques d'hydrotalcites contenant diverses quantités de nickel dans des couches de type brucite, (ii) évaluation des propriétés catalytiques d'hydrotalcites contenant du nickel activées à l'aide de Fe ou de La, (iii) évaluation de l'effet de la méthode d'introduction de La sur les propriétés catalytiques des Ni-hydrotalcites et (iv) optimisation des catalyseurs et examen de l'effet promoteur de La. Afin de corréler les modifications des propriétés physico-chimiques des matériaux préparés par co-précipitation, les catalyseurs ont été caractérisés par analyse élémentaire (ICP-MS ou XRF), DRX, IRTF, sorption de l'azote à basse température, H_2-TPR et CO_2-TPD. De plus, les catalyseurs sélectionnés ont été caractérisés par TEM, XANES et XES. Les tests catalytiques ont été effectués dans une plage de températures allant de 250°C à 450°C. Afin d'examiner l'effet de promotion de l'introduction du lanthane, les méthodes XANES et XES dans diverses conditions de réaction ont été mises en œuvre.

L'effet de la teneur en nickel a été évalué en comparant les propriétés physico-chimiques et l'activité catalytique d'hydrotalcites contenant 5, 10, 15, 25, 30 et 40% en poids de Ni (frais) préparées par co-précipitation dans une solution de Na_2CO_3. La caractérisation des matériaux préparés a confirmé la synthèse réussie de matériaux analogues à l'hydrotalcite. L'activité catalytique la plus élevée lors de la méthanation du

CO_2 a été constatée pour le catalyseur Ni40, qui a montré une conversion du CO_2 d'environ. 88% à 250°C. L'activité plus élevée a été attribuée à une réductibilité accrue et à une capacité d'adsorption de CO_2 bien supérieure à celle des échantillons contenant de plus faibles quantités de Ni.

L'influence de l'introduction de promoteurs a été évaluée par la préparation de matériaux contenant du Ni (15% en poids - frais), activés avec du Fe ou du La (1, 2 ou 4% en poids) par co-précipitation. Il a été prouvé que le fer était incorporé avec succès dans les couches de type brucite, tandis que le lanthane était déposé à la surface du matériau en tant que phase séparée. L'introduction de fer ou de lanthane a augmenté la réductibilité du matériau. Cependant, l'incorporation de quantités plus élevées de Fe entraînait une augmentation de la taille des cristallites de nickel métallique, tandis que l'incorporation de La diminuait quelque peu la taille des particules. En général, l'incorporation des promoteurs, 1% en poids de Fe et 2% en poids de La, a eu pour effet d'augmenter la capacité d'adsorption du CO_2, ce qui a eu une influence positive sur les performances catalytiques des catalyseurs. L'activité accrue lors de la méthanisation du CO_2 a été attribuée à la fois à une réductibilité et une capacité accrues d'adsorption du CO_2, en particulier un nombre plus élevé de sites basiques de force moyenne. Les tests sur 24h ont prouvé que ces catalyseurs sont restés stables.

En outre, l'influence de trois méthodes d'incorporation du lanthane a été étudiée : co-précipitation, adsorption à partir de solution La (EDTA) et imprégnation. Il a été constaté que l'introduction du lanthane par la méthode d'imprégnation avait entraîné une diminution de la capacité d'adsorption du CO_2 due au blocage partiel des sites basiques existants, ce qui influait négativement sur les performances du catalyseur. Cependant, l'introduction de La en utilisant la méthode d'adsorption (1% en poids de La) a entraîné

une augmentation significative du nombre de sites basiques modérés, ce qui a eu un effet positif sur les performances catalytiques. Cependant, l'incorporation de 2 et 4% en poids de La en utilisant cette technique n'influait pas de plus sur l'activité catalytique. Les tests de 24 heures ont prouvé que les catalyseurs restaient stables.

En outre, le catalyseur le plus actif contenant du nickel Ni40 a été activé avec 2% en poids de La afin d'optimiser ses propriétés catalytiques. Les catalyseurs optimisés Ni40La2 et Ni40 ont été examinés en utilisant les techniques XANES et XES. Les études XANES ont révélé que le lanthane avait une forte influence sur l'état d'oxydation du nickel dans diverses conditions de réaction, ce qui était l'effet de la chimisorption accrue du CO_2. La méthode de la Différence Absolue Intégrée utilisée pour Kβ s'est révélée être une méthode appropriée pour déterminer l'état d'oxydation du nickel dans les réactions in situ. Les résultats des mesures vtc-XES suggèrent que l'adsorption du CO_2 n'est pas l'étape déterminante de la vitesse de la réaction de méthanation.

Les meilleures performances catalytiques, par rapport à tous les matériaux étudiés, ont été observées pour les catalyseurs dérivés d'Hydrotalcites contenant du Ni et activés avec 1% en poids de La introduit par la méthode d'adsorption.

Academic achievements of the author

The results presented in this PhD Thesis were fully or partially published in the following journals with Impact Factor:

1. **D. Wierzbicki**, R. Dębek, M. Motak, T. Grzybek, M.E. Galvez, P. Da Costa,. „Novel Ni-La-hydrotalcite derived catalysts for CO_2 methanation", Catalysis Communications, vol. 83, 2016, p. 5-8, **IF=3.389**
2. H. Liu, **D. Wierzbicki**, R. Dębek, M. Motak, T. Grzybek, P. Da Costa, M.E. Galvez,. „ La-promoted Ni-hydrotalcite-derived catalysts for dry reforming of methane at low temperatures", Fuel, vol. 182, 2016, p. 8-16, **IF=3.611**
3. **D. Wierzbicki**, R. Baran, R. Dębek, M. Motak, T. Grzybek, M.E. Galvez, P. Da Costa,. „The influence of nickel content on the performance of hydrotalcite-derived catalysts in CO_2 methanation reaction", International Journal of Hydrogen Energy, vol. 42, 2017, 23548-23555, **IF=4.229**
4. **D. Wierzbicki**, M. Motak, T. Grzybek, M.E. Galvez, P. Da Costa,. „The influence of lanthanum incorporation method on the performance of nickel-containing hydrotalcite-derived catalysts in CO_2 methanation reaction", Catalysis Today, vol. 307, 2018, 205-211, **IF=4.667**
5. **D. Wierzbicki**, R. Baran, R. Dębek, M. Motak, M.E. Galvez, T. Grzybek, P. Da Costa, P. Glatzel,. „Examination of the influence of La promotion on Ni state in hydrotalcite-derived catalysts under CO_2 methanation reaction conditions: Operando X-ray absorption and emission spectroscopy investigation" Applied Catalysis B: Environmental, vol. 232, 2018, 409-419, **IF=11.698**

Other publications in journals with Impact Factor:

1. **D. Wierzbicki**, R. Dębek, J. Szczurowski, S. Basąg, M. Włodarczyk, M. Motak, R. Baran,. „Copper, cobalt and manganese: Modified hydrotalcite materials as catalysts for the selective catalytic reduction of NO with ammonia. The influence of manganese concentration", Comptes Rendus Chimie, vol. 18, 2015, 1074-1083, **IF=1.879**
2. R. Baran, F. Averseng, **D. Wierzbicki**, K. Chalupka, J-M. Krafft, T. Grzybek, S. Dzwigaj,. „Effect of postsynthesis preparation procedure on the state of copper in CuBEA zeolites and its catalytic properties in SCR of NO with NH_3", Applied Catalysis A: General, vol. 523, 2016, 332-342, **IF=4.012**
3. M. Radko, A. Kowalczyk, E. Bidzińska, S. Witkowski, S. Górecka, **D. Wierzbicki**, K. Pamin, L. Chmielarz,. „Titanium dioxide doped with vanadium as effective catalyst for selective oxidation to diphenyl sulfide to diphenyl sulfonate", Journal of Thermal Analysis and Calorimetry, 2018, **IF=2.209**

Chapters in monographs:

1. **D. Wierzbicki**, M. Motak, T. Grzybek,. „New hydrotalcite derived nano-oxide catalysts for NOx emission reduction", „Nowe nanotlenkowe hydrotalkitowe katalizatory do redukcji emisji Nox", Archiwum Gospodarki Odpadami i Ochrony Środowiska, 2015, 291-300
2. **D. Wierzbicki**, T. Piwowarczyk, M. Motak, L. Lietti, M. Martinelli, C.G. Visconti, T. Grzybek, „New nano-oxide catalysts for chemical utilization of CO_2", Archiwum Gospodarki Odpadami i Ochrony Środowiska, 2015, 301-312

Presentations at Polish and International conferences:

1. M. Radko, A. Kowalczyk, E. Bidzińska, S. Witkowski, S. Górecka, K. Pamin, **D. Wierzbicki**, L. Chmielarz, „V-doped titanium dioxides as efficient catalysts for selective oxidation of Ph_2S to sulfones with hydrogen peroxide, International conference on Catalysis and surface chemistry 2018, 18-23 March 2018, Kraków, Poland, p. 290
2. **D. Wierzbicki**, R. Baran, R. Dębek, M.E. Galvez, P. Da Costa, M. Motak, „Mechanism insight of CO_2 methanation on Ni-La hydrotalcite-derived catalysts by operando XAS and XES spectroscopy", International conference on Catalysis and surface chemistry 2018, 18-23 March 2018, Kraków, Poland, p. 79
3. **D. Wierzbicki**, R. Dębek, M. Bocheński, M. Motak, „Effect of thermal treatment on the stability and crystallite size of Cu-Mg-Fe hydrotalcite-derived materials", Energy and Fuels 2018, 19-21 September 2018, Kraków, Poland, p. 124
4. **D. Wierzbicki**, A. Drzyżdżyk, M. Motak, T. Grzybek, „Influence of pretreatment conditions of Ni-containing Fe-promoted hydrotalcite-like materials on Ni^0 crystallite size", Energy and Fuels 2018, 19-21 September 2018, Kraków, Poland, p. 123
5. R. Baran, **D. Wierzbicki**, R. Dębek, „Operando XANES study on Ni-containing La-promoted hydrotalcite-derived catalysts for CO_2 methanation, International symposium on Acid-Base Catalysis, 7-10 May 2017, Rio De Janeiro, Brazil.
6. K.V. Kaliappan, M.C. Bacariza, **D. Wierzbicki**, C. Henriques, T. Grzybek, M.F. Ribeiro, „Ni-hydrotalcite derived materials as CO_2 methanation catalysts", EuropaCAT, 27-31 August 2017, Florence, Italy.
7. **D. Wierzbicki**, M. Motak, M.E. Galvez, P. Da Costa, T. Grzybek, "The effect of different nickel content and lanthanum promotion on the performance of hydrotalcite-derived catalysts in CO_2 methanation", EuropaCAT, 27-31 August 2017, Florence, Italy.
8. **D. Wierzbicki**, M.E. Galvez, M. Motak, T. Grzybek, P. Da Costa, „Hydrotalcite-derived nickel containing catalysts for CO_2 methanation", International conference on Advanced Energy Materials, 12-14 September 2016, Guildford, England, p. 6
9. H. Liu, **D. Wierzbicki**, R. Dębek, M. Motak, T. Grzybek, P. Da Costa, M.E. Galvez, „La-promoted Ni-hydrotalcite-derived catalysts for methane dry

reforming at low temperatures", International conference on Advanced Energy Materials, 12-14 September 2016, Guildford, England, p. 7

10. **D. Wierzbicki**, R. Baran, K. Świrk, M. Krawczyk, R. Dębek, M. Motak, T. Grzybek, „Al-pillared, copper-containing vermiculites as prospective catalysts for NH_3-SCR", 13th Pannonian International symposium on catalysis, 19-23 September 2016, Siofok, Hungary, p. 147
11. K. Świrk, **D. Wierzbicki**, R. Baran, M. Krawczyk, R. Dębek, M. Motak, T. Grzybek, „Selective catalytic reduction of nitrogen oxides by NH_3 over iron-promoted vermiculites", 13th Pannonian International symposium on catalysis, 19-23 September 2016, Siofok, Hungary, p. 113
12. K.V. Kaliappan, M.C. Bacariza, **D. Wierzbicki**, T. Grzybek, C. Henriques, M.F. Ribeiro, "Methane production from CO_2 over Ni-hydrotalcite derived catalysts", Encorto Nacional de Catalise e Materiais Porosos, 19-20 May 2016, Lisboa, Portugal, p. 67
13. **D. Wierzbicki**, M. Motak, M.E. Galvez, P. Da Costa, T. Grzybek, „Effect of reduction temperature on catalytic activity of nickel-containing hydrotalcite-derived in CO_2 methanation reaction", 13th Pannonian International symposium on catalysis, 19-23 September 2016, Siofok, Hungary, p. 148
14. **D. Wierzbicki**, M. Motak, T. Grzybek, „Effect of reduction temperature on the structure of hydrotalcite-derived mixed oxides containing nickel and lanthanum", Energy and Fuels 2016, Kraków 21-23 September 2016, p. 126
15. M. Motak, D. Duraczyńska, R. Dębek, **D. Wierzbicki**, K. Świrk, B. Samojeden, „The SEM characterization of hydrotalcite-like catalysts in DRM process", XLVIII Polish Annual Conference on Catalysis, Kraków 16-18.03.2016, p. 339,
16. M. Motak, B. Samojeden, **D. Wierzbicki**, K. Świrk, T. Grzybek, „Modyfkowane materiały warstwowe jako katalizatory SCR", XLVIII Polish Annual Conference on Catalysis, Kraków 16-18.03.2016, p. 340,
17. **D. Wierzbicki**, R. Debek, J. Szczurowski, M. Włodarczyk, M. Motak, R. Baran, T. Grzybek, „Hydrotalcite-derived mixed oxides containing Cu, Co and Mn as efficient catalysts for low-temperature selective catalytic reduction of NO_x with ammonia" XLVII Ogólnopolskie Kolokwium Katalityczne, XLVII Polish Annual Conference on Catalysis, Kraków 16-18.03.2015, p.53,

18. **D. Wierzbicki**, T. Piwowarczyk, M. Motak, T. Grzybek, „Characterization of hydrotalcites containing iron, cobal and nickel as prospective catalysts for Fischer-Tropsch synthesis" XLVII Ogólnopolskie Kolokwium Katalityczne, XLVII Polish Annual Conference on Catalysis, Kraków 16-18.03.2015, p.314-315,
19. R. Dębek, M. Motak, M.E. Galvez, P. Da Costa, **D. Wierzbicki**, „Badania właściwości zasadowych materiałów pochodzenia hydrotalkitowego zawierających nikiel", Polska Chemia w mieście wolności, 58 zjazd naukowy Polskiego Towarzystwa Chemicznego w Gdańsku, 21-25 września 2015, p. 62
20. **D. Wierzbicki**, M. Motak, R. Dębek, R. Baran, T. Grzybek, B. Samojeden, „Nowe nanotlenkowe katalizatory do ochrony środowiska", Polska Chemia w mieście wolności, 58 zjazd naukowy Polskiego Towarzystwa Chemicznego w Gdańsku, 21-25 września 2015, p. 245
21. **D. Wierzbicki**, M. Motak, R. Dębek, „Nowe tlenkowe materiały do utylizacji", Polska Chemia w mieście wolności, 58 zjazd naukowy Polskiego Towarzystwa Chemicznego w Gdańsku, 21-25 września 2015, p. 275

List of Figures and Tables:

A. Appendix

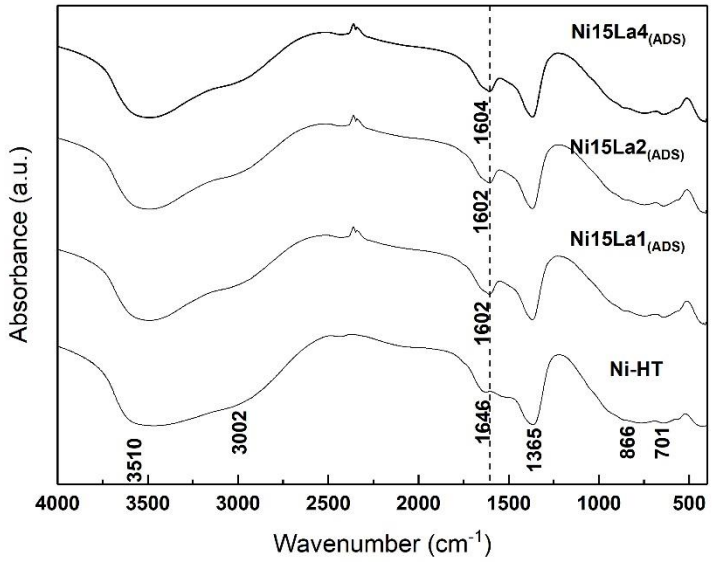

Figure A1 FTIR spectra for Ni-containing materials promoted with La using adsorption method

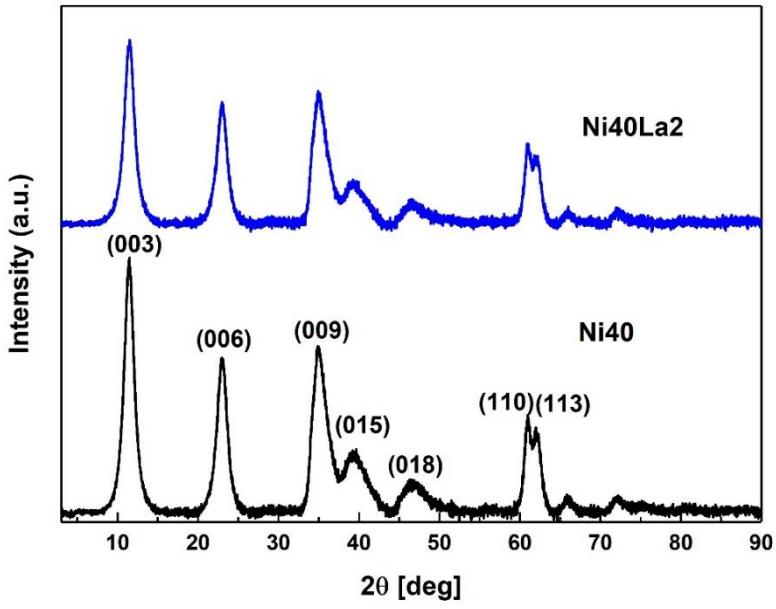

Figure A2 XRD patterns of as-synthesized hydrotalcite-like materials

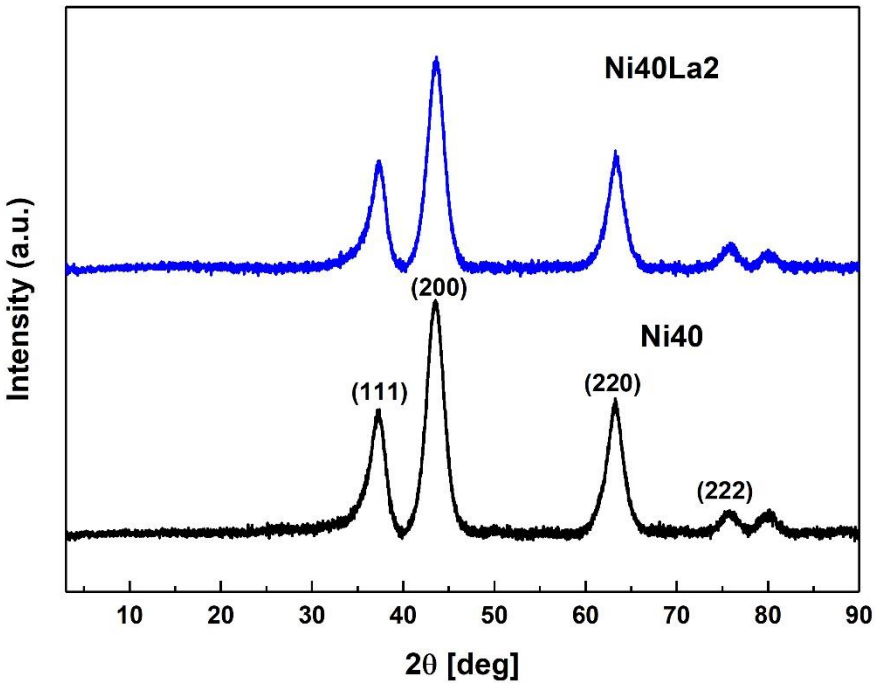

Figure A3 XRD patterns of hydrotalcite-derived mixed oxides obtained upon thermal treatment

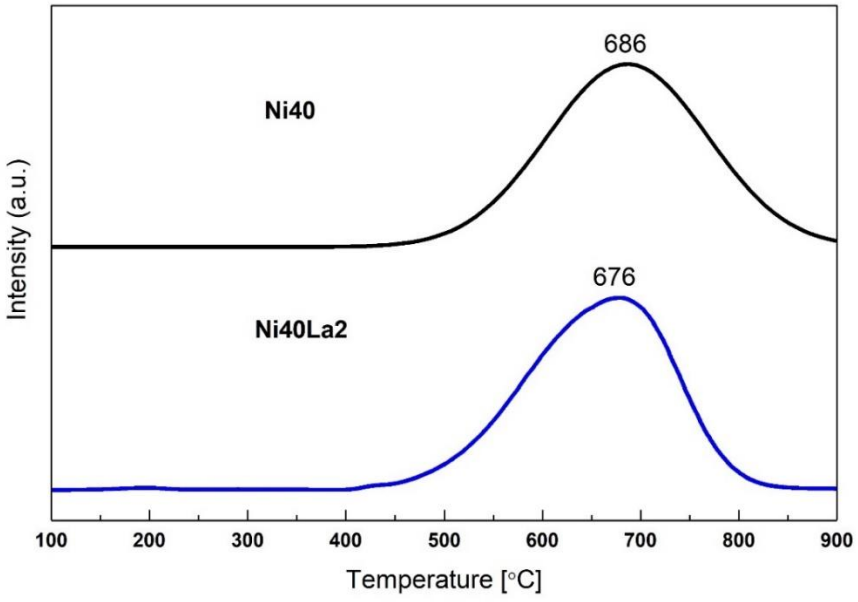

Figure A4 H_2-TPR profiles of the calcined materials

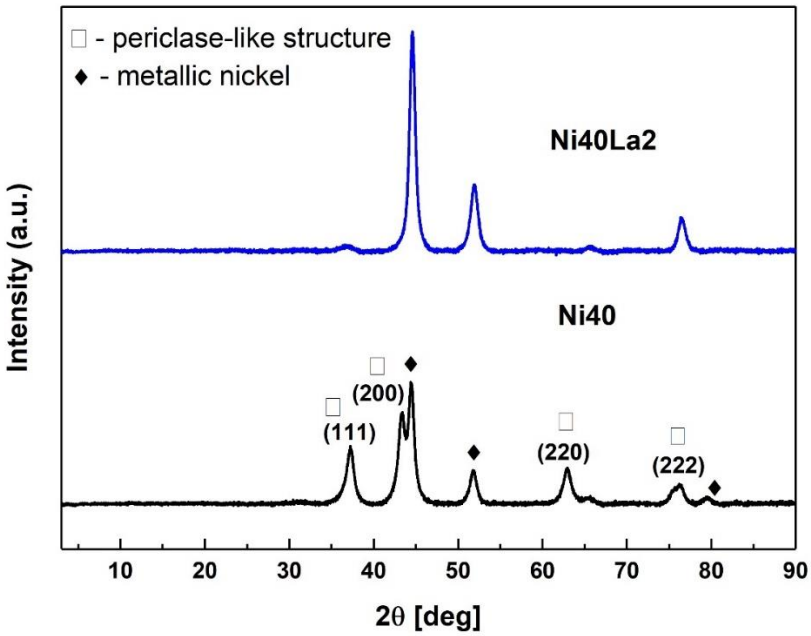

Figure A5 XRD patterns of reduced hydrotalcite-derived mixed oxides

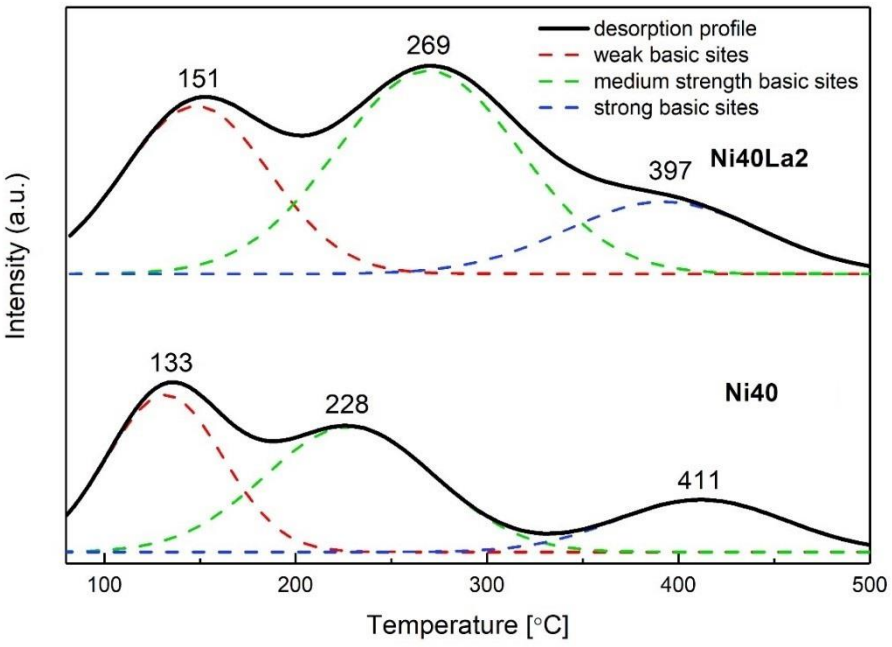

Figure A6 CO_2-TPD profiles of the reduced materials

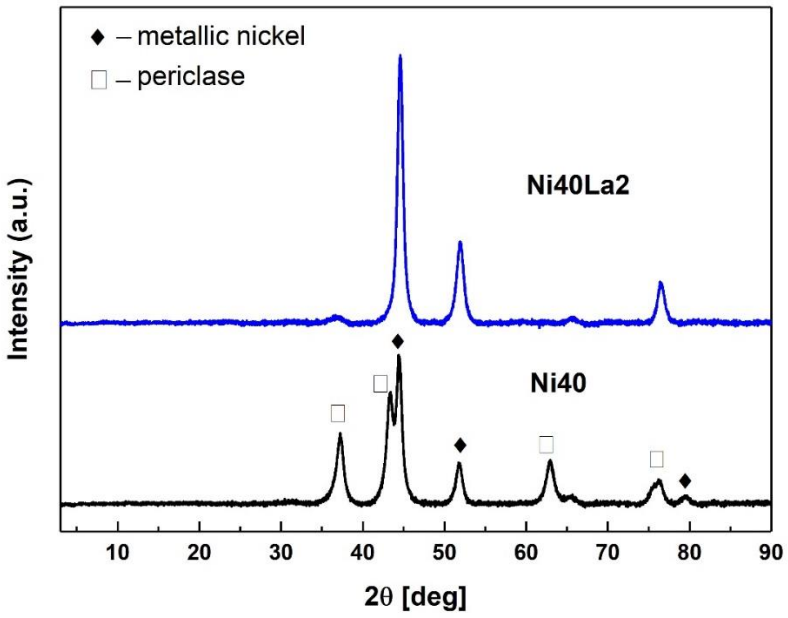

Figure A7 XRD patterns of spent catalysts